

**A Thesis Submitted for the Degree of PhD at the University of Warwick**

**Permanent WRAP URL:**

<http://wrap.warwick.ac.uk/111132>

**Copyright and reuse:**

This thesis is made available online and is protected by original copyright.

Please scroll down to view the document itself.

Please refer to the repository record for this item for information to help you to cite it.

Our policy information is available from the repository home page.

For more information, please contact the WRAP Team at: [wrap@warwick.ac.uk](mailto:wrap@warwick.ac.uk)

THE MEASUREMENT OF THE FLOW OF CEREBROSPINAL  
FLUID IN RESPONSE TO SHORT DURATION  
PRESSURE CHANGES

DAVID ROGER PRYTHERCH

A thesis submitted to the University of Warwick  
for the degree of Doctor of Philosophy.

October 1982.

For my late father, John  
and my mother, Gwenllian

For my late father, John  
and my mother, Gwenllian

MEMORANDUM

This dissertation is submitted to the University of Warwick in support of my application for admission to the degree of Doctor of Philosophy. It contains an account of my own work performed in the Department of Physics at the University of Warwick during the period October 1975 to July 1979 under the general supervision of Dr. M.J.A. Smith. No part of it has been used previously in a degree submitted to this or any other University. The work described in this thesis is the result of my own independent research except where specifically acknowledged in the text.

D.R. Prytherch

October 1982

#### ACKNOWLEDGEMENTS

I would like to express my thanks to those involved in the work presented in this thesis.

My supervisor, Dr. M.J.A. Smith, gave freely of his valuable time and advice. I am particularly grateful to Dr. Smith for his constant interest and enthusiasm which I found a great source of encouragement.

I wish to thank the Chairman of the Department of Physics for making the facilities of the Department available to me; and the Science Research Council for providing financial support.

I am grateful to Dr. G. Rowlands for helpful conversations concerning some of the mathematical aspects of this work; and to Mr. Cliff Randle for the technical support he so ably provided. I also wish to thank the members of the Department for the invigorating atmosphere they provided and for making my stay there a happy one.

The clinical aspects of this work were overseen by Mr. B.N. Williams, Consultant Neurosurgeon at the Midland Centre for Neurosurgery and Neurology, and I am deeply grateful to him for the time and effort he expended, and for his keen interest in this work. I also thank Dr. Clive Thursfield of the Medical Physics Department at the Midland Centre for the encouragement he gave and for his assistance in the clinical work.

Finally I wish to thank Mrs. Val Crozier who typed a somewhat difficult manuscript quickly and accurately, and my wife Deborah, who prepared the line drawings.

### ABSTRACT

This thesis describes the theory, development and use of an electrochemical flow transducer for the measurement of the flow of cerebrospinal fluid. The flow sensitive part of the flow transducer is a gold sphere cathode at which oxygen is reduced to hydroxyl ions. The rate of reduction of oxygen is limited by the transport of oxygen to the cathode by convective-diffusion and so the current flowing through the cathode is a function of flow past the cathode.

Theories are developed to describe the dependence of the output current on flow velocity, and other variables, for various cathode geometries. In all the cases considered the output current is proportional to the square root of the flow velocity magnitude and directly proportional to the oxygen concentration. The limiting time response of the transducer is that to a decrease in flow velocity and a theory to describe this is presented, for the cathode geometries considered.

Experiments were performed to investigate the dependence of the output current, of the various cathode geometries, on the main variables involved in the response to a steady flow, and in the time response to a decrease in flow. Good agreement was found between the experimental results and the theoretical predictions.

The development of the flow transducer used clinically is described, with the results of the final animal experiment performed to confirm the in-vivo operation of the flow transducer. In the form used clinically the flow transducer is small enough to enter the CSF pathways through an 18 gauge spinal needle whilst still allowing the simultaneous measurement of CSF pressure through the same needle. Typical results from the initial clinical trials are presented.

C O N T E N T S

	<u>Page</u>
<u>CHAPTER 1</u> THE CEREBROSPINAL FLUID (C.S.F.) AND THE C.S.F. PATHWAYS	1
1.1            Introduction	1
1.2            The C.S.F. and the C.S.F. pathways	4
1.3            The C.S.F. Pressure	6
1.3.1 General considerations	6
1.3.2 Rhythmical variations in C.S.F. pressure	8
1.3.3 Intermittent variations in C.S.F. pressure	9
 <u>CHAPTER 2</u> INVESTIGATIONS OF C.S.F. DYNAMICS	 12
2.1            Introduction	12
2.2            Pressure investigations	12
2.3            Flow investigations	14
2.3.1 Flow information derived from pressure movements	14
2.3.2 Flow information from radiographic procedures	15
2.4            Requirements for and choice of flow transducer	16
2.5            Conclusions	20
 <u>CHAPTER 3</u> THE STEADY-STATE RESPONSE OF THE OUTPUT CURRENT	 22
3.1            Introduction	22
3.2            Electrochemical Aspects	28
3.2.1 Introduction	28
3.2.2 The electrochemical reduction of oxygen	30
3.3            The convective-diffusion equation	32
3.4            The Navier-Stokes equation	36

<u>CHAPTER 3 (cont/d)</u>		<u>Page</u>
3.5	The current response of various electrodes	39
3.6	The calculation of the current response of an enamelled disc parallel to the flow	41
3.7	The calculation of the current response of an enamelled disc perpendicular to the flow	43
3.8	The calculation of the current response of a sphere	53
3.9	Discussion	57
	3.9.1 General	57
	3.9.2 Electrodes parallel to the flow	58
	3.9.3 Electrodes perpendicular to the flow	59
	3.9.4 The spherical electrodes	63
<u>CHAPTER 4</u>	<u>EXPERIMENTAL INVESTIGATIONS OF THE STEADY-STATE VELOCITY RESPONSE</u>	68
4.1	Introduction	68
4.2	The anode-cathode potential $V_{ac}$	69
4.3	The variation of I with $V_{ac}$ and $V_c$ and the choice of electrode materials	70
	4.3.1 The variation of I with $V_{ac}$	70
	4.3.2 The variation of I with $V_c$	70
	4.3.3 Choice of electrode materials	73
4.4	The variation of I with velocity of flow $U_0$	75
4.5	Dicussion	82
<u>CHAPTER 5</u>	<u>THE TIME RESPONSE OF THE OUTPUT CURRENT : THE RESPONSE TO A STEP DECREASE IN FLOW VELOCITY</u>	88
5.1	Introduction	88
5.2	A simple model of the time response	89
5.3	A more accurate model of the time response	92

<u>CHAPTER 5 (Cont/d)</u>		<u>Page</u>
5.4	The calculation of the time response of an enamelled disc parallel to the flow	99
5.5	The calculation of the time response of an enamelled disc perpendicular to the flow	103
5.6	The calculation of the time response of a sphere	105
5.7	The evaluation of the expressions obtained for the time response	108
5.8	Discussion	110
 <u>CHAPTER 6</u> EXPERIMENTAL INVESTIGATIONS OF THE TIME RESPONSE		112
6.1	Introduction	112
6.2	The experimental arrangement and method	113
6.3	Results	115
6.4	Discussion	119
	6.4.1 General	119
	6.4.2 Comparison of the derived value of D with accepted values	120
	6.4.3 The perpendicular disc	122
	6.4.4 Comparison of the time response results with the steady state results	123
	6.4.5 Scaling of electrodes	126
	6.4.6 Conclusions	127
 <u>CHAPTER 7</u> THE DEVELOPMENT AND CONSTRUCTION OF THE FLOW TRANSDUCER; AND THE EXTENSION OF ITS CALIBRATION TO C.S.F.		129
7.1	Introduction	129
7.2	Development of the cathode	129
	7.2.1 The copper enamelled parallel disc	129
	7.2.2 Copper sphere cathodes	131

<u>CHAPTER 7 (Cont/d)</u>		<u>Page</u>
	7.2.3 Gold sphere cathodes	132
7.3	The anode	134
	7.3.1 General considerations	134
	7.3.2 The reservoir	134
	7.3.3 Skin electrodes	135
7.4	The animal experiments	136
	7.4.1 Introduction	136
	7.4.2 Experimental arrangement and methods	137
	7.4.3 Results	139
7.5	Extension of the calibration to C.S.F.	142
	7.5.1 The constituents of the C.S.F.	142
	7.5.2 The effect of protein upon the velocity response	143
	7.5.3 The effect of pH upon the velocity response	146
7.6	Discussion	147
 <u>CHAPTER 8 THE CLINICAL TRIALS</u>		 149
8.1	Introduction	149
8.2	Electronics	150
8.3	Methods and procedures	152
8.4	Results	155
	8.4.1 General considerations	155
	8.4.2 Typical responses to the stimuli	157
8.5	Sources of Artefact	160
	8.5.1 ECG pick up	160
	8.5.2 The effects of skin impedance	165
	8.5.3 Motion artefact	167
8.6	Discussion	168



LIST OF FIGURES

	<u>following Page</u>
1.2.1	Schematic illustration of the CSF pathways - lateral view 5
1.2.2	Schematic illustration of the CSF pathways - posterior view 5
1.2.3	Schematic illustration of the contents of the (intracranial) CSF pathways 5
2.2.1	Illustration of lumbar puncture 12
2.2.2	Illustration of cisternal puncture 12
3.2.1	Illustration of the distribution of $V_{ac}$ at the electrodes 29
3.2.2	Illustration of the variation of current density $J$ with $V_c$ and $V_{ac}$ 29
3.3.1	Variation of concentration with distance normal to the reaction surface 35
3.4.1	The curvi-linear co-ordinates used for bodies of revolution 39
3.6.1	The usual form of enamelled parallel disc 41
3.6.2	The enamelled, parallel plate 41
3.6.3	The integration scheme for the parallel enamelled disc 42
3.6.4	The variation of $Q_{II}$ with $\chi$ 42
3.7.1	The geometry relevant to perpendicular electrodes 43
3.7.2	Potential flow past an elliptic cylinder 43
3.7.3	The variation of $d\phi/d\mu$ and $d^2\phi/d\mu^2$ with $\mu$ for the infinite perpendicular electrodes 47
3.7.4	The variation of $Q_1$ and $Q_1^*$ with $\chi$ 52
3.8.1	The geometry relevant to spherical electrodes 53
3.8.2	The variations of $df_1/d\mu$ , $df_3/d\mu$ and $df_5/d\mu$ with $\mu$ 53

FIGURES(Cont/d)following Page

3.9.1	The variation of diffusion layer thickness with position for the parallel plate and the perpendicular disc	58
3.9.2	The variation of hydrodynamic boundary layer thicknesses, with position for the parallel plate and the perpendicular disc	58
3.9.3	The variations of diffusion layer thickness for the perpendicular disc obtained by including and excluding the term $u\partial c/\partial x$ in the convective-diffusion equation	62
3.9.4	The variation of diffusion layer thickness with position for the sphere	63
3.9.5	The variation of $dI$ with position on the surface of a sphere	64
3.9.6	The variation of $Q_s$ with the separation point $\theta_s$	65
3.9.7	The spherical electrode with epoxy resin	65
3.9.8	The geometry of spherical electrodes with epoxy resin	65
3.9.9	The variation of $Q_{s2}$ with $\theta_c$	67
4.1.1	Values of the diffusion co-efficient of oxygen $D$ in water	69
4.1.2	The variation of the oxygen concentration $c_s$ with temperature	69
4.1.3	The variation of water vapour pressure $P_w$ with temperature	69
4.1.4	The variation of the kinematic viscosity $\nu$ with temperature	69
4.2.1	The voltage-clamp circuit used in the laboratory work	69
4.3.1	The variation of $I$ with $V_{ac}$ at different concentrations of sodium chloride	72
4.3.2	The variation of $I$ with $V_{ac}$ , $V_c$ and $V_a$	72
4.3.3	The variation of $I$ with $V_{ac}$ at different temperatures	72

<u>FIGURES(Cont/d)</u>	<u>following Page</u>	
3.9.1	The variation of diffusion layer thickness with position for the parallel plate and the perpendicular disc	58
3.9.2	The variation of hydrodynamic boundary layer thicknesses, with position for the parallel plate and the perpendicular disc	58
3.9.3	The variations of diffusion layer thickness for the perpendicular disc obtained by including and excluding the term $u\partial c/\partial x$ in the convective-diffusion equation	62
3.9.4	The variation of diffusion layer thickness with position for the sphere	63
3.9.5	The variation of $dI$ with position on the surface of a sphere	64
3.9.6	The variation of $Q_s$ with the separation point $\theta_s$	65
3.9.7	The spherical electrode with epoxy resin	65
3.9.8	The geometry of spherical electrodes with epoxy resin	65
3.9.9	The variation of $Q_{s2}$ with $\theta_c$	67
4.1.1	Values of the diffusion co-efficient of oxygen $D$ in water	69
4.1.2	The variation of the oxygen concentration $c_s$ with temperature	69
4.1.3	The variation of water vapour pressure $P_w$ with temperature	69
4.1.4	The variation of the kinematic viscosity $\nu$ with temperature	69
4.2.1	The voltage-clamp circuit used in the laboratory work	69
4.3.1	The variation of $I$ with $V_{ac}$ at different concentrations of sodium chloride	72
4.3.2	The variation of $I$ with $V_{ac}$ , $V_c$ and $V_a$	72
4.3.3	The variation of $I$ with $V_{ac}$ at different temperatures	72

<u>FIGURES</u> (Cont/d)	<u>following Page</u>	
4.4.1	The apparatus used in the investigation of the velocity response	74
4.4.2	The flow response of a parallel disc	75
4.4.3	The flow response of a perpendicular disc	75
4.4.4a	The flow response of a gold sphere	75
4.4.4b	The flow response of a copper sphere	75
4.4.5	The dependence of the flow response on oxygen concentration	79
4.4.6	The dependence of the flow response of disc electrodes on electrode radius	79
4.4.7	The dependence of the flow response of spherical electrodes on radius	81
4.4.8	The variation of the derived values of oxygen diffusion coefficient with temperature	81
4.4.9	The dependence of the flow response on temperature	81
5.3.1	The generalised electrode geometry used in the time response theory	93
5.7.1	The variation of I with C for the enamelled parallel disc	109
5.7.2	The variation of I with C for the enamelled perpendicular disc	109
5.7.3	The variation of I with C for the complete sphere	109
5.7.4	The variation of I with C for the epoxied sphere	109
6.2.1	Diagram of the apparatus used to obtain values of $U_f > U_c$	114
6.2.2	Diagram of the gold sphere constructed to eliminate the effects of epoxy resin	114
6.3.1	A typical time response curve for an enamelled parallel disc	115
6.3.2	A typical time response curve for an enamelled perpendicular disc	115

<u>FIGURES(Cont/d)</u>	<u>following Page</u>	
6.3.3	A typical time response curve for a spherical electrode	115
6.3.4	The application of the initial time response theory of section 5.2	115
6.3.5	The application of the time response theory of section 5.3	115
6.3.6	The variation of M with $I_f^2$ for the parallel disc	116
6.3.7	The variation of M with $I_f^2$ for the perpendicular disc	116
6.3.8	The radius dependence of the speed of the time response	117
6.3.9a	The variations of the derived values of oxygen diffusion coefficient with temperature for the disc electrodes	117
6.3.9b	The variations of the derived values of oxygen diffusion coefficient with temperature for the spherical electrodes	117
6.3.10	The effect of temperature on the speed of the time response	117
7.2.1	The initial design of flow transducer	131
7.2.2	The copper cathode flow transducer	131
7.2.3	Photographs of the construction of the gold cathode	134
7.2.4	The gold cathode flow transducer	134
7.3.1	Diagram of the reservoir and cathode assembly as used in practice	134
7.4.1	Schematic diagram of the animal experiment	138
7.4.2	Photograph of the animal experiment	138
7.4.3	The response of the flow transducer to an imposed flow of CSF	141
7.4.4	The response of the flow transducer to cardiac pulsation of the CSF	141
7.4.5	The response of the flow transducer to cardiac pulsation of the CSF	141

<u>FIGURES(Cont/d)</u>	<u>following Page</u>
7.5.1	The effect of protein upon the velocity response of the flow transducer 145
7.5.2	I-V <sub>ac</sub> curves at low values of pH 147
7.5.3	The variation of the plateau current with pH 147
8.2.1	The voltage-clamp circuit used in the clinical trials 150
8.2.2	The interface unit 150
8.3.1	Schematic illustration of the pressure measurements 153
8.4.1	The response to a series of coughs 157
8.4.2	The response to a series of blows 157
8.4.3	The response to Queckenstedt's test 157
8.4.4	The response to cardiac pulsation 157
8.4.5	The response to movement of the patient's arm 157
8.5.1	The simulation of ECG pick-up 161
8.5.2	The proposed equivalent circuit of the cathode to perturbations of V <sub>c</sub> 161
8.5.3	The results of the simulation of ECG pick-up with X = 0 Ω 163
8.5.4	The results of the simulation of ECG pick-up with X = 11.1kΩ 163
A.1.1	The variation of df/dμ with μ for the parallel plate 177
B.3.1	Simplified flow chart of the programs used to evaluate the time response expressions 189
C.1.1	Constant alternating voltage perturbation of the voltage-clamp 191

LIST OF TABLES

		<u>following Page</u>
2.3.1	Collected flow information	16
3.3.1	Symbols used in Chapter 3	32
3.5.1	Shape factors for the electrode geometries considered	40
3.7.1	Potential flow components for perpendicular electrodes	43
5.7.1	The effect on the time response of the enamelled parallel disc of varying $\chi$	109
5.7.2	The effect on the time response of the enamelled perpendicular disc of varying $\chi$	109
5.7.3	The effect on the time response of the complete sphere of varying $\theta_s$	109
5.7.4	The effect on the time response of the epoxied sphere of varying $\theta_c$	109
7.5.1	The properties and major constituents of C.S.F.	143
D.1.1	Materials and items used	192

CHAPTER 1

## CHAPTER 1

### THE CEREBROSPINAL FLUID (C.S.F.) AND THE C.S.F. PATHWAYS

#### 1.1 Introduction

This thesis describes the theory, development and use of a transducer for the measurement of the flow of cerebrospinal fluid (C.S.F.) in response to the various changes in pressure to which it is subject.

The flow sensitive part of the transducer is a gold sphere which acts as a cathode at which oxygen is electrochemically reduced to hydroxyl ions. The oxygen reaction is transport controlled by convective-diffusion of oxygen to the cathode, and the thickness of the diffusion layer established at the cathode is a function of the magnitude of flow past the cathode. Hence the current which flows through the cathode is a measure of the flow past it.

The electrochemical flow transducer is small enough to be inserted into the C.S.F. pathways through an 18 gauge spinal needle whilst allowing the simultaneous measurement of pressure through the same needle.

Chapters 3,4,5 and 6 present the theory of the transducer and the experiments performed to confirm the main functional variations. Chapter 7 describes the animal experiments performed to confirm the in-vivo functioning of the transducer and Chapter 8 describes the initial clinical trials.

The C.S.F. is the clear fluid that bathes the human central nervous system and is a dilute solution of salts, mainly sodium

chloride, and protein. The C.S.F. is in a state of constant movement, partly because of its continual production and absorption, but mainly because it is subject to pulsatile forces transmitted to it through the blood vessels which occupy the same region of the body.

At present only the pressure of the C.S.F. is routinely measured. Amongst the most sophisticated of these investigations is the simultaneous measurement, at two points, of the C.S.F. pressure in response to various stimuli (for example, a cough) which are expected to cause a pressure change and flow of C.S.F. (Lakke, 1969; Gilland, 1966; Williams, 1981a).

The only flow information available is limited to estimates of the volume of C.S.F. displaced during an event (Gilland, 1966), derived directly from pressure measurements; or to estimates of flow obtained by radiographic observation of an injected contrast medium (Du Boulay et al, 1972; Gilland et al, 1969).

Some diseases of the human central nervous system have an effect on, or are affected by, the C.S.F. and its flow through its pathways. Perhaps the most well known condition affecting the C.S.F. pathways is hydrocephalus, which involves a blockage of the pathways downstream of the site of production, so damming back the C.S.F. The C.S.F. continues to be produced and the pathways dilate applying pressure to the brain.

In some people severe disability is caused by the presence of a blockage, partial or complete, in the spinal subarachnoid space. This may be the result of a slipped disc, blood clot or lesion of some kind.

Syringomyelia (Barnett et al, 1973) is a condition in which there are fluid-containing cavities present within the spinal cord. These

cavities gradually destroy the cord from within. Syringobulbia is a similar condition in which the cavities extend into the hind brain. Infrequently, the fluid may have been exuded from a tumour within the cord. However, in most cases (Williams, 1973) the fluid is C.S.F. Barnett et al (1973) report that Williams has coined the term "communicating" syringomyelia to indicate his belief that the syrinx (cavity) communicates with the C.S.F. pathways.

There appear to be two main theories of the origin and progression of communicating syringomyelia, both of which cite the pulsation of the C.S.F. as being responsible for the progressive destructive enlargement of the cavity (Barnett et al, 1973). The theories differ mainly in that the first assumes the source of the destructive energy to be the cardiac derived pressure pulse (section 1.3.2) in the C.S.F. and therefore continuous; whilst the second assumes it is pressure pulses in the C.S.F. derived from the venous system (section 1.3.3) and therefore intermittent. Another condition in which pulsatile flow of the C.S.F. might play a part is in the filling of certain types of arachnoid cysts or pouches. The same disagreement about whether the filling force is arterial or venous in origin exists. Williams and Guthkelch (1974) believe it to be venous and O'Connell (1970) and Du Boulay (1966) arterial.

These conditions, and any others affecting the C.S.F. pathways, can be expected to alter to some extent both the flow of C.S.F. and the propagation of pressure pulses within the pathways. A greater knowledge of the dynamics of the C.S.F. might aid in the understanding of the origins and progressions (and possibly diagnosis) of some conditions affecting the C.S.F. pathways. Also, C.S.F. is in a continual state of movement, and since it bathes some of the most

important structures in the body knowledge of its flow could be of considerable importance.

### 1.2 The C.S.F. and the C.S.F. Pathways

The C.S.F. is mainly water. Bell et al (1980) state it has a pH of 7.33, specific gravity of 1.005 and contains not more than 5 lymphocytes per  $\text{mm}^3$ . In composition it is very similar to plasma, the major difference being it contains approximately 200 times less protein. Table 7.5.1 gives a comparison of the constituents of the two fluids.

The central nervous system is covered by three membranes, or meninges. The outer one is the dura mater which is tough and fibrous. The dura adheres to the walls of the cranium (Davson, 1967) but in the spine it is separated from the vertebral canal by an epidural layer of fat. Under the dura are the two further membranes, the leptomeninges. The innermost is the pia mater which closely follows the surface of the brain dipping into all fissures and apertures. The middle membrane, the arachnoid mater, is very thin and is separated from the dura by the subdural space. This is very narrow and contains a little tissue fluid. The arachnoid is separated from the pia by the subarachnoid space which contains C.S.F. No communication exists between the subdural and subarachnoid spaces. Unlike the epidural space, the subarachnoid space varies considerably in width, being widest at the base of the brain forming the spaces known as the cisterns, of which the largest is the cisterna magna. The subarachnoid space communicates directly with the ventricles of the brain through apertures in the roof of the fourth ventricle. The C.S.F. pathways thus consist of the subarachnoid space and the ventricles

(Davson, 1967). Figures 1.2.1 and 1.2.2 are schematic illustrations of the C.S.F. pathways.

In addition to C.S.F. the subarachnoid space also contains many strands of arachnoid tissue connecting the arachnoid and pia, and blood vessels and nerves passing through it (Figure 1.2.3). These blood vessels are covered with two layers of arachnoid. Branches of the vessels penetrating the brain, and also the cranial and spinal nerve roots, are accompanied by extensions of the subarachnoid space so that to some extent the C.S.F. penetrates the substance of the central nervous system.

The C.S.F. is continuously produced (Lakke, 1969; Eversden, 1973) as a secretion in the choroid plexuses (rich networks of arteries projecting into the ventricles). As the C.S.F. is continuously produced and yet its volume is relatively constant it must be re-absorbed at a rate equal to its formation. Absorption is thought to take place at the arachnoid villi (Eversden, 1973; O'Connell, 1970; Davson, 1967) which are invaginations of the subarachnoid space which contain valve like structures.

The volume of C.S.F. increases with growth and represents about one tenth of the intradural contents by volume. O'Connell (1970) reports the average volume in adults to be  $135 \text{ cm}^3$ ,  $35 \text{ cm}^3$  in the ventricles and the remainder in the subarachnoid space, of which  $25 \text{ cm}^3$  is in the skull and  $75 \text{ cm}^3$  in the spinal canal. The rate of absorption (and therefore formation) is equivalent to  $500 \text{ cm}^3$  every 24 hours (Davson, 1967). The skull represents an essentially rigid container and its contents, the brain matter, blood and C.S.F. are incompressible. Therefore an increase in the volume of one of the contents can only occur at the expense of another. This is the

(Davson, 1967). Figures 1.2.1 and 1.2.2 are schematic illustrations of the C.S.F. pathways.

In addition to C.S.F. the subarachnoid space also contains many strands of arachnoid tissue connecting the arachnoid and pia, and blood vessels and nerves passing through it (Figure 1.2.3). These blood vessels are covered with two layers of arachnoid. Branches of the vessels penetrating the brain, and also the cranial and spinal nerve roots, are accompanied by extensions of the subarachnoid space so that to some extent the C.S.F. penetrates the substance of the central nervous system.

The C.S.F. is continuously produced (Lakke, 1969; Eversden, 1973) as a secretion in the choroid plexuses (rich networks of arteries projecting into the ventricles). As the C.S.F. is continuously produced and yet its volume is relatively constant it must be reabsorbed at a rate equal to its formation. Absorption is thought to take place at the arachnoid villi (Eversden, 1973; O'Connell, 1970; Davson, 1967) which are invaginations of the subarachnoid space which contain valve like structures.

The volume of C.S.F. increases with growth and represents about one tenth of the intradural contents by volume. O'Connell (1970) reports the average volume in adults to be  $135 \text{ cm}^3$ ,  $35 \text{ cm}^3$  in the ventricles and the remainder in the subarachnoid space, of which  $25 \text{ cm}^3$  is in the skull and  $75 \text{ cm}^3$  in the spinal canal. The rate of absorption (and therefore formation) is equivalent to  $500 \text{ cm}^3$  every 24 hours (Davson, 1967). The skull represents an essentially rigid container and its contents, the brain matter, blood and C.S.F. are incompressible. Therefore an increase in the volume of one of the contents can only occur at the expense of another. This is the

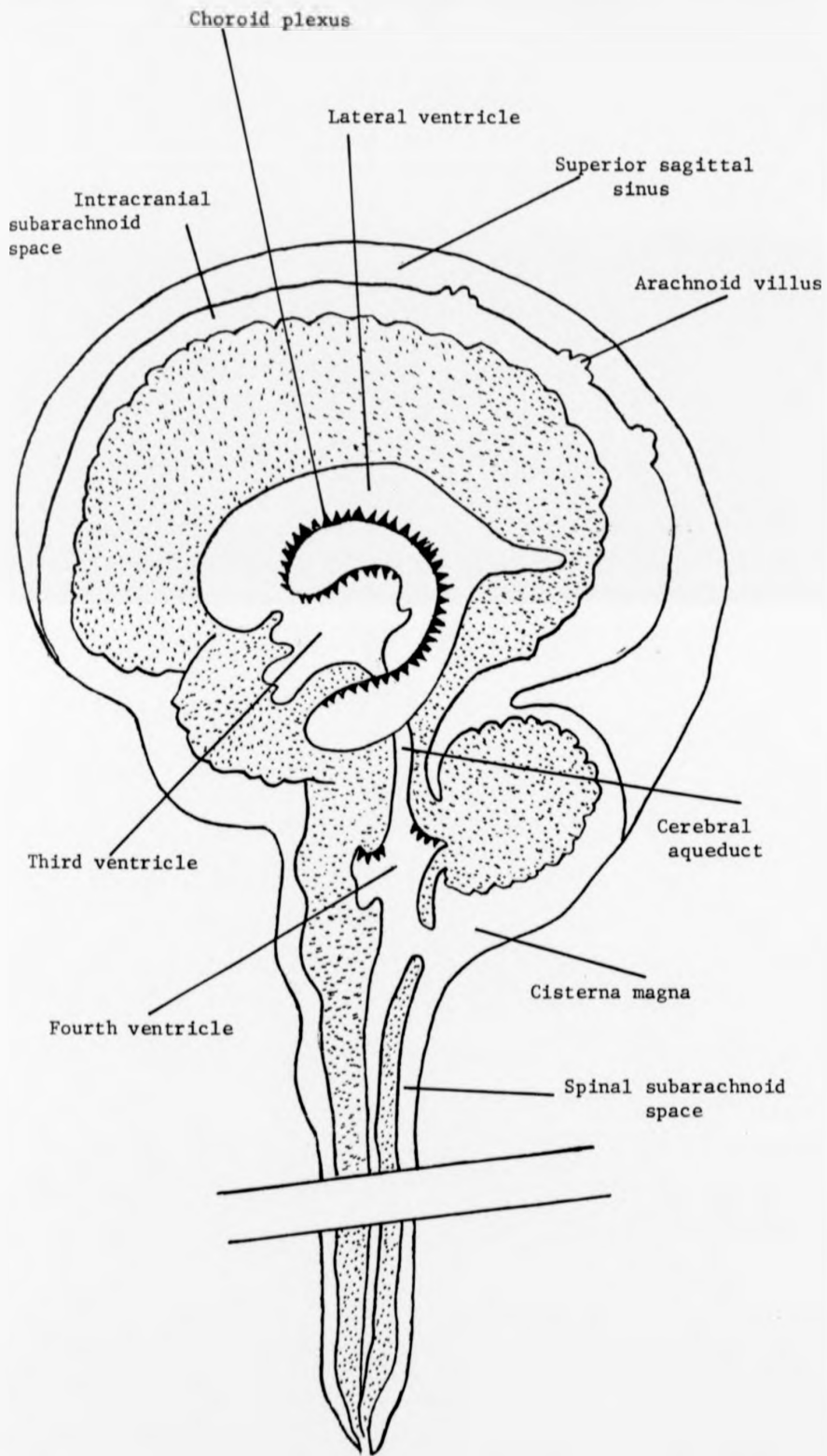


Figure 1.2.1 Schematic illustration of the CSF pathways - lateral view.

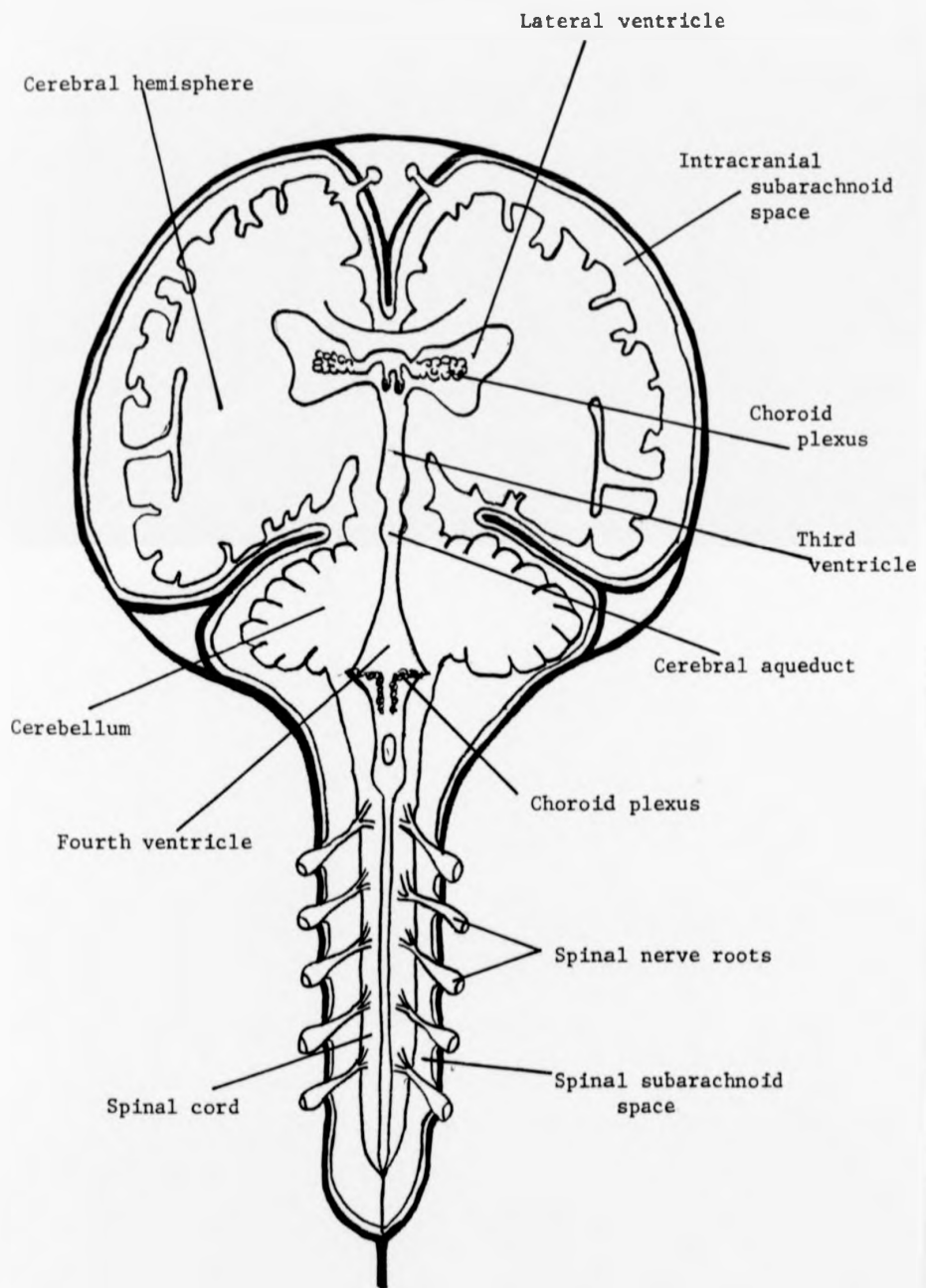


Figure 1.2.2 Schematic illustration of the CSF pathways - posterior view

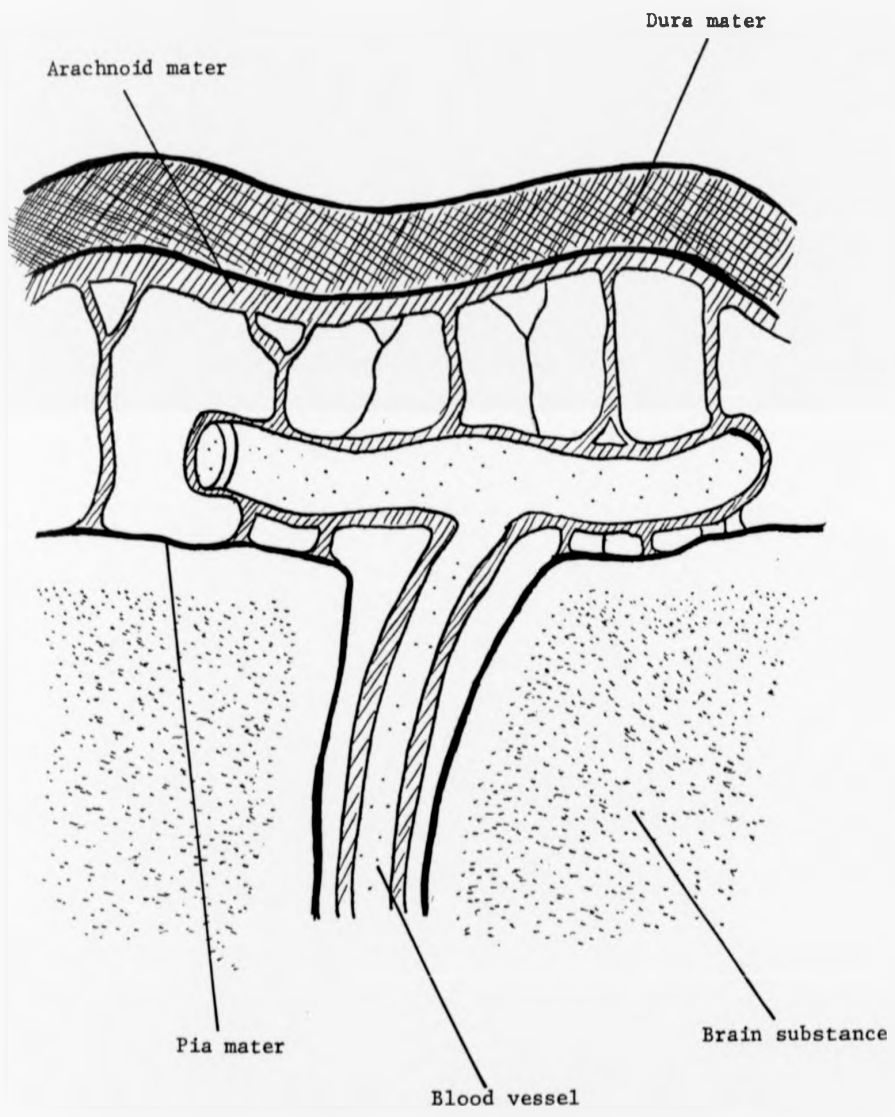


Figure 1.2.3 Schematic illustration of the contents of the (intracranial) CSF pathways.

Monro-Kellie doctrine (Lakke, 1969; Eversden, 1973).

After its production in the choroid plexuses the C.S.F. moves via various channels in the brain into the subarachnoid space. The C.S.F. does not circulate in the sense that blood does. Rather it tends to drift between sites of production and absorption aided by the pressure of production and by the pulsatile forces discussed below.

### 1.3 The C.S.F. Pressure

#### 1.3.1 General considerations

The mean pressure of the C.S.F. is particularly dependent upon the venous pressure, and is typically 10mm of Hg above resting venous pressure (Lockey et al, 1975). Venous pressure is a function of both posture and muscle activity. In the normal adult, with the body in the horizontal lateral position, O'Connell (1970) reports the mean pressure at lumbar puncture is 150mm of saline, values between 60 and 180mm being considered normal.

The importance of venous pressure in determining mean C.S.F. pressure is illustrated by the following example. O'Connell (1953, 1970) reports that the difference in lumbar and cisternal pressures with the patient sitting is equal to the height of the fluid column separating them, the pressures being similar with the patient horizontal. However, the increase in lumbar pressure from the horizontal to the sitting position is only 40% of that expected because the point at which venous pressure is equal to atmospheric pressure is posture dependent.

The blood vessels in, and close to the C.S.F. pathways also impart impulsive forces to the C.S.F. which in general, as the pathways

possess elasticity, can be expected to cause a flow of C.S.F. The blood vessels transmit pressure by an expansion of their walls (Davson, 1967), and in arteries possibly also by movement of the vessel (Williams and Guthkelch, 1974). Unlike arteries, where an increase in vessel diameter caused by an increase in pressure is resisted by the elastic tension of the walls, the veins distend and collapse easily. Veins, therefore, transmit pressure pulses to the C.S.F. more efficiently than do arteries.

The C.S.F. pathways possess compliance and elasticity so flow of C.S.F. can occur. Differing opinions are held as to which structures give rise to this compliance and elasticity. Du Boulay (1966) and Du Boulay et al (1972) are of the opinion that most of the elasticity of the C.S.F. pathways is due to the veins and imply the dura possesses little, if any, elasticity, merely being compliant. However, Tunturi (1977) has demonstrated that the dura of dog is elastic and this is likely to be true in humans. It is likely that both the dura and the venous system adjacent to the C.S.F. pathways contribute to the elastic and compliant properties of the C.S.F. pathways.

The amplitude of C.S.F. movements within the head is generally smaller than in the spinal canal. This is consistent with the intracranial pathways having a larger capacitance (or compliance). Williams (1974, 1976) reports the capacitance of the C.S.F. pathways at the top of the spine is always likely to be great, unless the foramen magnum is blocked or there is an intracranial space occupying lesion, since the head contains a large number of compressible veins.

Du Boulay (1966) and Du Boulay et al (1972) report the elasticity of the head as being partly due to the ventricular system at the expense of the subarachnoid space, and chiefly due to the large veins.

Both Williams and Du Boulay emphasise the importance of the degree of filling of the venous system and the venous pressure in influencing the capacitance and elasticity of the pathways, thus having an important effect on the transfer of pressure pulses to the C.S.F. and their propagation along the C.S.F. pathways. When empty the veins have little capacitance. The degree of filling of the veins and their pressure is posture dependent, so the propagation and transmission of pressure pulses can be expected to be influenced by posture.

#### 1.3.2 Rhythmical variations in C.S.F. pressure

These are the variations in C.S.F. pressure caused by the cardiac and respiratory activity of the body. Arterial blood enters the head in a pulsatile manner (Eversden, 1973) and in spite of the muscular walls of the arteries causes an expansion of the arterial bed at systole and a corresponding collapse at diastole.

O'Connell (1970) found the average peak to peak variation due to the cardiac pulse to be 45mm of C.S.F. and that due to respiration 35mm of C.S.F., which when they add is a total variation of 80mm. These measurements were made in patients with raised intracranial pressure and it is known that factors which raise the mean pressure also affect the magnitude of pulsation. Nonetheless, these figures are illustrative of the typical variations. The rhythmic pressure variations have been shown, using radiographic techniques (Du Boulay et al, 1972), to cause a rhythmic to and fro flow of C.S.F.

Several sites have been proposed as the primary origin of the cardiac derived pressure pulse. Bering (1955) suggested the main

source was systolic expansion of the choroid plexuses whilst Laitinen (1968) favoured the basal arteries. Dereymaeker et al (1971) report the pressure waveform as having venous characteristics at high arterial pressure and arterial characteristics at normal and low arterial pressure. Du Boulay (1966) and Du Boulay et al (1972) conclude that cardiac pulsatile movements of the C.S.F. are due to an arterial pump in the head and to a venous pump in the spinal canal, the former being by far the stronger. They cite the pulsatile flow into the arteries of the cerebrum as chiefly responsible, the choroid plexuses and the basal arteries contributing little.

It is generally accepted that the major contributions to the respiratory fluctuations in C.S.F. pressure are mediated by the venous system, reflecting changes in intrathoracic and abdominal pressures. Eversden (1973) reports they are due to changes of impedance of venous outflow from the head in inspiratory and expiratory phases. Gardner (1945) and O'Connell (1953) report that usually the C.S.F. pressure falls on inspiration and rises on expiration. However, it appears that in general the effects are dependent upon both posture and the type of respiration (Du Boulay et al, 1972).

### 1.3.3 Intermittent variations in C.S.F. pressure

These are all the variations in C.S.F. pressure other than the rhythmic cardiac and respiratory pulses. Generally these variations are mediated almost entirely by the venous system and are of considerably greater magnitude than either of the rhythmic variations.

Between the dura and the vertebrae is the epidural space. The epidural space contains, on the surface of the dura, a little fat and a plexus of epidural veins lying mainly on the front side of the dura

in the form of two vertical channels (Lockey et al, 1975). These channels are cross linked and supplied with anastomoses (valveless connecting vessels) to the veins from the bones of the spines, veins within surrounding muscles, and to the veins of the abdominal and thoracic cavities via the perivertebral plexus. The anastomatic veins occur at each segmental level and all but the topmost seven vertebrae (the cervical vertebrae) are intimately connected to the abdominal and thoracic cavities. The extensive connections which exist between the epidural venous plexus and the venous system outside the vertebrae suggest that blood can freely flow in and out of the spinal canal (Lakke, 1969).

If for any reason the pressure in either the thoracic or abdominal cavities increases, then the veins in these cavities are subjected to higher pressure causing blood to move into the epidural veins, thus transmitting most of the pressure increase. Du Boulay et al (1972) report that during a cough the spinal canal is considerably compressed by the tissues around it, and state that only the epidural veins are capable of such an action. The rise in pressure is transmitted across the walls of the veins, the dura and the arachnoid, into the C.S.F. The increased pressure in the spinal subarachnoid space causes C.S.F. to flow from the spinal canal into the head, this C.S.F. returning to the spinal C.S.F. pathways when the pressure is released (in the normal case). If it were not for the elastic, or pliable, properties of the dura surrounding the spinal C.S.F. pathways, there would be no flow out of, or into, the spinal canal to or from the skull (Lakke, 1969). For there to be a flow there must be a change in the volume of the dural sac and this is easily compensated for by the enormous, valveless epidural venous plexus.

The other veins within the skull and spinal canal play a much smaller, if any, part in the transmission of pressure from the venous system to the C.S.F. Compared to the epidural veins, the veins within the subarachnoid space are few and small (Lakke, 1969). The epidural system within the skull is in a very different situation to that in the spinal canal. The intracranial venous dural sinuses are encased within rigid meninges and thus cannot transmit pressure changes.

Williams (1976, 1977) reports that in coughs lasting 0.6 to 0.9s the lumbar pressure rises by between 19 and 97mm of Hg, a moderate cough producing typically 50mm of Hg rise, whilst most patients can comfortably cause a rise of over 100mm of Hg. In the normal case the rise in cisternal pressure is about 70% of that at the lumbar region and occurs about 0.04s later. Williams is careful to stress that this delay does not necessarily imply that the pressure pulse starts at, or below, the lumbar region and propagates upwards.

If the veins in the neck which drain blood from the head are compressed as in Queckenstedt's test (Davson, 1967) the pressure in the skull is increased causing a flow of C.S.F. from the head into the spinal canal, which returns on release. Gilland (1966) and Lakke (1969) report the rise in cisternal pressure during Queckenstedt's test to be typically of the order of 400mm of H<sub>2</sub>O.

Pressures transmitted to the C.S.F from the venous system, other than the respiratory fluctuation, are considerably greater than the arterially transmitted cardiac pulse. Consequently venous derived pressure pulses can be expected to impart far more energy to the C.S.F. than the cardiac derived pulse. The C.S.F. is in a state of continual movement as a result of the heart beat and pressure changes in the abdominal and thoracic cavities, the latter being caused by practically any activity or movement.

CHAPTER 2

## CHAPTER 2

### INVESTIGATIONS OF C.S.F. DYNAMICS

#### 2.1 Introduction

This chapter includes a resumé of the various techniques and measurements used in the investigation of C.S.F. dynamics. Techniques of pressure measurement are well developed and are of proven value but are limited by the absence of a method of obtaining simultaneous flow information.

Two methods have been used to estimate C.S.F. flow caused by a pressure pulse in the C.S.F. pathways. One of these techniques (section 2.3.1) infers volume flow from pressure measurements. Many instances of this technique reported are concerned with secretion and absorption rates of C.S.F., rather than its flow during a pressure pulse even though the word "hydrodynamic" is often included in the title (for example, Guinane, 1972; Ekstedt, 1977; Ekstedt, 1978).

Also discussed in this chapter are the requirements a C.S.F. flow transducer should satisfy, and the choice of flow transducer.

#### 2.2 Pressure Investigations

A sample of C.S.F. can be obtained by inserting a needle into the lumbar or cisternal pathways as shown in figures 2.2.1 and 2.2.2. To measure the pressure a pressure transducer need only be connected to needles entering the C.S.F. pathways at these sites, which in adults are about 50cm apart. Of these two sites for

## CHAPTER 2

### INVESTIGATIONS OF C.S.F. DYNAMICS

#### 2.1 Introduction

This chapter includes a resumé of the various techniques and measurements used in the investigation of C.S.F. dynamics. Techniques of pressure measurement are well developed and are of proven value but are limited by the absence of a method of obtaining simultaneous flow information.

Two methods have been used to estimate C.S.F. flow caused by a pressure pulse in the C.S.F. pathways. One of these techniques (section 2.3.1) infers volume flow from pressure measurements. Many instances of this technique reported are concerned with secretion and absorption rates of C.S.F., rather than its flow during a pressure pulse even though the word "hydrodynamic" is often included in the title (for example, Guinane, 1972; Ekstedt, 1977; Ekstedt, 1978).

Also discussed in this chapter are the requirements a C.S.F. flow transducer should satisfy, and the choice of flow transducer.

#### 2.2 Pressure Investigations

A sample of C.S.F. can be obtained by inserting a needle into the lumbar or cisternal pathways as shown in figures 2.2.1 and 2.2.2. To measure the pressure a pressure transducer need only be connected to needles entering the C.S.F. pathways at these sites, which in adults are about 50cm apart. Of these two sites for

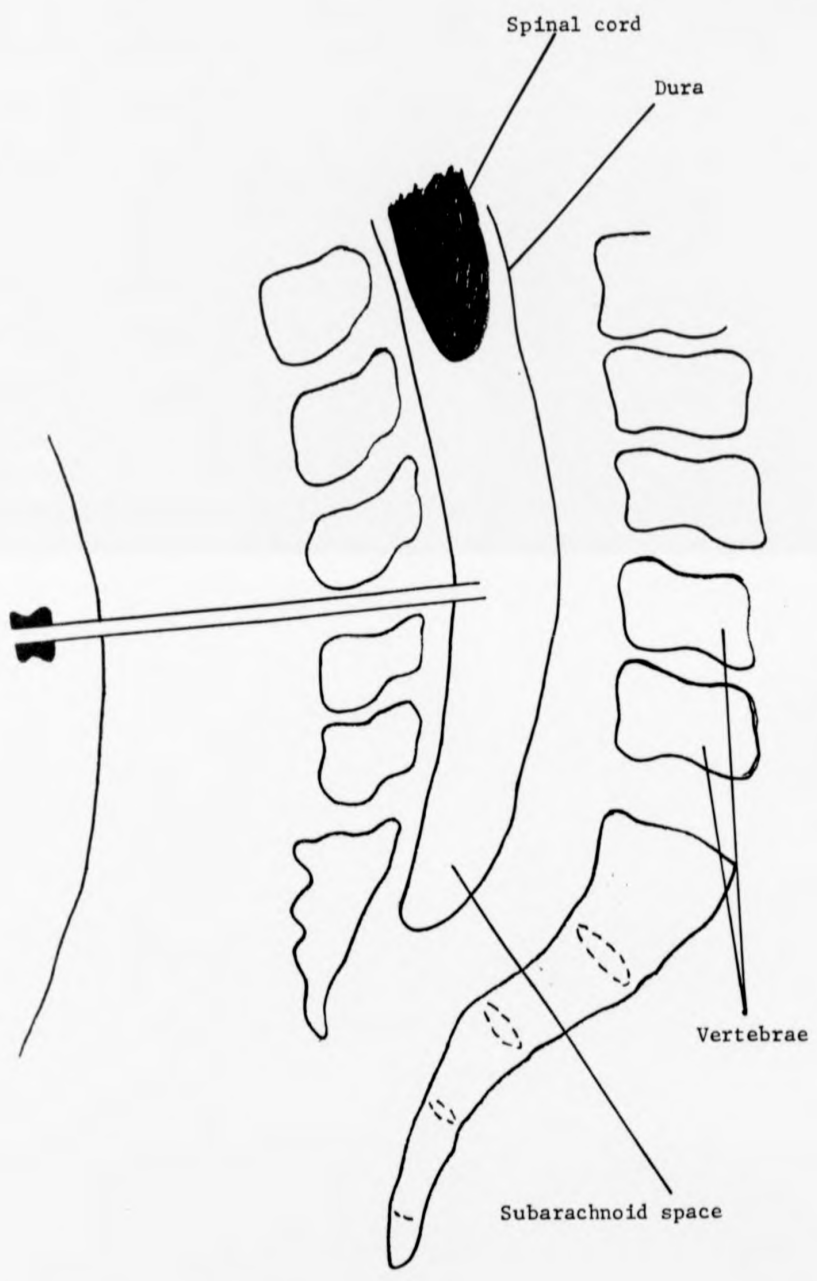


Figure 2.2.1 Illustration of lumbar puncture.

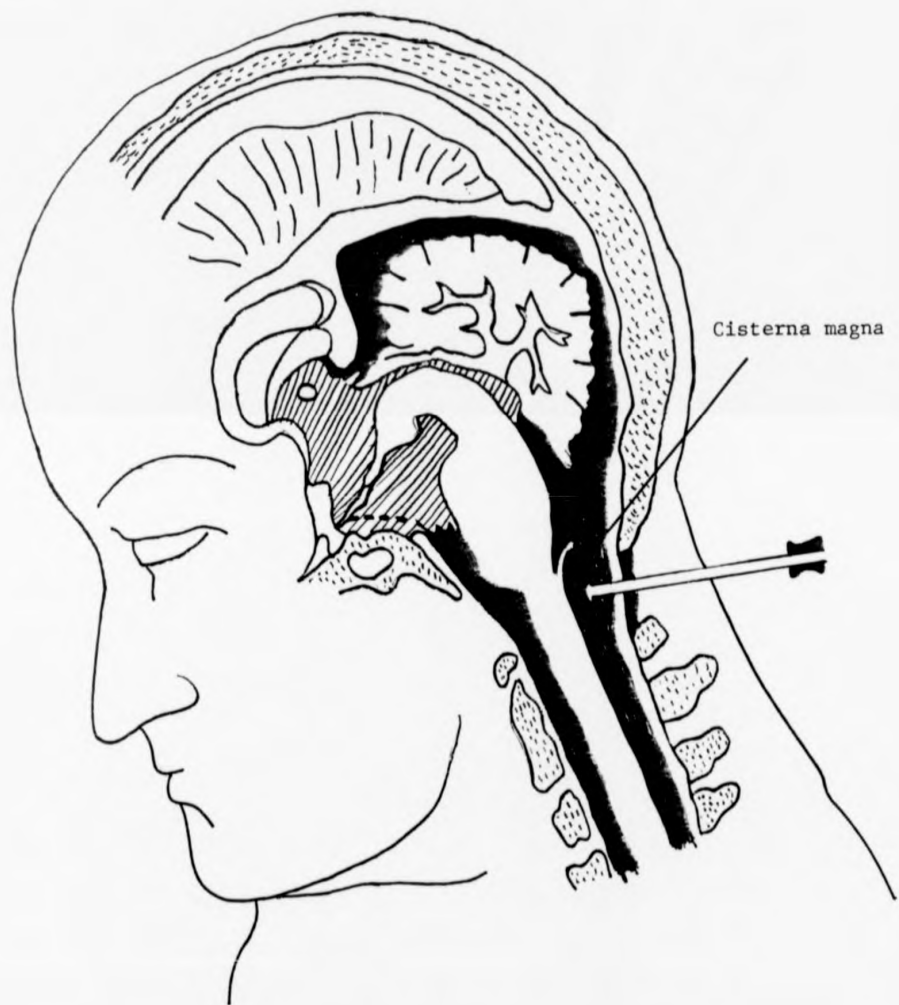


Figure 2.2.2 Illustration of cisternal puncture.

puncture the lumbar is the safest as the spinal cord ends above this point in the spinal canal. A third point of entry is often preferred to cisternal puncture. That is to insert a needle into the ventricles through a hole drilled in the forehead. The sub-arachnoid space in the lumbar region, even though the cord does not reach this far, still contains very many nerves, blood vessels and connective tissue and compared to the cisterna magna is very cluttered. Du Boulay et al (1972) suggest as much as three quarters of the lower spinal subarachnoid space is occupied by nerve roots.

The pressure waves in the C.S.F. usually studied in the investigation of the C.S.F. pathways are those derived from the venous system (Gilland, 1966; Lakke, 1969; Williams, 1980; 1981b; 1981c; 1981d), since they are of greater magnitude than those from the arterial system. The arterial pulse is, however, studied (for example, Chopp, 1980; Spertell, 1981), often in the investigation of raised intracranial pressure. The response of the C.S.F. pathways to the rapid injection or withdrawal of a small volume of C.S.F. is also investigated (Shapiro, 1980), to obtain information about the compliance of the C.S.F. pathways especially in cases of raised intracranial pressure.

The stimuli used to cause a venous derived pressure wave in the C.S.F. are Queckenstedt's test, a cough or series of coughs and Valsalva's manoeuvre. Queckenstedt's test (Gilland, 1966; Lakke, 1969) involves compressing the veins in the neck which drain blood from the head, usually with the fingers, so damming back the blood in the skull and raising the intracranial pressure. Normally this increase in pressure will be transmitted to the spinal canal with a flow of C.S.F. in that direction. Gilland et al (1969) report that in the normal case the lumbar pressure reaches a

plateau value within 0.5s, the fall on release being equally fast.

Unlike Queckenstedt's test a cough causes a flow of C.S.F. towards the head, which returns when the cough is over. Lockey et al (1975) state a normal cough may last 0.9s and produce a pressure in the abdomen, which is efficiently transmitted to the C.S.F. (section 1.3.3) of typically 75mm of Hg.

The pressure pulse produced by a cough is of greater amplitude than that caused by Queckenstedt's test, and faster in rise and fall. In either test any obstruction will interfere with the propagation of the pressure pulse and the associated flow of C.S.F. A complete blockage of the C.S.F. pathways would be expected to totally halt the propagation of the pressure, whilst a partial obstruction decreases the rise and fall of pressure at any measuring site beyond the obstruction.

The Valsalva manoeuvre (Lakke, 1969) has similar effects to the cough. It involves forced expiration through an open glottis and a closed mouth and nostrils. The same effect occurs when blowing against an obstruction and the pressure rise can be kept constant if a measure of the pressure can be seen by the patient.

## 2.3 Flow Investigations

### 2.3.1 Flow information derived from pressure measurements

Lakke (1969) reports that A.Verjaal estimated the volume of C.S.F. displaced from the head during Queckenstedt's test to be 20 to 40cm<sup>3</sup>. This was done by withdrawing measured amounts of C.S.F. and recording the mean pressure and the pressure reached on jugular compression, after each withdrawal. When the pressure on jugular compression equalled the original mean pressure it was reasoned that the volume withdrawn was equal to that of the extra blood dammed back, and therefore of the C.S.F. displaced from the head.

Gilland (1966), in three patients with complete spinal block injected up to  $9\text{cm}^3$  of fluid into the lumbar region, whilst recording the pressure. This fluid, and more, was then removed, the pressure falling below its initial value. The pressure was found to vary exponentially with the volume of fluid added or removed. Using these pressure-volume data, Gilland assumed the volume of fluid entering the lumbar dural sac, in the normal case, during jugular compression to be that volume in the data necessary to produce the pressure observed. The volume entering the lumbar region was estimated to be 2 to  $7\text{cm}^3$ .

### 2.3.2 Flow information from radiographic procedures

Movements of radiographic contrast media in response to pressure pulses in the C.S.F. pathways have been reported by many authors. These include Reitan (1941), Lakke (1969), Gilland et al (1969), Du Boulay (1966) and Du Boulay et al (1972).

Lakke observed the movements of a cisternally injected contrast medium during jugular compression, when a prominent downward movement was seen, the reverse occurring on release.

Du Boulay (1966) observed the movements of contrast media in response to the arterial pulse. Pulsatile movement of the same frequency as the arterial pulse was found in the spinal canal, the movement being considerable in the cervical canal diminishing towards the lumbar canal. In the lower lumbar canal it was only rarely observable. No movement was found distal of a complete block. When the spinal subarachnoid space was narrowed, but not completely blocked, the amplitude of the cardiac induced movement was greatly increased, in one case being more than 2.5cm to and fro. In most patients there

was a great difference in amplitude of movement above and below the foramen magnum. Slightly above the movement was so small as to be easily missed, while that below was of considerable amplitude.

Gilland et al studied the movement of a contrast medium during jugular compression. Movement was found to be greatest in the cervical canal, almost as great in the thoracic canal but far less in the lumbar canal where the main movement was expansion of the dural sac.

Du Boulay et al studied the movement of contrast media in response to coughs in 12 patients with no obstruction of the spinal canal. The coughs usually consisted of a short, sharp inspiration, followed by explosive expiration against the partly closed glottis. With the patient semi-erect the upper level of the contrast medium dropped sharply on inspiration followed at the cough by an upwards movement of usually about 1cm, but sometimes as much as two vertebral bodies. The upwards movement was accompanied by a lateral narrowing of the lower dural sac of about 50%.

In the cervical canal with the patient prone, or with head down, a cough propelled the contrast medium towards, and sometimes into, the head. A Valsalva manoeuvre compressed the lower dural sac propelling the contrast medium towards the head, whilst cardiac pulsations caused a downward movement at systole.

Table 2.3 summarises the flow information from the pressure and radiographic studies.

#### 2.4 Requirements for and Choice of Flow Transducer

The clinical aspects of this work (Chapter 8) were performed

Table 2.3.1 Collected Flow Information

Source	Event	Patient	Contrast medium	Observations
Verjaal (Lakke 1969)	JC	Lateral recumbent	pressure derived	20 to 40 mls displaced from head
Gilland (1966)	JC	Lateral recumbent	pressure derived	Prominent downwards movement on compression. Reverse on release
Du Boulay et al (1972)	C	Semi-erect	lower lumbar	Upward movement typically 1cm with narrowing of spinal sac of order of 50%. Est 2-9 ml CSF displaced.
	C	Horizontal or head down	cervical	Movement towards head, some into head. Typical distance moved upto 4 cervical vertebrae. Est 4-8 ml CSF into head.
	V	Various	lumbar	CSF towards head
	A	Various	spinal canal	Movement usually away from head (at systole) - opposite in some abnormal cases.
	A	Sitting	head	Typically 1 ml displaced from basal cisterns towards spinal canal. Order of 0.1 ml displaced from 3rd ventricle.
Gilland et al (1969)	JC	Horizontal prone	cervical canal	Average time from onset to Vmax 1/15 s. Vmax 11-43 cm/s. Average velocity 5-15 cm/s. Max distance moved 3-10 cm.
	JC	Horizontal prone	thoracic canal	Average time from onset to Vmax 1/15 s. Vmax 9-23 cm/s. Average velocity 8-13 cm/s. Max distance moved 1.5-5 cm/s.
	JC	Horizontal prone	lumbar canal	Slow downward movement in upper lumbar canal. Mainly lateral distention in lower lumbar canal with 28 to 50% increase in lateral diameter.

JC=jugular compression; A=arterial pulse; C=cough; V=Valsalva manoeuvre

at the Midland Centre for Neurology and Neurosurgery, Smethwick, West Midlands in conjunction with Mr. B.N. Williams, Consultant Neurosurgeon. Mr. Williams regularly performs pressure measurements of the C.S.F. pathways in response to the various stimuli detailed earlier. He gains access to the C.S.F. pathways through 18 gauge spinal needles. The techniques used are described in Chapter 8 and in numerous publications by Williams (for example, Williams, 1981a).

It was intended to perform the flow measurements simultaneously with the pressure measurements. The pressure measurements are of proven value, whilst any flow measurements, at least initially, would be experimental in nature. Therefore, a major requirement of any flow transducer used was that it did not interfere with the pressure measurements to an unacceptable extent, and that the flow measurements be as small an extension of the clinical procedure as possible. The other requirements of a suitable C.S.F. flow transducer can be itemised as follows. The transducer should :

- i) be safe
- ii) be accurate; it should not significantly perturb the flow being measured
- iii) preferably measure instantaneous volume flow
- iv) preferably be non-invasive
- v) if invasive it must be capable of entering the C.S.F. pathways through an 18 gauge spinal needle whilst still allowing the simultaneous measurement of pressure through the same needle
- vi) be capable of measuring the small (cf. blood) flow rates expected
- vii) be able to respond to pulsatile flow

The obvious starting point is to consider blood flow meters (Woodcock, 1976; Roberts, 1972). Requirements i and ii are common to all clinical flow meters. It was believed requirement iii could not be met. Instruments which measure volume flow require access to both sides of the vessel, for example, cuff type electromagnetic (EM) flowmeters (Webster, 1978) or implantation in the vessel as in cannulating EM flowmeters and rotameters. Neither of these were possibilities. It was also thought unlikely that any transducer small enough to enter the pathways through an 18 gauge needle would provide volume flow information.

The only flow transducer capable of meeting requirement iv was considered to be a Doppler ultrasound flow meter. This technique is unsuitable as C.S.F. contains very few scattering centres, and also because the bone surrounding the C.S.F. pathways and the many structures in the pathways would probably give rise to many spurious signals (Jenkins and White, 1972). Nuclear magnetic resonance flowmeters were considered totally unsuitable at their current state of development (Battocletti et al, 1975).

The flow transducer must therefore be invasive. Requirement v essentially states that the transducer must have a very small diameter. EM flowmeters are of three basic types; cuff, cannulating and catheterised. Only the catheterised type could possibly be of use here. They primarily measure flow velocity at a point (Bevir, 1971) but are still influenced by flow some distance away and are sensitive to the attitude of the flow. Catheterised EM flow meters were considered unsuitable, however, mainly because it was thought unlikely that one of small enough diameter could be constructed.

Bristle flowmeters (Woodcock, 1976) were rejected because of their insensitivity to low flows and the difficulty in making the bristle sufficiently small and rigid to operate along the length of a spinal needle whilst retaining sensitivity. Methods employing the Pitot principle are reported by Jackson and Williams (1979) to be inapplicable where, as here, the pressure wave propagates slowly. An inseparable admixture of the changing difference in pressure between the two pressure ports caused by the pressure wave and the flow caused pressure difference is obtained.

The blood flow measurement technique which came closest to meeting the requirements is that of resistance thermometry (Woodcock, 1976), principally because of the potentially very small size of such a device. These devices are of two types, the thin film and the thermistor, of which the thin film is considered superior (Woodcock, 1976). Both types measure flow velocity, not volume flow.

The thin film probe, as described for example by Bellhouse and Bellhouse (1968), Bellhouse et al (1969), Seed and Wood (1970a) and Clark (1974) has been used in measuring blood flow (Ling, 1968; Seed and Wood, 1970b; Bellhouse et al, 1972; and Seed, 1972). The probes are held at a constant temperature, usually 1 to 5°C above blood temperature, the power required to maintain this temperature being a measure of the blood flow.

Thin film probes are sensitive to their exact attitude to the flow (Clark, 1974). Also, Seed and Wood (1970a) report that errors at low flows ( $10\text{cm}\cdot\text{s}^{-1}$  and below) become large, particularly when the direction of flow rapidly reverses, as would be expected in the C.S.F. pathways during a cough, for example. These devices work

by transferring heat to the fluid. As C.S.F. does not circulate in the sense that blood does, but is contained in the essentially closed C.S.F. pathways, it was thought likely that a thin film device might give rise to convection currents of magnitude comparable to the flow to be measured. The thin film probe was rejected because of the above considerations.

## 2.5 Conclusions

The technique of deriving volume flow information from pressure studies (section 2.3.1) was rejected because of the gross perturbation of the system under investigation that it occasions, and also because the technique does not allow the simultaneous measurement of flow and pressure.

Radiographic contrast studies, when used to provide flow information (section 2.3.2), also perturb the flow being measured. If the contrast medium used is denser than C.S.F. it tends to sink, and vice versa. If a contrast medium miscible with C.S.F. is used then it quickly forms a diffuse front with the C.S.F. In all cases the presence of the contrast medium perturbs the fluid movement because of differences in viscosity and density. Further this technique is inconvenient and prone to errors, for example the volume occupied by the contents of the C.S.F. pathways has to be estimated to allow the estimation of volume flow of C.S.F.

The search for a suitable C.S.F. flow transducer amongst those used to measure blood flow was unsuccessful largely because of the differences between C.S.F. and the C.S.F. pathways, and blood and blood vessels. The C.S.F. contains very few scattering centres and does not circulate. Further, the C.S.F. pathways are enclosed by

bone, access is very limited and the pathways contain blood vessels, nerves and connective tissue in addition to the C.S.F.

As no suitable C.S.F. flow transducer was found it was considered worthwhile to develop the electrochemical flow transducer. The active part of this device is the cathode, at which oxygen is reduced to hydroxyl ions, the current flowing being a measure of the flow velocity adjacent to the cathode. That is, the electrochemical flow transducer measures flow velocity, not volume flow. The flow transducer, as developed, is small enough to enter the C.S.F. pathways through an 18 gauge spinal needle and allow the simultaneous measurement of pressure through the same needle.

The theory of the electrochemical flow transducer, the experiments performed to confirm the theory, and the development of the transducer used clinically are presented in Chapters 3 to 7.

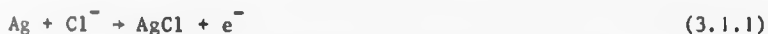
CHAPTER 3

## CHAPTER 3

THE STEADY-STATE RESPONSE OF THE OUTPUT CURRENT3.1 Introduction

The operation of the electrochemical flow transducer relies upon the presence of oxygen, physically dissolved in an electrolyte such as saline or CSF. If a cathode is immersed in the electrolyte and its potential is set correctly, and held, against a supporting anode, a current passes which is proportional to the square root of the velocity of flow past the cathode. This current is also a function of several other variables, such as the geometry of the cathode and the oxygen concentration.

At the cathode oxygen molecules are reduced to hydroxyl ions, while at the anode the particular reaction depends upon the nature of the anode. For example, for a silver/silver chloride anode the reaction is



The potential difference applied between the two electrodes must be such that the rate of reaction at the cathode is limited by the transport of oxygen to the cathode rather than the kinetics of the reaction. The response of the current to flow can be explained by assuming the existence of a diffusion layer, inside the hydrodynamic or viscous boundary layer, across which most of the change in oxygen concentration occurs.

A theoretical description of this effect is presented, which is capable of explaining, at least in part, the dependences of the current upon the variables involved. For example, theories are advanced which describe the responses of electrodes of different shapes and attitudes to the flow, such as discs parallel and perpendicular to the flow and a sphere. The most important result is that, for the electrodes the current is proportional to the square root of velocity as shown in equation

3.1.2.

$$\bar{J} = S m e c_s D^{2/3} \nu^{-1/6} U_o^{1/2} \quad (3.1.2)$$

$\bar{J}$  is the current divided by the available area of the cathode. The word 'available' is necessary since some electrodes possess regions which are insulated and therefore do not contribute current to the total output.  $S$  is the shape factor which depends upon the geometry and size of the electrode. In effect, calculations for various electrodes reduce to finding  $S$ .  $U_o$  is the free stream velocity;  $D$  is the diffusion coefficient of oxygen in the solution;  $\nu$  is the kinematic viscosity of the solution;  $c_s$  the oxygen concentration of the bulk of the solution;  $e$  the electronic charge and  $m$  the number of electrons required to reduce one oxygen molecule.

The response of a disc electrode to a given flow depends upon its attitude to the flow and consequently, if used in a blind situation such as the CSF pathways, the flow information would be ambiguous since the attitude of the flow to the disc would be unknown and probably varying. Spherical electrodes have been used in clinical trials to remove this ambiguity, although at the cost of all directional information.

From equation 3.1.2 it can be seen that a knowledge of the oxygen concentration  $c_s$  is required to obtain quantitative flow information. Clinically this did not prove to be a disadvantage since a sample of the CSF was anyway always taken for analysis.

The limiting time response is that to a decrease in flow and this is described in detail in Chapters 5 and 6. The response of the output current to a step decrease in flow is initially fast, but is then followed by a slow tail. The response to an increase in flow is very fast. Work has been concentrated upon the response to a decrease as this is the limiting response.

Advantages of the electrochemical flow transducer include its small size. Spheres of less than 1 mm diameter have been used in clinical trials. Whilst the flow transducer is invasive, it only requires access to the CSF pathways (or any other vessel) from one side. Also, the flow transducer is extremely sensitive to low flow velocities because of its square root dependence upon flow. A further advantage is that it is relatively simple to construct and that its operation does not require extremely complex electronic circuitry.

It must be emphasised here that this device measures flow velocity in its immediate vicinity, effectively at a point, rather than volume flow.

The electrochemical flow transducer utilises the same effect as  $pO_2$  electrodes. In suitable form  $pO_2$  electrodes can be used invasively, as skin electrodes, or, if provided with their own electrolyte, to monitor the oxygen content of gas mixtures. Their operation relies upon the proportionality of output current to oxygen concentration. They are widely described in the literature, the following references being a few of the many present: Clark (1956), Cater Silver and Wilson (1959) and Meldrum Watson and Becker (1973). Many authors, for example Zick (1976), report that  $pO_2$  electrodes possess a flow sensitivity, or stirring artefact. This is considered to be a disadvantage and considerable effort is devoted to overcoming it. The usual technique is to cover the cathode with an oxygen permeable membrane of sufficient thickness to totally enclose the diffusion layer, thus removing the flow sensitivity. A disadvantage of this approach is that it severely increases the response time of the electrode as the membrane invariably possesses a smaller oxygen diffusion coefficient than the fluid in which it is immersed. This approach does, however, lead to great theoretical simplification, allowing Fick's Law to be used with accuracy.

Parker and Scopes (1971) in an effort to improve the response time of their  $pO_2$  electrode, used a membrane so thin it only totally covered the diffusion layer at velocities greater than  $5 \text{ cm s}^{-1}$  at  $37^\circ\text{C}$ . Up to this velocity the graph presented of current versus flow velocity shows the usual square root dependence upon flow.

Oeseburg, Zijlstra and Ing (1968) report an interesting approach to removing flow sensitivity. They decreased the applied potential between anode and cathode to below the point where the reaction is transport controlled and apparently found their platinum electrode continued to function correctly. They explain this by stating "lowering the polarizing voltage down to the point where the diffusion layer is always thinner than the hydrodynamic boundary layer results in an adequate suppression of the flow effects on the oxygen cathode output". The theoretical discussion below shows that, when the reaction is transport controlled and so flow sensitive, the diffusion layer is about ten times thinner than the hydrodynamic boundary layer. If the applied potential is decreased, then as the reaction becomes no longer transport controlled, the diffusion layer grows to infinity as the concentration of oxygen at the cathode grows from zero and approaches that of the bulk of the solution. In reducing the applied potential, Oeseburg allowed competition for control of the reaction rate between the reaction kinetics and oxygen transport. It may perhaps be that in this intermediate state flow sensitivity is reduced whilst the dependence of current upon oxygen concentration remains.

Mackay (1970) reports that it is possible, using  $pO_2$  electrodes, to estimate the flow in a blood vessel provided that directional information is not required and considerable inaccuracy can be tolerated. It is one of the aims of this work to show that oxygen reducing cathodes can measure physiological flow velocities as accurately as other available techniques. Whilst the clinical trials reported here were performed with

directionally insensitive electrodes it is possible, using for example an electrode array, to obtain direction, certainly in a blood vessel where the directions of main interest are away from or towards the heart. Directional forms will not be discussed in any greater detail.

The main difference between the electrochemical flow probe and  $pO_2$  electrodes is that flow sensitivity is optimised rather than suppressed.

When this work was at an advanced stage a reference to Mochizuki, Koyama and Yokata (1962) was found in Oeseburg (1968). Mochizuki and his co-workers report, in their monograph, a considerable amount of work using oxygen reducing cathodes to measure blood flow in dogs and humans. However, in their theoretical section they appear unaware of the work of Levich (1962), and their treatment is naive leading to the incorrect conclusion that current is directly proportional to flow velocity. Further, when presenting velocity calibrations of their electrode systems a graph is given which shows the usual square root dependence upon free stream velocity. However, they persist in assuming direct proportionality, in fact drawing a straight line through the apparently linear high velocity portion of the parabola. They attribute the failure of their theory to explain the experimental results to a difference between convection and flow, which is "too difficult to consider theoretically". It is possible that Oeseburg's fallacious comments on the diffusion layer derive from this naive treatment.

The theoretical treatment given here of the response of electrodes parallel to the flow is based upon the work of Levich (1962), who derived the expression for the semi-infinite parallel plate. Levich (1962) did much work on the diffusion layer, showing the inadequacy of the previous Nernst approach (Bockris and Reddy, 1970; Eyring, Henderson and Jost, 1970) which assumed that the diffusion layer consists of totally static fluid.

Theoretical descriptions of infinite perpendicular electrodes already exist (Arvia and Marchiano, 1971), but are inadequate in this context and so a theoretical treatment is developed for finite perpendicular electrodes. For the sphere a theoretical treatment again already exists (Matsuda, 1967) but is only applicable to a small area around the stagnation point where the effects of curvature are negligible and the diffusion layer may be considered constant. A theory is advanced here to describe the sphere up to the point at which the hydrodynamic boundary separates from the sphere.

It is possible to consider the type of reaction involved as consisting of three major sequential steps: the first in which the reacting species arrives at the cathode; the second in which the reaction occurs (this may itself consist of many steps); and the third in which the products leave the reaction site

Each of these consecutive steps will have a rate constant associated with it. The step with the smallest rate constant, at the conditions pertaining, will control the overall reaction rate. In the reduction of oxygen at a cathode when the correct potential is applied the reaction is transport limited, or controlled. That is as fast as the oxygen molecules arrive they are reduced to hydroxyl ions since the rate constant of the second state is under these conditions, considerably greater than that of the first. To ensure the rate of reaction is controlled by the rate of arrival of oxygen, the rate of removal of hydroxyl ions from the reaction site must be sufficiently great. (This, and above statements, assume that hydroxyl ions are the only product of importance). Three factors ensure the rate constant of the third stage is sufficiently high: first, the diffusion coefficient of hydroxyl ions in saline (or CSF) is of the same order as that of oxygen; second, the hydroxyl ion is negatively charged, as is the cathode, and will therefore experience coulombic repulsion; and third, the concentration gradient of hydroxyl ions, except perhaps at very high values of pH, caused by the reaction is such as to cause the hydroxyl ions to diffuse away. It therefore seems reasonable to assume that the third step is always fast enough to never exert any control over the reaction rate.

electronation current density  $\bar{j}$  caused by oxidation reactions; and the electronation current density  $\bar{j}$  caused by reduction reactions.

If the overpotential is large and negative then the interface is a cathode and  $\bar{j} \gg \bar{j}$  and equation 3.2.2 may be written

$$j = -\bar{j} = -j_0 e^{\alpha e |V_c|/kT} \quad (3.2.3)$$

The minus sign in equation 3.2.3 refers only to the interface under consideration, showing that it is a cathode. In further references to the current density at the cathode this conventional minus sign will be omitted.  $V_c$ , the overpotential at the cathode, is now used to replace  $V$ . Equation 3.2.3 holds for values of  $V_c$  more negative than  $\sim -0.1$  V.

The situation which occurs at an electrode/electrolyte interface is complex and unnecessary for this discussion. In general if a potential difference  $V_{ac}$  is applied across an anode and cathode then the majority of the potential appears across a very narrow region (of the order of a few molecular diameters) at each interface, as the overpotentials at the anode  $V_a$ , and the cathode  $V_c$ . For direct currents the electrolyte between the electrodes may be considered purely resistive and therefore there is also a potential difference across the electrolyte. For fairly strong electrolytes, provided the distance between the electrodes is not excessive, the ohmic potential across the electrolyte may be considered negligible. Thus, in full

$$V_{ac} = V_a + V_c + IR \quad (3.2.4)$$

where  $I$  is the current flowing and  $R$  the resistance of the electrolyte.

This situation is shown schematically in figure 3.2.1.

Theoretical descriptions of infinite perpendicular electrodes already exist (Arvia and Marchiano, 1971), but are inadequate in this context and so a theoretical treatment is developed for finite perpendicular electrodes. For the sphere a theoretical treatment again already exists (Matsuda, 1967) but is only applicable to a small area around the stagnation point where the effects of curvature are negligible and the diffusion layer may be considered constant. A theory is advanced here to describe the sphere up to the point at which the hydrodynamic boundary separates from the sphere.

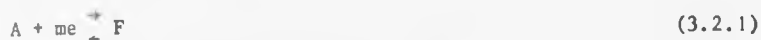
It is possible to consider the type of reaction involved as consisting of three major sequential steps: the first in which the reacting species arrives at the cathode; the second in which the reaction occurs (this may itself consist of many steps); and the third in which the products leave the reaction site

Each of these consecutive steps will have a rate constant associated with it. The step with the smallest rate constant, at the conditions pertaining, will control the overall reaction rate. In the reduction of oxygen at a cathode when the correct potential is applied the reaction is transport limited, or controlled. That is as fast as the oxygen molecules arrive they are reduced to hydroxyl ions since the rate constant of the second state is under these conditions, considerably greater than that of the first. To ensure the rate of reaction is controlled by the rate of arrival of oxygen, the rate of removal of hydroxyl ions from the reaction site must be sufficiently great. (This, and above statements, assume that hydroxyl ions are the only product of importance). Three factors ensure the rate constant of the third stage is sufficiently high: first, the diffusion coefficient of hydroxyl ions in saline (or CSF) is of the same order as that of oxygen; second, the hydroxyl ion is negatively charged, as is the cathode, and will therefore experience coulombic repulsion; and third, the concentration gradient of hydroxyl ions, except perhaps at very high values of pH, caused by the reaction is such as to cause the hydroxyl ions to diffuse away. It therefore seems reasonable to assume that the third step is always fast enough to never exert any control over the reaction rate.

## 3.2 Electrochemical Aspects

### 3.2.1 Introduction

At an electrode/electrolyte interface away from equilibrium, at which an oxidation-reduction (redox) reaction involving  $m$  electrons is taking place, that is



the current density through the interface is given by

$$J = J_0 \left[ e^{(1-\alpha) eV/kT} - e^{-\alpha eV/kT} \right] \quad (3.2.2)$$

This is the Butler-Volmer equation and is discussed in detail in the standard electrochemical texts, for example Bockris and Reddy (1970). If a single metal electrode is immersed in saline then  $J_0$ , the equilibrium exchange current density, represents the current in each reaction direction, the net current being zero. In the case of such a single electrode, if the solution is disturbed by, say, flow of the electrolyte, then the equilibrium will be disturbed as the ions entering solution are swept away, thereby causing further ions to enter the solution by dissolution of the electrode.

The symmetry factor  $\alpha$  often has the value of approximately 0.5, but depends upon the properties of the particular interface.

The actual potential which exists across an electrode/electrolyte interface is impossible to measure since this requires the presence of a second electrode/electrolyte interface. However, it is possible to measure the deviation of the potential across the interface when the equilibrium is disturbed if the second, reference, electrode is maintained at equilibrium. This change in the potential is the overpotential across the interface  $V$  and here it may be thought of as the force driving the current flow. Whilst the reaction rate is limited only by electrochemical factors, the overpotential is the rate determining factor.

The right hand side of equation 3.2.2 contains two terms: first the de-

electronation current density  $\bar{J}$  caused by oxidation reactions; and the electronation current density  $\bar{J}$  caused by reduction reactions.

If the overpotential is large and negative then the interface is a cathode and  $\bar{J} \gg \bar{J}$  and equation 3.2.2 may be written

$$J = -\bar{J} = -J_0 e^{ae|V_c|/kT} \quad (3.2.3)$$

The minus sign in equation 3.2.3 refers only to the interface under consideration, showing that it is a cathode. In further references to the current density at the cathode this conventional minus sign will be omitted.  $V_c$ , the overpotential at the cathode, is now used to replace  $V$ . Equation 3.2.3 holds for values of  $V_c$  more negative than  $\sim -0.1V$ .

The situation which occurs at an electrode/electrolyte interface is complex and unnecessary for this discussion. In general if a potential difference  $V_{ac}$  is applied across an anode and cathode then the majority of the potential appears across a very narrow region (of the order of a few molecular diameters) at each interface, as the overpotentials at the anode  $V_a$ , and the cathode  $V_c$ . For direct currents the electrolyte between the electrodes may be considered purely resistive and therefore there is also a potential difference across the electrolyte. For fairly strong electrolytes, provided the distance between the electrodes is not excessive, the ohmic potential across the electrolyte may be considered negligible. Thus, in full

$$V_{ac} = V_a + V_c + IR \quad (3.2.4)$$

where  $I$  is the current flowing and  $R$  the resistance of the electrolyte.

This situation is shown schematically in figure 3.2.1.

electronation current density  $\bar{J}$  caused by oxidation reactions; and the electronation current density  $\bar{J}$  caused by reduction reactions.

If the overpotential is large and negative then the interface is a cathode and  $\bar{J} \gg \bar{J}$  and equation 3.2.2 may be written

$$J = -\bar{J} = -J_0 e^{ae |V_c| / kT} \quad (3.2.3)$$

The minus sign in equation 3.2.3 refers only to the interface under consideration, showing that it is a cathode. In further references to the current density at the cathode this conventional minus sign will be omitted.  $V_c$ , the overpotential at the cathode, is now used to replace  $V$ . Equation 3.2.3 holds for values of  $V_c$  more negative than  $\sim -0.1V$ .

The situation which occurs at an electrode/electrolyte interface is complex and unnecessary for this discussion. In general if a potential difference  $V_{ac}$  is applied across an anode and cathode then the majority of the potential appears across a very narrow region (of the order of a few molecular diameters) at each interface, as the overpotentials at the anode  $V_a$ , and the cathode  $V_c$ . For direct currents the electrolyte between the electrodes may be considered purely resistive and therefore there is also a potential difference across the electrolyte. For fairly strong electrolytes, provided the distance between the electrodes is not excessive, the ohmic potential across the electrolyte may be considered negligible. Thus, in full

$$V_{ac} = V_a + V_c + IR \quad (3.2.4)$$

where  $I$  is the current flowing and  $R$  the resistance of the electrolyte.

This situation is shown schematically in figure 3.2.1.

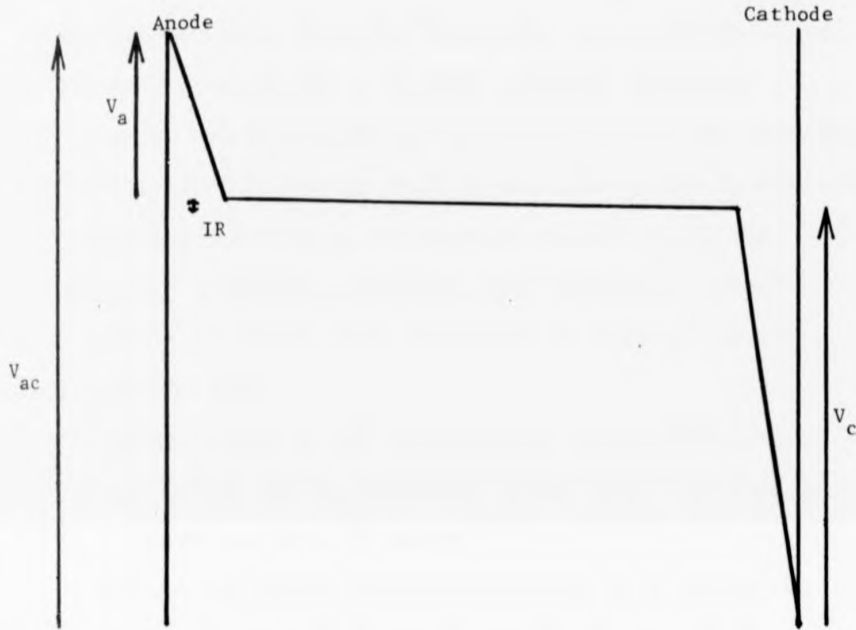


Figure 3.2.1 The distribution of  $V_{ac}$  at the electrodes.

$$V_c, V_a \gg IR$$

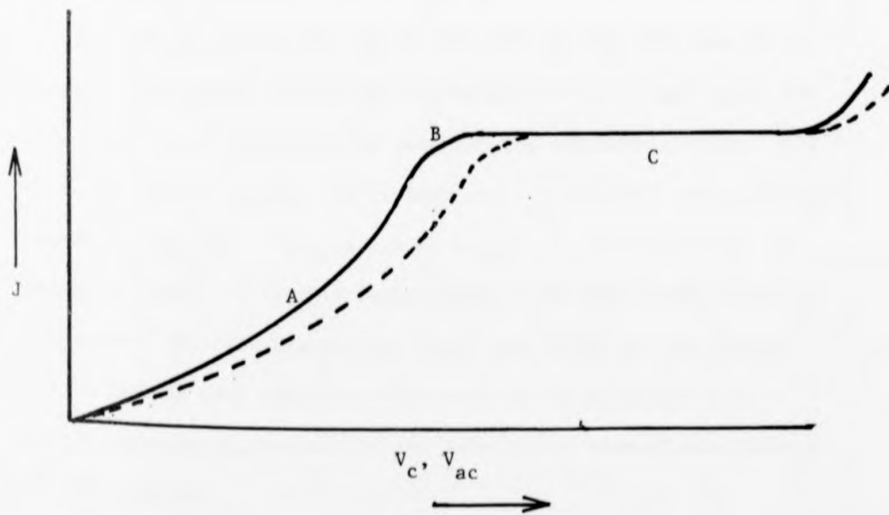


Figure 3.2.2 The variation of current density  $J$ , with  $V_c$  (—) and  $V_{ac}$  (-----).

### 3.2.2 The electrochemical reduction of oxygen

The electrochemical discussion so far has been general in nature and only strictly applicable to electrode reactions involving a single step. However, in a complex multi-step reaction, such as the reduction of oxygen, the above discussion still applies. Most electrode reactions obey a relationship similar to that given by equation 3.2.3; the main difference in multi-step reactions being that  $\alpha$  is no longer a simple variable but depends upon the details of each step and each possible reaction path.

The current density at the cathode during oxygen reduction is found to vary with  $V_c$  and  $V_{ac}$  as shown in figure 3.2.2. Experimental details and values are given in Chapter 4.

In region A the current obeys a relationship of the type given by equation 3.2.3, that is the reaction rate is controlled by the overpotential  $V_c$ . In region B the overpotential at the cathode and the rate of arrival of oxygen are in conflict for control of the reaction rate and the properties of an electrode in this region are indeterminate.

In region C, where the current is constant the reaction is transport controlled since oxygen molecules can no longer reach the cathode at a rate sufficient to maintain the exponential rise. All oxygen molecules reaching the cathode are, effectively instantaneously, reduced so that the concentration of oxygen at the surface of the cathode is zero. It is this region which is of importance to the operation of the flow transducer, since the height of the current plateau depends upon the rate of arrival of oxygen which in turn depends upon the square root of the velocity of flow of electrolyte past the cathode.

When  $V_c$  is increased sufficiently, the current increases from

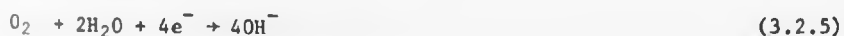
the plateau as other reactions are activated. If the electrolyte contained no oxygen then this region would descend to the origin in a way similar to region A.

The value of  $V_{ac}$  at which the plateau begins in the  $J - V_{ac}$  curve depends upon the electrode materials. A graph of  $V_a$  versus the current density at the anode would exhibit a relationship of the kind described by equation 3.2.3. No plateau is present in the region of interest since an anode of suitable material and sufficient size to ensure a very large rate constant will have been chosen. Requirements for the anode to ensure correct functioning are discussed in Chapter 4.

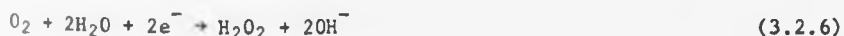
The current density for a given flow depends upon the number of electrons involved in the reduction of one molecule of oxygen. However, given that the reaction, in the plateau region is fast enough to maintain the oxygen concentration at the cathode at zero, this is the only way in which the exact mechanism is of importance to the functioning and description of the flow transducer.

According to Charlot et al (1962) the first reaction to occur in an electrochemical cell, that is at the lowest value of applied potential difference  $V_{ac}$ , is the reduction of oxygen, even though the current so obtained may be negligible.

Charlot et al report that for  $5 < \text{pH} < 12$  oxygen is reduced to hydroxyl ions by one of the following paths: either



or



In both of these cases four electrons are required to reduce one molecule of oxygen so that, in the present situation, it is not necessary to distinguish between them.

Most workers with  $pO_2$  electrodes assume the reaction to involve four electrons. However, most electrochemical texts report hydrogen peroxide as either an intermediary or an end product of the reaction. So, uncertainty exists as to whether some, or even all, of the hydrogen peroxide formed diffuses away from the cathode surface before further reacting to form hydroxyl ions. It is also possible that more than one reaction path exist in parallel, the end product of some being hydrogen peroxide and that of others hydroxyl ions. Thus the average number of electrons involved per oxygen molecule could, in this case, lie between two and four.

Damjanovic (1969) in his review article reports that the reaction mechanism and products depend upon the pH and  $pO_2$  of the solution, the particular metal or alloy used as the electrode and the details of its surface structure (for example any oxide state).

At present it will be assumed that, at the gold and copper cathodes used in this work, four electrons are involved in the reduction of one oxygen molecule (that is  $m = 4$ ). This is considered again in the discussion of Chapter 6.

### 3.3 The Convective-Diffusion Equation

It is first necessary to define the symbols used in the remainder of this chapter. This is done in table 3.3.1. As shown below, the fluid can be divided into two regions: that where viscous effects are negligible, the potential flow region; and that where viscous forces

Table 3.3.1 Symbols used in chapter 3

General

$U_0$  - the free stream velocity, i.e., the fluid velocity immediately downstream of the electrode.

$\underline{v}$  - a general fluid velocity anywhere in the fluid. In Cartesian co-ordinates its components in the x, y and z directions are  $v_x$ ,  $v_y$  and  $v_z$ .

Cartesian co-ordinates - used for the parallel disc and plate and perpendicular plate electrodes.

y - the outward normal to the surface

x, z - orthogonal co-ordinates on the surface

U, V, W - components of the potential flow in the x, y and z directions.

u, v, w - components, in the x, y and z directions, of the flow within the hydrodynamic boundary layer.

For parallel electrodes  $U_0$  impinges along the x direction and  $U_0 = U$ ,  $V = 0$ .

For the perpendicular plate  $U_0$  impinges along the negative y direction.  $U_0 \neq V$ .

Curvilinear co-ordinates - used for the perpendicular disc and the sphere.

x - along the surface away from the stagnation point (the point at which the flow impinges).

y - the outward normal to the surface.

U, V - the potential flow components in the x and y directions.

u, v - components, in the x and y directions, of the flow within the hydrodynamic boundary layer.

For the perpendicular disc these co-ordinates are equivalent to cylindrical polar co-ordinates and  $x = r$ .

are important, the hydrodynamic boundary layer. Different symbols are used to represent the flow in these regions, but it must be emphasised that  $\underline{v}$  and its components  $v_x$ ,  $v_y$  and  $v_z$  represent a general flow anywhere.

The operation of the electrochemical flow transducer depends upon the transport of oxygen to the cathode. The transport of matter added to a liquid (or gas) forming a solution is described by the convective-diffusion equation. Therefore, a solution of this equation for a given electrode arrangement and attitude to the flow will define the expected response of the electrode. The equation which is derived fully by Levich (1962) may be written

$$\frac{\partial c}{\partial t} + \underline{v} \text{ grad } c = D \nabla^2 c \quad (3.3.1)$$

or in cartesian co-ordinates as

$$\frac{\partial c}{\partial t} + v_x \frac{\partial c}{\partial x} + v_y \frac{\partial c}{\partial y} + v_z \frac{\partial c}{\partial z} = D \left( \frac{\partial^2 c}{\partial x^2} + \frac{\partial^2 c}{\partial y^2} + \frac{\partial^2 c}{\partial z^2} \right) \quad (3.3.2)$$

$c$  is the concentration, in this case of oxygen, at any point.  $D$  is written as being independent of position since at low concentrations the variation of the diffusion coefficient with concentration is negligible (Levich 1962).

Since the velocity of the liquid is a function of position, the convective-diffusion equation is a second order partial differential equation with variable coefficients. To determine the variation of concentration with position for a particular problem it is also necessary to know the boundary and initial conditions. Here only the steady state is of interest, that is  $\partial c / \partial t \equiv 0$ , and equation 3.3.1 becomes

$$\underline{v} \text{ grad } c = D \nabla^2 c \quad (3.3.3)$$

If  $v = 0$  equation 3.3.1 would become Fick's Law for molecular diffusion.

The convective-diffusion equation is similar to the Navier-Stokes equation and a dimensionless number, the Peclet number  $Pe$  can be derived which is analogous to the Reynolds number  $Re$ .

$$Pe = \frac{U L}{D} \quad (3.3.4)$$

where  $L$  is a characteristic length along which the major change in concentration occurs.

The left hand side of the convective-diffusion equation represents the convective transport of matter in the liquid and the right hand its transport by molecular diffusion. When  $Pe \ll 1$  transport by molecular diffusion predominates (Levich 1962) and when  $Pe \gg 1$  transport by convection dominates, unless there is a large concentration gradient along one of the co-ordinates. So, in this last case, it is not possible to neglect the right hand side of equation 3.3.3 because of the large value of one of the derivatives.

The ratio  $Pe/Re$  is the Prandtl number  $Pr$

$$Pr = Pe/Re = \frac{U L}{D} / \frac{U L}{\nu} = \frac{\nu}{D} \quad (3.3.5)$$

In liquids  $\nu$ , the kinematic viscosity is  $\sim 10^{-6} \text{ m}^2 \cdot \text{s}^{-1}$  and  $D \sim 10^{-9} \text{ m}^2 \cdot \text{s}^{-1}$  and therefore  $Pr \sim 10^3$ . So, even for  $Re$  as small as  $10^{-2}$ ,  $Pe$  is still greater than unity. That is, even for very small flow velocities the convective transport of matter dominates and equation 3.3.3 becomes, in cartesian co-ordinates

$$v_x \frac{\partial c}{\partial x} + v_y \frac{\partial c}{\partial y} + v_z \frac{\partial c}{\partial z} = 0 \quad (3.3.6)$$

Equation 3.3.6 is applicable to the present case, far from the reaction surface and a solution to it is that  $c$  is constant. However, close to

the reaction surface the concentration gradients will be large since the concentration of oxygen at the reaction surface is zero because the reaction is transport limited. In this region equation 3.3.3 must be used in full. Therefore, at high  $Pe$ , the liquid is divided into two regions: the first far away from the reaction surface where the concentration is constant; and the second, close to the surface where the concentration changes rapidly. In the latter case the concentration is zero at the reaction surface and quickly approaches the constant bulk value away from it. This is analogous to flow at high  $Re$  past a body, in which two regions can also be defined, one where viscosity is of importance and the other where it is neglected.

Again, as in viscous flow past a body where a viscous (hydrodynamic) boundary layer is defined, a diffusion layer  $\delta$  can be defined here by

$$\left. \frac{\partial c}{\partial y} \right|_{y=0} = \frac{c_s - c_e}{\delta} = \frac{c_s}{\delta} \quad (3.3.7)$$

where  $y$  is the outward normal to the surface and  $c_e = 0$ , the concentration at the reaction surface. This is a linearization of the concentration profile which increases proportionally with  $y$  at small  $y$  and then asymptotically approaches the bulk concentration value  $c_s$  as shown in figure 3.3.1.

Thus, the convective-diffusion equation leads to a diffusion layer, as does Nernst's theory (Bockris and Reddy 1970; Levich 1962; Eyring, Henderson and Jost 1970) except that Nernst's diffusion layer is completely static and of constant thickness with position. It will be shown below that  $\delta$  varies rapidly with position and is not static since it occupies the same space as the non-static viscous boundary layer.

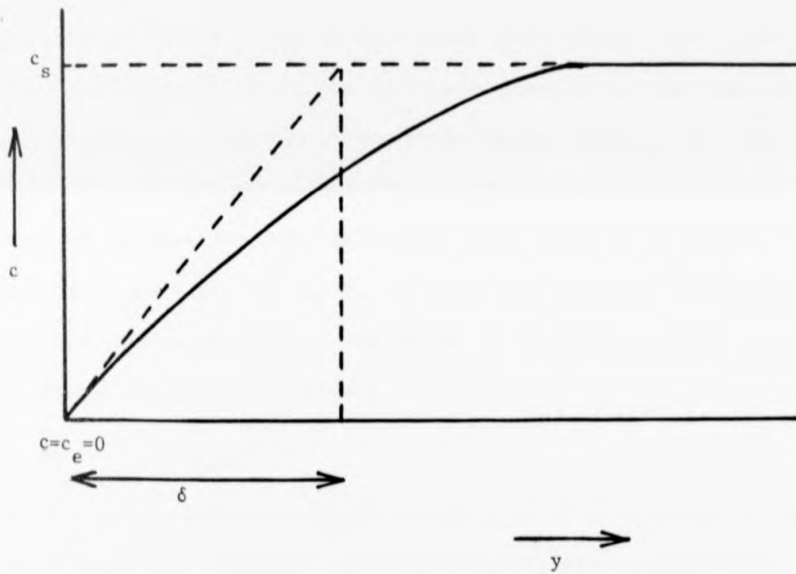


Figure 3.3.1 The variation of concentration  $c$  with distance normal to the reaction surface.

### 3.4 The Navier-Stokes Equation

To solve the convective-diffusion equation it is necessary to know the velocity components. To gain this knowledge it is necessary to solve the Navier-Stokes equation, which is difficult because of its complexity. The region of interest is that close to the electrode surface (within the hydrodynamic (viscous) boundary layer), solutions to the Navier-Stokes equation here only being attainable in series form with coefficients evaluated numerically. At very small  $y$  the first term of such a series is sufficient (Schlichting 1960). Two factors show that to obtain the current response of an electrode it is only necessary to solve the convective-diffusion equation for small values of  $y$ , that is the velocity components need to be known only at small  $y$ . The first is that, as Levich (1962) shows in an initial approximate analysis,  $\delta \sim \delta_h/10$ ,  $\delta_h$  being the thickness of the hydrodynamic boundary layer. The second is the flux of oxygen molecules arriving at the electrode surface  $N$  is

$$N = D \left. \frac{\partial c}{\partial y} \right|_{y=0} \quad (3.4.1)$$

So, to solve the convective-diffusion equation it is necessary to find the values of the components  $u$ ,  $v$  and  $w$  of the flow velocity within the hydrodynamic boundary layer, as  $y \rightarrow 0$ .

For an incompressible fluid the Navier-Stokes equation can be written

$$\frac{\partial \underline{v}}{\partial t} + (\underline{v} \cdot \nabla) \underline{v} = \nu \nabla^2 \underline{v} - \frac{\nabla p}{\rho} \quad (3.4.2)$$

The kinematic viscosity  $\nu$  is assumed independent of position, in effect stipulating constant temperature. Also, all body forces have been neglected, which is reasonable when there are no free surfaces and the fluid density  $\rho$  is constant. It is assumed that the change in density close to the reaction surface caused by the change in oxygen concentration there is negligible.

In addition to equation 3.4.2 the equation of continuity

$$\nabla \cdot \underline{v} = 0 \quad (3.4.3)$$

is required. As for the convective-diffusion equation only the steady state is of interest, that is  $\partial v / \partial t \equiv 0$

$$(\underline{v} \cdot \nabla) \underline{v} = \nu \nabla^2 \underline{v} - \frac{\nabla p}{\rho} \quad (3.4.4)$$

Even neglecting body forces, the Navier-Stokes equation is a non-linear second order partial differential equation for which there is no general solution. Exact solutions can be obtained for any value of  $\nu$  only when the equation is linear because of a particular flow pattern.

In the case of viscous fluids with a solid boundary the velocity normal to the surface is, of course, zero at the surface, but the existence of viscosity also demands that the tangential velocity be zero at the surface. This is the condition of no slip.

Equation 3.4.4 can, by the introduction of a characteristic velocity, length and pressure, be made dimensionless leading to the definition of the Reynolds number given earlier (equation 3.3.5). When  $Re \gg 1$ , the case of interest here, the viscosity term in equation 3.4.4 can be neglected provided there is no large velocity gradient along one of the co-ordinates. When the viscosity can be neglected, which is the case for flow at high  $Re$  far from a solid boundary, the velocity vector can be represented as the gradient of a potential, where the potential satisfies the Laplace equation. Thus

$$\underline{v} = \text{grad } \phi \quad (3.4.5)$$

and

$$\nabla^2 \phi = 0 \quad (3.4.6)$$

Then, the viscosity terms become identically zero and the viscosity free flow is known as potential flow. However, close to the boundary, because of the condition of no slip, the velocity gradient normal to

the surface is large (the gradients along the surface are much smaller and are neglected) so the viscosity term in equation 3.4.4 must be retained because of the large value of this one derivative.

Prandtl (Schlichting 1960; Prandtl 1963) first defined these two separate regions. For the two dimensional case Prandtl simplified the Navier-Stokes equation to the following, known as Prandtl's boundary layer equations, which apply to the viscous flow region:

$$u \frac{\partial u}{\partial x} + v \frac{\partial u}{\partial y} = -\frac{1}{\rho} \frac{\partial p}{\partial x} + \nu \frac{\partial^2 u}{\partial y^2} \quad (3.4.7)$$

$$\frac{\partial u}{\partial x} + \frac{\partial v}{\partial y} = 0 \quad (3.4.8)$$

with boundary conditions

$$y = 0 : u = v = 0 \quad ; \quad y \rightarrow \infty : u \rightarrow U \quad (3.4.9)$$

where the potential flow components  $U$  and  $V$  are considered known.

Equation 3.4.7 is arrived at by neglecting terms of first and higher order in  $\delta_h$ , the viscous boundary layer thickness. The pressure across the boundary layer, at constant  $x$ , is almost constant, so that  $\frac{\partial p}{\partial y}$  may be neglected, and can be set equal to that at the outer edge of the boundary layer where it is determined by the potential flow (Schlichting 1960). In steady flow the pressure may be obtained from the integrated Bernoulli equation

$$p + \rho \frac{U^2}{2} = \text{constant} \quad (3.4.10)$$

In solving the Prandtl equations it is necessary to assume a velocity profile at the initial point, either the leading edge or the stagnation point. This assumed function is similar in form to the potential flow nearby. Therefore, for a given problem the potential flow distribution must be known so as to obtain the assumed profile at the initial point and also to obtain the pressure term, via the Bernoulli equation.

Boundary layer equations can also be obtained for bodies of revolution. The flow is assumed to be parallel to the axis. Curvi-linear coordinates are used as shown in figure 3.4.1, with  $y$  again the outward normal to the surface. The distance from the stagnation point (where the flow impinges) along a contour is  $x$  and the shape of the body is given by  $r(x)$ , the perpendicular distance from the axis to the point  $x$ . Of principal importance is that there should be no sharp corners, so that  $d^2r/dx^2$  does not become very large. The boundary layer equations for a body of revolution are then (Schlichting 1960) in the steady state

$$u \frac{\partial u}{\partial x} + v \frac{\partial u}{\partial y} = -\frac{1}{\rho} \frac{\partial p}{\partial x} + \nu \frac{\partial^2 u}{\partial y^2} \quad (3.4.11)$$

$$\frac{\partial(ur)}{\partial x} + \frac{\partial(vr)}{\partial y} = 0 \quad (3.4.12)$$

with boundary conditions

$$y = 0 : u = v = 0 ; \quad y \rightarrow \infty : u \rightarrow U \quad (3.4.13)$$

The term  $\partial p/\partial y$  is again neglected as being small compared to  $\partial p/\partial x$  (Schlichting 1960).

### 3.5 The Current Response of Various Electrodes

Obtaining the steady state output currents, for the transport-limited electrodes of interest here, can be divided into the following distinct steps:

- i) Obtain the potential flow distribution around the geometry of interest. This is not always trivial.
- ii) Then, using the potential flow distribution as a guide to the form of the velocity components inside the hydrodynamic boundary layer at the initial point, obtain the velocity components as  $y \rightarrow 0$ .
- iii) Insert these into the convective-diffusion equation and solve to obtain the current density as a function of position on the electrode surface.
- iv) Integrate the current density over the surface of the electrode, finally obtaining the response of the electrode to a given steady flow.

Following these steps for the electrodes under consideration always

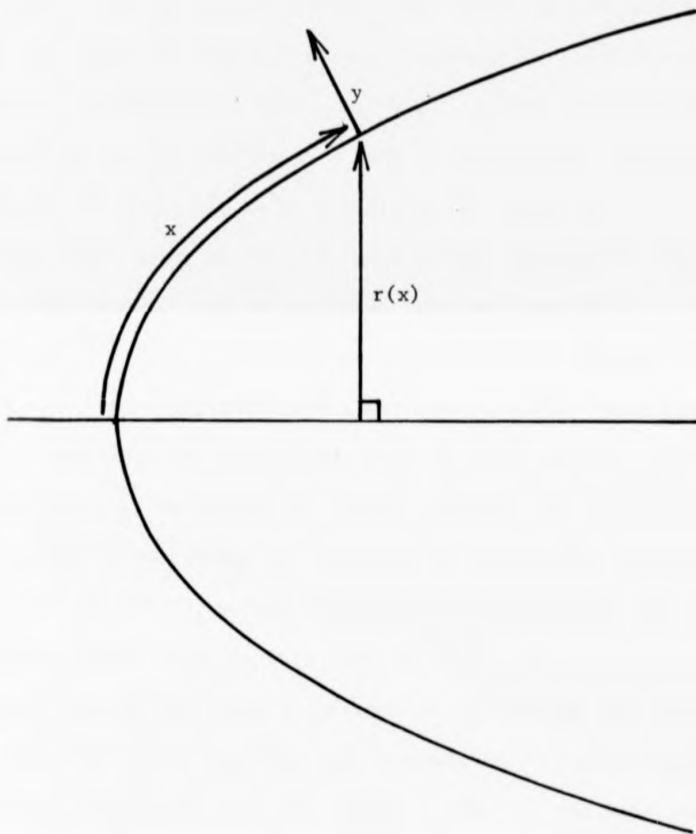


Figure 3.4.1 The curvi-linear co-ordinates used for bodies of revolution.

leads to the relationship given by equation 3.1.2, that is

$$\bar{j} = S \text{ mec}_s D^{2/3} v^{-1/6} U_0^{1/2} \quad (3.5.1)$$

where

$$\bar{j} = I. (\text{Available area of the electrode})^{-1/2} \quad (3.5.2)$$

$I$  is the current output of the electrode. The most important result is that the current (or average current density) for all these electrodes is proportional to the square root of the free stream velocity. The electrodes considered may be thought of as being 'exterior' in that they are either flat surfaces or the outside surface of a body of revolution. In contrast, Levich (1962) found that for an interior electrode, the inside of a tube, the current was proportional to the cube root of the velocity of flow.

The shape factor  $S$  can be separated into two components

$$S = K(L)^{-1/2} \quad (3.5.3)$$

$K$  being a numerical coefficient and  $L$  the characteristic dimension of the particular electrode. Since all electrodes of interest here obey equation 3.5.1 the problem of obtaining the current response for a given electrode is in effect, that of evaluating  $K$ . The results obtained for various electrodes are given in table 3.5.1, whilst details of the calculations for particular electrodes are given later in this chapter.

The area of the electrode to be used in calculating the average current density (equation 3.5.2) requires some explanation. Usually, the disc electrodes used in this work consisted simply of the cut, and sometimes polished, end of an enamelled (insulated) copper wire, the enamelling forming an annulus around the circular metal face. The flow distribution around the electrode is governed by the total radius. However, in calculating the average current density the inner radius, that of the metal surface is used, since the insulated region contributes no current. The area used to calculate the average current density for an enamelled disc electrode is, therefore

$$\text{Available area of electrode} = \pi r^2 R^2 \quad (3.5.4)$$

$R$  being the total radius and  $r$  that of the metal surface. Naturally, the integration (step(iv), above) is only carried out over the metal surface.

Table 3.5.1

## Shape factors

For all electrodes

$$\bar{J} = S m e c_b D^{2/3} \nu^{-1/6} U_0^{1/2} \quad (3.5.1)$$

$$\bar{J} = I / \text{Available reaction area} \quad (3.3.2)$$

$$S = K L^{-1/2} \quad (3.5.3)$$

For disc electrodes

$$\text{Available area} = \pi X^2 R^2 \quad (3.5.4)$$

Electrode	Attitude to flow	L	K	Comments
Infinite plate	Perp.	X	0.91	Infinite flow distribution applied to finite plate. Area=XZ, X<<Z
Finite plate	Para.	X	0.68	Edge effects in z direction assumed negligible. Area=XZ
Infinite disc	Perp.	R	0.84	Infinite flow distribution applied to finite disc. Diffusion layer constant.
Finite disc. enamelled	Para.	R	$\frac{0.43Q_{\parallel}}{X^2}$	$Q_{\parallel}$ given by equation 3.6.5
Finite disc. No enamel	Para.	R	0.54	X=1 => $Q_{\parallel}=1.236$
Finite disc. enamelled	Perp.	R	$\frac{1.67Q_{\perp}}{X^2}$	$Q_{\perp}$ given by equation 3.7.53
Finite disc. No enamel	Perp.	R	1.28	X=1 => $Q_{\perp}=10/13$
Sphere with epoxy	--	R	$\frac{1.04R(Q_{s1}+Q_{s2})}{(b+R)}$	$Q_{s1}$ given by equation 3.9.13 $Q_{s2}$ given by equation 3.9.14
Sphere No epoxy	--	R	0.48	$Q_s$ given by equation 3.9.5 b=R, $Q_{s2}=0$ , $Q_{s1}=Q_s=0.921$

For a sphere, the hydrodynamic boundary layer separates from the surface at  $109.6^\circ$  from the stagnation point (Schlichting 1960) and after this point the diffusion layer is considered infinite, so that current contributions from beyond the point of separation are considered to be zero. In practice there must be some small, but assumed negligible, contribution from this region since it is still in contact with oxygenated fluid. So, the integration is only taken to the point of separation, but, for consistency the total metal surface area of the sphere is used in calculating the average current density. That is, for all electrodes, when calculating the average current density the total available reaction area is used, whether or not it all contributes current. The sphere electrodes used clinically were partly covered by epoxy resin (as a mechanical support) which decreased their available area.

### 3.6 The Calculation of The Current Response of an Enamelled Disc

#### Parallel to the Flow

The relevant geometry is shown in figure 3.6.1. The calculation for the parallel disc follows directly from that for the parallel plate. This was performed by Levich (1962) and is given in appendix A.1, where Schlichting's (1960) form of the velocity components in the hydrodynamic boundary layer is used rather than that used by Levich (the two forms are equivalent). The geometry relevant to the parallel, enamelled plate is shown in figure 3.6.2.

For the enamelled parallel plate, Levich (1962) found the current density to vary with position as

$$J = 0.34 \text{ mec}_s D^{2/3} \nu^{-1/6} U_o^{1/2} x^{-1/2} \left[ 1 - \left( \frac{h}{x} \right)^{3/4} \right]^{-1/3} \quad (3.6.1)$$

If  $h = 0$ , that is there is no enamel, then equation 3.6.1 represents the parallel plate without enamelling. Equation 3.6.1 can easily be integrated to give the output current for a plate, provided that edge effects in the  $z$ -direction are negligible so that integration in that direction is finite. The theory also assumes that the  $x$  co-ordinate extends to  $+\infty$ . In practice

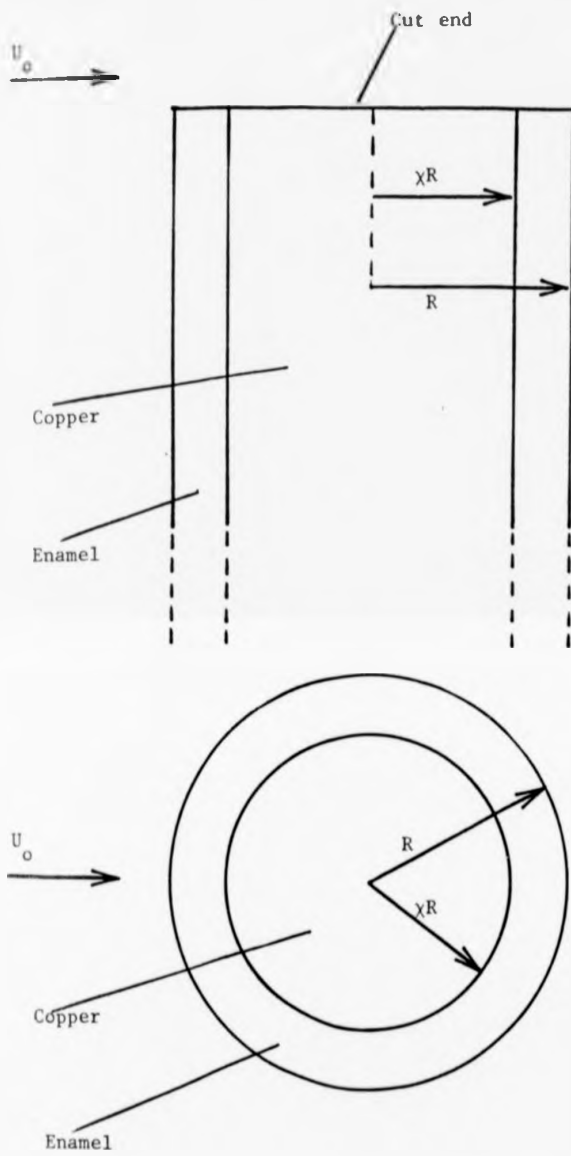


Figure 3.6.1 The usual form of enamelled disc parallel to the flow  $U_0$ .

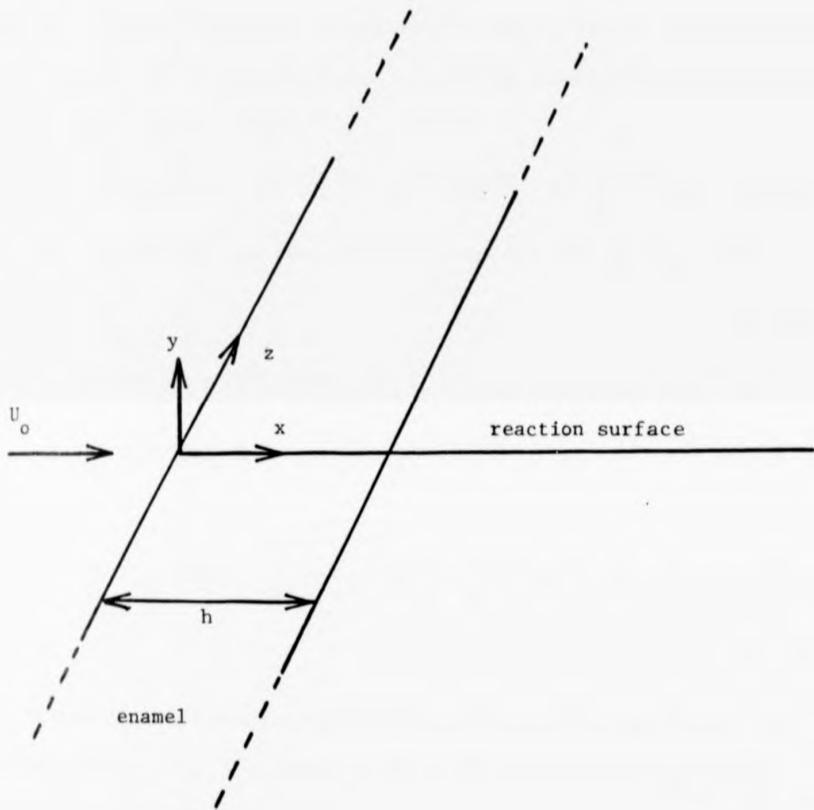


Figure 3.6.2 The enamelled, parallel plate.

$x$  is finite and the integration is therefore curtailed. It is assumed that the finite value of  $X$ , the extent of the plate in the  $x$ -direction, has no effect on the concentration profile set up around the electrode.

Obtaining the total current for the parallel enamelled disc is more difficult. The situation is illustrated in figure 3.6.3. Equation 3.6.1 can be integrated to give the total current  $dI$  flowing from the elemental strip shown in figure 3.6.3.

$$dI = 2 \times 0.34 \text{ mec}_s D^{2/3} v^{-1/6} U_o^{1/2} \left[ l^{3/4} - h^{3/4} \right]^{2/3} db \quad (3.6.2)$$

The total current for the disc surrounded by the insulating enamel ring is

$$I = 2 \times \int_0^{XR} dI \quad (3.6.3)$$

with  $b = \epsilon R$ , and  $db = R d\epsilon$ , then

$$I = 4 \times 0.34 \text{ mec}_s D^{2/3} v^{-1/6} U_o^{1/2} R^{3/2} \times Q_{11} \quad (3.6.4)$$

where

$$Q_{11} = \int_0^X \left[ \left( \sqrt{1 - \epsilon^2} + \sqrt{\chi^2 - \epsilon^2} \right)^{3/4} - \left( \sqrt{1 - \epsilon^2} - \sqrt{\chi^2 - \epsilon^2} \right)^{3/4} \right]^{2/3} d\epsilon \quad (3.6.5)$$

The integral  $Q_{11}$  is dimensionless and can be evaluated numerically for various values of  $\chi$ . The computer generated variation of  $Q_{11}$  with  $\chi$  is shown in figure 3.6.4.

The area of the electrode which is available for the reaction to take place at is  $\pi \chi^2 R^2$  and therefore the average current density  $\bar{J}$  is

$$\bar{J} = \frac{I}{\pi (\chi R)^2} = \frac{0.43}{\chi^2} Q_{11} R^{-1/2} \text{ mec}_s D^{2/3} v^{-1/6} U_o^{1/2} \quad (3.6.6)$$

For the enamelled parallel disc the shape factor is

$$S = \frac{0.43}{\chi^2} Q_{11} R^{-1/2} \quad (3.6.7)$$

$S$  is, therefore, a function of the degree of enamelling. If  $\chi = 1$ , that is there is no enamel, then  $Q_{11} = 1.236$  and the shape factor becomes

$$S = 0.54 R^{-1/2} \quad (3.6.8)$$

$x$  is finite and the integration is therefore curtailed. It is assumed that the finite value of  $X$ , the extent of the plate in the  $x$ -direction, has no effect on the concentration profile set up around the electrode.

Obtaining the total current for the parallel enamelled disc is more difficult. The situation is illustrated in figure 3.6.3. Equation 3.6.1 can be integrated to give the total current  $dI$  flowing from the elemental strip shown in figure 3.6.3.

$$dI = 2 \times 0.34 \text{ mec}_s D^{2/3} v^{-1/6} U_o^{1/2} \left( l^{3/4} - h^{3/4} \right)^{2/3} db \quad (3.6.2)$$

The total current for the disc surrounded by the insulating enamel ring is

$$I = 2 \times \int_0^{\chi R} dI \quad (3.6.3)$$

with  $b = \epsilon R$ , and  $db = R d\epsilon$ , then

$$I = 4 \times 0.34 \text{ mec}_s D^{2/3} v^{-1/6} U_o^{1/2} R^{3/2} \times Q_{II} \quad (3.6.4)$$

where

$$Q_{II} = \int_0^{\chi} \left[ \left( \sqrt{1 - \epsilon^2} + \sqrt{\chi^2 - \epsilon^2} \right)^{3/4} - \left( \sqrt{1 - \epsilon^2} - \sqrt{\chi^2 - \epsilon^2} \right)^{3/4} \right]^{2/3} d\epsilon \quad (3.6.5)$$

The integral  $Q_{II}$  is dimensionless and can be evaluated numerically for various values of  $\chi$ . The computer generated variation of  $Q_{II}$  with  $\chi$  is shown in figure 3.6.4.

The area of the electrode which is available for the reaction to take place at is  $\pi \chi^2 R^2$  and therefore the average current density  $\bar{J}$  is

$$\bar{J} = \frac{I}{\pi (\chi R)^2} = \frac{0.43}{\chi^2} Q_{II} R^{-1/2} \text{ mec}_s D^{2/3} v^{-1/6} U_o^{1/2} \quad (3.6.6)$$

For the enamelled parallel disc the shape factor is

$$S = \frac{0.43}{\chi^2} Q_{II} R^{-1/2} \quad (3.6.7)$$

$S$  is, therefore, a function of the degree of enamelling. If  $\chi = 1$ , that is there is no enamel, then  $Q_{II} = 1.236$  and the shape factor becomes

$$S = 0.54 R^{-1/2} \quad (3.6.8)$$

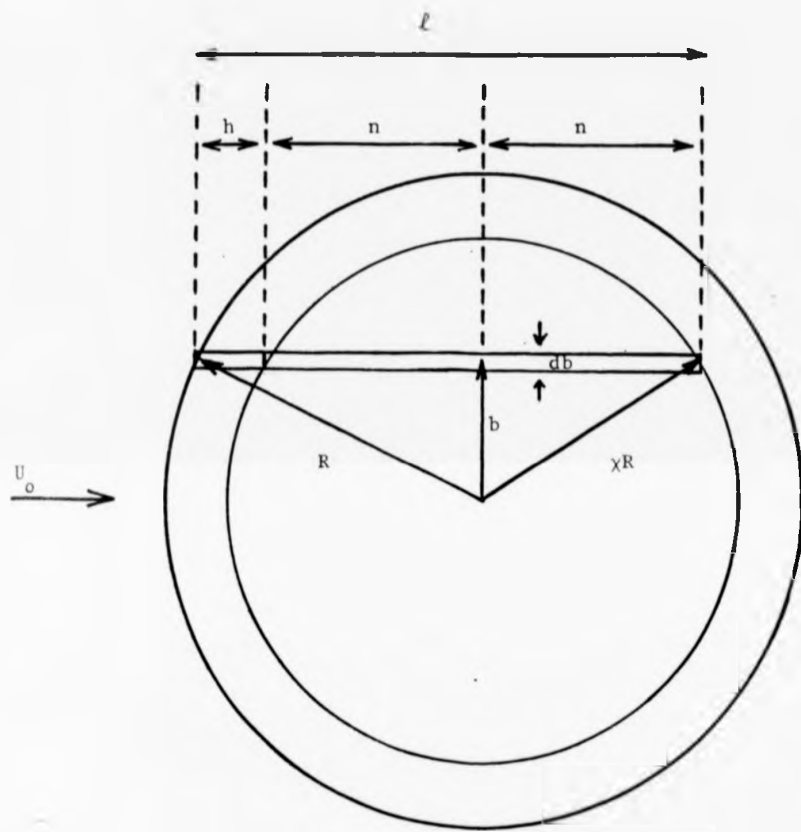


Figure 3.6.3 The scheme of integration used for the parallel enamelled disc.

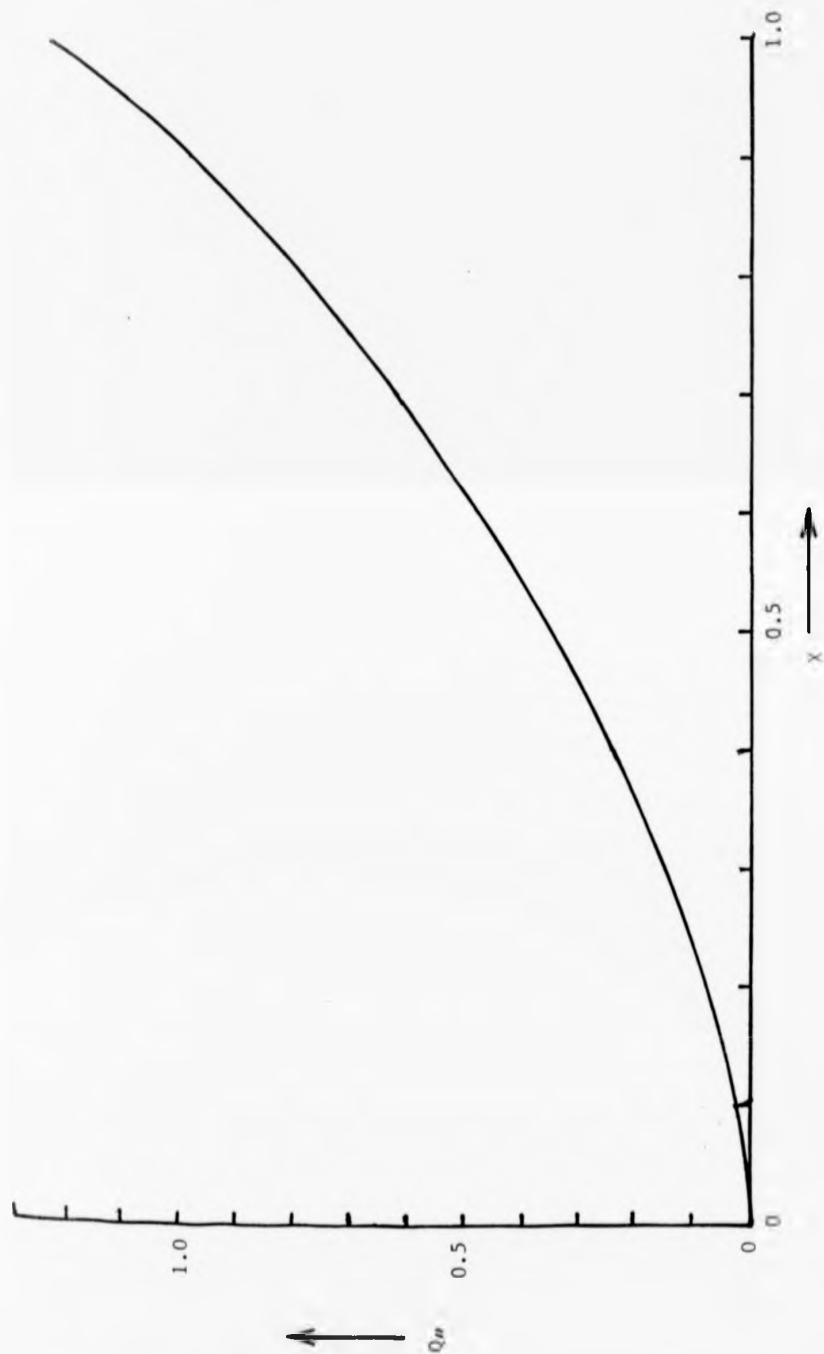


Figure 3.6.4 The variation of  $Q''$  with  $x$

### 3.7 The Calculation of the Current Response of an Enamelled Disc Perpendicular to the Flow

For the plate perpendicular to the flow and the infinite disc (the axisymmetric case) the solutions of the Laplace equation necessary to find the potential flow are relatively easily obtained, and are shown in table 3.7.1. The geometry relevant to perpendicular electrodes is shown in figure 3.7.1.

Finding the potential flow distribution for finite electrodes is not so easy. Complex variable theory is used to find the potential flow for the finite perpendicular plate (Spiegel 1964). The complex potential  $\Omega(z)$  for fluid flow past the cylinder shown in figure 3.7.2 is

$$\Omega(z) = U_0 \left[ \zeta + \frac{(a+b)^2}{4\zeta} \right] \quad (3.7.1)$$

where

$$\zeta = \frac{1}{2} \left[ z + \sqrt{z^2 - c^2} \right] \quad \text{and} \quad c^2 = a^2 - b^2 \quad (3.7.2)$$

To convert this problem into that for the finite perpendicular plate it is necessary to rotate the flow through  $90^\circ$ , achieved by multiplying  $\zeta$  by  $e^{-i\pi/2}$  and letting the minor axis  $b$  go to zero.

Solution of the problem is expedited by transforming to elliptic co-ordinates  $u, v$  where

$$z = x + iy = c \cosh(u + iv) \quad (3.7.3)$$

In the complex plane the complex potential,  $\Omega(z)$

$$\Omega(z) = \phi(x,y) + i\psi(x,y) \quad (3.7.4)$$

where  $\phi(x,y)$  is the potential satisfying the Laplace equation and  $\psi(x,y)$  is the stream function. Therefore it is the real part of  $\Omega(z)$  that is required. Solution leads to

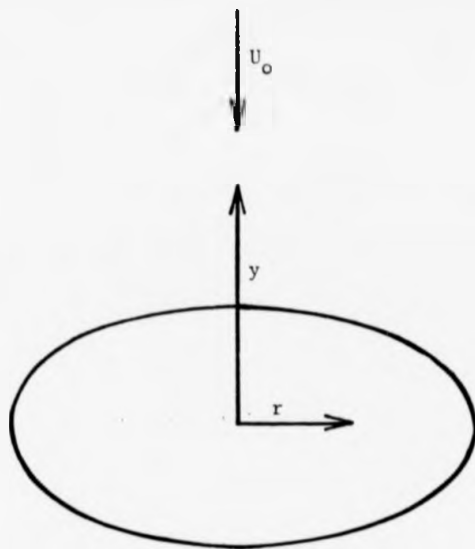


Figure 3.7.1a The geometry of perpendicular disc electrodes.

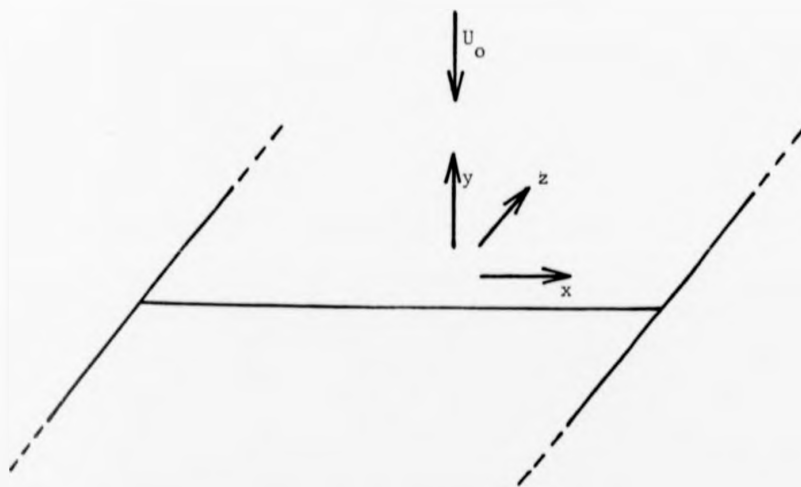


Figure 3.7.1b The perpendicular plate. For finite plates edge effects in the  $z$  direction are assumed negligible.

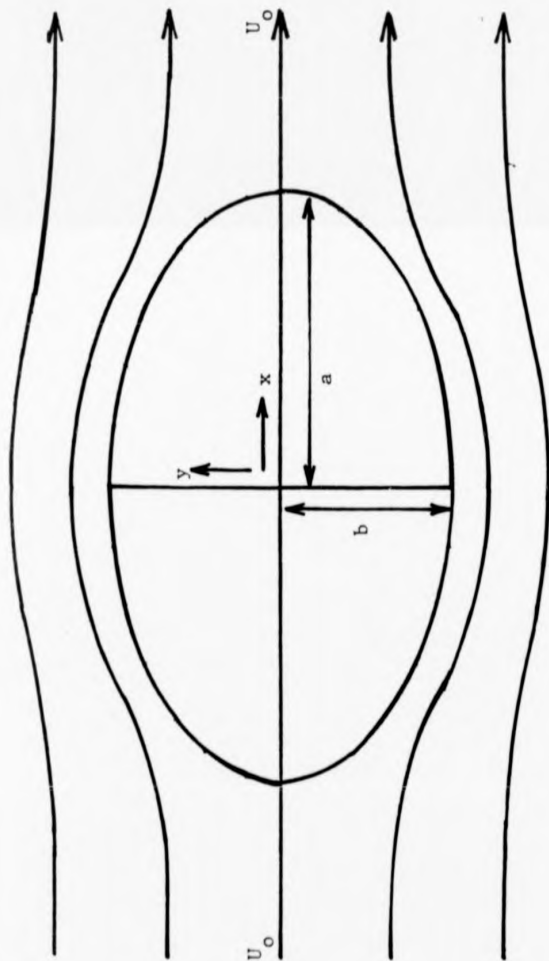


Figure 3.7.2 Potential flow past an elliptic cylinder.

Table 3.7.1 Potential Flow components for perpendicular electrodes.

Electrode	Perpendicular component	Parallel component	
Infinite plate	$V = -dy$	$U = dx$	(i)
Infinite disc	$V = -2dy$	$U = dr$	(i)
Finite plate	$V = -\frac{a^2 U_0 y}{(a^2 - x^2)^{3/2}}$	$U = \frac{U_0 x}{(a^2 - x^2)^{1/2}}$	(ii)
Finite disc	$V = -\frac{2R^2 U_0 y}{(R^2 - r^2)^{3/2}}$	$U = \frac{U_0 r}{(R^2 - r^2)^{1/2}}$	(iii)
	$V = -\frac{U_0 (2R^2 - r^2) y}{(R^2 - r^2)^{3/2}}$	$U = \frac{U_0 r}{(R^2 - r^2)^{1/2}}$	(iv)

Notes:

- (i)  $d$  is a constant
- (ii)  $a = X/2$ ,  $X$  being the characteristic dimension of the finite plate.
- (iii) These are proposed terms, from inspection of those for the infinite plate and disc and the finite plate. However, they do not satisfy continuity.
- (iv) These terms satisfy continuity and are considered to be the desired expressions.

$$\phi(u,v) = U_0 a \sin v \cosh u \quad (3.7.5)$$

or, in cartesian co-ordinates

$$\phi(x,y) = \frac{U_0}{2\sqrt{2}} \left\{ y^2 - x^2 + a^2 + \left[ (x^2 + y^2 - a^2)^2 + 4a^2 y^2 \right]^{1/2} \right\}^{1/2} \quad (3.7.6)$$

The velocity components in the x and y directions respectively are given by  $\frac{\partial \phi}{\partial x}$  and  $\frac{\partial \phi}{\partial y}$ .

To obtain the velocity distribution in the viscous boundary layer, values of  $U = \frac{\partial \phi}{\partial x}$  and  $V = \frac{\partial \phi}{\partial y}$  are required as y tends to zero. In obtaining these values care must be taken to approach zero correctly and it is necessary to expand, using the binomial theory, terms involving y inside square roots. The required expressions for U and V are then

$$U = \left( \frac{\partial \phi}{\partial x} \right)_{y \rightarrow 0} = \frac{U_0 x}{(a^2 - x^2)^{1/2}} \quad (3.7.7)$$

$$V = \left( \frac{\partial \phi}{\partial y} \right)_{y \rightarrow 0} = \frac{-a^2 U_0 x}{(a^2 - x^2)^{3/2}} \quad (3.7.8)$$

It is easy to verify that these expressions satisfy the Laplace equation.

The above process cannot be used to obtain the required potential flow velocities for the three dimensional finite perpendicular disc since complex variable theory is two dimensional. It is, however, possible to obtain the potential flow using the above process in an indirect way, that is by analogy with those for the other perpendicular electrodes. A study of table 3.7.1 shows that it is reasonable to expect the velocity components for the finite disc to be

$$U = \frac{U_0 r}{(R^2 - r^2)^{1/2}} \quad (3.7.9)$$

$$V = \frac{-2R^2 U_0 y}{(R^2 - r^2)^{3/2}} \quad (3.7.10)$$

However, such values fail to satisfy the equation of continuity. For an axisymmetric flow distribution it is possible, as in two dimensional flow, to define a stream function  $\psi$  (Yuan 1967) amongst whose properties are the following

$$U = \frac{\partial \phi}{\partial r} = \frac{-1}{r} \frac{\partial \psi}{\partial y} \quad \text{and} \quad V = \frac{\partial \phi}{\partial y} = \frac{1}{r} \frac{\partial \psi}{\partial r}$$

It follows that if

$$U = \frac{U_0 r}{(R^2 - r^2)^{1/2}} \quad (3.7.11)$$

that

$$V = \frac{-(2R^2 - r^2)U_0 y}{(R^2 - r^2)^{3/2}} \quad (3.7.12)$$

These values do satisfy the equation of continuity and will be considered to be the required potential velocity components.

For the remainder of this discussion of perpendicular electrodes only the finite disc will be considered since its solution is the most complex. For the finite disc, the boundary layer equation 3.4.11 and the continuity equation 3.4.12 become, since  $r(x) = x$

$$u \frac{\partial u}{\partial r} + v \frac{\partial u}{\partial y} = \frac{-1}{\rho} \frac{\partial p}{\partial r} + v \frac{\partial^2 u}{\partial y^2} \quad (3.7.13)$$

$$\frac{\partial u}{\partial r} + \frac{u}{r} + \frac{\partial v}{\partial y} = 0 \quad (3.7.14)$$

with boundary conditions

$$y = 0 : u = v = 0 \quad ; \quad y \rightarrow \infty : u \rightarrow U \quad (3.7.15)$$

Equation 3.7.13 does not apply at the edge of the disc since there  $\frac{d^2 r}{dx^2}$  attains an extremely high value. The assumption  $\frac{\partial p}{\partial r} > \frac{\partial p}{\partial y}$  allows the above pressure term to be found by applying Bernoulli's equation to the potential flow component  $U$ . Thus

$$-\frac{1}{\rho} \frac{\partial p}{\partial r} = \frac{U_0 R^2 r}{(R^2 - r^2)^2} \quad (3.7.16)$$

By analogy with the potential flow components the velocity components within the boundary layer are assumed to be

$$u = \frac{U_0 r f'(y)}{(R^2 - r^2)^{1/2}} \quad (3.7.17)$$

and

$$v = \frac{-U_0 (2R^2 - r^2) f(y)}{(R^2 - r^2)^{3/2}} \quad (3.7.18)$$

where the function  $f(y)$  is to be found and the prime denotes differentiation with respect to  $y$ . The above expressions satisfy continuity identically. On substitution equation 3.7.13 becomes, with

$$r = \epsilon R \quad (3.7.19)$$

and

$$h = \frac{U_0 R^2}{(R - r^2)^{3/2}} \quad (3.7.20)$$

$$h f'^2 - h(2 - \epsilon^2) f f'' = h + v f''' \quad (3.7.21)$$

with boundary conditions

$$y = 0 : f = f' = 0 ; \quad y \rightarrow \infty : f' \rightarrow 1 \quad (3.7.22)$$

This equation cannot be solved in closed form and to aid its numerical solution the following substitutions are made

$$f(y) = \left(\frac{v}{h}\right)^{1/2} \phi(\mu) \quad (3.7.23)$$

where

$$\mu = \left(\frac{h}{v}\right)^{1/2} y \quad (3.7.24)$$

Equation 3.7.21 then becomes

$$\phi''' + (2 - \epsilon^2) \phi \phi'' - \phi'^2 + 1 = 0 \quad (3.7.25)$$

the prime now denoting differentiation with respect to  $\mu$ . The boundary conditions are :

$$\mu = 0 : \phi = \phi' = 0 ; \quad \mu \rightarrow \infty : \phi' \rightarrow 1 \quad (3.7.26)$$

Now,  $\epsilon$  varies between 0 and 1 as  $r$  varies between 0 and  $R$ . When  $\epsilon = 0$  equation 3.7.25, with its boundary conditions, is identical to that obtained by Schlichting (1960) for the infinite perpendicular disc and when  $\epsilon = 1$  the equation is identical to that obtained by him for the infinite perpendicular plate. Numerical solutions, in these cases, can be obtained around  $\mu = 0$  by using Blasius expansions, as for the parallel plate (appendix A1), though not necessarily of identical form. The variations of  $\frac{d\phi}{d\mu}$  and  $\frac{d^2\phi}{d\mu^2}$  with  $\mu$  for the infinite perpendicular plate and disc are shown in figure 3.7.3.

In solving the convective-diffusion equation values of  $\phi(\mu)$  are only required at  $\mu \sim 0$ , when

$$\phi(\mu) \sim \beta\mu^2 \quad (3.7.27)$$

For  $\epsilon = 0$ ,  $\beta = \beta_0 = 0.656$  (figure 3.7.3) and for  $\epsilon = 1$ ,  $\beta = \beta_1 = 0.616$ . It seems reasonable to assume that as  $\epsilon$  varies from 0 to 1 that  $\beta$  varies smoothly between  $\beta_0$  and  $\beta_1$ . Further,  $\beta$  appears in the expression below for  $J$  at a point as  $(\beta)^{1/3}$ , when the percentage difference caused will be even smaller. Thus,  $\beta$  will be considered to be constant.

It will be shown below that  $J$  increases as  $r$  approaches  $R$  and since the electrode is circular such regions will contribute by far the greatest proportion of the total current. Therefore, the value  $\beta_1$  is taken as that for  $\beta$  since this is most likely to be closest to the true value.

Collecting terms

$$u = \frac{U_0^{3/2} 2\beta}{R^{3/2} \sqrt{v}} \frac{yr}{(1-r^2/R^2)^{5/4}} \quad (3.7.28)$$

$$v = -\frac{U_0^{3/2} 2\beta}{R^{3/2} \sqrt{v}} y^2 \frac{(1-r^2/2R^2)}{(1-r^2/R^2)^{9/4}} \quad (3.7.29)$$

when  $r = R$  both  $u$  and  $v$  become infinite. This is to be expected because equation 3.7.13 fails at  $r = R$  when  $d^2 r(x)/dx^2$  achieves an

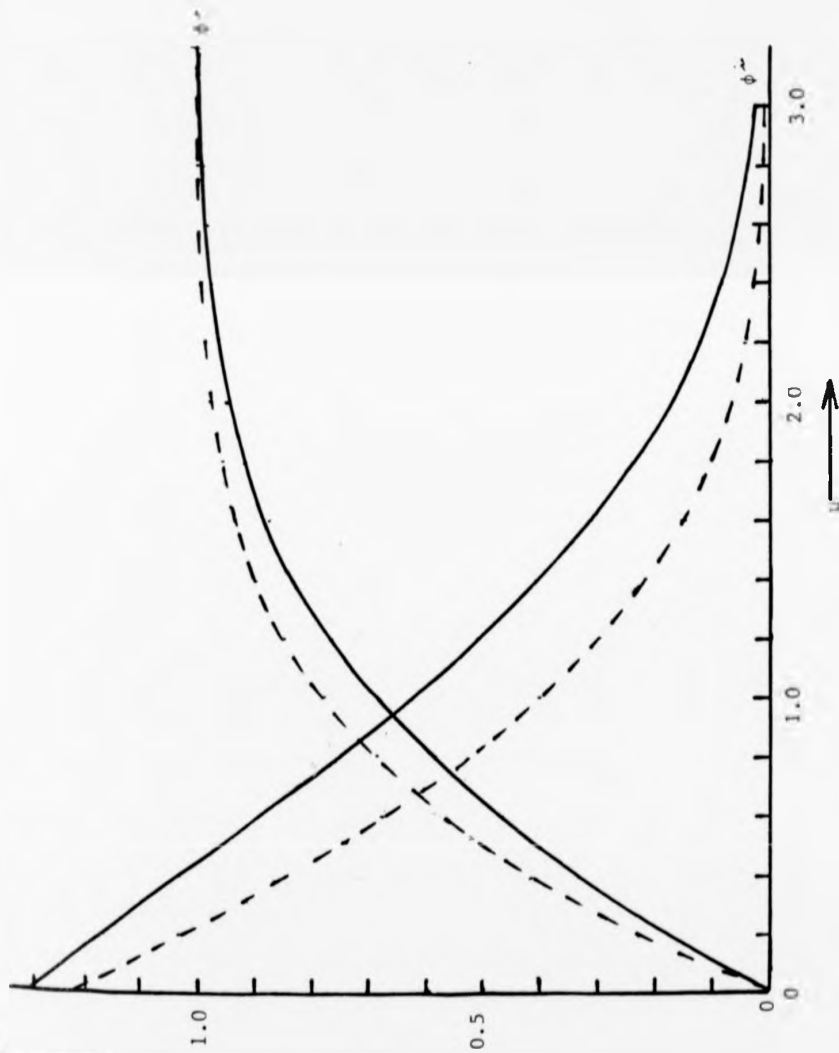


Figure 3.7.3 The variation of  $d\phi/d\nu$  and  $d^2\phi/d\nu^2$  with  $\nu$  for the infinite perpendicular disc (—) and the infinite perpendicular plate (---), from Schlichting (1960)

excessively high value. [The method (appendix A.3) applied to obtain the viscous flow components for the sphere can be applied here. Values of  $u$  and  $v$  similar to the above are obtained except at  $r = R$  when  $u$  and  $v$  do not tend to infinity because of the form of the expansions for  $u$  and  $v$  obtained. Equations 3.7.28 and 3.7.29 for  $u$  and  $v$  are thought preferable because the discontinuity is inherent to the boundary layer equations].

It is now possible to proceed with the solution of the convective-diffusion equation for the enamelled perpendicular disc. The convective-diffusion equation (equation 3.3.1) in cylindrical co-ordinates is

$$v_r \frac{\partial c}{\partial r} + v_y \frac{\partial c}{\partial y} + \frac{v_\phi}{r} \frac{\partial c}{\partial \phi} = D \left( \frac{\partial^2 c}{\partial y^2} + \frac{\partial^2 c}{\partial r^2} + \frac{1}{r} \frac{\partial c}{\partial r} + \frac{1}{r^2} \frac{\partial^2 c}{\partial \phi^2} \right) \quad (3.7.30)$$

In this case  $v_\phi \equiv 0$ ,  $\frac{\partial}{\partial \phi} \equiv 0$ ,  $v_r \equiv u$  and  $v_y \equiv v$ . Further over the entire surface, except perhaps at  $r \sim R$  when the theory breaks down,  $\frac{\partial c}{\partial y} > \frac{\partial c}{\partial r}$ .

Thus

$$u \frac{\partial c}{\partial r} + v \frac{\partial c}{\partial y} = D \frac{\partial^2 c}{\partial y^2} \quad (3.7.31)$$

with boundary conditions

$$y = 0 : c = 0 \quad ; \quad y = \infty : c = c_s \quad (3.7.32)$$

$$\text{If } v > u \text{ then } v \frac{\partial c}{\partial y} > u \frac{\partial c}{\partial x}$$

and

$$v \frac{\partial c}{\partial y} \sim D \frac{\partial^2 c}{\partial y^2} \quad (3.7.33)$$

At small  $r$  the approximation  $v > u$  is true but it becomes progressively worse as  $r$  tends to  $R$ . Assuming  $c = c(\mu)$ , equation 3.7.33 can be written in terms of  $\mu$

$$\frac{d^2 c}{d\mu^2} = -\frac{v}{D} (2 - \epsilon^2) \beta \mu^2 \frac{dc}{d\mu} \quad (3.7.34)$$

where  $r = \epsilon R$  and the boundary conditions are

$$\mu = 0 : c = 0 \quad ; \quad \mu = \infty : c = c_s \quad (3.7.35)$$

Equation 3.7.34 may be solved by integration giving

$$c(\nu) = \frac{c_s}{\int_0^{\infty} \exp\left[-\frac{\nu}{D} \frac{(2-\epsilon^2)}{3} \beta \mu^3\right] d\mu} \cdot \int_0^{\nu} \exp\left[-\frac{\nu}{D} \frac{(2-\epsilon^2)}{3} \beta \mu^3\right] d\mu \quad (3.7.36)$$

Now

$$\int_0^{\infty} e^{-(gx)^k} dx = \frac{1}{kg} \Gamma\left(\frac{1}{k}\right) \quad \text{if } g, k > 0 \quad (3.7.37)$$

(Dwight, 1961)

Therefore, using the boundary conditions and since

$$J = D \text{ me } \left. \frac{\partial c}{\partial y} \right|_{y=0} \quad (3.7.38)$$

$$J = 0.66 R^{-1/2} \text{ mec}_s D^{2/3} \nu^{-1/6} U_o^{1/2} \frac{(2-\epsilon^2)^{1/3}}{(1-\epsilon^2)^{3/4}} \quad (3.7.39)$$

At  $\epsilon = 1$ , that is  $r = R$ ,  $J \rightarrow \infty$ , which is to be expected because of the failure of the boundary layer equation 3.7.13 at the sharp edge.

The total current obtained from the disc  $I$  is obtained by integration over the available surface, the presence of an enamelled outer ring being accounted for by limiting the integration to the available area.

Thus

$$I = \int_0^{2\pi} d\theta \int_0^{\chi R} J(r) r dr = 2\pi \int_0^{\chi R} J(r) r dr \quad (3.7.40)$$

and

$$\bar{J} = \frac{I}{\pi(\chi R)^2} = \frac{1.32}{\chi} Q_1^* R^{-1/2} \text{ mec}_s D^{2/3} \nu^{-1/6} U_o^{1/2} \quad (3.7.41)$$

where

$$Q_1^* = \int_0^{\chi} \epsilon \frac{(2-\epsilon^2)^{1/3}}{(1-\epsilon^2)^{3/4}} d\epsilon \quad (3.7.42)$$

The variation of  $Q_1^*$  with  $z$  is given in figure 3.7.4 where it will be seen that at  $\chi = 1$   $Q_1^*$  becomes infinite. For a parallel electrode without enamelling (disc or plate) it will be seen that  $J$  is infinite at  $x = 0$  (equation 3.6.1), but when the integration is performed the total current is finite. Here the discontinuity in  $J$  is due to the failure of the hydrodynamic boundary layer equation (the same is true at  $x = 0$  for parallel electrodes), but the infinite value of  $\bar{J}$  for an electrode with no enamelling occurs because of the neglect of the term  $u \partial c / \partial x$  in equation 3.7.31. If this term is retained and the above method of solution is used the following solution is obtained

$$c(\mu) = \frac{c_s}{\int_0^{\mu} \exp\left[-2(1-2\epsilon^2) \frac{v}{D} \frac{\beta\mu^3}{3}\right] d\mu} \cdot \int_0^{\mu} \exp\left[-2(1-2\epsilon^2) \frac{v}{D} \frac{\beta\mu^3}{3}\right] d\mu \quad (3.7.43)$$

Comparing this expression with equation (3.7.37) shows that for  $r \geq R/\sqrt{2}$ ,  $c(\mu) = 0$  for all  $\mu$  (or  $y$ ). This contradiction means that the assumption that the concentration  $c$  is a function of  $\mu$  only, is false. Consequently, another approach to the solution of equation 3.7.31 with its boundary conditions, equation 3.7.32, is required.

[It was mentioned earlier that the method of appendix A.3 could be used to give the viscous flow components for a perpendicular disc,  $u$  and  $v$ . These values, if inserted into equation 3.7.33 do not give  $J$  infinite at  $\epsilon = 1$  or  $Q_1^*$  infinite for  $\chi = 1$  because the expansions for  $u$  and  $v$  themselves do not become infinite at  $\epsilon = 1$ ].

Appendix A.2 describes a series expansion solution of the convective-diffusion equation (3.7.31), given that the viscous flow components can be expanded in a converging series in  $x^2/R^2$ .

Equations 3.7.28 and 3.7.29 can be expanded using the binomial theorem to give

$$u = \frac{U_0^{3/2} 2B}{R^{3/2} \sqrt{v}} y r \left[ 1 + \frac{5}{4} \frac{r^2}{R^2} + \frac{45}{32} \frac{r^4}{R^4} + \dots \right] \quad (3.7.44)$$

$$v = -\frac{U_0^{3/2} 2B}{R^{3/2} \sqrt{v}} y^2 \left[ 1 + \frac{7}{4} \frac{r^2}{R^2} + \frac{81}{32} \frac{r^4}{R^4} + \dots \right] \quad (3.7.45)$$

Note, that here  $r \equiv x$ .

Comparison with equations A.2.3 and A.2.4 shows that

$$u_0 \equiv \frac{U_0^{3/2} 2B}{R^{3/2} \sqrt{v}} ; m_2 = \frac{5}{4} ; n_2 = \frac{7}{4} ; n_4 = \frac{81}{32} \quad (3.7.46)$$

Substitution of these values into equation A.2.25 gives

$$J = \frac{c_s}{\Gamma(4/3)} \left( \frac{U_0^{3/2} 2B}{R^{3/2} \sqrt{v} \cdot 3D} \right)^{1/3} me D \left[ 1 + \frac{7}{20} \frac{r^2}{R^2} + \alpha \frac{r^4}{R^4} \right] \quad (3.7.47)$$

and  $\alpha = 0.2191$  on evaluation. That is, the current density at a point for the disc can be written

$$J = 0.8325 R^{-1/2} me c_s D^{2/3} v^{-1/6} U_0^{1/2} \left( 1 + 0.35 \frac{r^2}{R^2} + 0.2191 \frac{r^4}{R^4} \right) \quad (3.7.48)$$

The reason for adopting this approach to the solution of the equation 3.7.31 is to obtain a value for  $\bar{J}$  that is finite when  $x = 1$  whilst  $J$  becomes infinite when  $\epsilon (= r/R) = 1$ . The above form of  $J$  does not satisfy the latter criterion.

However,

$$\left( 1 - r^2/R^2 \right)^{-7/20} = 1 + 0.35 \frac{r^2}{R^2} + 0.2365 \frac{r^4}{R^4} + \dots \quad (3.7.49)$$

when expanded using the binomial theorem. Equation 3.7.49 is used to replace the series in equation 3.7.48 because of the similarity between the two. Thus, it is assumed that, had an exact solution of equation 3.7.31 been possible it would have been of the form

$$J = 0.8325 R^{-1/2} \text{mec}_s D^{2/3} v^{-1/6} \frac{U_o^{1/2}}{(1-r^2/R^2)^{1/20}} \quad (3.7.50)$$

Equation 3.7.50 for J does become infinite at  $r = R$  ( $\epsilon = 1$ ). The average current density for the enamelled perpendicular disc is given by

$$\bar{J} = \frac{I}{\pi(\chi R)^2} = \frac{2}{(\chi R)^2} \int_0^{\chi R} Jrdr \quad (3.7.51)$$

with  $\epsilon = r/R$ ,

$$\bar{J} = \frac{1.67}{\chi^2} R^{-1/2} Q_1 \text{mec}_s D^{2/3} v^{-1/6} U_o^{1/2} \quad (3.7.52)$$

where

$$Q_1 = \int_0^{\chi} \epsilon(1-\epsilon^2)^{-7/20} d\epsilon = \frac{10}{13} \left[ 1 - (1-\chi^2)^{13/20} \right] \quad (3.7.53)$$

The integral  $Q_1$  is dimensionless and its variation with  $\chi$  is shown in figure 3.7.4, where it is also compared with  $Q_1^*$ .

Thus the shape factor may be written

$$S = \frac{1.67}{\chi^2} Q_1 R^{-1/2} \quad (3.7.54)$$

S is, as for the parallel disc, a function of the degree of enamelling.

If  $\chi = 1$ , that is there is no enamel, then  $Q_1 = 10/13$  and the shape factor becomes

$$S = 1.28 R^{-1/2}$$

So, the criteria above, for a satisfactory solution of equation 3.7.31 are satisfied. That is J becomes infinite when  $\epsilon = 1$ , yet the average current density is finite when there is no enamelling as must be the case physically.

when expanded using the binomial theorem. Equation 3.7.49 is used to replace the series in equation 3.7.48 because of the similarity between the two. Thus, it is assumed that, had an exact solution of equation 3.7.31 been possible it would have been of the form

$$J = 0.8325 R^{-1/2} \text{mec}_s D^{2/3} v^{-1/6} \frac{U_o^{1/2}}{(1-r^2/R^2)^{7/20}} \quad (3.7.50)$$

Equation 3.7.50 for J does become infinite at  $r = R$  ( $\epsilon = 1$ ). The average current density for the enamelled perpendicular disc is given by

$$\bar{J} = \frac{I}{\pi(\chi R)^2} = \frac{2}{(\chi R)^2} \int_0^{\chi R} Jrdr \quad (3.7.51)$$

with  $\epsilon = r/R$ ,

$$\bar{J} = \frac{1.67}{\chi^2} R^{-1/2} Q_1 \text{mec}_s D^{2/3} v^{-1/6} U_o^{1/2} \quad (3.7.52)$$

where

$$Q_1 = \int_0^{\chi} \epsilon(1-\epsilon^2)^{-7/20} d\epsilon = \frac{10}{13} \left[ 1 - (1-\chi^2)^{13/20} \right] \quad (3.7.53)$$

The integral  $Q_1$  is dimensionless and its variation with  $\chi$  is shown in figure 3.7.4, where it is also compared with  $Q_1^*$ .

Thus the shape factor may be written

$$S = \frac{1.67}{\chi^2} Q_1 R^{-1/2} \quad (3.7.54)$$

S is, as for the parallel disc, a function of the degree of enamelling.

If  $\chi = 1$ , that is there is no enamel, then  $Q_1 = 10/13$  and the shape factor becomes

$$S = 1.28 R^{-1/2}$$

So, the criteria above, for a satisfactory solution of equation 3.7.31 are satisfied. That is J becomes infinite when  $\epsilon = 1$ , yet the average current density is finite when there is no enamelling as must be the case physically.

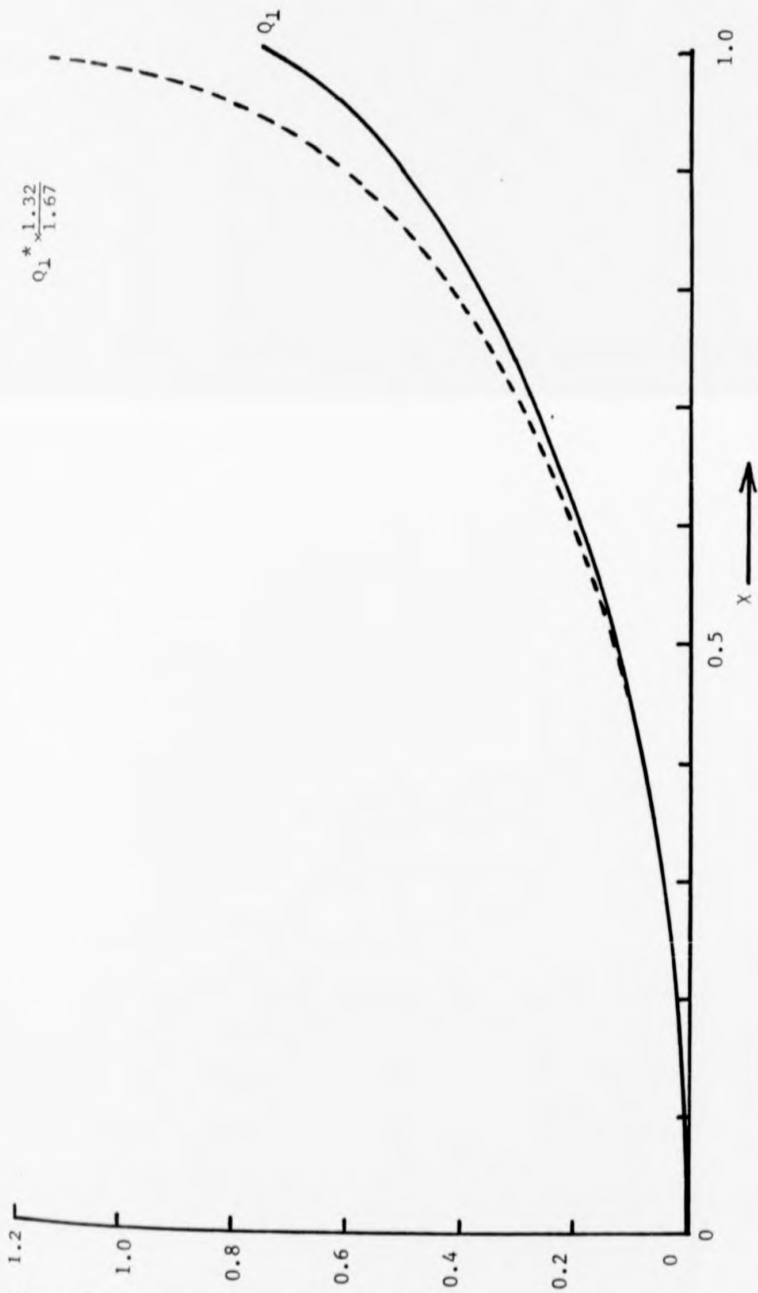


Figure 3.7.4 The variations of  $Q_1$  and  $Q_1^*$  with  $x$

### 3.8 The Calculation of the Current Response of a Sphere

The geometry and co-ordinate system used are shown in figure 3.4.1 and 3.8.1. In this co-ordinate system the potential flow component  $U$  in the  $x$ -direction is (Schlichting 1960)

$$U = \frac{3}{2} U_0 \sin \left( \frac{x}{R} \right) \approx \frac{3}{2} U_0 \left( \frac{x}{R} - \frac{x^3}{R^3 \cdot 3!} + \frac{x^5}{R^5 \cdot 5!} - \dots \right) \quad (3.8.1)$$

The body contour,  $r(x)$ , is

$$r(x) = R \sin \left( \frac{x}{R} \right) \approx R \left( \frac{x}{R} - \frac{x^3}{R^3 \cdot 3!} + \frac{x^5}{R^5 \cdot 5!} - \dots \right) \quad (3.8.2)$$

Comparison of these equations with equations A.3.6 and A.3.7 gives the values of the coefficients used in equation A.3.9, A.3.10 and A.3.11.

That is, the stream function is

$$\psi(x, y) = \sqrt{\frac{\nu R}{3U_0}} \left( \frac{3}{2} \frac{U_0}{R} x f_1(\mu) - \frac{U_0 x^3}{2R^3} f_3(\mu) + \frac{3}{80} \frac{U_0 x^5}{R^5} f_5(\mu) - \dots \right) \quad (3.8.3)$$

with

$$f_3 = g_3 + h_3 \quad (3.8.4)$$

and

$$f_5 = g_5 + h_5 + \frac{10}{3} (k_5 + j_5 + q_5) \quad (3.8.5)$$

Figure 3.8.2 shows the variations of  $df_1/d\mu$ ,  $df_3/d\mu$  and  $df_5/d\mu$  with  $\mu$ .

At small  $\mu$  (or  $y$ ), which is the region of interest here for the solution of the convective-diffusion equation, each of the derivatives is proportional to  $\mu$ . That is, at small  $\mu$ , it is possible to write

$$f_1 \approx \alpha_1 \mu^2 ; f_3 \approx \alpha_3 \mu^2 ; f_5 \approx \alpha_5 \mu^2 \quad (3.8.6)$$

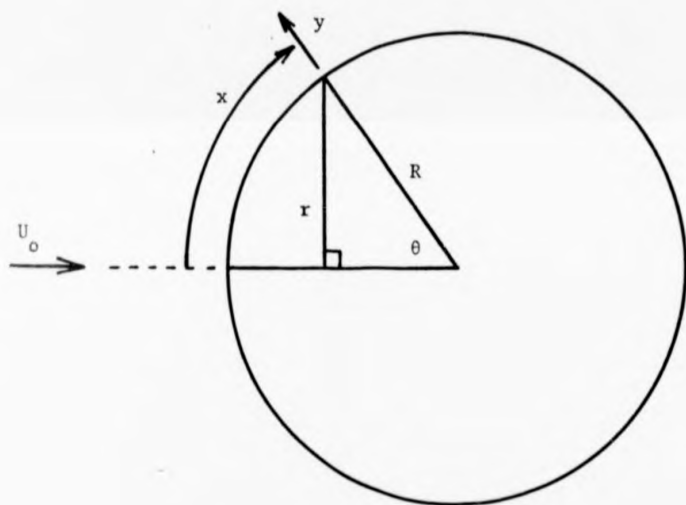


Figure 3.8.1 The sphere.

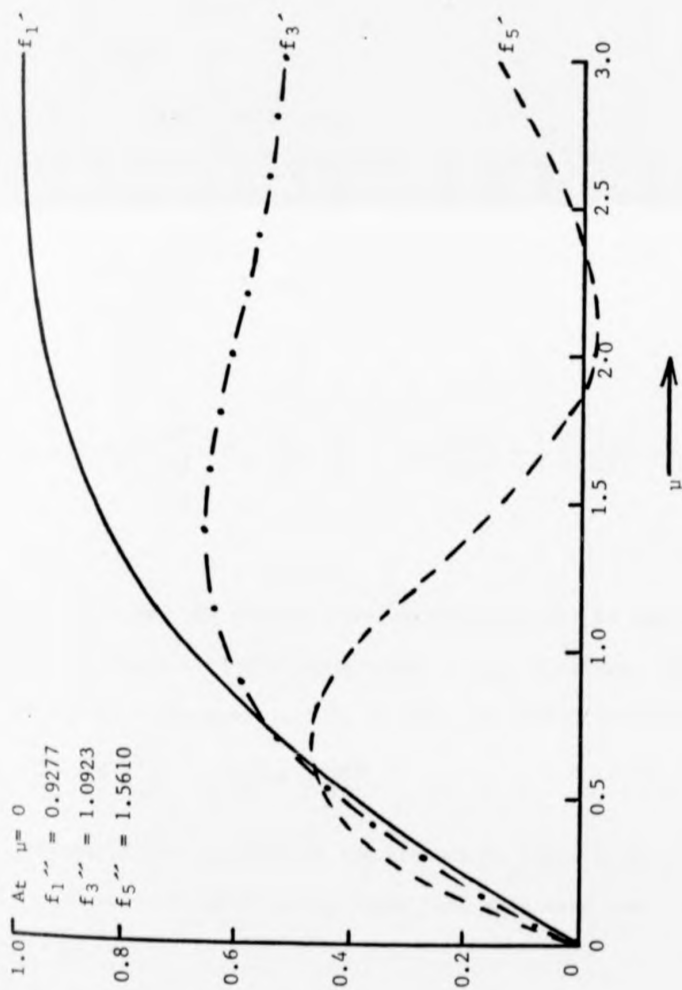


Figure 3.8.2 The variation of  $df_1/d\mu$ ,  $df_3/d\mu$  and  $df_5/d\mu$  with  $\mu$  adapted from Schlichting (1960).

The stream function  $\psi(x, y)$  now becomes, for small  $y$ ,

$$\psi(x, y) \approx \frac{3^{3/2} U_0^{3/2} \alpha_1}{2R^{3/2} \nu^{1/2}} y^2 x \left( 1 - \frac{1}{3} \left( \frac{x}{R} \right)^2 \frac{\alpha_3}{\alpha_1} + \frac{1}{40} \left( \frac{x}{R} \right)^4 \frac{\alpha_5}{\alpha_1} \dots \right) \quad (3.8.7)$$

Then, using the properties of the stream function, that is

$$u = \frac{\partial \psi}{\partial y} \quad (3.8.8)$$

and

$$v = -\frac{1}{r} \frac{\partial(\psi r)}{\partial x} \quad (3.8.9)$$

the viscous flow components at small  $y$  are

$$u = \frac{3^{3/2} U_0^{3/2} \alpha_1}{R^{3/2} \nu^{1/2}} y x \left( 1 - \frac{1}{3} \left( \frac{x}{R} \right)^2 \frac{\alpha_3}{\alpha_1} + \frac{1}{40} \left( \frac{x}{R} \right)^4 \frac{\alpha_5}{\alpha_1} \dots \right) \quad (3.8.10)$$

$$v = -\frac{y^2 3^{3/2} U_0^{3/2}}{R^{3/2} \nu^{1/2}} \frac{\alpha_1}{2} F(x) \quad (3.8.11)$$

where

$$F(x) = 1 - \frac{\alpha_3}{\alpha_1} \left( \frac{x}{R} \right)^2 + \frac{1}{8} \left( \frac{x}{R} \right)^4 \frac{\alpha_5}{\alpha_1} + \text{ctn} \left( \frac{x}{R} \right) \left[ \frac{x}{R} - \frac{1}{3} \frac{\alpha_3}{\alpha_1} \left( \frac{x}{R} \right)^3 + \frac{1}{40} \left( \frac{x}{R} \right)^5 \frac{\alpha_5}{\alpha_1} \right] \quad (3.8.12)$$

Now, having obtained the viscous flow components close to the surface of the sphere the convective-diffusion equation can be solved. The convective-diffusion equation (equation 3.3.3) in spherical polar co-ordinates is

$$v_r \frac{\partial c}{\partial r} + \frac{v_\theta}{r} \frac{\partial c}{\partial \theta} = D \left( \frac{\partial^2 c}{\partial r^2} + \frac{2}{r} \frac{\partial c}{\partial r} \right) \quad (3.8.13)$$

where, because of the symmetry of the situation, there is no azimuthal variation and terms in  $\partial/\partial\theta$  on the right hand side have been neglected since  $\frac{\partial c}{\partial r} > \frac{\partial c}{\partial \theta}$ .

In the co-ordinate system used here the convective-diffusion equation becomes

$$u \frac{\partial c}{\partial x} + v \frac{\partial c}{\partial y} = D \left( \frac{\partial^2 c}{\partial y^2} + \frac{2}{R} \frac{\partial c}{\partial y} \right) \quad (3.8.14)$$

since for small  $y$

$$r = R + y \approx R \quad \text{and} \quad \theta = x/R$$

Further, at small  $y$ ,  $\frac{\partial^2 c}{\partial y^2} \gg \frac{2}{R} \frac{\partial c}{\partial y}$  and the convective-diffusion equation becomes

$$u \frac{\partial c}{\partial x} + v \frac{\partial c}{\partial y} = D \frac{\partial^2 c}{\partial y^2} \quad (3.8.15)$$

with boundary conditions

$$y = 0 : c = 0 \quad ; \quad y + \infty : c \rightarrow c_s$$

Transforming equation 3.8.15 into terms of  $\mu$ , that is assuming  $c = c(\mu)$ , to aid its solution fails because of two reasons. The first is that  $\mu$  is not a function of  $x$  and therefore the term  $u \frac{\partial c}{\partial x}$  is lost. The second is that  $F(x)$  becomes negative for  $x/R \approx 68.5^0$  leading to a similar contradiction to that encountered in equation 3.7.43.

Appendix A.2 describes a series expansion solution of the convective-diffusion equation (3.8.15), given that the viscous flow components can be expanded in a converging series in  $x^2/R^2$ . It is, therefore, necessary to expand the cotangent term in  $F(x)$  (3.8.12) giving

$$u = \frac{3^{3/2} U_0^{3/2} \alpha_1}{R^{3/2} \nu^{1/2}} y x \left( 1 - \frac{1}{3} \left( \frac{x}{R} \right)^2 \frac{\alpha_3}{\alpha_1} + \frac{1}{40} \left( \frac{x}{R} \right)^4 \frac{\alpha_5}{\alpha_1} \right) \quad (3.8.16)$$

$$v = - \frac{3^{3/2} U_0^{3/2} \alpha_1}{R^{3/2} \nu^{1/2}} y^2 \left( 1 - \frac{1}{2} \left( \frac{x}{R} \right)^2 \left( \frac{4}{3} \frac{\alpha_3}{\alpha_1} + \frac{1}{3} \right) + \left( \frac{x}{R} \right)^4 \frac{1}{2} \left( \frac{3}{20} \frac{\alpha_5}{\alpha_1} + \frac{1}{4} \cdot \frac{\alpha_3}{\alpha_1} - \frac{1}{45} \right) \right) \quad (3.8.17)$$

From figure 3.8.2  $\alpha_1 = 0.464$  ;  $\alpha_3 = 0.546$  ;  $\alpha_5 = 0.781$ . Substitution of these values into equations 3.8.16 and 3.8.17 and comparison with equations A.2.3 and A.2.4 shows that

$$u_0 = \frac{3^{3/2} U_0^{3/2} \alpha_1}{R^{3/2} \nu^{1/2}} \quad ; \quad m_2 = -0.393 \quad ; \quad n_2 = -0.952 \quad ; \quad n_4 = 0.181 \quad (3.8.18)$$

Substitution of these values into equation A.2.25 gives the current density at a point on the sphere as

$$J = \frac{c_s}{\Gamma(4/3)} \left( \frac{3^{3/2} U_0^{3/2} \alpha_1}{R^{3/2} \nu^{1/2} 3D} \right)^{1/3} \text{meD} \left( 1 - 0.190 \left( \frac{x}{R} \right)^2 - 7.31 \times 10^{-4} \left( \frac{x}{R} \right)^4 \right) \quad (3.8.19)$$

that is

$$J = 1.04 R^{-1/2} \text{mec}_s D^{2/3} \nu^{-1/6} U_0^{1/2} \left( 1 - 0.190 \theta^2 - 7.31 \times 10^{-4} \theta^4 \right) \quad (3.8.20)$$

since  $x = \theta R$

The hydrodynamic boundary layer separates from the surface of the sphere at  $\theta = \theta_s = 109.6^\circ$  (Schlichting 1960). After the separation point the diffusion layer is considered to be infinite. Consequently, when calculating the total current output the integration is curtailed at  $\theta = \theta_s$  and the total output current becomes

$$I = \int_0^{\theta_s} 2\pi R^2 J(\theta) \sin \theta d\theta \quad (3.8.21)$$

or

$$I = 2\pi R^{3/2} \times 1.04 \text{mec}_s D^{2/3} \nu^{-1/6} U_0^{1/2} \times \int_0^{\theta_s} \left( 1 - 0.190 \theta^2 - 7.31 \times 10^{-4} \theta^4 \right) \sin \theta d\theta \quad (3.8.22)$$

The value of the integral is 0.921. In calculating the average current density the total area of the sphere is used, since this is available even if its contributions to the total are negligible. Therefore, the average current density is

$$\bar{J} = \frac{I}{4\pi R^2} = 0.48 R^{-1/2} \text{mec}_s D^{2/3} \nu^{-1/6} U_0^{1/2} \quad (3.8.23)$$

and the shape factor for the sphere is

$$S = 0.48 R^{-1/2} \quad (3.8.24)$$

### 3.9 Discussion

#### 3.9.1 General

The theoretical description applies only to laminar flow in the hydrodynamic boundary layer. Levich (1962) predicts that for turbulent flow the current would vary with the flow velocity raised to some power between  $1/2$  and  $1$ . The theory also assumes ideal conditions, not necessarily easily achievable in practice. That is the geometry is exactly as stated, the electrode surface is totally smooth, and the surface reactivity is constant (that is the concentration of oxygen at the electrode is everywhere zero) except where stated.

A major difference exists in the descriptions of parallel and perpendicular electrodes arising from the different regions which give the largest current density since they have the thinnest diffusion layer (figure 3.9.1). For parallel electrodes it is possible to use a semi-infinite theory and then limit the integration since the downstream regions contribute progressively less of the total current. For perpendicular electrodes the current density  $J$  increases away from the stagnation point towards the edges. This precludes the use of a theory based upon infinite electrodes when the current density would be constant with position.

A further difference between parallel and perpendicular electrodes is the way the existence of enamelling is accounted for. In the case of perpendicular electrodes the enamelling is allowed for simply by limiting the integration over the surface to the metal area. For parallel electrodes the enamelling radically changes the boundary conditions.

Spherical electrodes are very similar to perpendicular ones in that they also possess a stagnation point and the solution of the convective-diffusion equation for both is similar. For spheres, however, no problem arises because of sharp edges and the diffusion layer is at its thinnest at the stagnation point, increasing away from it.

The electrodes shown in table 3.5.1, other than the sphere and enamelled discs, are very difficult to implement in practice and thus little work has been done to confirm these expressions. The results for these electrodes should, therefore, be regarded as intermediates in, or by products of, the results for the enamelled discs. Similarly, the results given in Prytherch and Smith (1979) should be considered interim, the perpendicular electrode values quoted there being obtained from an initial, more approximate theory. This accounts for the incorrect assertion that enamelling has only a small effect.

### 3.9.2 Electrodes parallel to the flow

Figures 3.9.1 and 3.9.2 show the variation of  $\delta$  and  $\delta_h$  with position, for the parallel plate, with and without enamelling. The definition of  $\delta$  is given by equation 3.3.7, whilst  $\delta_h$  is that value of  $y$  at which the viscous flow parallel to the surface  $u$  becomes ninety nine per cent of the potential flow parallel to the surface  $U$ . For the enamelled plate it is necessary to go considerably downstream before  $\delta$  approaches the value it would have had if not for the enamelling. So, whilst the total current from an enamelled electrode will be smaller here, the current density at each point is larger. For the parallel plate  $\delta$  is  $\sim \delta_h/10$ , as stated earlier.

For the parallel plate (and therefore the disc) Prandtl's boundary layer equation does not apply very close to the leading edge since the underlying assumption, that  $|\partial^2 u / \partial y^2| \ll |\partial^2 v / \partial y^2|$ , no longer applies there (Schlichting 1960). At, and near to, the leading edge an accurate description can only be obtained by the application of the full Navier-Stokes equations. Near the leading edge the failure of Prandtl's equation probably only leads to an inaccurate coefficient in the expression for the current density at that point, whilst giving the correct functional variation with free stream velocity  $U_0$ . However, at the leading edge, that is at  $x = 0$ , the insufficiency of the Prandtl equation leads to the

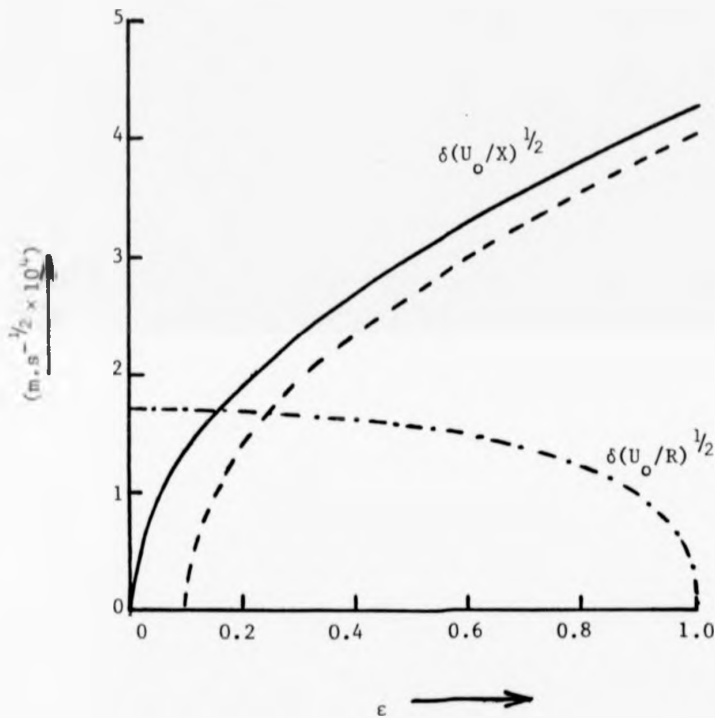
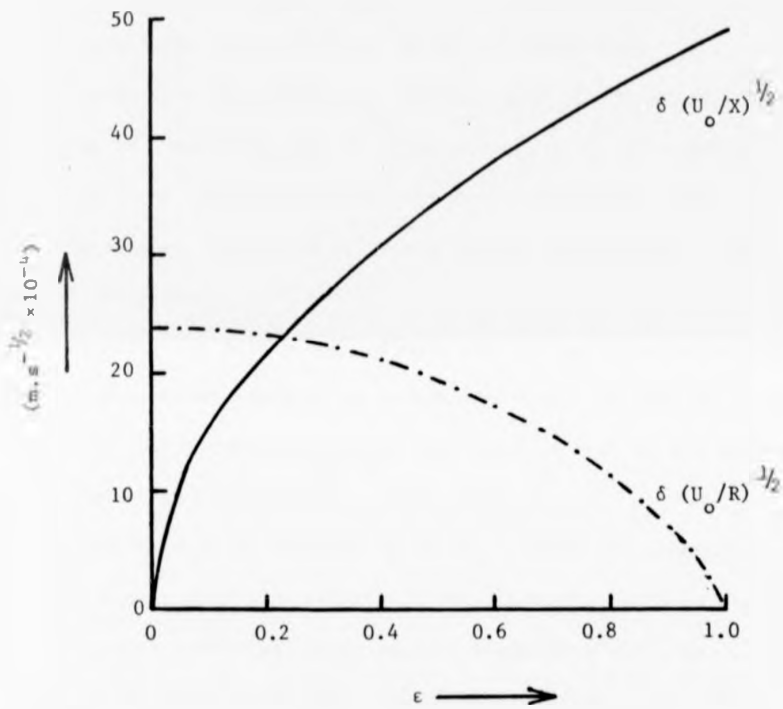


Figure 3.9.1 The variation of diffusion layer thickness  $\delta$  with position, for the parallel plate with (----) and without (—) enamelling and the perpendicular disc (-.-.-),  $\nu = 10^{-6} \text{m}^2 \cdot \text{s}^{-1}$ ;  $D = 3 \times 10^{-9} \text{m}^2 \cdot \text{s}^{-1}$ ;  $h = X/10$ .



**Figure 3.9.2** The variation of hydrodynamic boundary layer thickness  $\delta_h$  with position for the parallel plate (—) and the perpendicular disc (---).  
 $\nu = 10^{-6} m^2 \cdot s^{-1}$ .

predicted current density being infinite. Whilst physically that is incorrect, in practice it is of little consequence since the infinite current density only exists over an infinitesimally small area and the infinity therefore vanishes upon integration. If the electrode area does not extend to the leading edge, that is it is enamelled, then the failure of the boundary layer equation there is of no consequence.

The unenamelled electrode is a limiting case of the enamelled disc. As the degree of enamelling goes to zero, that is  $\chi \rightarrow 1$  in equation 3.6.5, the predicted output current smoothly approaches the finite value for no enamelling (figure 3.6.4) and is thus a further indication of the adequacy of the theory.

The theories for finite and infinite plates, parallel or perpendicular to the flow, assume the plate to be infinitely wide. In practice this means they must be of sufficient width that edge effects in the  $z$ -direction can be ignored, that is  $Z \gg X$ .

The parallel disc is obtained by integration of the expression for the parallel plate, when edge effects at the boundaries between elemental plates are assumed infinitesimally small. Enamelling will, again, decrease the impact of any  $z$ -direction edge effects at the sides of the disc. The expression for the parallel disc, unlike that for the perpendicular disc, is, therefore, obtained indirectly, being derived from the parallel plate instead of by solution of the full convective-diffusion equation including the term  $w\partial c/\partial z$  ( $w$  is the viscous flow component in the  $z$ -direction). The neglect of the term  $w\partial c/\partial z$  is reasonable, since for the parallel disc  $w$  will be much less than  $u$  or  $v$ .

### 3.9.3 Electrodes perpendicular to the flow

Figures 3.9.1 and 3.9.2 also show the variation of  $\delta$  and  $\delta_h$  with position for the perpendicular disc. For the perpendicular disc the diffusion layer and the hydrodynamic layer are symmetrical, being thinnest at

the edges, whilst for the parallel electrodes they are asymmetric being thinnest at the leading edge. The leading edge of a parallel electrode may be regarded as its initial point at which the diffusion layer has its minimum value. The initial point for a perpendicular disc (or plate) is the stagnation point which is the centre of the electrode where the diffusion layer is thickest. For the perpendicular plate  $\delta \approx \delta_H/10$ , again.

As for the parallel plate the hydrodynamic boundary layer equations do not hold for all points on the surface of the perpendicular disc (or plate). The boundary layer equations fail at sharp edges, when  $d^2r(x)/dx^2$  becomes large (Rosenhead 1963). Therefore, a discontinuity (infinity) is expected at  $r = R$  ( $\epsilon = 1$ ) for the disc. The method of obtaining the viscous flow outlined in appendix A.3 (and used for the sphere) is rejected for the disc since because of its series form, it fails to give infinite  $u$  and  $v$  at  $\epsilon = 1$  and further the values of  $u$  and  $v$  given as  $\epsilon$  approaches unity will not be accurate because of the limited number of terms in the series. Therefore, for the disc (the form given in appendix A.3 is adequate for the sphere since there are then no sharp edges) the viscous flow components are obtained by the method of section 3.7.

Having obtained the viscous flow components close to the reaction surface several different approaches can be taken to the solution of the convective-diffusion equation. It is necessary to establish criteria to be met by a particular solution if it is to be considered satisfactory. These are taken to be those already met by the solution of the convective-diffusion equation obtained for the parallel plate and disc. First the current density at the edge ( $\epsilon = 1$ ) of the disc (or plate) must be infinite, a required consequence of the infinite values of  $u$  and  $v$  there. Second, the total output current obtained by integrating the current density  $J$  over the entire surface, that is for no enamelling, must be finite. Therefore, the expression obtained for the current density at a point must be of such a form that the infinity at  $\epsilon = 1$  exists only for an infinitesimally small extent. Two solutions to the convective-

diffusion equation for the disc are given in section 3.7, the first meeting only the first criteria, the second both.

The first method of solution assumes that the concentration  $c$  is a function of the dimensionless variable  $\mu$  only. A consistent solution is then possible if the term  $u\partial c/\partial x$  is neglected compared to the term  $v\partial c/\partial y$  and equation 3.7.31 becomes equation 3.7.33. For all electrodes, when the concentration of oxygen is zero at the surface,  $\partial c/\partial y \gg \partial c/\partial x$  and therefore  $u\partial c/\partial x \ll v\partial c/\partial y$  if  $v \gg u$ . This last assumption is true at the centre of the disc but becomes progressively worse as  $\epsilon$  approaches 1. Solution of equation 3.7.33 gives a predicted current density accurate close to the stagnation point (centre of the disc), but becoming progressively less so as  $\epsilon$  approaches 1. Figure 3.9.3 shows the variation of the diffusion layer, predicted by this approach, with position. At small  $\epsilon$   $\delta$  is almost constant, since the theory for a disc of infinite extent, which leads to a diffusion layer thickness constant with position, applies near to the centre of the disc. The solution to equation 3.7.33, equation 3.7.39, may be regarded as a first order correction to applying the theory for an infinite disc to a finite one.

The predicted current density (equation 3.7.39) is infinite at  $\epsilon = 1$  and, therefore, satisfies the first criterion. However, because of the neglect of  $u\partial c/\partial x$  in equation 3.7.33, equation 3.7.39 is of such a form that, when integrated over the surface of the electrode to  $\chi = 1$  (no enamelling), the predicted output current (equation 3.7.41) is infinite and so the second criterion is not satisfied. This model, whilst not successful, is useful as a guide to the accuracy of any other model, since both should agree near the stagnation point.

It is necessary, therefore, to retain the term  $u\partial c/\partial x$ , but doing so and assuming  $c = c(\mu)$  leads to a contradiction (equation 3.7.43). A series method of solution of equation 3.7.31 (appendix A.2) was found successful, the number of terms in the expansion being limited only by the practicalities of the algebra. The expression obtained for the

current density, equation 3.7.47, is in series form and so does not satisfy the first criterion above. However, the use of the approximation given in equation 3.7.49 leads to equation 3.7.50 which does satisfy the criterion. Equation 3.7.47, because of the limited number of terms in the series is increasingly inaccurate as  $\epsilon$  approaches 1, (for example it does not become infinite at  $\epsilon = 1$ ). It seems likely, in view of the accuracy of equation 3.7.49 that if a complete solution to equation 3.7.31 had been possible, it would have been of the form given by equation 3.7.50. Even if this is not so, any error caused by the use of equation 3.7.49 will be small.

Upon integration of equation 3.7.50 over the electrode surface for the case of no enamelling ( $\chi = 1$ ) the output current obtained is finite and so this model satisfies both criteria. Some support for the accuracy of this model is given by figure 3.7.4 and figure 3.9.3. Figure 3.7.4 compares  $Q_{\perp}$  with a form of  $Q_{\perp}^*$  normalised so as to remove the differences in coefficients of the respective shape factors. Over much of the range of  $\epsilon$ ,  $Q_{\perp}$  and  $Q_{\perp}^*$  are identical, that is they agree well in the region where the theory neglecting  $u\partial c/\partial x$  is known to be accurate and diverge where it is known to be inaccurate. Figure 3.9.3 compares the variations of the diffusion layers, predicted by the two models, with  $\epsilon$ . Again, the two models agree well at small  $\epsilon$ , where they should, the main difference being that at larger  $\epsilon$  the diffusion layer from the model neglecting  $u\partial c/\partial x$  is smaller.

Any inaccuracy that does exist in the preferred form of solution will be greatest as  $\epsilon$  approaches unity, but in practice the existence of enamelling will greatly diminish the effects of any such error.

One last point remains. The way the enamelling is accounted for means that any diffusion of oxygen back from the oxygen depleted solution above the enamelled region to the active surface has been neglected as this effect is almost certainly negligible.

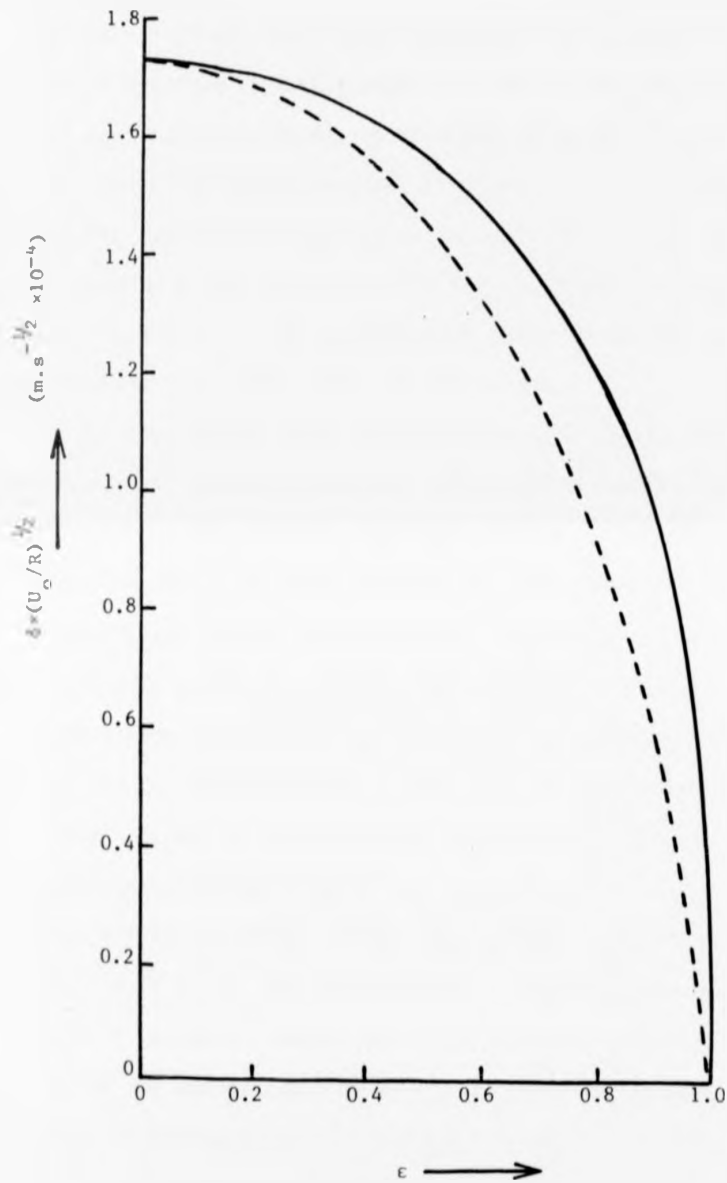


**Figure 3.9.3** Comparison of the variations of  $\delta$ , for the perpendicular disc, predicted by including (----) and excluding (—) the term  $u \frac{dc}{dx}$  in the convective diffusion equation  
 $v = 10^{-6} \text{m}^2 \cdot \text{s}^{-1}$ ;  $D = 3 \times 10^{-9} \text{m}^2 \cdot \text{s}^{-1}$

#### 3.9.4 The spherical electrode

Spherical electrodes are similar in several ways to perpendicular discs. Both types of electrode possess a stagnation point around which the diffusion layer is relatively constant in thickness (figures 3.9.1, 3.9.4). For the sphere though, the diffusion layer is thinnest at the stagnation point, whilst for the perpendicular disc it is thickest there. Also, the same method of solution of the convective-diffusion equation is necessary for both types. Again, as for the perpendicular disc, the assumption  $c = c(\nu)$  does not hold for the reasons given in section 3.8.

There is no problem of sharp edges reducing the region of applicability of the hydrodynamic boundary equations, and the method of appendix A.3 is used to find the viscous flow components near to the surface. The viscous flow components are then inserted into the general solution of the convective-diffusion equation (appendix A.2), to give an expression for the current density at a point J in series form (equation 3.8.20).

For the sphere, there is no need to use an approximation like that of equation 3.7.49 for the perpendicular disc since no discontinuity is required. The convoluted origins of  $u$  and  $v$  almost preclude a sensible form of this type of approximation being found.

It is difficult to comment, other than generally, upon the accuracy of equation 3.8.20 for J. The accuracy will be best at small values of  $\theta$ , decreasing as  $\theta$  increases. Separation of the viscous boundary layer from the surface of the sphere occurs at  $\theta = \theta_g = 109.6^\circ$  (Schlichting 1960). Past  $\theta_g$  both the viscous boundary layer and the diffusion layer are considered infinite. Therefore, the largest value of  $\theta$  inserted into equation 3.8.20 will be approximately 2 radians. (A discontinuity exists in equation 3.8.20 for J at  $\theta \sim 130^\circ$  but since this occurs after separation it is of no consequence). For  $\theta \sim 2$  rad the third term in equation 3.8.20 is less than 2% of the second. Whilst this is not absolute proof, it does imply equation 3.8.20 converges so rapidly that two terms are sufficient, even

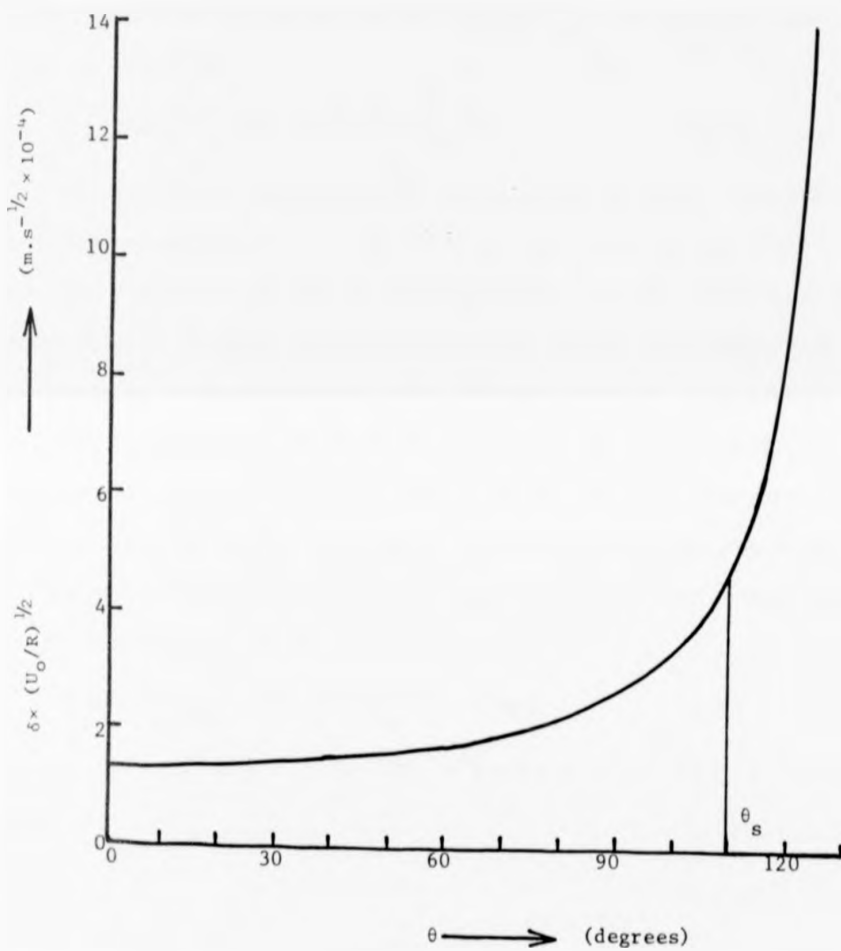


Figure 3.9.4 The variation of diffusion layer thickness  $\delta$ , with position  $\theta$  for the sphere.

$$\nu = 10^{-6} \text{m}^2 \cdot \text{s}^{-1}; \quad D = 3 \times 10^{-9} \text{m}^2 \cdot \text{s}^{-1}.$$

at the largest relevant value of  $\theta$ .

Further support for this model of spherical electrodes is obtained by comparison with the expression obtained by Matsuda (1967) for the current density at a point on the surface of a sphere. In the symbolism used here, Matsuda found:

$$J = 1.04 R^{-1/2} \text{mec}_s D^{2/3} \nu^{-1/6} U_0^{1/2} \quad (3.9.1)$$

This equation is independent of position and can only, therefore, be applied to regions where  $\delta$  and  $J$  are approximately constant with position, that is within  $23^\circ$  of the stagnation point (for 3% accuracy, figure 3.9.4). At small values of  $\theta$  equation 3.8.20, which applies to all points up to the separation point, becomes identical to equation 3.9.1.

The importance, to the total output current (equation 3.8.22), of any inaccuracy in equation 3.8.20 at large  $\theta$  is decreased to some extent by the fact that  $J$  is smaller at large  $\theta$ . However, the current contribution  $dI$  from each elemental segment of the sphere's surface also varies with  $\theta$ . The definition of  $dI$  is

$$dI = R^{-1/2} \text{mec}_s D^{2/3} \nu^{-1/6} U_0^{1/2} \times 2.08\pi R \times \\ (1 - 0.190 \theta^2 - 7.31 \times 10^{-4} \theta^4) \sin \theta d\theta \quad (3.9.2)$$

where

$$I = \int_0^{\theta_s} dI \quad (3.9.3)$$

The variation of  $\delta$  and  $dI$  with  $\theta$  are shown in figures 3.9.4 and 3.9.5. Whilst  $\delta$  continually increases with  $\theta$  (becoming infinite at  $\theta \sim 130^\circ$  and negative thereafter)  $dI$  has a maximum at  $\theta \sim 60^\circ$ . At  $\theta \sim 60^\circ$  the third term in equation 3.8.20 is far less than 1% of the second, and equation 3.8.20 must be considered accurate here, this point being relatively close to the stagnation point.

Past the separation point  $\theta_s$  there must still be some current contributed to the total since this part of the sphere is also in contact

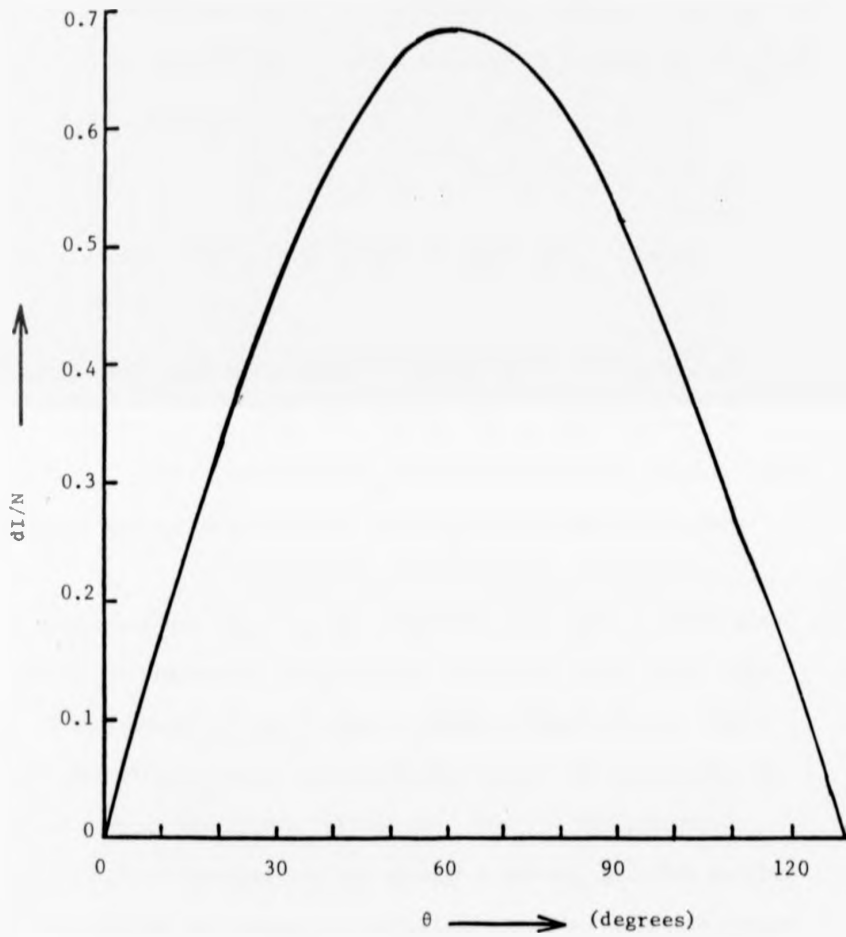


Figure 3.9.5 The variation of  $dI$  with  $\theta$

$$N = (R^{-1/2} \text{mec} D^{2/3} v^{-1/6} U_o^{1/2}) \times 2\pi R \times 1.041 d\theta$$

(equation 3.9.2)

with the oxygenated solution. It is, however, assumed to be negligible.

Therefore, the integration of equation 3.8.20 over the surface, to obtain the total current output, is curtailed at  $\theta_s$ , which is taken to be  $109.6^\circ$  (Schlichting 1960). To illustrate the effects of any inaccuracy in  $\theta_s$ , it is possible to define the average current density  $\bar{j}$  as

$$\bar{j} = \frac{I}{4\pi R^2} = 0.52 Q_s R^{-1/2} \text{mec}_s D^{2/3} \nu^{-1/6} U_o^{1/2} \quad (3.9.4)$$

where

$$Q_s = \int_0^{\theta_s} (1 - 0.190 \theta^2 - 7.31 \times 10^{-4} \theta^4) \sin \theta \, d\theta \quad (3.9.5)$$

The variation of  $Q_s$  with  $\theta_s$  is shown in figure 3.9.6. A ten degree increase or decrease in  $\theta_s$ , from 109 degrees causes approximately a 5% change in  $Q_s$ . Any dependence of  $Q_s$  upon the free stream velocity would be seen in the experimental results, but no such dependence has been observed.

The analysis given for a sphere assumes the electrode to be a complete sphere. In practice a connection to the sphere must exist. The geometry of the spheres actually used is shown in figure 3.9.7. The electrodes used clinically had a considerable extent of epoxy resin to minimise the risk of the sphere falling off, into the CSF pathways.

Figure 3.9.8a is a cross-section through a sphere, parallel to the flow. Figure 3.9.8b is a slice, at any point, through the sphere perpendicular to the flow. The profile of the epoxy resin is idealised in figures 3.9.8a and 3.9.8b, that is it is assumed to be infinitely thin and to follow exactly the surface of the sphere. This idealised profile is also assumed in the following analysis.

Two separate cases exist. The extent of epoxy resin given by  $\theta_c$ , either does or does not extend beyond the separation point  $\theta_s$ . In the electrodes used the epoxy resin always extended beyond  $\theta_s$  and this is the only case considered. Therefore, to obtain the total current two

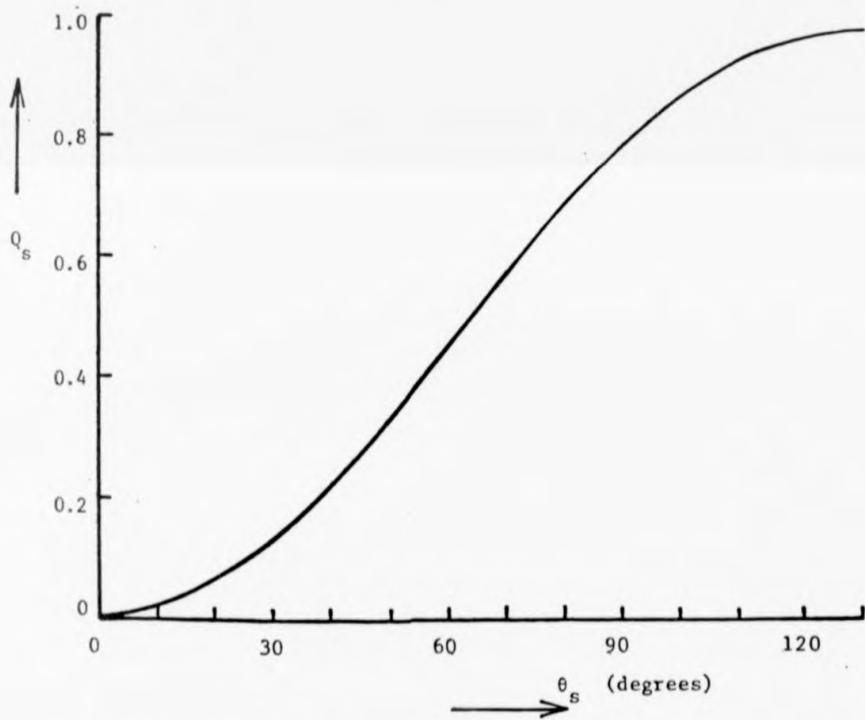


Figure 3.9.6 The variation of  $Q_s$  with  $\theta_s$

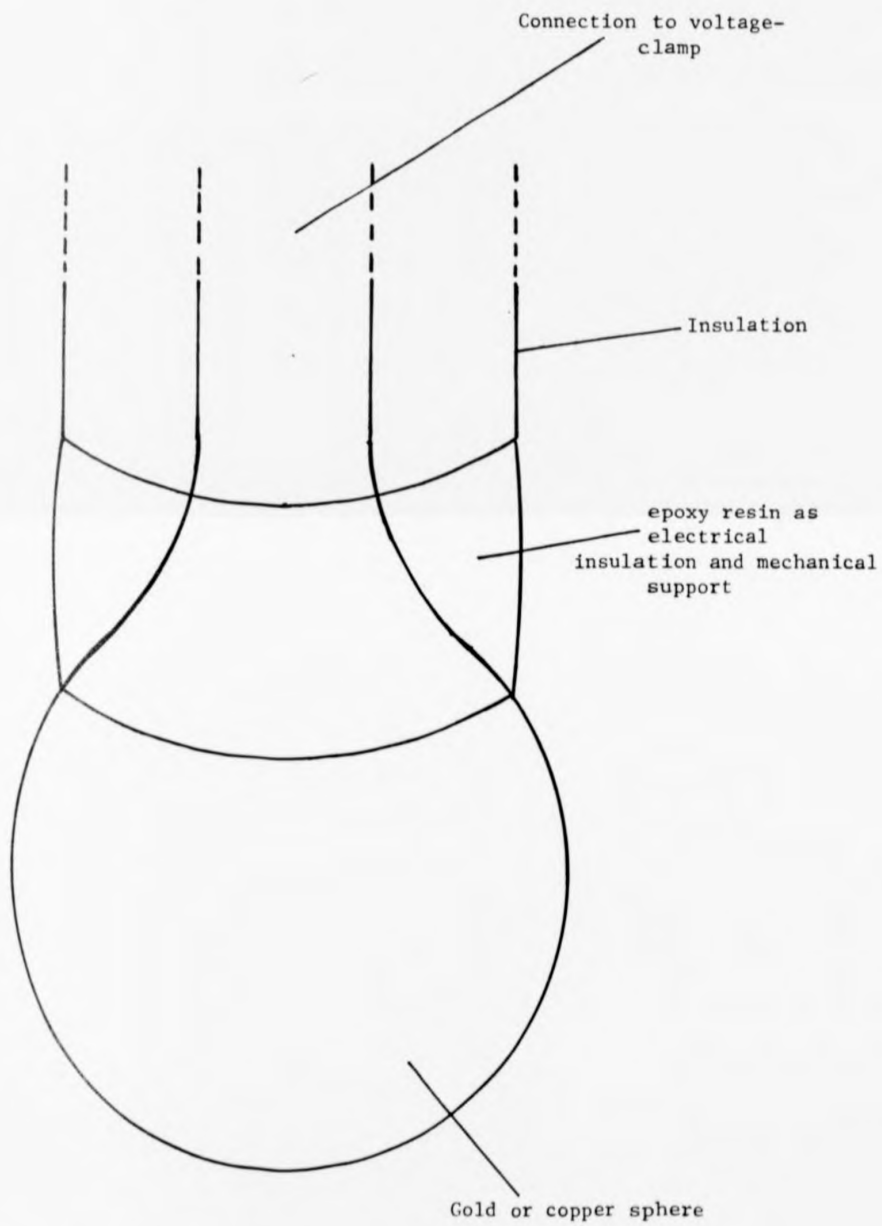


Figure 3.9.7 The spherical electrode with epoxy resin.

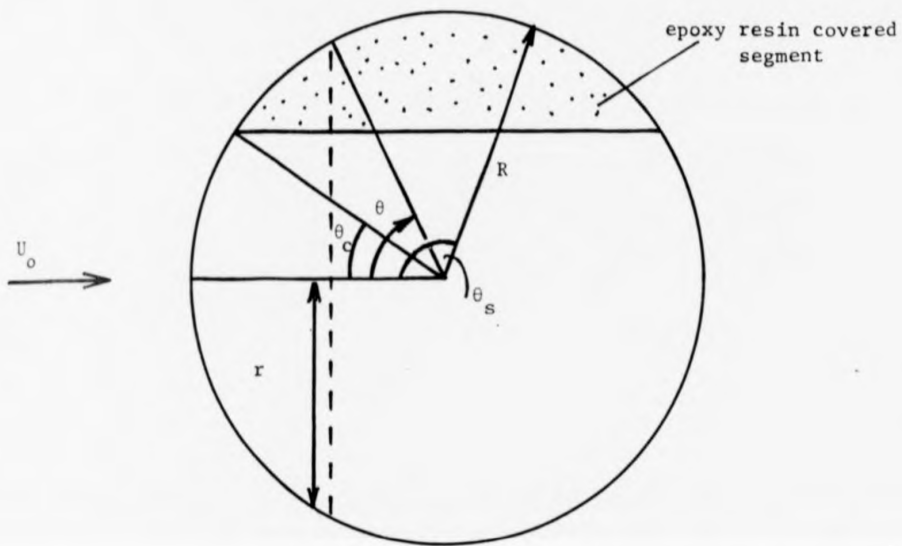


Figure 3.9.8a Cross-section through centre of sphere, parallel to flow.

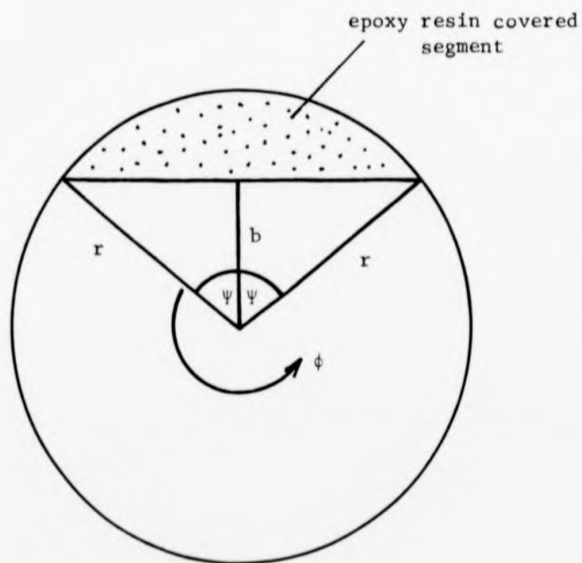


Figure 3.9.8b Cross-section through sphere perpendicular to flow.

regions of integration (of equation 3.8.20) exist, the first from  $\theta = 0$  to  $\theta = \theta_c$  and the second from  $\theta_c$  to  $\theta_s$ . In the first region the integration over  $\phi$  is from 0 to  $2\pi$  and in the second region the integration over  $\phi$  is as shown in figure 3.9.8b.

Since

$$b = R \sin \theta_c \quad (3.9.6)$$

$$r = R \sin \theta \quad (3.9.7)$$

and

$$\cos \psi = b/r = \frac{\sin \theta_c}{\sin \theta} \quad (3.9.8)$$

it follows that

$$\psi = \cos^{-1} \left( \frac{\sin \theta_c}{\sin \theta} \right) \quad (3.9.9)$$

The total current then becomes

$$I = \int_0^{\theta_c} \int_0^{2\pi} d\phi r R J(\theta) d\theta + \int_{\theta_c}^{\theta_s} \int_0^{2(\pi-\psi)} d\phi r R J(\theta) d\theta \quad (3.9.10)$$

where  $J(\theta)$  is given by equation 3.8.20.

That is

$$I = 2\pi R^2 \int_0^{\theta_c} \sin \theta J(\theta) d\theta + 2\pi R^2 \int_{\theta_c}^{\theta_s} \frac{1}{\pi} (\pi - \psi) R^2 \sin \theta J(\theta) d\theta \quad (3.9.11)$$

or

$$I = 2\pi \times 1.04 R^{3/2} (Q_{S_1} + Q_{S_2}) \text{mec}_s D^{2/3} v^{-1/6} U_o^{1/2} \quad (3.9.12)$$

where

$$Q_{S_1} = \int_0^{\theta_c} (1 - 0.190 \theta^2 - 7.31 \times 10^{-4} \theta^4) \sin \theta d\theta \quad (3.9.13)$$

and

$$Q_{S_2} = \int_{\theta_c}^{\theta_s} \frac{1}{\pi} \left[ \pi - \cos^{-1} \left( \frac{\sin \theta_c}{\sin \theta} \right) \right] (1 - 0.190 \theta^2 - 7.31 \times 10^{-4} \theta^4) \times \sin \theta d\theta \quad (3.9.14)$$

Since the epoxy resin extends beyond  $\theta_s$ ,  $\theta_c \ll 70^\circ$ . The variation of  $Q_{s1}$  with  $\theta_c$  can be obtained from figure 3.9.6, for  $\theta_c \ll 70^\circ$ . The variation of  $Q_{s2}$ , assuming  $\theta_s = 109.6^\circ$ , is given in figure 3.9.9.

To obtain the average current density  $\bar{J}$  the available area of the electrode is used, that is the free electrode surface, which is  $\frac{b+R}{2R} \times 4\pi R^2$ .

$\bar{J}$  is then given by

$$\bar{J} = \frac{I}{(b+R)4\pi R^2} \times 2R = \left( \frac{R}{b+R} \right) 1.04 R^{-1/2} (Q_{s1} + Q_{s2}) \text{mec}_s D^{2/3} U_o^{-1/6} \quad (3.9.15)$$

and the shape factor for a practical sphere becomes

$$S = \left( \frac{R}{b+R} \right) 1.04 (Q_{s1} + Q_{s2}) R^{-1/2} \quad (3.9.16)$$

If there is no epoxy resin then  $b = R$ ,  $Q_{s1} = Q_{s2} = 0$  and equation 3.9.16 becomes identical to equation 3.8.24 for the complete sphere.

Since the epoxy resin extends beyond  $\theta_s$ ,  $\theta_c \ll 70^\circ$ . The variation of  $Q_{s1}$  with  $\theta_c$  can be obtained from figure 3.9.6, for  $\theta_c \ll 70^\circ$ . The variation of  $Q_{s2}$ , assuming  $\theta_s = 109.6^\circ$ , is given in figure 3.9.9.

To obtain the average current density  $\bar{J}$  the available area of the electrode is used, that is the free electrode surface, which is  $\frac{b+R}{2R} \times 4\pi R^2$ .

$\bar{J}$  is then given by

$$\bar{J} = \frac{I}{(b+R)4\pi R^2} \times 2R = \left( \frac{R}{(b+R)} \right) 1.04 R^{-1/2} (Q_{s1} + Q_{s2}) \text{ mec}_s D^{2/3} U_o^{-1/6} U_o^{1/2} \quad (3.9.15)$$

and the shape factor for a practical sphere becomes

$$S = \left( \frac{R}{b+R} \right) 1.04 (Q_{s1} + Q_{s2}) R^{-1/2} \quad (3.9.16)$$

If there is no epoxy resin then  $b = R$ ,  $Q_{s1} = Q_s$ ,  $Q_{s2} = 0$  and equation 3.9.16 becomes identical to equation 3.8.24 for the complete sphere.

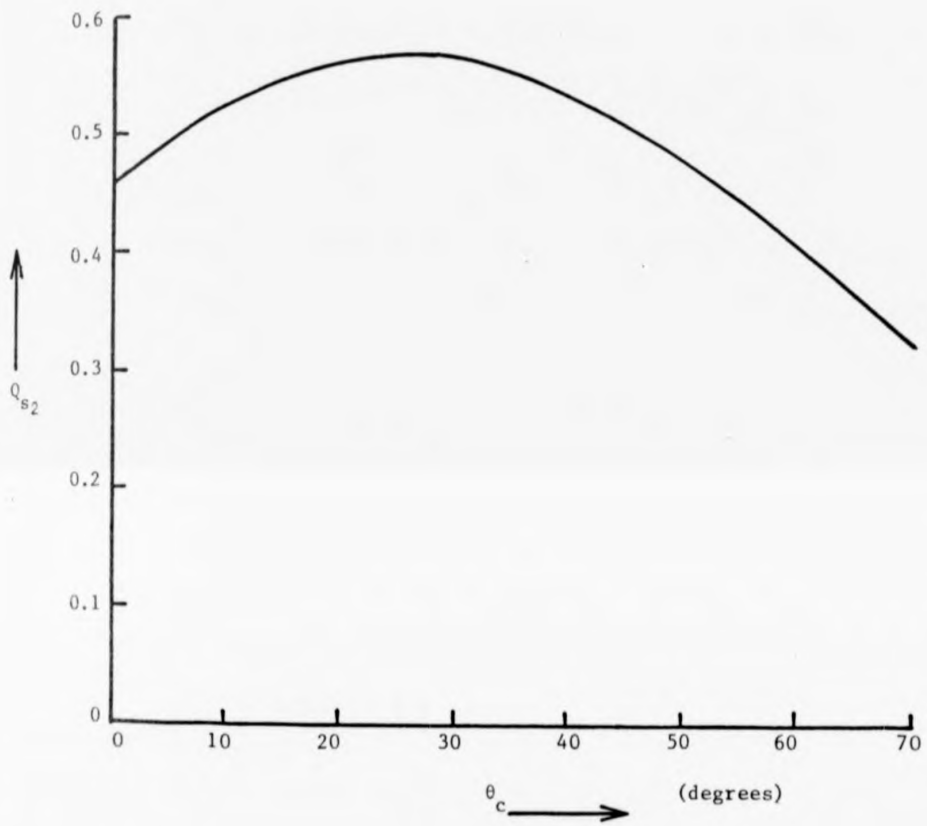


Figure 3.9.9 The variation of  $Q_{s2}$  with  $\theta_c$ .

CHAPTER 4

CHAPTER 4EXPERIMENTAL INVESTIGATIONS OF THE STEADY-STATE VELOCITY RESPONSE4.1 Introduction

This chapter describes the experimental investigations of the steady-state velocity response of the parallel disc, the perpendicular disc and the sphere. The velocity response of a given electrode is a function of many variables and it was not practicable to investigate all dependencies for all electrodes. The theoretical descriptions of the various electrodes, as given in Chapter 3, did not exist in such an advanced form at the time these in-vitro investigations were performed. The earlier theories did not fully illustrate the importance of enamelling and therefore only a limited range of  $\chi$  has been used.

The results obtained show, for all electrode shapes, that at a given temperature the current is proportional to the square root of the flow velocity and directly proportional to the oxygen concentration. It was also found that the response was constant with time. These results are sufficient to enable the calibration and use of this device as a flow transducer.

The only experimentally independent variable in equation 3.1.2 for the velocity response of an electrode is the diffusion coefficient  $D$  of oxygen. The accuracy of the theories of Chapter 3 can therefore be investigated by applying them to the experimental results and deriving a value of  $D$  which may be compared with accepted values. Figure 4.1.1 shows values of  $D$ , at different temperatures, obtained from Landolt-Börnstein (1969). The value of  $D$  in 0.15M NaCl (the solution used in most experiments) is assumed to be equal to that in distilled water.

To obtain  $D$  it is necessary to know the oxygen concentration  $c_g$

and the kinematic viscosity  $\nu$ . A knowledge of the atmospheric pressure  $P_a$ , water vapour pressure  $P_w$ , temperature and the composition of the gas mixture above the solution allow  $c_s$  to be calculated using tabulated values of the Bunsen absorption coefficient (Perry, 1963). Figure 4.1.2 shows the variation of  $c_s$  with temperature assuming a partial pressure of oxygen of 152mm of Hg and 0.15M NaCl.

Figure 4.1.3 shows the variation of  $P_w$  with temperature (Weast, 1978). Figure 4.1.4 shows the variation of  $\nu$ , for 0.15M NaCl, with temperature, the values being derived from tables given by Washburn (1929).

#### 4.2 The Anode-Cathode Potential $V_{ac}$

It is necessary for the correct functioning of the flow transducer for the potential difference  $V_{ac}$  applied between the anode and the cathode to remain constant, whatever the current flowing. That is, a voltage clamp is required. The value of  $V_{ac}$  can then be maintained on the plateau (transport limited region) of the  $I$ - $V_{ac}$  characteristic. The electronic circuit used to maintain constant  $V_{ac}$  and to detect the current  $I$  flowing is shown in figure 4.2.1.

The operational amplifier in the first (voltage clamp) stage is a standard low noise JFET device. When  $I$  is zero the output of the voltage clamp stage is equal to  $V_{ac}$  and it is usually necessary to back-off this value (if, for example, the output is to be squared). The back-off is achieved with the second stage by setting S2, P2 and P3. Automatic back-off of  $V_{ac}$  could have been used but it was found more convenient, especially in the early stages, to have control over all circuit variables. With no back-off, the output  $V_o$  is

$$V_o = IR_f + V_{ac} \quad (4.2.1)$$

Therefore, with  $V_{ac}$  backed-off exactly

$$I = V_o/R_f \quad (4.2.2)$$

$V_o$  is then proportional to the square root of the magnitude of the flow velocity past the cathode.  $V_{ac}$  was measured with a Keithley

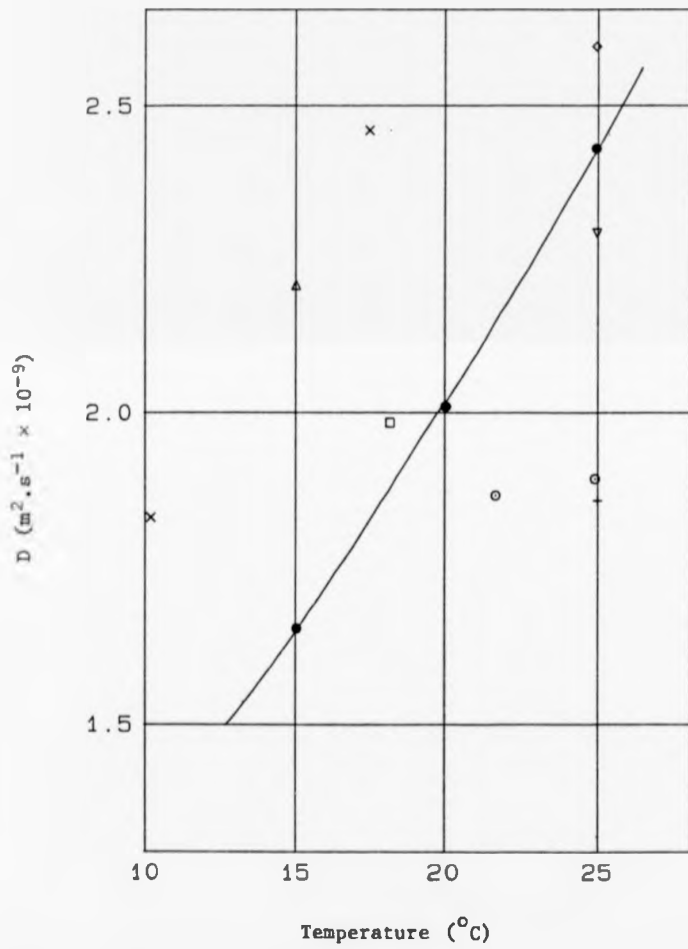


Figure 4.1.1 Values of the diffusion coefficient of oxygen in water from Landolt-Börnstein (1969)

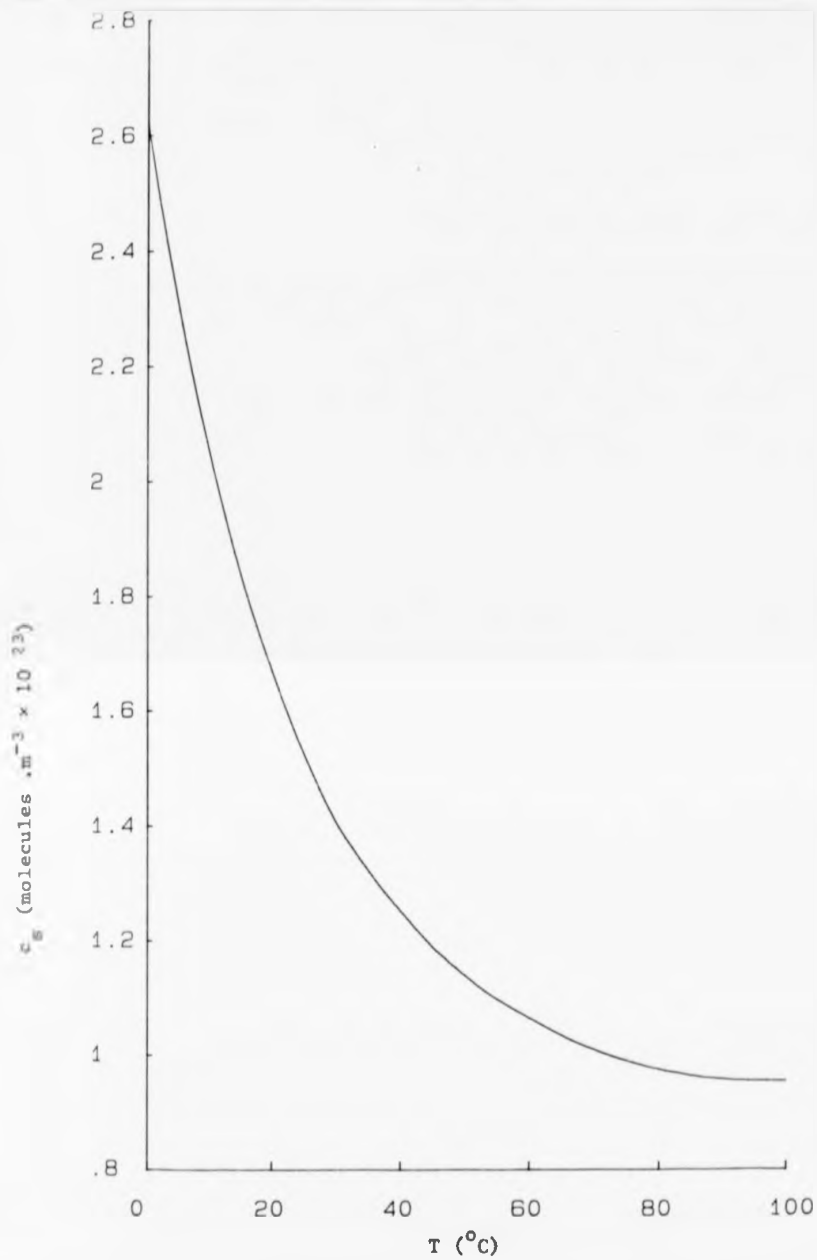


Figure 4.1.2 The variation of  $c_g$  with temperature assuming a partial pressure of oxygen of  $\frac{1}{5}$  atmosphere ( $p_{\text{O}_2} = 152\text{mm of Hg}$ )

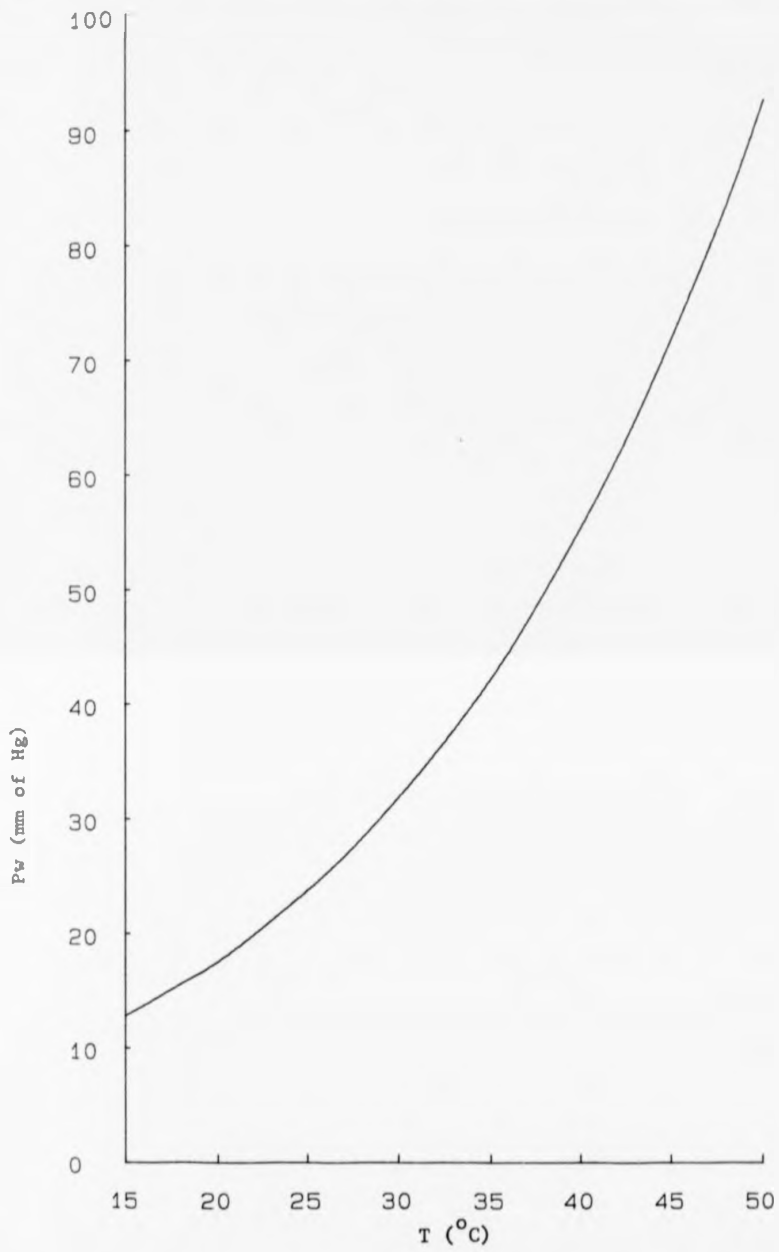


Figure 4.1.3 The variation of water vapour pressure with temperature from Weast (1978)

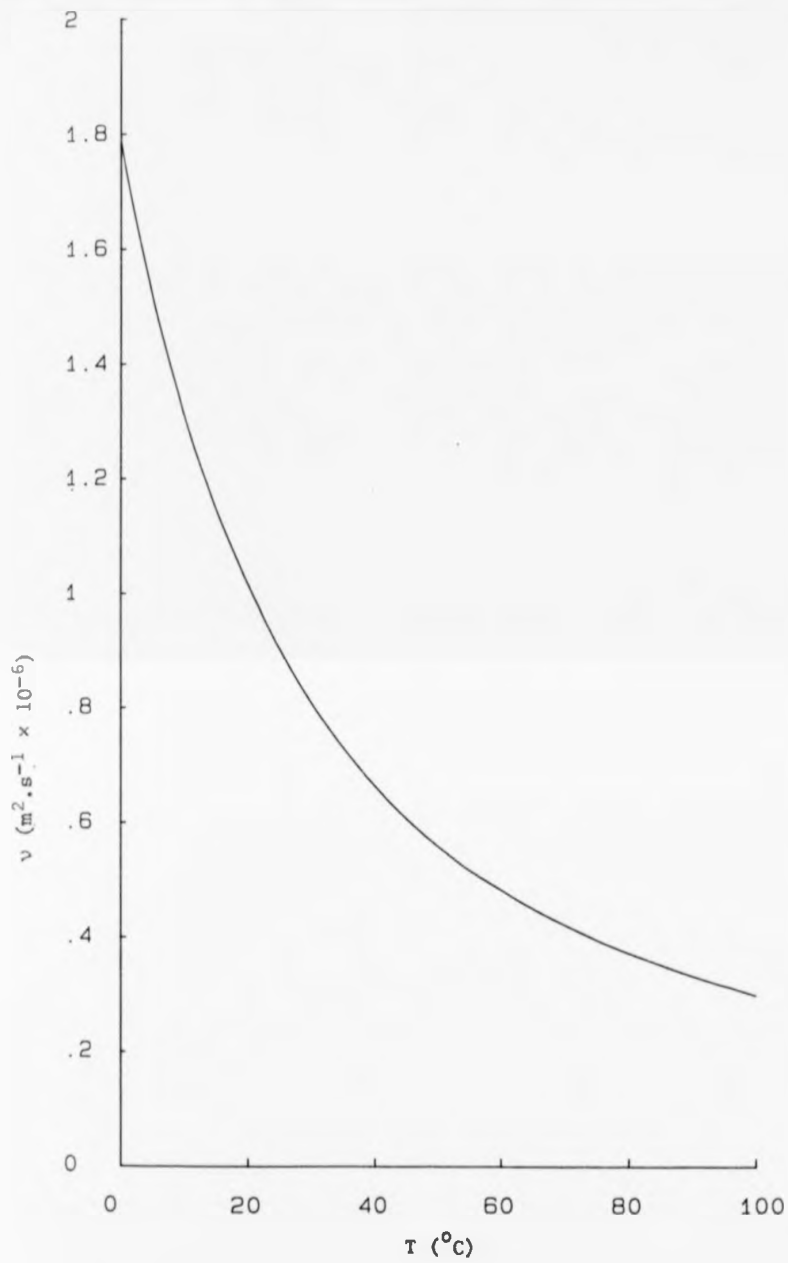


Figure 4.1.4 The variation of the kinematic viscosity  $v$  of 0.15M NaCl with temperature



model 602 electrometer of input impedance  $10^{14}$  ohms. The voltage clamp stage was calibrated using a resistance box.

#### 4.3 The Variation of I with $V_{ac}$ and $V_c$ and the Choice of Electrode Materials

##### 4.3.1 The Variation of I with $V_{ac}$

Usually the anode and cathode were both in a bath of 0.15M NaCl (physiological concentration), itself surrounded by a water bath. Initially at  $V_{ac} = 0$  a small current was often observed. After a few minutes this became zero (being anyway very small, approximately 1% or less of the plateau current  $I_p$ ).  $V_{ac}$  was increased in 50mV or 100mV steps. After each step typically one minute was allowed for the electrodes to stabilise. Below the plateau I was very constant with time. As the plateau was approached a random current component occurred as the cathode became sensitive to flow and responded to the naturally occurring free convection in the saline.

The free convection occurred because of the existence of temperature gradients in the saline caused by the heated water bath. The random nature of the free convection often led to very considerable scatter in the points on the plateau of the I- $V_{ac}$  characteristic. The scatter could be reduced by placing the cathode in a small container of saline inside the main bath (connected by saline to the main bath). This had the effect of reducing the free convection past the cathode.

##### 4.3.2 The Variation of I with $V_c$

It is impossible to measure the actual potential difference across an electrode/electrolyte interface (Bockris and Reddy, 1970) since to do so requires the existence of another electrode/electrolyte interface across which another unknown potential difference will exist. It is, though, possible to measure the change in potential which occurs if a current

flows through the interface. This change in potential is known as the overpotential and can be measured by the use of a third (in addition to the anode and cathode) reference electrode through which no current is allowed to pass. The potential difference across the electrode/electrolyte interface of the reference electrode is therefore maintained at its equilibrium (zero current) value.

First, with  $V_{ac} = 0$  ( $I = 0$ ) the potential differences between the reference electrode and the anode, and the reference electrode and the cathode were measured. Then  $V_{ac}$  was increased ( $I > 0$ ) and the same potential differences measured for each value of  $V_{ac}$ . The overpotentials at the anode  $V_a$ , and the cathode  $V_c$  were found by subtraction of the zero current values.

In practice, a small copper electrode was used as the reference electrode, the condition of no current flow through the reference electrode being satisfied by the use of the Keithley electrometer ( $10^{14}$  ohms input impedance) to measure the potential differences. Often two reference electrodes were used, one very close to the anode and the other very close to the cathode. The potential difference between the two reference electrodes, caused by the current flow through the electrolyte was found to be negligible, so that

$$V_{ac} = V_a + V_c \quad (4.3.1)$$

Figure 4.3.1 shows  $I$ - $V_{ac}$  curves obtained at different NaCl concentrations with a pair of copper electrodes. The attitude of the electrodes is of no importance since the electrodes were stationary. Except at zero NaCl concentration, plateaux of approximately equal width were obtained in all cases. At zero NaCl concentration, the de-ionised water still contains electrolytes because of the dissolution of carbon dioxide, but the conductivity was too low to obtain a plateau with the range of potential available.

In all cases the heights of the plateaux are equal, within the scatter caused by the random free convection, and the reaction rate of the transport controlled region is therefore independent of NaCl concentration. The effect of increasing NaCl concentration is to move the plateau to lower values of  $V_{ac}$  as the conductivity of the solution increases. The curves obtained for 0.1M NaCl and 0.2M NaCl (not shown, for clarity) were essentially identical to that for 0.15M NaCl. At these higher values of NaCl concentration the resistance of the solution (as measured using the reference electrodes) was negligible, so the anode-cathode separation could be varied without causing a significant potential difference across the electrolyte.

Velocity responses (obtained as described below) were independent of NaCl concentration except when zero. Plots of  $I$  against  $V_c$  at different NaCl concentrations were also identical within the scatter caused by free convection. All other experiments reported were therefore performed in 0.15M NaCl, this being approximately the physiological concentration.

Figure 4.3.2 shows the variation of  $I$  with  $V_{ac}$ ,  $V_c$  and  $V_a$  in 0.15M NaCl. As the potential lost across the electrolyte was negligible the variation of  $I$  with  $V_a$  can be obtained from equation 4.3.1. Here,  $V_c$  and  $V_a$  were measured using separate reference electrodes. Agreement with equation 4.3.1 varied within 3%, justifying the assumption that the potential lost across the electrolyte was negligible.

Similar  $I$ - $V_{ac}$  curves were obtained at different values of  $c_s$ , when the plateau currents  $I_p$  were proportional to  $c_s$ , within the scatter caused by free convection.

Figure 4.3.3 shows a set of  $I$ - $V_{ac}$  curves obtained with a gold sphere cathode and an Ag/AgCl anode (section 4.3.3), at different temperatures. Here, the variation in plateau current caused by different levels of free convection is of the same order as that caused directly by the change in temperature.

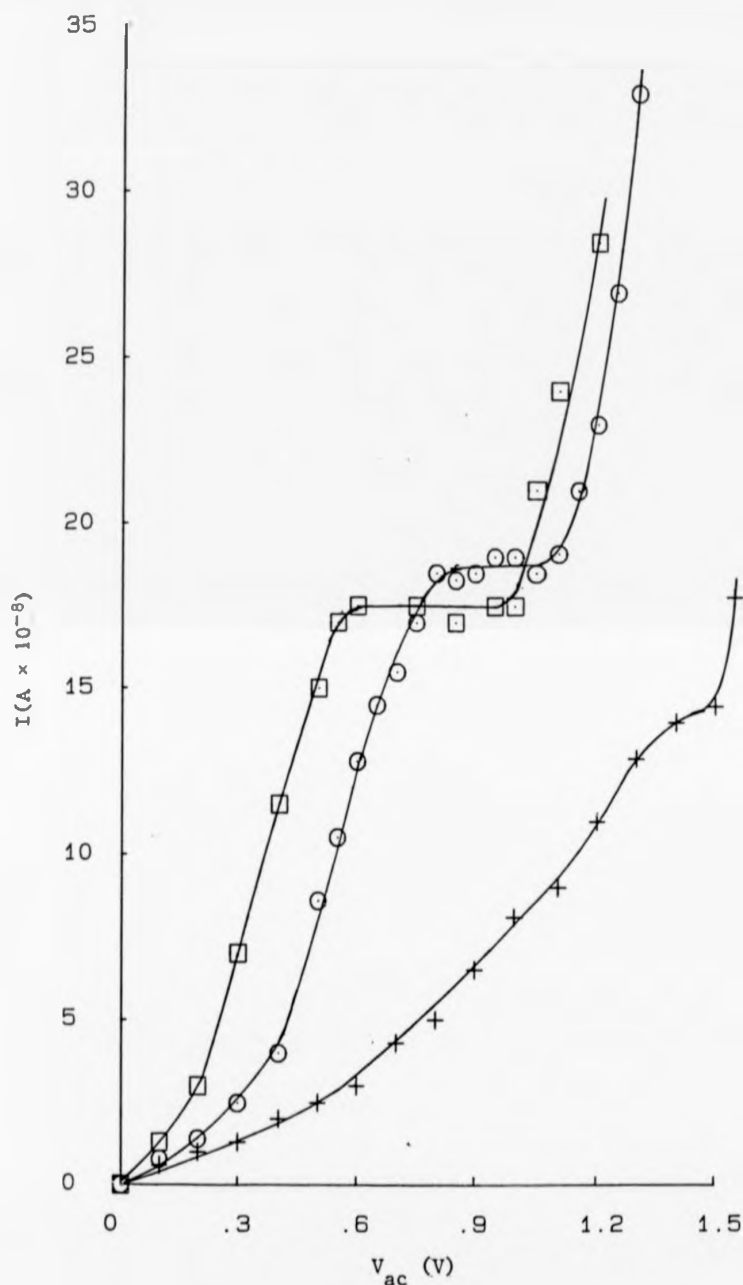


**Figure 4.3.1** The variation of  $I$  with  $V_{ac}$  at different  $[NaCl]$ , for a copper anode and a copper disc cathode ( $R = 1.3 \times 10^{-4}m$ ,  $\chi = 0.73$ ) at  $16^{\circ}C$  in an air equilibrated solution.  
 $+$   $[NaCl] = 0$ ;  $O$   $[NaCl] = 0.01M$ ;  $\square$   $[NaCl] = 0.15M$

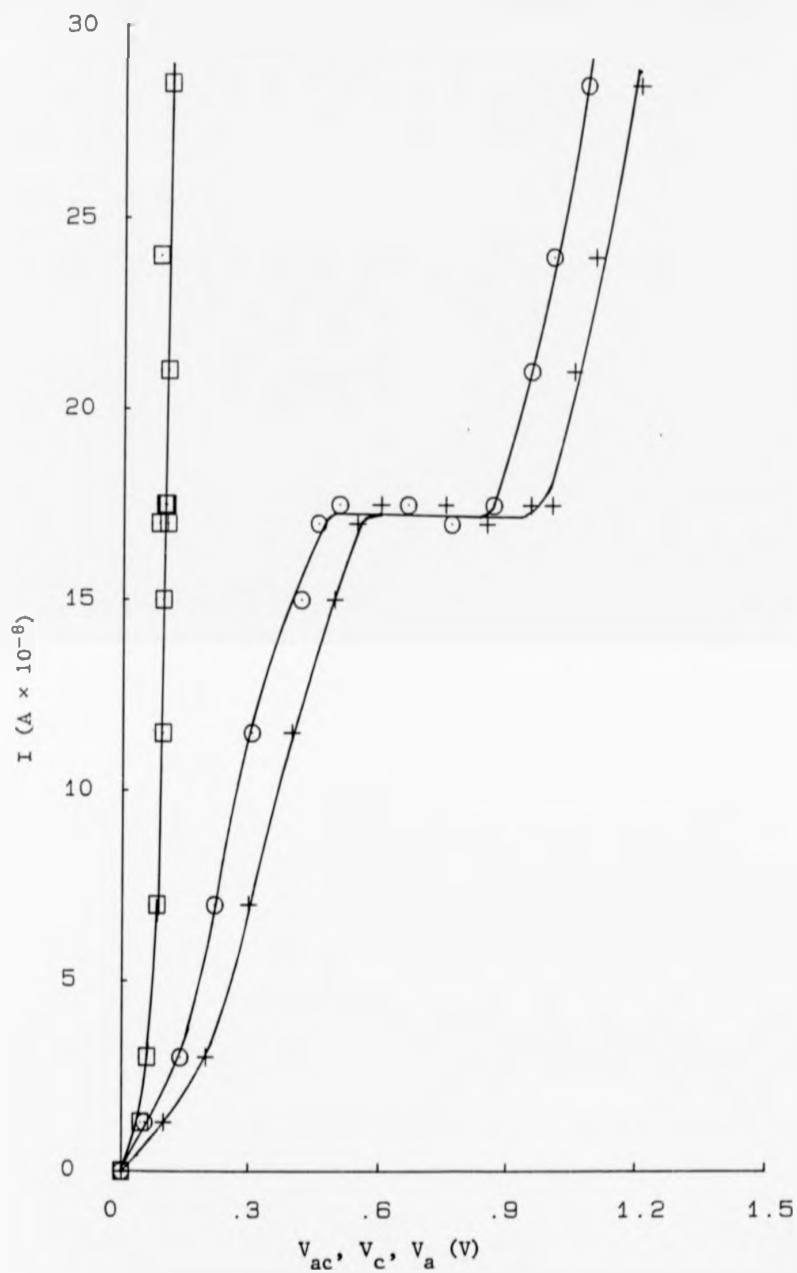


Figure 4.3.2 The variation of  $I$  with  $V_{ac}$  (+),  $V_c$  (O) and  $V_a$  (□), for a copper anode and copper disc cathode ( $R = 1.3 \times 10^{-4} m$ ,  $\chi = 0.73$ ) at  $16^\circ C$  in air equilibrated 0.15M NaCl.

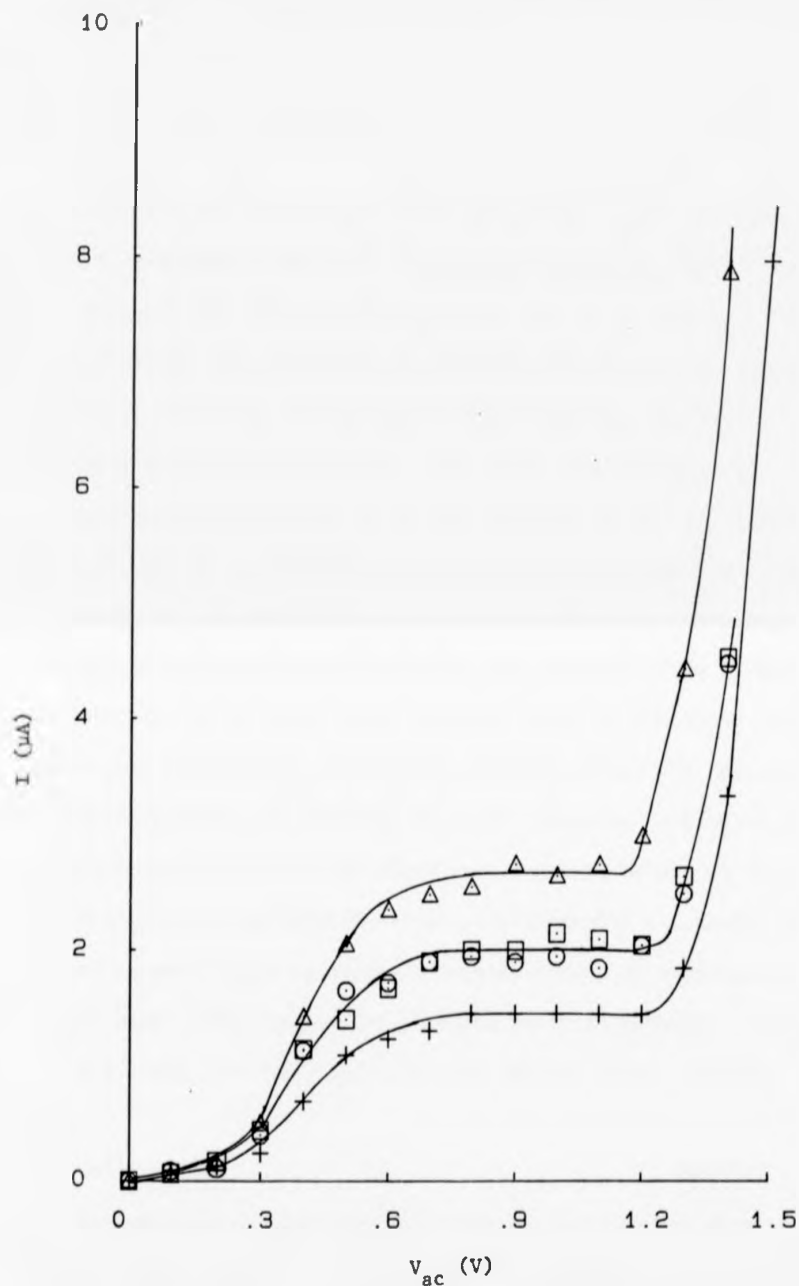
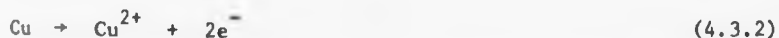


Figure 4.3.3 The variation of  $I$  with  $V_{ac}$  at different temperatures for a Ag/AgCl anode and a gold sphere cathode ( $R = 0.35\text{mm}$ ,  $b = 0.08\text{mm}$ ) in air equilibrated  $0.15\text{M NaCl}$ .  
 $+ 16^\circ\text{C}$ ;  $\text{O } 28^\circ\text{C}$ ;  $\square 35^\circ\text{C}$ ;  $\triangle 42^\circ\text{C}$

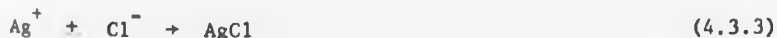
#### 4.3.3 Choice of Electrode Materials

An  $I-V_a$  curve is similar in shape to an  $I-V_c$  curve except it possesses no plateau (Fig. 4.3.2). A suitable anode should be stable with time and the value of  $V_a$  required to maintain the plateau current  $I_p$  should not be excessive. Further, the area of the electrode should be such that the plateau current is on the steeply rising part of the  $I-V_a$  curve. Then an increase in  $I$ , caused by an increase in flow velocity, can be accommodated by a small increase in  $V_a$ . This last requirement is of importance because experimentally it is only possible to set the value of  $V_{ac}$ , and not the way it is distributed between the electrodes. For the optimum operation of the electrochemical flow transducer an operating point close to the maximum of the plateau of the  $I-V_{ac}$  curve is chosen. Then, any decrease in  $V_c$  caused by a increase in  $V_a$ , or resistive losses in the electrolyte between the electrodes, will not affect the operation of the transducer because the reaction is still transport controlled.

The above requirements for the anode were found to be not at all severe. Both copper and silver/silver chloride ( $Ag/AgCl$ ) electrodes were found to function adequately as anodes. Usually anodes of approximate area  $2\text{cm}^2$  were used. The reaction at a copper anode is probably as given by equation 4.3.2 but the reaction could also involve singly charged copper ions.



Copper is a poison to most biological systems and the use of an anode which dissolves copper ions into solution is best avoided in use in humans. The reaction at a  $Ag/AgCl$  anode is given in equation 4.3.3 and overcomes this objection.



The material chosen for the cathode should be one that does not

dissolve and which is stable in use. Copper, again, was found to be perfectly adequate, remaining bright when continually used as the cathode. The choice of copper was, to a large degree, pragmatic in that copper is readily available as enamelled (insulated) wires of various diameters. Gold was found to behave very similarly to copper, with the added advantage that it did not oxidise, as did copper when not in use. It was necessary, with copper electrodes, either to clean them by polishing or dipping in dilute acid, or to construct a new electrode just before use. The optimum choice of electrodes is, therefore, a gold cathode and a Ag/AgCl anode, though extensive use was made of copper anodes and cathodes during the laboratory work.

The  $I(\bar{J}) - V_{ac}, V_c$  curves and therefore the operating potential chosen, depend upon the electrode materials chosen, as shown by figures 4.3.2 and 4.3.3. For gold and Ag/AgCl an operating potential of 1 volt was used whilst for copper/copper 0.8 volts was used.

The copper anodes used were either copper sheets or bare wires, whilst the Ag/AgCl anodes were the button type commonly used to record electro-encephelograms. The copper cathodes were either the cut-end of an enamelled wire, or the appropriate shape was cut from copper sheet and soldered onto the cut end of a wire, insulating laquer being used as necessary to define the required electrode shape. Figure 3.6.1 illustrates schematically the geometry of the wire-end copper cathodes. The construction of the gold sphere electrodes used is described in Chapter 7. The geometry of a practical sphere is shown in Figure 3.9.7.

Short trials were performed with silver and platinum cathodes. Silver was found to be an adequate cathode material but possessed no advantage over copper. Platinum cathodes were found to be unpredictable possibly because of surface oxide states (Damjanovic, 1969). As copper

\* See Table D.1.1

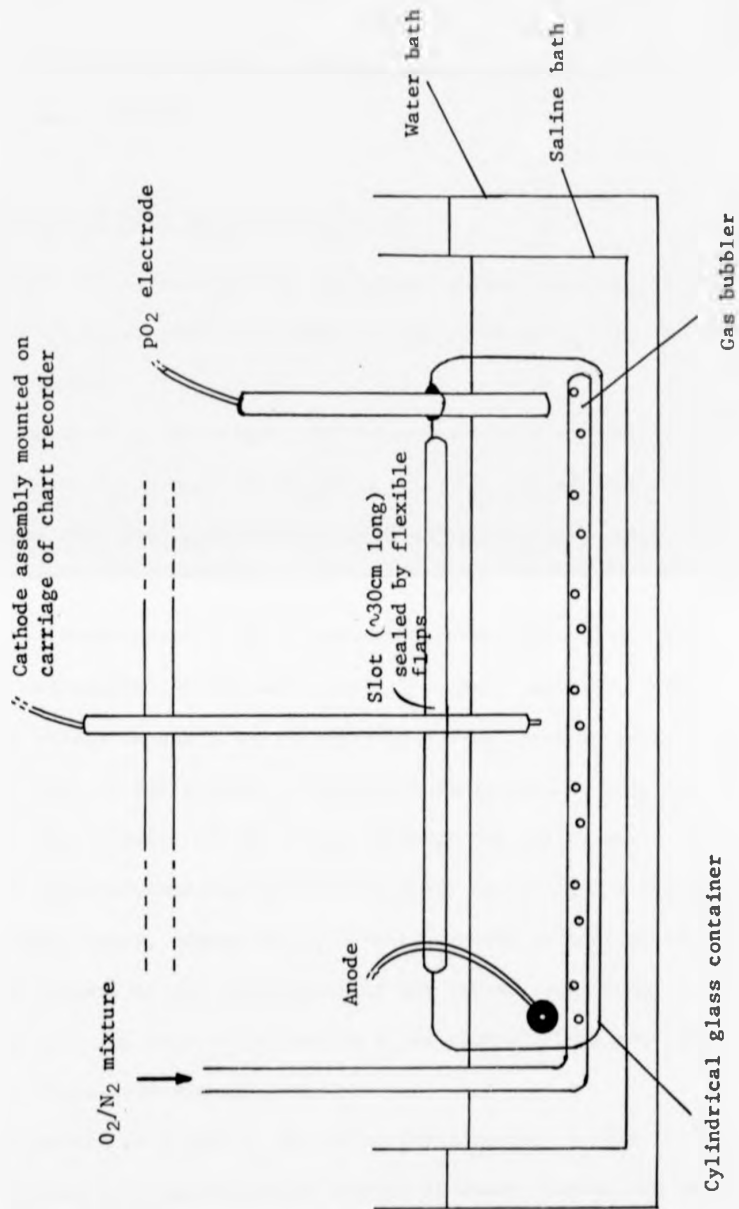


Figure 4.4.1 Diagram of the apparatus used in the investigation of the velocity response. The cylindrical glass container was only used when the effect of varying  $c_g$  was being investigated.

and gold were satisfactory no further investigation of other possible cathode materials was performed.

#### 4.4 The Variation of I with Velocity of Flow $U_0$

It is assumed that movement of the transducer whilst the fluid is stationary is exactly equivalent to movement of the fluid whilst the transducer is stationary.

The apparatus used to investigate the variation of the current I with the flow velocity  $U_0$  is shown in Figure 4.4.1. The cylindrical container shown was only used when the effects of varying  $c_g$  were being investigated.

The anode was stationary in the temperature controlled saline. The cathode assembly was mounted on the moving arm of a chart recorder. The cathode was moved either manually, or by applying a ramp input to the chart recorder though it was generally found more convenient to move the cathode by hand. The velocity of the cathode through the saline was obtained from the phase-advance tachogenerator of the recorder, the output of the tachogenerator being, conveniently, 1 volt when the cathode moved at  $1 \text{ m.s}^{-1}$ . The outputs of the tachogenerator and the voltage-clamp circuit were displayed and recorded either on a two channel chart recorder or on a Tektronix model 7633 storage oscilloscope.

When the variation of I with  $c_g$  was being investigated,  $c_g$  was controlled by allowing an oxygen-nitrogen mixture of known composition to bubble through the saline.  $c_g$  was calculated using the Bunsen absorption coefficient for oxygen and checked, particularly for constancy, using the commercial oxygen concentration probe. The flow of the gas mixture was halted when measurements were taken, to remove the stirring caused by the bubbling of the gas. The plastic flaps arranged around the top of the

• See Table D.1.1

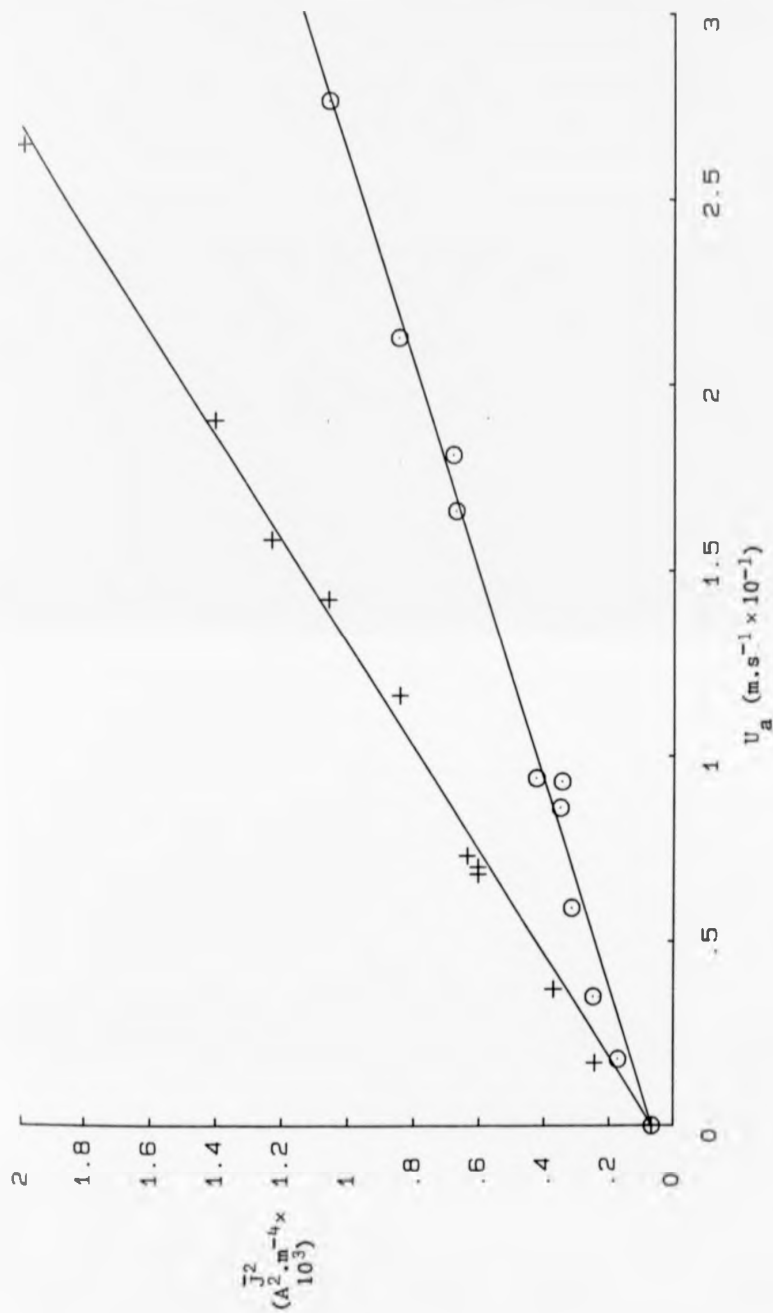


Figure 4.4.2 The variation of  $\bar{J}^2$  with  $U_a$  for a parallel enamelled disc ( $R = 1.3 \times 10^{-4} m$ ,  $\chi = 0.73$ ) at  $37.5^\circ C$ .  $c_g = 1.26 \times 10^{23}$  molecules. $m^{-3}$ . + , O movement in reciprocal directions  
 +  $G = 7.16 \pm 0.21 \times 10^3 A^2 \cdot m^{-5} \cdot s$ ; O  $G = 3.56 \pm 0.18 \times 10^3 A^2 \cdot m^{-5} \cdot s$

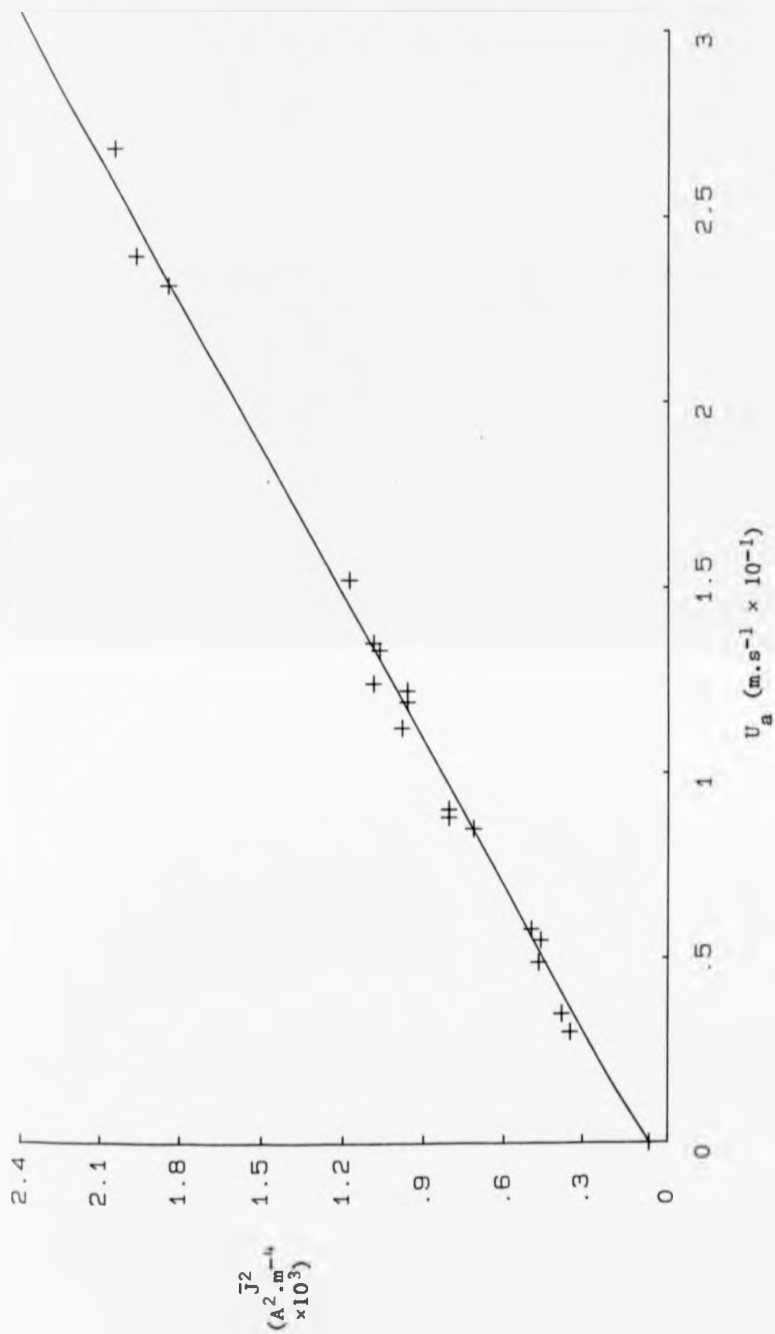


Figure 4.4.3 The variation of  $\bar{J}^2$  with  $U_a$  for a perpendicular enamelled disc ( $R = 1.3 \times 10^{-4} \text{ m}$ ,  $\chi = 0.73$ ) at  $37.5^\circ\text{C}$ .  $c_g = 1.26 \times 10^{23} \text{ molecules.m}^{-3}$   $C = 7.63 \pm 0.20 \times 10^3 \text{ A}^2.\text{m}^{-5}.\text{s}$

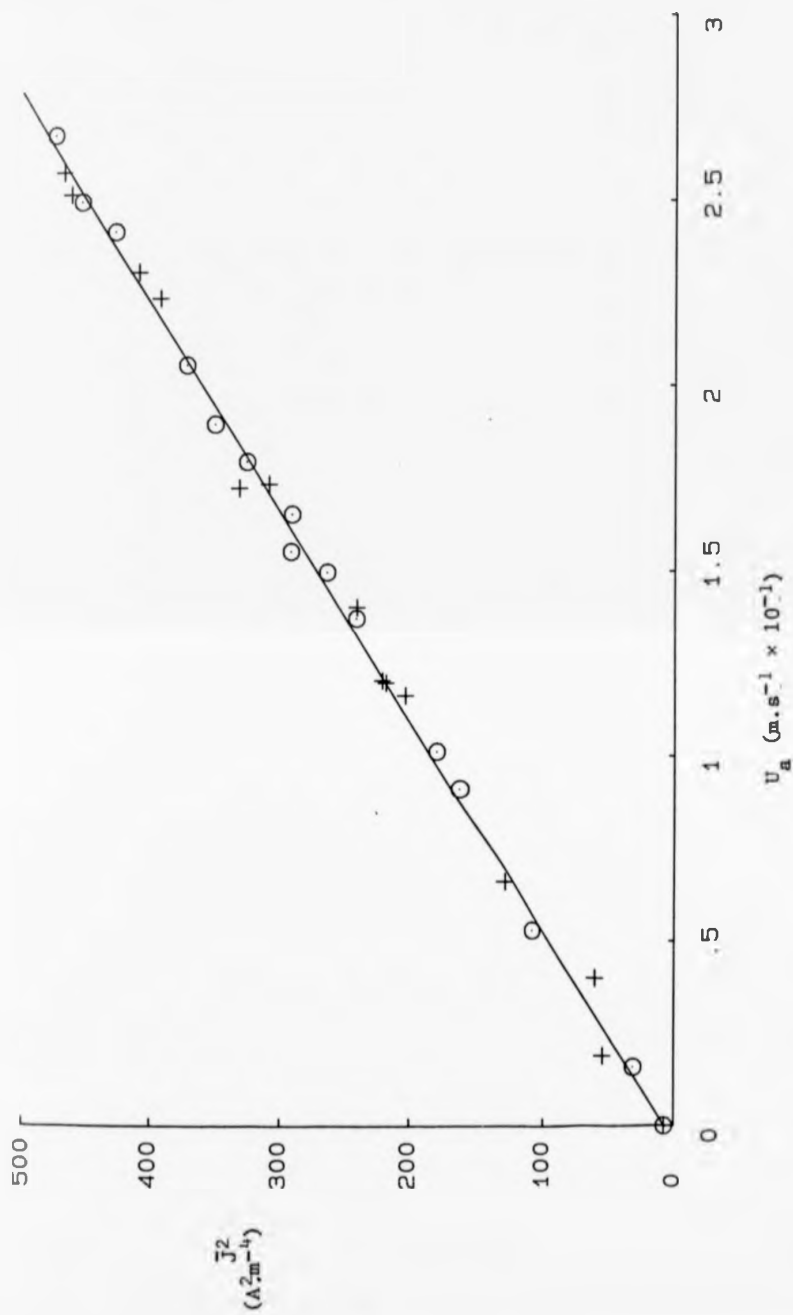


Figure 4.4.4a The variation of  $\bar{J}^2$  with  $U_a$  for an epoxied gold sphere ( $R = 0.31mm$ ,  $b = 0.14mm$ ) at  $37.5^\circ C$ .  $c_g = 1.25 \times 10^{23}$  molecules. $m^{-3}$ . +,  $\circ$  movement in reciprocal directions  $G = 1.77 \pm 0.03 \times 10^3$   $A^2.m^{-5}.s$

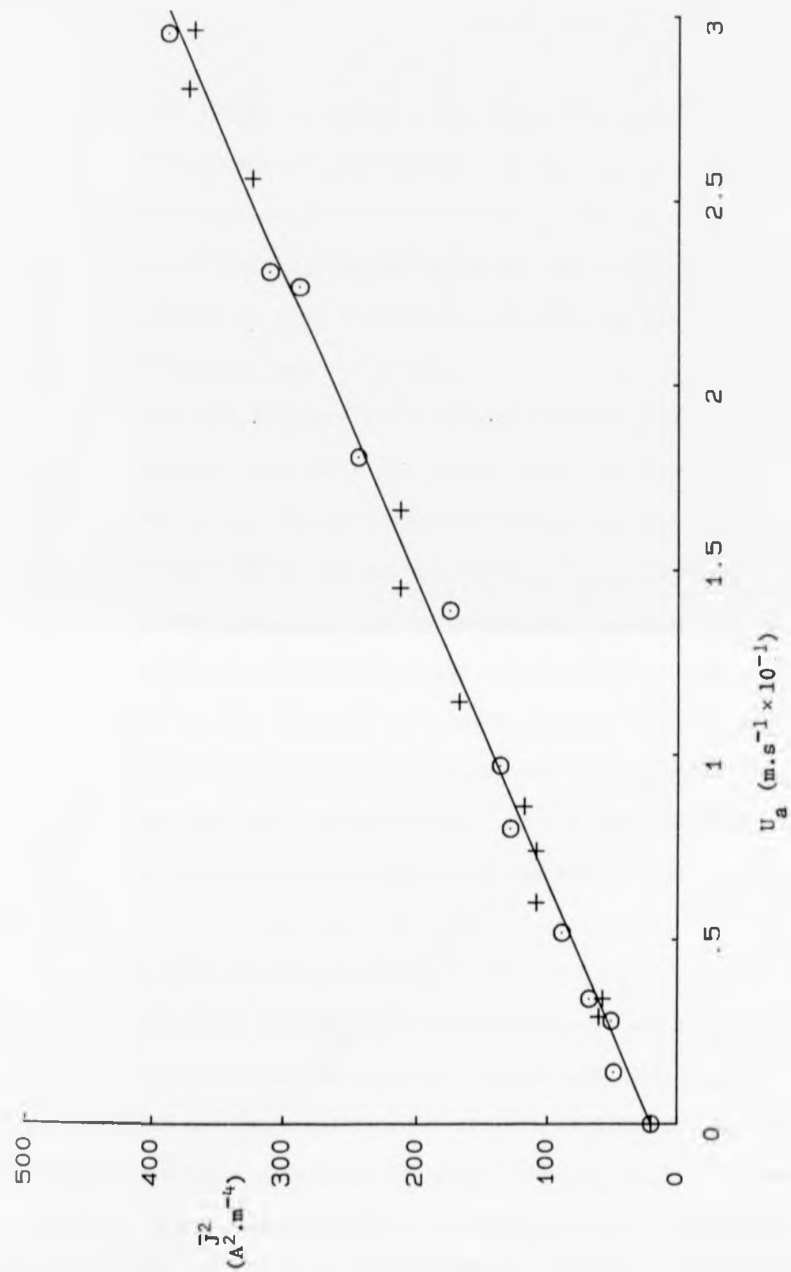


Figure 4.4.4b The variation of  $J^2$  with  $U_a$  for an epoxied copper sphere ( $R = 0.46\text{mm}$ ,  $b = 0.39\text{mm}$ ) at  $37.5^\circ\text{C}$ .  $c_g = 1.26 \times 10^{23}$  molecules. $\text{m}^{-3}$ . +, O movement in reciprocal directions  $G = 1.23 \pm 0.03 \times 10^3 \text{ A}^2 \cdot \text{m}^{-5} \cdot \text{s}$

cylindrical container helped to preserve the composition of the gas mixture above, and therefore in, the saline. It was, though, necessary to take the measurements with some speed so that  $c_g$  did not change appreciably.  $c_g$  was constantly checked using the oxygen concentration probe, and if it changed by more than 5% the gas flow was restarted to return  $c_g$  to the desired value.

Since the anode was stationary, the anode-cathode distance varied during the measurements. Any variation in potential lost across the solution (the potential lost being anyway very small) was negligible and could easily be accommodated by the plateau of the  $I-V_{ac}$  curve.

Figures 4.4.2 and 4.4.3 show the variation of  $\bar{J}^2$  with applied velocity  $U_a$  (the velocity of movement of the cathode) for an enamelled copper disc parallel to the flow and an enamelled copper disc perpendicular to the flow. Figures 4.4.4(a) and 4.4.4(b) show the variation of  $\bar{J}^2$  with  $U_a$  for a gold sphere and for a copper sphere. In all cases the variation of  $\bar{J}^2$  with  $U_a$  is as predicted by the theory of Chapter 3, but some features require comment.

In all the graphs a finite value of  $\bar{J}^2$  exists at  $U_a = 0$ . This is the plateau current of the  $J(I)-V_{ac}$  curve and represents the random free convection which exists in the saline bath. Whilst the direction of flow might well alter the current response, the current is always of the same polarity and in this sense rectifies the flow. Further, at low velocities, such as those of free convection, the time response of the current to a decrease in flow velocity is very slow (Chapters 5 and 6). The rectifying effect, together with the slow time response to a decrease in flow (the response to an increase is effectively instantaneous when the new velocity corresponds to a greater current than that already existing) act to give the plateau current which is a smoothed representation of the magnitude of the free convection. The point plotted at  $U_a = 0$  is the square of the

average value of  $\bar{J}$  at  $U_a = 0$ , and thus represents an averaged value of the free convection, weighted towards its peak value.

If the random free convection velocity is  $U_c$ , then the magnitude of the velocity seen by the cathode will be

$$|U_o| = |U_a \pm U_c| \quad (4.4.1)$$

Since  $U_c$  varies in direction and magnitude with both position and time, a scatter in the points of Figures 4.4.2, 4.4.3 and 4.4.4 of approximately  $2\bar{J}^2$  (at  $U_a=0$ ) should exist. Such a scatter does exist. In Figures 4.4.2, 4.4.3 and 4.4.4 the intercepts on the velocity axis correspond to free convection velocities in the range 10 to 20  $\text{mm.s}^{-1}$ , a not unreasonable value.

The convective-diffusion equation can be applied when the Peclet number  $Pe \gg 1$ . For an electrode of diameter 1mm, with  $D \sim 2 \times 10^{-9} \text{ m}^2 \cdot \text{s}^{-1}$ , the convective diffusion equation applies when  $U_o \gg 2 \times 10^{-6} \text{ m.s}^{-1}$ . However, the analysis of Chapter 3 requires the existence of a viscous boundary layer. Separation of the fluid into regions of viscous and potential flow occurs when the Reynolds number  $Re \gg 1$ , that is for a 1mm diameter electrode ( $\nu \sim 10^{-6} \text{ m}^2 \cdot \text{s}^{-1}$ ) when  $U_o \gg 1 \text{ mm.s}^{-1}$ . The smallest electrodes used here (discs) were approximately 0.2mm in diameter and should function as predicted down to velocities of  $\sim 5 \text{ mm.s}^{-1}$ . This could not be adequately tested with the experimental arrangement used because of the large (in comparison) values of free convection.

Electrodes up to 2mm in diameter were found to behave as predicted up to velocities of at least 800  $\text{mm.s}^{-1}$ , this velocity being the practical upper limit of the experimental arrangement.

For the parallel disc (Figure 4.4.2) different responses were obtained for movement in reciprocal directions. This is easily explained if the disc was not exactly parallel to  $U_a$ . It was found possible with

care, and using the response of the electrode as a guide, to align the electrode so that equal responses were obtained in reciprocal directions.

For all electrodes, the gradient of the  $\bar{J}^2 - U_a$  graph is defined as G. From equation 3.1.2 it follows that

$$G^{1/2} = S \text{ mec}_s D^{2/3} v^{-1/2} \quad (4.4.2)$$

For parallel disc electrodes it was found that when no difference in response (to movement in reciprocal directions) occurred, that G was approximately equal to the average value of G when a difference was observed. Therefore, in the absence of a better approach, when a difference occurred the square root of the average value  $(G_{av})^{1/2}$  was used in equation 4.4.2.

For perpendicular disc electrodes a meaningful response could naturally only be obtained in one direction. To some extent this was a disadvantage since the reciprocal responses of the cathode provided little information about the accuracy of its alignment.

All the errors quoted in the results presented in this Chapter refer only to the precision of the points plotted. In all the graphs presented there is uncertainty both in the ordinate and the abscissa. Consequently, the line drawn was evaluated from a least squares fit assuming independent uncertainties in both co-ordinates, the values and errors quoted being derived from this procedure. Further consideration of the errors is given in the discussion.

The value of D, at 37.5°C, obtained using the value of  $(G_{av})^{1/2}$  for Figure 4.4.2 is  $2.43 \pm 0.07 \times 10^{-9} \text{ m}^2 \cdot \text{s}^{-1}$ . The value of D obtained from Figure 4.4.3 for the perpendicular disc is  $1.41 \pm 0.04 \times 10^{-9} \text{ m}^2 \cdot \text{s}^{-1}$ . Similar results were obtained with parallel and perpendicular discs up to 2mm in diameter (the largest used).

The electrode used to obtain Figure 4.4.4(a) for the gold sphere was

actually used in humans. To decrease the risk of the gold sphere falling off into the C.S.F. pathways a considerable degree of epoxy resin was used (the construction is described in Chapter 7) which accounts for the small value of the dimension  $b$ . The current densities were calculated using the available area of gold (the exposed area) and the value of  $D$ , at  $37.5^{\circ}\text{C}$  obtained was  $2.48 \pm 0.05 \times 10^{-9} \text{ m}^2 \cdot \text{s}^{-1}$  using equations 3.9.15 and 4.4.2.

Figure 4.4.4(b) was obtained with a copper sphere with a lesser degree of epoxy resin. The value of  $D$  at  $37.5^{\circ}\text{C}$  obtained,  $2.51 \pm 0.05 \times 10^{-9} \text{ m}^2 \cdot \text{s}^{-1}$ , is very similar to that for the gold sphere, indicating that the reduction of oxygen at gold and copper electrodes involves the same number of electrons, whatever the actual reaction paths, and that in this work no distinction need be made between gold and copper so far as the value of  $m$  is concerned.

The dependence of current upon  $c_g$  is shown in Figure 4.4.5 where  $(G_{av})^{\frac{1}{2}}$ , for a parallel enamelled copper disc, is plotted against  $c_g$ . As predicted the current obtained for a given velocity is proportional to  $c_g$ . The value of  $D$  obtained, at  $37.5^{\circ}\text{C}$ , is  $2.4 \pm 0.4 \times 10^{-9} \text{ m}^2 \cdot \text{s}^{-1}$ . Similar results were obtained for parallel disc electrodes covering the range of size shown in Figure 4.4.6. With the apparatus used it was not possible to perform this experiment at  $c_g = 0$ . The intercept obtained in Figure 4.4.5 is  $2 \pm 4 \text{ A} \cdot \text{m}^{-5/2} \cdot \text{s}^{1/2}$  which is consistent with there being zero current at  $c_g = 0$ .

The effect of varying the radius, for both parallel and perpendicular discs, is shown in Figure 4.4.6. Again the variation is as predicted. The value of  $D$  for the parallel discs is  $2.48 \pm 0.05 \times 10^{-9} \text{ m}^2 \cdot \text{s}^{-1}$  and for the perpendicular discs is  $1.5 \pm 0.3 \text{ m}^2 \cdot \text{s}^{-1}$  at  $37.5^{\circ}\text{C}$ . In Figure 4.4.6 the origin is plotted as an experimental point, since without the cathode no current flows. The intercept for the parallel disc is

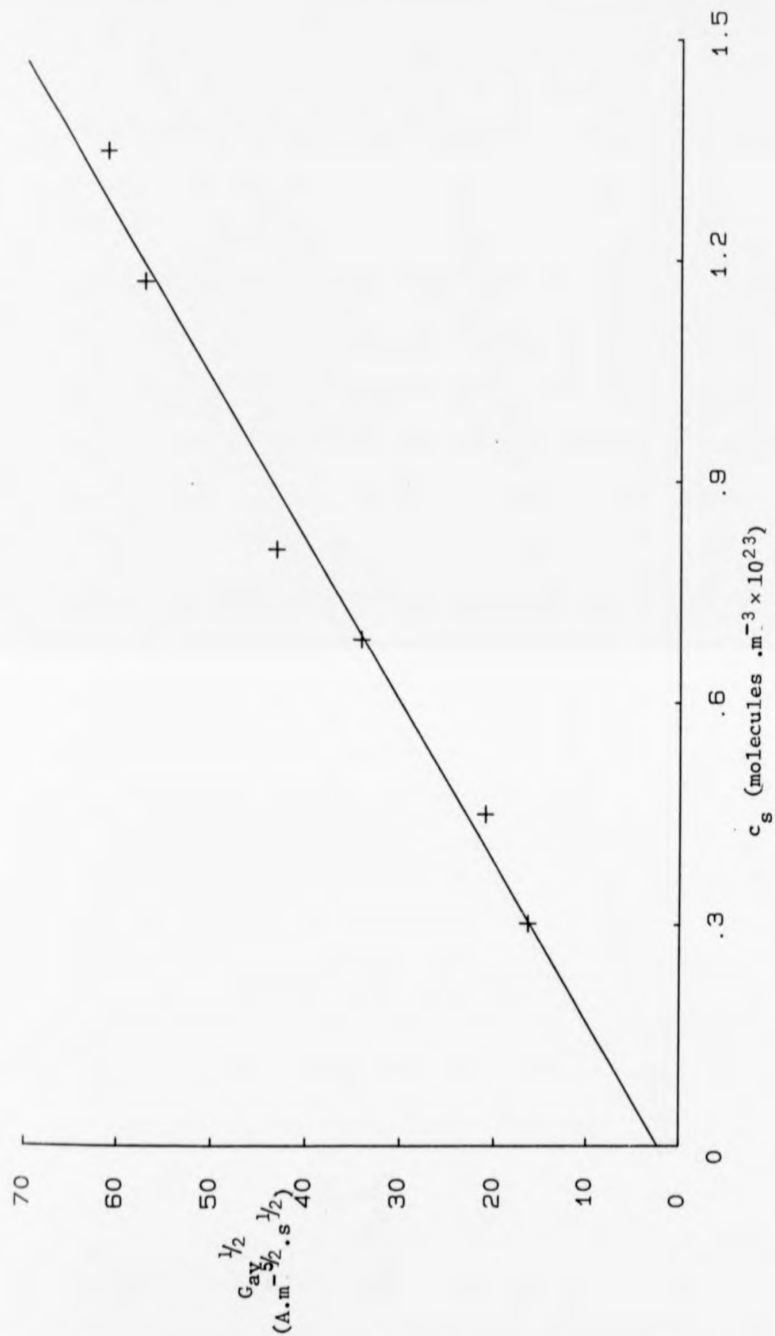


Figure 4.4.5 The variation of  $G_{av}^{1/2}$  with oxygen concentration  $c_s$ , for a parallel enamelled disc ( $R = 1.9 \times 10^{-4}m$ ,  $\chi = 0.87$ ) at  $37.5^\circ C$ .  
 $grad = 4.62 \pm 0.42 \times 10^{-22} \text{ A} \cdot m^{1/2} \cdot s^{1/2}$

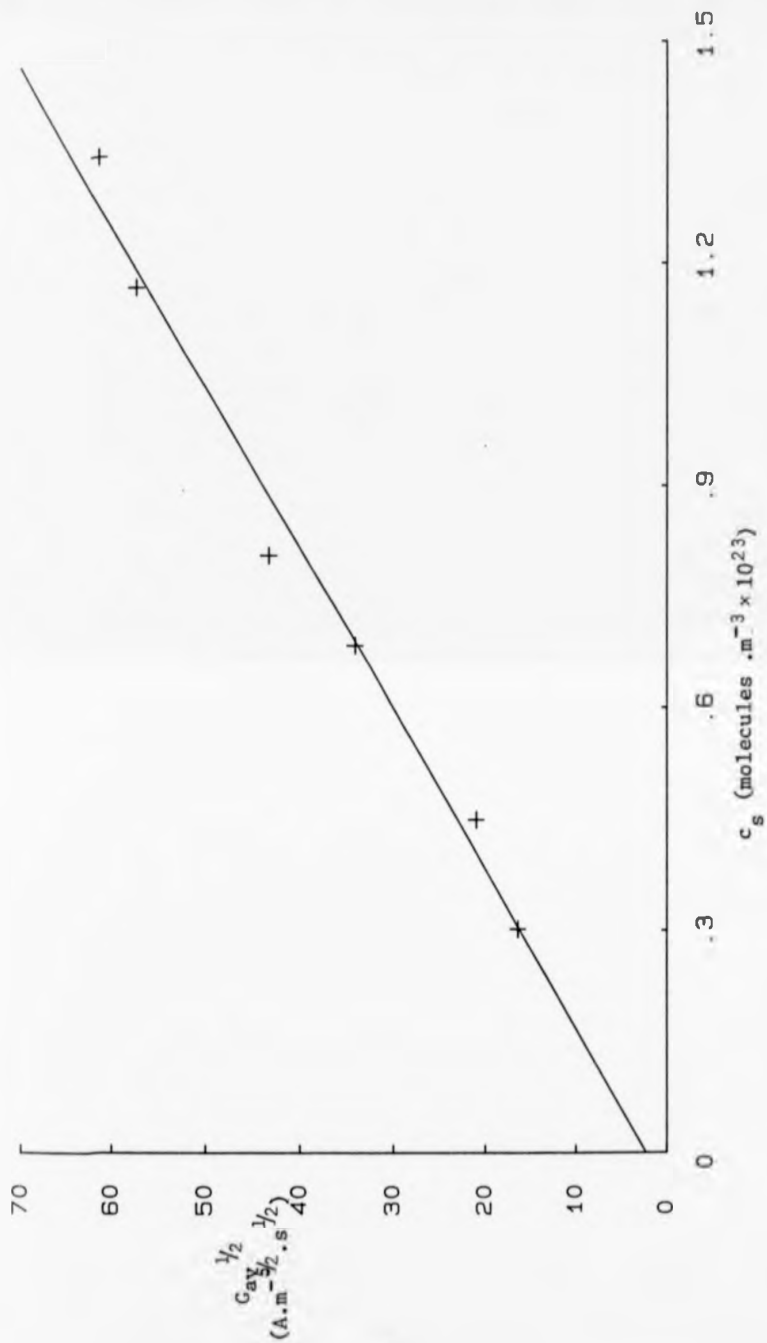


Figure 4.4.5 The variation of  $G_{av}^{1/2}$  with oxygen concentration  $c_s$ , for a parallel enamelled disc ( $R = 1.9 \times 10^{-4}\text{m}$ ,  $\chi = 0.87$ ) at  $37.5^\circ\text{C}$ .  
 $\text{grad} = 4.62 \pm 0.42 \times 10^{-22} \text{ A.m}^{1/2}.\text{s}^{1/2}$

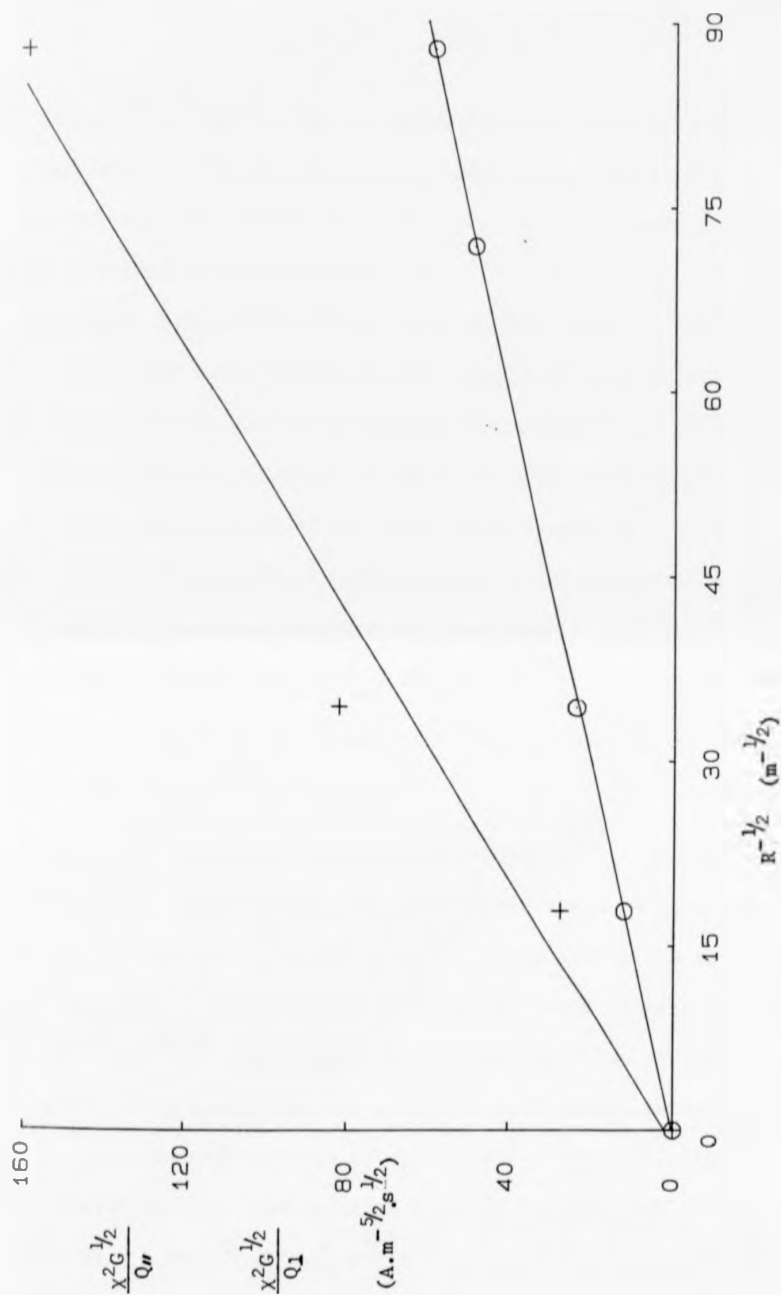


Figure 4.4.6 The variation of  $G^{1/2}$  with radius  $R$  for enamelled discs parallel

( $\circ$ ) and perpendicular ( $+$ ) to the flow, at  $37.5^\circ\text{C}$ .

$c_s$  within 1% of  $1.25 \times 10^{23}$  molecules  $\cdot\text{m}^{-3}$

$\circ$  gradient =  $0.67 \pm 0.01$  ;  $+$  gradient =  $1.86 \pm 0.29$

$\text{A}\cdot\text{m}^{-2}\cdot\text{s}^{1/2}$

$\text{A}\cdot\text{m}^{-2}\cdot\text{s}^{1/2}$

$0.4 \pm 0.5 \text{ A.m}^{-5/2} \cdot \text{s}^{1/2}$  and for the perpendicular disc is  $2 \pm 13 \text{ A.m}^{-5/2} \cdot \text{s}^{1/2}$ .

The effect of the degree of enamelling was not explicitly investigated, but the results given in Figure 4.4.6 do cover a considerable range of  $\chi$ , from  $\chi = 0.73$  to  $\chi = 1$ .

The sphere electrodes did not span the same range of radius as did the disc electrodes and if  $G^1$  is plotted against  $R^{-1/2}$ , as in Figure 4.4.6 for the discs, all the points are grouped close together. The effect of radius upon the output current of a sphere is best shown by plotting the square root of the gradient of the  $I^2-U_a$  graph against  $R^{3/2}$ . The gradient of the  $I^2-U_a$  graph is defined as  $g$ . From equation 3.9.12 for the response of an epoxied sphere it follows that

$$g^{1/2} = 2\pi \times 1.04 R^{3/2} (Q_{s1} + Q_{s2}) \text{ mec}_s D^{2/3} v^{-1/6} \quad (4.4.3)$$

Combining equations 4.4.3 and 3.9.15 for the epoxied sphere gives

$$g^{1/2} = 2\pi R (b+R) G^{1/2} \quad (4.4.4)$$

Figure 4.4.7 shows the variation of  $g^{1/2}$  with  $R^{3/2}$ . The line drawn in Figure 4.4.7 is only for the gold epoxied spheres, and gives a value of  $D$  at  $37.5^\circ\text{C}$  of  $2.5 \pm 0.2 \times 10^{-9} \text{ m}^2 \cdot \text{s}^{-1}$ . Again the origin is an experimental point. The intercept given by the least squares fit is  $0 \pm 0.2 \times 10^{-5} \text{ A.m}^{-1/2} \cdot \text{s}^{1/2}$ . For completeness points are also plotted for a copper sphere (with epoxy) and for a special gold sphere constructed to attempt to eliminate the effects of epoxy resin (Chapter 6, Figure 6.2.2).

For the special sphere, from equation 3.9.4 it follows that

$$g^{1/2} = 2\pi \times 1.04 R^{3/2} Q_s \text{ mec}_s D^{2/3} v^{-1/6} \quad (4.4.5)$$

The effect of varying the dimension  $b$  was not explicitly investigated. For the epoxied spheres the ratio  $b/R$  varied between 0.20 and 0.84. For the special sphere  $b/R$  was nominally 1.

The variation of the values of  $D$  obtained with temperature is shown in Figure 4.4.8, for the parallel and perpendicular discs and for

the gold epoxied spheres. To obtain the results shown an electrode of each type was used to perform velocity responses at the different temperatures. Whilst the results do seem to confirm that  $\ln_e D$  varies as  $1/T$ , the range of temperature (from  $17^{\circ}\text{C}$  to  $45^{\circ}\text{C}$ ) is possibly too small.

The same results (as for Figure 4.4.8) were used to produce Figure 4.4.9 where the variation of output current with temperature is shown by plotting  $G^{\frac{1}{2}}$  against temperature. If the gradients of the lines drawn are normalised against the values of  $G^{\frac{1}{2}}$  at, say  $37^{\circ}\text{C}$ , the percentage increase in the output current (caused by a given velocity) per degree centigrade is obtained. For the parallel disc the increase is  $1.3 \pm 0.2\%/\text{C}$ , for the perpendicular disc  $0.9 \pm 0.4\%/\text{C}$  and for the sphere is  $1.1 \pm 0.2\%/\text{C}$ . So, to a large extent the effect upon output current of the increase of  $D$  with temperature is offset by the decrease in  $c_g$ .

Some final points require mention. For gold sphere electrodes, when the velocity response was retested at intervals over periods of months, the responses were found to be equal, within the scatter, when changes in  $c_g$  had been allowed for. Such long term testing was not possible for copper electrodes because of surface oxidation when not in use. However, if kept working continually the velocity response did not change over several days. Usually the electrodes failed when the response markedly increased, becoming random in nature. This was attributed to breakdown of the insulating enamel after prolonged immersion.

Occasionally, after operation in dusty conditions (a dust film being observed on the surface of the saline) a decrease in response of the electrodes was observed. On inspection the surface of the electrode could be seen to be covered by a greyish deposit, which could be removed by wiping, when the response of the electrode usually returned to its original value.

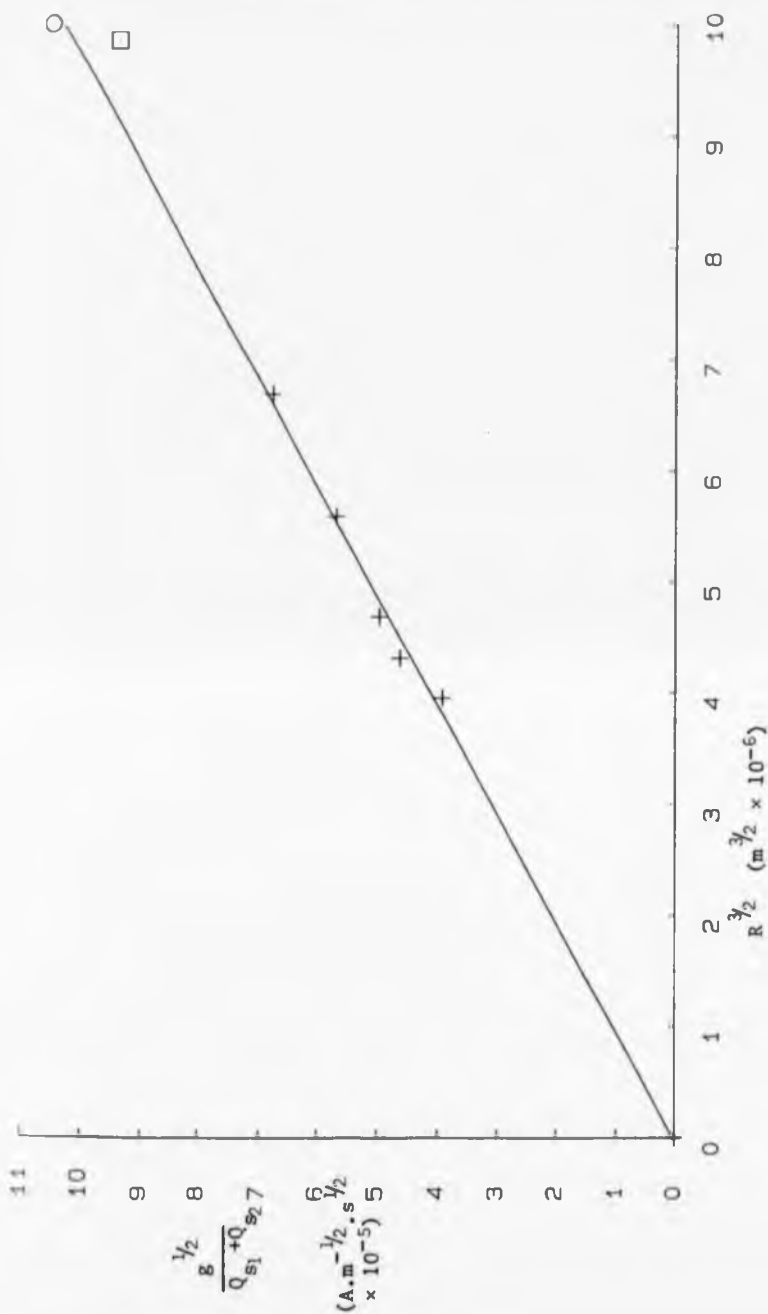


Figure 4.4.7 The variation of  $g^{1/2}$  with radius for the epoxied gold sphere cathode at  $37.5^{\circ}\text{C}$ .  $c_g$  within 1% of  $1.25 \pm 10^{23}$  molecules. $\text{m}^{-3}$   
 gradient =  $10.2 \pm 0.4$   $\text{A.m}^{-2}.\text{s}^{1/2}$

□ special gold sphere; ○ copper sphere (figure 4.4.4b)

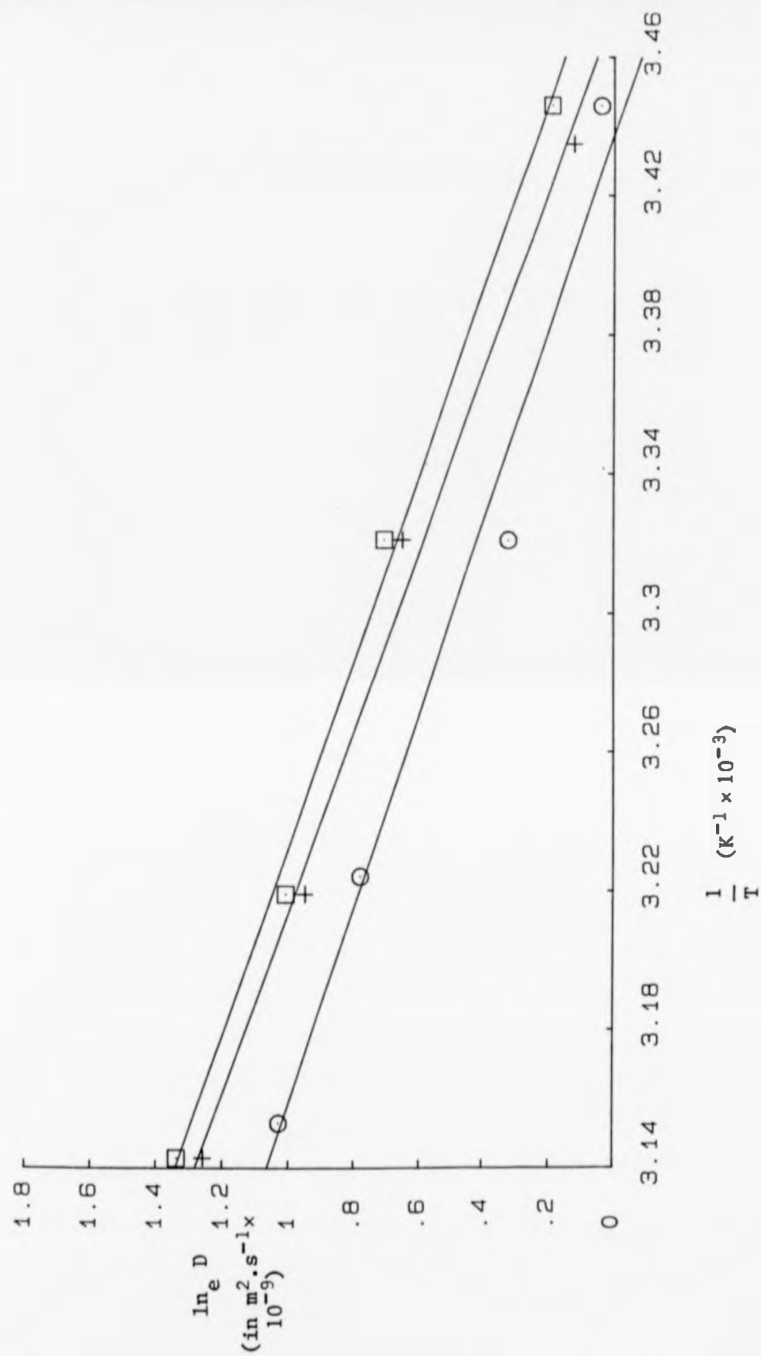


Figure 4.4.8 The variation of the values of  $D$  derived, with temperature.

Parallel disc (+) gradient =  $-3.8 \pm 0.4 \times 10^3 \text{K}$

Perpendicular disc (O) gradient =  $-3.6 \pm 0.6 \times 10^3 \text{K}$

Epoxied sphere (square) gradient =  $-3.7 \pm 0.3 \times 10^3 \text{K}$

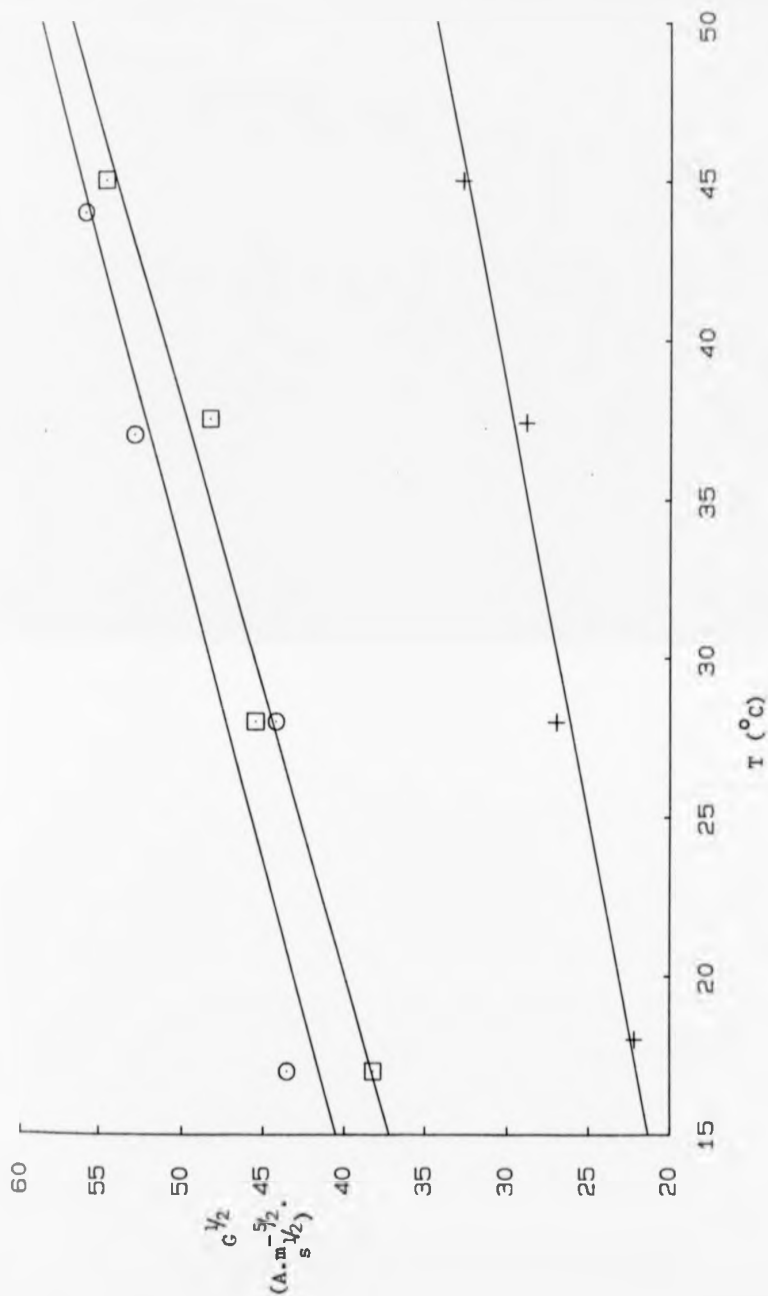


Figure 4.4.9 The variation of  $C^{1/2}$  with temperature.

+ Parallel disc  $R = 8.5 \times 10^{-4}\text{m}$ ,  $\chi = 0.93$ , gradient =  
 $0.37 \pm 0.06 \text{ A.m}^{-5/2} \cdot \text{s}^{1/2} / ^\circ\text{C}$

o Perpendicular disc  $R = 8.5 \times 10^{-4}\text{m}$ ,  $\chi = 0.93$ , gradient =  
 $0.5 \pm 0.2 \text{ A.m}^{-5/2} \cdot \text{s}^{1/2} / ^\circ\text{C}$

□ Epoxied sphere  $R = 2.6 \times 10^{-4}\text{m}$ ,  $b = 1.8 \times 10^{-4}\text{m}$   
 gradient =  $0.56 \pm 0.09 \text{ A.m}^{-5/2} \cdot \text{s}^{1/2} / ^\circ\text{C}$

If, after construction, a copper electrode was exposed to air for some time its response, whilst still exhibiting the normal dependencies, was considerably reduced in magnitude. Similarly, if immersed in saline for some time with no potential applied, a decreased response was observed when the electrode was tested. Such effects were attributed to oxidation of the copper surface. Consequently, care was taken to minimise the time between construction and use, but the presence of some oxidation on the surface of the copper electrodes used cannot be excluded.

#### 4.5 Discussion

The results presented in section 4.3 confirm the basic electro-chemistry and require no further comment. The results of section 4.4 show conclusively that the variations of current, predicted by the theories of Chapter 3, with the magnitude of flow velocity, oxygen concentration and electrode dimensions are obtained. Also, the velocity response results were found to be repeatable. This is sufficient for the device to be used as a practical flow transducer.

To investigate the detailed accuracy of the theories of Chapter 3, values of the diffusion coefficient of oxygen have been derived from the results, with the assumption that the number of electrons involved in the reduction of one oxygen molecule is 4. The values of  $D$  plotted for the parallel disc, at  $37.5^{\circ}\text{C}$ , are in the range  $2.4$  to  $3.0 \times 10^{-9} \text{ m}^2 \cdot \text{s}^{-1}$ , whilst those for the sphere are in the range  $2.2$  to  $2.7 \times 10^{-9} \text{ m}^2 \cdot \text{s}^{-1}$ . Those for the perpendicular disc lie between  $1.4$  and  $2.2 \times 10^{-9} \text{ m}^2 \cdot \text{s}^{-1}$ . The values of  $D$  given in Landolt-Börnstein (Figure 4.1.1) do not extend to such a high temperature, but the values of  $D$  obtained for the parallel disc and the sphere are not unreasonable in comparison. The values of  $D$  for the perpendicular disc are, however, certainly too low, possible reasons

for which are discussed below.

For each electrode type the values of  $D$  are consistent over a considerable range of oxygen concentration and electrode dimensions, reflecting favourably upon the theory of Chapter 3. The predicted dependencies of current upon the main variables have been satisfactorily confirmed. It remains to discuss the confirmation, or otherwise, of the details of the theory.

It must first be stated that the experiments conducted were designed to investigate the variation of current with the main variables, and not to test the accuracy of details of particular theories. Therefore, it is possible that the experiments are in some sense deficient for this second purpose.

Comparison of the values of  $D$  obtained with those given in Figure 4.1.1 is difficult because of the wide scatter of the points of Figure 4.1.1. However, a true value of  $D$  must exist and any difference between this and the values obtained in this work could be caused by any combination of the following factors.

- (a) The value of  $m$  used is too high. Since  $D$  is proportional to  $m^{-3/2}$  (equation 3.1.2) any overestimate of  $m$  would cause a disproportionate decrease in the value of  $D$  derived.
- (b) One of the potential flow distributions used may be in error. Since the predicted variations with the main variables have been obtained, any such theoretical inadequacy could only manifest itself in the coefficient of  $S$ . Indeed if any realistic flow distribution around an electrode is assumed then an equation of the form of equation 3.1.2 will be obtained. Differences between various flow distributions could only exist in the coefficient of  $S$ .
- (c) The theory is being applied to an experimental situation which it does not exactly describe, or rather that the experimental situation does

not reflect closely enough the idealised theoretical model. For example, the theory assumes a perfectly smooth electrode surface of constant surface reactivity. In the case of copper electrodes oxidation may well "deactivate" scattered regions of the surface, and even gold sphere electrodes which are perfectly smooth in construction easily suffer damage to their soft surfaces during handling.

Also the disc electrodes were usually the ends of cylinders (though the largest electrodes were discs and behaved in a similar manner - Figure 4.4.6) and consequently the flow distribution might differ from that assumed. Similarly, with spheres the existence of the structural epoxy resin was assumed to only insulate some of the sphere and not to affect the flow pattern. Misalignment of disc electrodes is another possibility.

All of these effects if present, except misalignment of the parallel disc, would probably act to reduce the current and so the value of  $D$  obtained.

(d) Inaccuracies in the measurements of the dimensions of the electrodes, that is  $R$ ,  $\chi$  and  $b$ , and in the oxygen concentration  $c_g$  when the effect of  $c_g$  upon the current response was being investigated.

Up to this point all errors quoted refer only to scatter in the points of the graphs presented, that is to the precision of the results. All dimensions given are average values in that several measurements in different positions were taken of each electrode and averaged. The measurements, therefore, include any deviation from the correct shape for a particular electrode, such as non-uniformity of enamelling. Typically the dimensions are accurate to within  $\pm 5\%$ , but current not current density is the fundamental measurement and current is proportional to  $R^{3/2}$  so the error in  $R$  becomes an error of  $\pm 8\%$  in the expression for  $D^{2/3}$ . (Any error or non-linearity in the calibration of the voltage-clamp circuitry and the

recording system was far smaller than this.)

When  $c_g$  was varied it was held constant to within  $\pm 5\%$ . An uncertainty of  $\pm 5\%$  has already been quoted in  $D$ , caused by the scatter of the points of the graphs. Using a naive analysis (a more sophisticated approach is not worthwhile) in the worst case these errors would be additive to give an uncertainty in  $D^{2/3}$  approaching  $\pm 20\%$  and in  $D$  of  $\pm 30\%$ .

It would be surprising though, if the degree of error due to these factors was anywhere near this limit because the values of  $D$  obtained in different ways, for each electrode type are so consistent. The most likely causes of error in  $D$  must be those listed under (a) to (c).

The different derivations of  $D$  for the sphere and the parallel disc are very close. Whilst those for the perpendicular disc agree reasonably well they are consistently smaller. The perpendicular disc therefore requires special attention for possible sources of error particular to itself.

As far as reliability of the theory is concerned, that for the perpendicular disc is probably least so, whilst that for the parallel disc is most. Also whilst the end faces of cylinders, that is the cut end of a wire, were used often for both perpendicular and parallel discs, it is possible that the disturbance of the flow pattern was greatest for the perpendicular disc.

Given that the theory for the perpendicular disc is adequate the most likely cause of disagreement is misalignment of the disc away from the perpendicular. This problem does not exist for the sphere since it was easy to align the edge of the epoxy resin parallel to the flow and the response to reciprocal movements allowed this to be checked. With the parallel disc any misalignment was detectable and could either be corrected or allowed for by averaging the reciprocal responses, which was found adequate. For the perpendicular disc misalignment was not easy to detect because there was only one meaningful direction of motion. Also, the

perpendicular disc is unique in that it has to be correctly aligned in two orthogonal planes.

It seems very likely that the flow distribution caused by flow exactly perpendicular to a finite electrode is an unstable one. That is, any small component of flow parallel to the surface would cause a radical change in the flow pattern towards that for the parallel case. After this large change caused by the initial very small misalignment, any further misalignment would have only a comparatively small effect.

If the above reasoning is correct, then the existence of the random free convection makes it effectively impossible to reliably obtain the perpendicular flow distribution even though the electrode might be exactly perpendicular to its direction of movement. If the perpendicular flow distribution is not achieved then the current obtained will be smaller and the value of  $D$  derived smaller also. The conclusion must be that some other experimental arrangement is necessary to obtain the correct flow pattern.

The above discussion is probably overcritical since there is no proof that the values of  $D$  obtained from the sphere and parallel disc are inaccurate. An attempt has been made to include every reasonable criticism. It should be emphasised that the experiments reported were designed to investigate the dependence of the output current upon the main variables, not to confirm the accuracy of any theory in all its detail. The experimental arrangement was perfectly adequate for this purpose, providing the information required and in the process confirming the form of equation 3.1.2, for the three types of electrode considered. The experiments also confirm in large part the accuracy of the theories of Chapter 3. With respect to confirming these theories though, certain inadequacies do exist, especially in the case of the perpendicular disc, where a different type of experimental arrangement is necessary to fully test the theory. An arrangement with

the electrode stationary and the fluid impinging upon it would probably suffice.

It is clear from the results presented that in a "blind" situation, such as the CSF pathways, only magnitude information can be obtained from any single electrode. To ensure that this information is unambiguous the electrode should be a sphere. However, the existence of the necessary connection to the sphere does mean that some of its directional insensitivity is lost. For use in humans the spherical cathode should be gold since it is unaffected by storage and cannot inject unacceptable ions in the case of an accidental reversal of electrode polarity. An Ag/AgCl anode is recommended to again avoid the injection of foreign ions.

In short, the above work confirms the practicability of using the oxygen-reduction electrode as a flow transducer for physiological applications.

CHAPTER 5

CHAPTER 5THE TIME RESPONSE OF THE OUTPUT CURRENT:THE RESPONSE TO A STEP DECREASE IN FLOW VELOCITY5.1 Introduction

The time response to a step decrease in flow will be considered in this chapter since it provides the limiting response and is also probably closest to that occurring during cough impulses in the CSF. Often, the velocity responses of the previous chapter were obtained by suddenly moving the cathode, and then equally suddenly stopping it. The response of the current to an increase in flow was sufficiently fast for this convenient method to be satisfactory. However, the response of the current to a decrease in flow was so much slower that the actual decrease in flow imposed could be considered to be a step. The response of the current to this step decrease in flow was initially fast and then followed by a slow tail. Figures 6.3.1, 6.3.2 and 6.3.3 show typical responses of a parallel disc, a perpendicular disc and a sphere respectively. These responses, whilst similar do differ in some respects.

The time response was found to be extremely complex, but always of the same shape for each type of electrode. The time taken to fully respond was found to depend upon the final current, corresponding to the final velocity and on the ratio of the initial and final currents as well as on the size of the electrode and the temperature. The shape of the time response defied attempts to fit it with any simple curve.

In principle the complete description of the time response requires the solution, with the requisite boundary, initial and final conditions, of the time dependent convective diffusion equation (equation 3.3.1). However, considering the difficulty of solving the steady state convective diffusion equation (equation 3.3.3) this was not thought a profitable course of action.

If when there is a decrease in velocity the hydrodynamic boundary layer responds much faster than the diffusion layer, it may well be possible to describe the time response of the current by a solution of the time dependent diffusion equation

$$\frac{\partial c}{\partial t} = D\nabla^2 c \quad (5.1.1)$$

That is, the hydrodynamic boundary layer is assumed to respond so quickly that sufficient account can be taken of convective effects in the boundary, initial and final conditions.

Two approaches to the solution of equation 5.1.1 are presented. The first, given for completeness, assumes simplified non-specific initial and boundary conditions and is of limited applicability but is still probably an advance on treatments found elsewhere (Bockris and Reddy, 1970). This approach does not draw upon the theory of Chapter 3 and is independent of the type of electrode. Its limited usefulness prompted the second approach.

The second approach employs much more realistic initial and boundary conditions and draws heavily on the theory of Chapter 3. It was found to be completely successful, being able to reproduce accurately the shapes of the time responses of the various electrodes (not a trivial matter) and when compared with experiment gave values of the diffusion coefficient of oxygen which compare favourably with those in the literature. Since this approach depends upon the theory of Chapter 3, its success is very good support for the accuracy of that theory.

## 5.2 A simple model of the time response

As stated above, the assumption is made that the response to a step decrease in velocity can be described by a solution of equation 5.1.1. It is first necessary to define the terminology. The initial free stream velocity is  $U_{oi}$ , but will be written  $U_i$  for simplicity and the corresponding

average current density is  $\bar{J}_i$ . Similarly, the final free stream velocity is  $U_f$  and the corresponding average current density is  $\bar{J}_f$ .

As for the steady state, changes in concentration normal to the electrode surface are much greater than those parallel to the surface. That is  $\partial c/\partial y > \partial c/\partial x$  and  $\partial^2 c/\partial y^2 \gg \partial^2 c/\partial x^2$ . So, a solution to the following one dimensional form of equation 5.1.1 is required

$$\frac{\partial c}{\partial t} = D \frac{\partial^2 c}{\partial y^2} \quad (5.2.1)$$

with the initial and boundary conditions

$$t < 0 \quad : \quad c = c_s \quad \text{for } y \geq 0 \quad (5.2.2)$$

$$t > 0 \quad : \quad c = 0 \quad \text{at } y = 0 \quad (5.2.3)$$

$$c = c_s \quad \text{at } y = \infty$$

The solution, with these conditions is

$$c = c_s \operatorname{erf} \left( \frac{y^2}{4Dt} \right)^{1/2} \quad (5.2.4)$$

To obtain the current density  $J$  at a point (following Chapter 3)

$\frac{\partial c}{\partial y} \Big|_{y=0}$  is required. That is

$$\frac{\partial c}{\partial y} \Big|_{y=0} = \frac{c_s}{(Dt\pi)^{1/2}} \quad (5.2.5)$$

Since

$$J = Dme \frac{\partial c}{\partial y} \Big|_{y=0} \quad (5.2.6)$$

the current density at a point is

$$J = (\pi^{-1/2} mec_s D^{1/2}) t^{-1/2} \quad (5.2.7)$$

This equation is independent of position on the cathode surface and therefore, the average current density is equal to the current density at

any point. That is

$$\bar{J} = (\pi^{-1/2} \text{mec}_s D^{1/2}) t^{-1/2} \quad (5.2.8)$$

Weaknesses in this approach are already apparent. Equation 5.2.7 is independent of position, implying all points on the surface are equivalent and is therefore, in conflict with the theory of Chapter 3. Also equations 5.2.7 and 5.2.8 are independent of the particular electrode type. These results are a consequence of the simple, non-specific boundary conditions employed, which themselves require further comment.

The condition for  $t < 0$  (equation 5.2.2) states in effect that the diffusion layer thickness  $\delta$  is zero. There are two ways in which this could be so. First, that the cathode is switched off, merely placed in the fluid. The second, that there is an infinite flow and therefore an infinite current. (This raises a related point which is discussed here for convenience. If the cathode is immersed switched off in oxygen containing saline, there is in contact with it a reservoir of oxygen and equation 5.2.2 applies. On switching on this oxygen is immediately available and in principle should give rise to an infinite current until the excess is consumed. In practice, a large but finite current is obtained, since until the current becomes transport controlled it is, initially limited by the reaction kinetics).

In equations 5.2.7 and 5.2.8 the time  $t$  is measured from the instant of the step decrease. However, the condition 5.2.3 assumes the initial current is infinite. To accommodate a finite initial current the time,  $\tau$ , is introduced. Whilst  $t = 0$  is the time at which the step decrease in velocity occurs,  $t = -\tau$  is the notional time at which  $\delta = 0$ . If  $U_1 \gg 0$ , then  $\tau$  will be small compared to the total diffusion time. Initially,  $\delta$  will be very small if  $U_1 \gg 0$  and then for  $t > \tau$  distances normal to the surface measured relative to either  $y = 0$  or the initial  $\delta$ , will become equivalent and condition 5.2.2 hold.

Further, in deriving equation 5.2.8 it is assumed that  $U_i$  is completely removed by the step decrease in velocity, that is  $U_f = 0$  and the response continues until  $\delta$  is infinite and  $\bar{J}_f$  zero. In practice a finite free convection velocity always exists (Marchiano and Arvia, 1968) causing a finite final current,  $\bar{J}_f$ . If  $U_i \gg U_f$  ( $\approx 0$ ), then  $\tau$  and  $\bar{J}_f$  may be included in equation 5.2.8 to take account of the non-infinite initial current and the non-zero final current, to give

$$\bar{J} - \bar{J}_f = (\pi^{-1/2} \text{me} c_s D^{1/2}) (t + \tau)^{-1/2} \quad (5.2.9)$$

where  $t = 0$  is the time at which the step decrease in velocity occurs and  $t = -\tau$  is the notional time at which  $\delta = 0$ .

Implicit in equation 5.2.9 is the assumption that all time responses (of all types of electrode), to a given final current density, are described by the same curve, the response proceeding from the initial current as if from an infinite current. Equation 5.2.9 only applies to situations where  $U_i \gg U_f$  ( $\approx 0$ ) and therefore its usefulness is limited. The success, and otherwise, of this description of the time response is detailed in Chapter 6.

The main points of criticism are as follows: the finite initial and non-zero final currents are taken account of in what is possibly an ad-hoc manner; the simplified, non-specific initial and boundary conditions result in an expression which is independent of position on the electrode surface, and which is also independent of the electrode type. The approach of the next section, at the cost of greatly increased complexity, uses much more sophisticated initial and boundary conditions and successfully overcomes these criticisms.

### 5.3 A More Accurate Model of the Time Response

The second approach is again a solution of the time dependent diffusion equation (equation 5.1.1). As before the assumption is made

that convective effects can be satisfactorily accounted for by the boundary initial and final conditions. To improve the description of the situation existing, over that of the preceding section, the boundary, initial and final conditions used are linearised concentration profiles of the type

$$c(y) = \frac{c_s y}{\delta} \quad (5.3.1)$$

Linearised concentration profiles (the diffusion layer model) are used instead of the actual concentration profiles, for mathematical simplicity. This is justified since, as in the solution of the steady state convective-diffusion equation (Chapter 3) when the actual concentration profiles were obtained, the variation of  $\partial c/\partial y$  at  $y = 0$  is sought. The linearised concentration profile is only an extension of  $\partial c/\partial y$  at  $y = 0$ .

When conditions of the form of equation 5.3.1 are used the system is finite and linear with boundaries at  $y = 0$  and  $y = \delta_f$ ,  $\delta_f$  being the final value of the diffusion layer thickness. The boundaries along the surface of the electrode (that is in the  $x$  and  $z$  directions for, say, a flat plate) need not be infinite but should be parallel to the normal to the surface. The initial and boundary conditions should be functions of  $y$  only.

It is assumed that only diffusion normal to the surface need be considered, as in the solutions of the steady state convective diffusion equation in Chapter 3. That is, the equation to be solved, is again

$$\frac{\partial c}{\partial t} = D \frac{\partial^2 c}{\partial y^2} \quad (5.3.2)$$

The model assumed here is shown schematically in figure 5.3.1. As always  $x$  is the distance along the surface from either the stagnation point or the point at which the flow impinges, and  $y$  is the normal to the surface. It is assumed that the diffusion layer thickness, varies slowly with  $x$ , so that it can be considered constant over the small distance  $dx$ . The

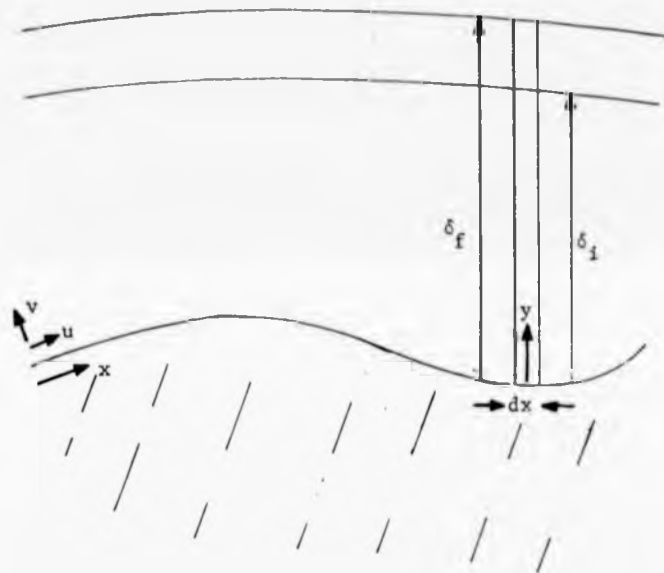


Figure 5.3.1 The generalised electrode geometry assumed in the time response theory.

time dependence of  $J$  in the small element  $dx$  will be obtained, the total current from a particular electrode, then being obtainable by integration over the surface of the electrode.

A solution to equation 5.3.2 is sought, subject to the following conditions:

$$\text{Initial: } t = 0 \quad ; \quad c = \phi_i(y) \quad \text{for } 0 \leq y \leq \delta_f \quad (5.3.3)$$

$$\text{where } \phi_i(y) = \frac{c_s y}{\delta_i} \quad 0 \leq y \leq \delta_i$$

$$\text{and } \phi_i(y) = c_s \quad \delta_i \leq y \leq \delta_f$$

$$\text{Final: } t \rightarrow \infty \quad ; \quad c = \frac{c_s y}{\delta_f} \quad (5.3.4)$$

$$\text{Boundary: } c = 0 \quad \text{for } y = 0 \quad (5.3.5)$$

$$c = c_s \quad \text{for } y = \delta_f \quad \text{when } t > 0$$

$$\text{Let } c = c_1 + c_2 + c_3 \quad (5.3.6)$$

where  $c_1$ ,  $c_2$  and  $c_3$  satisfy the following conditions

$$\text{Initial: for } 0 \leq y \leq \delta_f \quad \text{at } t = 0$$

$$c_1 = \phi_i(y) \quad (5.3.7)$$

$$c_2 = \phi_i^*(y) \quad (5.3.8)$$

$$\text{Boundary: for } t > 0 \quad \text{at } y = 0 \quad \text{and } y = \delta_f$$

$$c_1 = 0 \quad (5.3.9)$$

$$c_2 = 0 \quad (5.3.10)$$

$$\text{For all } t, c_3 = \frac{c_s y}{\delta_f} \quad (5.3.11)$$

$$\text{where } \phi_i(y) = \frac{c_s y}{\delta_i} \quad \text{for } 0 \leq y \leq \delta_i \quad (5.3.12)$$

$$\text{and } \phi_i(y) = c_s \quad \text{for } \delta_i \leq y \leq \delta_f$$

$$\text{and } \phi_i^*(y) = \frac{c_s y}{\delta_f} \quad (5.3.13)$$

With  $c_1$ ,  $c_2$  and  $c_3$  satisfying these conditions  $c$  satisfies conditions 5.3.3., 5.3.4. and 5.3.5.

The solution for  $c_3$  is trivial. Therefore only solutions for  $c_1$  and  $c_2$  are required, and these are equivalent. To avoid confusion, the dummy variable  $b$  is introduced. Therefore, a solution of the following equation is required

$$\frac{\partial b}{\partial t} = D \frac{\partial^2 b}{\partial y^2} \quad (5.3.14)$$

subject to the conditions

$$\text{Initial: } b = \phi(y) \text{ for } 0 \leq y \leq \delta_f \text{ at } t = 0 \quad (5.3.15)$$

$$\text{Boundary: For } t > 0, b = 0 \text{ at } x = 0, x = \delta_f \quad (5.3.16)$$

The method of the separation of variables is used (Crank, 1975). That is

$$\text{let } b = Y(y) \cdot T(t) \quad (5.3.17)$$

$$\text{so that } \frac{1}{T} \frac{\partial T}{\partial t} = \frac{D}{Y} \frac{\partial^2 Y}{\partial y^2} \quad (5.3.18)$$

The left hand side and the right hand side of equation 5.3.18 must equal the same constant, say  $-\lambda^2 D$ . That is

$$\frac{1}{T} \frac{\partial T}{\partial t} = -\lambda^2 D \quad (5.3.19)$$

$$\text{and } \frac{1}{Y} \frac{\partial^2 Y}{\partial y^2} = -\lambda^2 \quad (5.3.20)$$

The solutions are

$$T = \exp(-\lambda^2 Dt) \quad (5.3.21)$$

$$\text{and } Y = A \cos \lambda y + B \sin \lambda y \quad (5.3.22)$$

where  $A$  and  $B$  are constants.

Therefore

$$b = \exp(-\lambda^2 Dt) (A \cos \lambda y + B \sin \lambda y) \quad (5.3.23)$$

Applying the boundary condition 5.3.16 gives  $A = 0$  and  $\lambda = \frac{n\pi}{\delta_f}$   
where  $n = 0, 1, 2, \text{etc.}$

$$\text{That is } b = \exp \left[ -\frac{n^2 \pi^2 Dt}{\delta_f^2} \right] B \sin \left[ \frac{n\pi y}{\delta_f} \right] \quad (5.3.24)$$

This is only one of many possible solutions. The most general solution is the sum of all such solutions,

$$b = \sum_{n=1}^{\infty} \exp \left[ -\frac{n^2 \pi^2 Dt}{\delta_f^2} \right] B_n \sin \left[ \frac{n\pi y}{\delta_f} \right] \quad (5.3.25)$$

since the term for  $n = 0$  is zero.

An explicit expression for the coefficient  $B_n$  is required. The initial condition 5.3.15 is applied. Both sides of equation 5.3.25 are multiplied by  $\sin \left( \frac{p\pi y}{\delta_f} \right)$  ( $p$  is any integer) and integrated over  $\delta_f$  with  $b = \phi(y)$  and  $t = 0$ , to give

$$\int_0^{\delta_f} \phi(y) \sin \left[ \frac{p\pi y}{\delta_f} \right] dy = \sum_{n=1}^{\infty} \int_0^{\delta_f} B_n \sin \left[ \frac{p\pi y}{\delta_f} \right] \cdot \sin \left[ \frac{n\pi y}{\delta_f} \right] dy \quad (5.3.26)$$

$$\begin{aligned} \text{Now } \int_0^{\delta_f} \sin \left[ \frac{p\pi y}{\delta_f} \right] \sin \left[ \frac{s\pi y}{\delta_f} \right] dy &= 0 \quad s \neq p \quad (5.3.27) \\ &= \frac{\delta_f}{2} \quad s = p \quad (\text{Dwight, 1961}) \end{aligned}$$

and therefore

$$B_n = \frac{2}{\delta_f} \int_0^{\delta_f} \phi(y) \sin \left[ \frac{n\pi y}{\delta_f} \right] dy \quad (5.3.28)$$

That is the solution of equation (5.3.14) with the conditions 5.3.15 and 5.3.16 is

$$b = \sum_{n=1}^{\infty} B_n \exp \left[ - \frac{\pi^2 D t n^2}{\delta_f^2} \right] \sin \left[ \frac{n \pi y}{\delta_f} \right] \quad (5.3.29)$$

with the coefficients  $B_n$  being given by equation 5.3.28.

The expressions for  $c_1$  and  $c_2$  are obtained by substituting the initial conditions (equation 5.3.7) into equation 5.3.29, that is

$$c_1 = \frac{2}{\delta_f} \sum_{n=1}^{\infty} \exp \left[ - \frac{\pi^2 D t n^2}{\delta_f^2} \right] \sin \left[ \frac{n \pi y}{\delta_f} \right] \int_0^{\delta_f} \phi_i(y) \sin \left[ \frac{n \pi y}{\delta_f} \right] dy \quad (5.3.30)$$

$$c_2 = \frac{2}{\delta_f} \sum_{n=1}^{\infty} \exp \left[ - \pi^2 \frac{D t n^2}{\delta_f^2} \right] \sin \left[ \frac{n \pi y}{\delta_f} \right] \int_c^{\delta_f} \phi_i^*(y) \sin \left[ \frac{n \pi y}{\delta_f} \right] dy \quad (5.3.31)$$

Since  $\int x \sin x dx = \sin x - x \cos x$  (Dwight, 1961)

it follows that

$$\int_0^{\delta_f} \phi_i(y) \sin \left[ \frac{n \pi y}{\delta_f} \right] dy = \frac{c_s \delta_f}{n \pi} \left[ \frac{1}{a n} \sin(a n) - (-1)^n \right] \quad (5.3.32)$$

$$\text{and } \int_c^{\delta_f} \phi_i^*(y) \sin \left[ \frac{n \pi y}{\delta_f} \right] dy = \frac{c_s \delta_f}{n \pi} (-1)^n \quad (5.3.33)$$

where  $a = \frac{\pi \delta_i}{\delta_f}$  (5.3.34)

Therefore, from equation 5.3.6

$$c = \frac{c_s y}{\delta_f} + \frac{2}{\delta_f} \sum_{n=1}^{\infty} \exp \left[ - \frac{\pi^2 D t n^2}{\delta_f^2} \right] \sin \left[ \frac{n \pi y}{\delta_f} \right] \frac{c_s \delta_f}{n^2} \frac{\sin(an)}{an} \quad (5.3.35)$$

and

$$\frac{\partial c}{\partial y} = \frac{c_s}{\delta_f} + \frac{2c_s}{\delta_f} \sum_{n=1}^{\infty} \exp \left[ - \frac{\pi^2 D t n^2}{\delta_f^2} \right] \cos \left[ \frac{n \pi y}{\delta_f} \right] \frac{\sin(an)}{an} \quad (5.3.36)$$

Therefore

$$\frac{\partial c}{\partial y} \Big|_{y=0} = \frac{c_s}{\delta_f} + \frac{2c_s}{\delta_f} \sum_{n=1}^{\infty} \exp \left[ - \frac{\pi^2 D t n^2}{\delta_f^2} \right] \frac{\sin(an)}{an} \quad (5.3.37)$$

Since  $\frac{\partial c}{\partial y} \Big|_{y=0} = \frac{c_s}{\delta}$  (equation 3.3.7)

$$\frac{1}{\delta} = \frac{1}{\delta_f} + \frac{2}{\delta_f} \sum_{n=1}^{\infty} \exp \left[ - \frac{\pi^2 D t n^2}{\delta_f^2} \right] \frac{\sin(an)}{an} \quad (5.3.38)$$

and since  $J = D m e \frac{\partial c}{\partial y} \Big|_{y=0}$  (equation 3.7.38)

$$J(x,t) = J_f(x) + 2 J_f(x) \sum_{n=1}^{\infty} \exp \left[ - \frac{\pi^2 D t n^2 J_f^2}{D^2 m^2 e^2 c_s^2} \right] \frac{\sin(an)}{an} \quad (5.3.39)$$

where  $a = \frac{\pi \delta_i}{\delta_f} = \frac{\pi J_f}{J_i} = \frac{\pi \bar{J}_f}{\bar{J}_i}$  (5.3.40)

Equations 5.3.38 and 5.3.39 are equivalent and are the required expressions, both  $\delta$  and  $J$  being functions both of position on the electrode surface and of time. Expressions for the response of the total current of particular electrodes are obtained by integration of equation 5.3.39. This process, for the electrode types previously considered, is described in the following sections.

5.4. The calculation of the time response of an enamelled disc parallel to the flow.

The geometry relevant to this calculation is given in figure 3.6.3. As for the calculation of the steady state response of a parallel disc, the response of an elemental rectangular strip must be introduced. The current density  $J$ , at a point on an enamelled plate parallel to the flow is given by equation 3.6.1.

$$J(x) = 0.34 \text{ m e c}_s D^{2/3} v^{-1/6} U_o^{1/2} x^{-1/2} \left[ 1 - \left( \frac{h}{x} \right)^{3/4} \right]^{-1/3}$$

(5.4.1)

The total current  $dI$ , from the elemental strip of figure 3.6.3 can be written

$$dI = \int_h^l J dx \quad (5.4.2)$$

and therefore, from equation 3.6.3 the total current  $I$ , from the disc may be written

$$I = 2 \int_0^{XR} db \int_h^l J dx \quad (5.4.3)$$

or in integrated form, from equations 3.6.4 and 3.6.5

$$I = 4 \times 0.34 \text{ m e c}_s D^{2/3} v^{-1/6} U_o^{1/2} R^{3/2} Q_{II} \quad (5.4.4)$$

Introducing the subscript  $f$ , to show that current variables correspond to a final flow velocity  $U_{of}$ , equations 5.4.1 and 5.4.4 can be combined to give

$$J_f(x) = \frac{I_f}{4R^{3/2} Q_{II}} \cdot \frac{1}{x^{1/4}(x^{3/4} - h^{3/4})^{1/3}} \quad (5.4.5)$$

$J_f(x)$  is the current density at a point corresponding to the final steady velocity  $U_f$  (the subscript  $o$  being dropped for simplicity). Equation 5.4.5. can be substituted into equation 5.3.39 to give the time dependent current density at a point  $J(x,t)$

$$J(x,t) = \frac{I_f}{4R^{3/2} Q_{II}} \cdot \frac{1}{x^{1/4}(x^{3/4} - h^{3/4})^{1/3}} +$$

$$\frac{2I_f}{4R^{3/2} Q_{II}} \cdot \frac{1}{x^{1/4}(x^{3/4} - h^{3/4})^{1/3}} \left[ \sum_{n=1}^{\infty} \frac{\sin an}{an} \exp \left( - \frac{C n^2 R}{x^{1/2}(x^{3/4} - h^{3/4})^{2/3}} \right) \right] \quad (5.4.6)$$

where

$$C = \left( \frac{\pi I_f}{4D \text{ m e c}_s Q_{II} R^2} \right)^2 D t \quad (5.4.7)$$

Writing  $C$  in this way effectively introduces an extra term  $R$  on the top and the bottom of the exponential term of equation 5.4.6. This is done so that the final expression is dimensionless, simplifying the computing of the expression.

The time varying current from the disc is obtained by performing the double integration of equation 5.4.3 upon equation 5.4.6.

$$I(t) = \frac{I_f}{2R^{3/2} Q_u} \int_0^{xR} db \int_h^{\ell} \frac{1}{x^{1/4} (x^{3/4} - h^{3/4})^{1/3}} dx + \frac{I_f}{R^{3/2} Q_u} x$$

$$\sum_{n=1}^{\infty} \frac{\sin an}{an} \int_0^{xR} db \int_h^{\ell} \frac{1}{x^{1/4} (x^{3/4} - h^{3/4})^{1/3}} \exp \left[ -\frac{C_D^2 R}{x^{1/2} (x^{3/4} - h^{3/4})^{2/3}} \right] dx$$

(5.4.8)

The first double integral has been evaluated in section 3.6 to find the steady state response and is equal to  $2R^{3/2} Q_u$ . That is, the first term of equation 5.4.8 is  $I_f$ . The aim of the remainder of the equation is to render the second double integral dimensionless, so as to aid in computation.

The variable  $x$  ranges from  $h$  to  $\ell$  (figure 3.6.3).

$$\text{By setting } x = \beta h \text{ where } 1 \leq \beta \leq \ell/h \quad (5.4.9)$$

$$\text{and } z = (\beta^{3/4} - 1)^{2/3} \quad (5.4.10)$$

the second double integral becomes

$$\int_0^{xR} \int_h^{\ell} = 2 \int_0^{xR} db h^{1/2} \int_0^{\left(\left(\frac{\ell}{h}\right)^{3/4} - 1\right)^{2/3}} \exp \left[ -\frac{C_D^2 R}{(z^{3/2} + 1)^{2/3} zh} \right] dz \quad (5.4.11)$$

From section 3.6 and figure 3.6.3

$$b = \epsilon R \quad (5.4.12)$$

$$\ell = R \left( \sqrt{1 - \epsilon^2} + \sqrt{\chi^2 - \epsilon^2} \right) = R \ell' \quad (5.4.13)$$

$$h = R \left( \sqrt{1 - \epsilon^2} - \sqrt{\chi^2 - \epsilon^2} \right) = R h' \quad (5.4.14)$$

The new variables  $\epsilon$ ,  $\ell'$  and  $h'$  are inserted into equation 5.4.11 so that the double integral becomes

$$\int_0^{\chi R} \int_0^{\ell} = 2 R^{3/2} \int_0^{\chi} d\epsilon h'^{1/2} \exp \left[ \frac{-Cn^2}{h' z (z^3 + 1)^{2/3}} \right] dz \quad (5.4.15)$$

$I(t)$  then becomes

$$I(t) = I_f + \frac{2I_f}{Qn} \int_{n=1}^{\infty} \frac{\sin an}{an} \int_0^{\chi} d\epsilon h'^{1/2} \exp \left[ \frac{-Cn^2}{h' z (z^3 + 1)^{2/3}} \right] dz \quad (5.4.16)$$

The double integral is now dimensionless. Its numerical solution only requires a value of  $\chi$ . Values for  $I(t)$  from equation 5.4.16, for a given initial current  $I_i$  and final current  $I_f$ , are obtained by computation. The evaluation of equation 5.4.16 is discussed in section 5.7.

If there is no enamel then  $h = 0$  and equation 5.4.9 and all subsequent equations no longer apply. The expression for a disc with no enamel is obtained by setting  $h = 0$  and  $\chi = 1$  in equation 5.4.8, to give

$$I(t) = I_f + \frac{2I_f}{Q_{in}} \int_{n=1}^{\infty} \frac{\sin an}{an} \int_0^1 \left[ \left( 2(1-\epsilon^2)^{1/2} \right)^{1/2} \cdot \exp \left( - \frac{Cn^2}{2(1-\epsilon^2)^{1/2}} \right) - \sqrt{\pi Cn^2} \left[ 1 - \operatorname{erf} \left( \frac{Cn^2}{2\sqrt{1-\epsilon^2}} \right)^{1/2} \right] \right] d\epsilon \quad (5.4.17)$$

The derivation of equation 5.4.17 is given in detail in appendix B.1.

#### 5.5. The calculation of the time response of an enamelled disc perpendicular to the flow

The geometry relevant to this calculation is shown in figure 3.7.1. The current density at a point on the surface of the disc  $J$ , is given by equation 3.7.50.

$$J = 0.83 R^{-1/2} \operatorname{mecc}_B D^{2/3} v^{-1/6} \frac{U_0^{1/2}}{(1-\epsilon^2)^{7/20}} \quad (5.5.1)$$

with  $\epsilon = r/R$ .

The total current from the disc  $I$ , may be written, from equation 3.7.51

$$I = 2\pi R^2 \int_0^1 J \epsilon d\epsilon \quad (5.5.2)$$

or in integrated form, from equation 3.7.52.

$$I = 1.67 \pi R^{3/2} Q_{\perp} \text{mec}_s D^{2/3} v^{-1/6} U_o^{1/2} \quad (5.5.3.)$$

As in the previous section the subscript  $f$  is introduced.

Equations 5.5.1. and 5.5.3. are then combined to give the current density at a point  $J_f$ , corresponding the final velocity state  $U_f$ .

$$J_f(\epsilon) = \frac{I_f}{(1-\epsilon^2)^{7/20}} \cdot \frac{1}{2\pi R^2 Q_{\perp}} \quad (5.5.4)$$

In equation 5.3.39  $x$  is the general dimension parallel to the surface,  $\epsilon$  being the specific dimension here. Therefore equation 5.5.4. can be substituted into equation 5.3.39 to give the time dependent current density at a point  $J(\epsilon, t)$ .

$$J(\epsilon, t) = \frac{I_f}{(1-\epsilon^2)^{7/20}} \frac{1}{2\pi R^2 Q_{\perp}} +$$

$$\left[ \frac{2I_f}{(1-\epsilon^2)^{7/20}} \frac{1}{2\pi R^2 Q_{\perp}} \right]_{n=1}^{\infty} \frac{\sin an}{an} \exp \left( \frac{-Cn^2}{(1-\epsilon^2)^{14/20}} \right) \quad (5.5.5.)$$

$$\text{where } C = \left( \frac{I_f}{D \text{mec}_s 2R^2 Q_{\perp}} \right)^2 D\tau \quad (5.5.6.)$$

The time varying current from the disc is obtained by performing the integration of equation 5.5.2. upon the terms of equation 5.5.5. That is

$$I(t) = \frac{2\pi R^2}{2\pi R^2 Q_L} I_f \int_0^{\chi} \frac{\epsilon}{(1-\epsilon^2)^{7/20}} d\epsilon + \frac{2\pi R^2 2I_f}{2\pi R^2 Q_L} * \int_{n=1}^{\infty} \frac{\sin an}{an} \int_0^{\chi} \frac{\epsilon}{(1-\epsilon^2)^{7/20}} \exp\left(\frac{-Cn^2}{(1-\epsilon^2)^{14/20}}\right) d\epsilon \quad (5.5.7)$$

From equation 3.7.53 the integral of the first term is equal to  $Q_L$ .

Therefore  $I(t)$  is given by

$$I(t) = I_f + \frac{2I_f}{Q_L} \int_{n=1}^{\infty} \frac{\sin an}{an} \int_0^{\chi} \frac{\epsilon}{(1-\epsilon^2)^{7/20}} \exp\left(\frac{-Cn^2}{(1-\epsilon^2)^{14/20}}\right) d\epsilon \quad (5.5.8.)$$

The integral of equation 5.5.8 is dimensionless. Only the value of  $\chi$  is required for its numerical evaluation. Given values of  $I_i$ ,  $I_f$  and  $\chi$  the variation of  $I(t)$  with  $C$  (which is proportional to  $t$ ) can be found by computation.

Unlike the parallel disc (section 5.4) the time response of a perpendicular disc with no enamelling can be obtained directly from that for the enamelled disc. That is, by setting  $\chi = 1$  in equation 5.5.8.

### 5.6. The calculation of the time response of a sphere

The geometry and co-ordinate system relevant to this calculation are shown in figures 3.4.1 and 3.8.1. From equation 3.8.20 the current density  $J$ , at a point on the surface of the sphere is

$$J(\theta) = 1.04 R^{-1/2} \text{mec}_s D^{2/3} v^{-1/6} U_o^{1/2} F(\theta) \quad (5.6.1)$$

$$\text{where } F(\theta) = 1 - 0.190 \theta^2 - 7.31 \times 10^{-4} \theta^4 \quad (5.6.2).$$

The total current is, from equations 3.8.21 and 3.8.22

$$I = \int_0^{\theta_s} 2\pi R^2 J(\theta) \sin \theta d\theta \quad (5.6.3)$$

or

$$I = 2\pi R^{3/2} \times 1.04 \text{ mec}_s^{2/3} v^{-1/6} U_o^{1/2} Q_s \quad (5.6.4)$$

where  $Q_s = 0.921$ .

Again the subscript  $f$  is introduced and equations 5.6.1 and 5.6.4 are combined to give

$$J_f(\theta) = \frac{I_f F(\theta)}{2\pi R^2 Q_s} \quad (5.6.5)$$

Equation 5.6.5. is then substituted into equation 5.3.39 to give

$$J(\theta, t) = \frac{I_f F(\theta)}{2\pi R^2 Q_s} + \frac{2I_f F(\theta)}{2\pi R^2 Q_s} \int_{n=1}^{\infty} \frac{\sin an}{an} \exp \left[ -Cn^2 F(\theta)^2 \right] \quad (5.6.6)$$

where

$$C = \left( \frac{I_f}{D \text{mec}_s 2R^2 Q_s} \right)^2 Dt \quad (5.6.7)$$

The time varying total current  $I(t)$  is obtained by performing the integration of equation 5.6.3. upon the terms of equation 5.6.6. That is

$$I(t) = \frac{I_f}{Q_s} \int_0^{\theta_s} F(\theta) \sin\theta \, d\theta +$$

$$\frac{2I_f}{Q_s} \int_{n=1}^{\infty} \frac{\sin n\theta}{n} \int_0^{\theta_s} F(\theta) \sin\theta \exp\left[-Cn^2 F(\theta)^2\right] d\theta \quad (5.6.8)$$

From equation 3.9.5 the integral of the first term of equation 5.6.8 is equal to  $Q_s$ . Therefore

$$I(t) = I_f + \frac{2I_f}{Q_s} \int_{n=1}^{\infty} \frac{\sin n\theta}{n} \int_0^{\theta_s} F(\theta) \sin\theta \exp\left[-Cn^2 F(\theta)^2\right] d\theta \quad (5.6.9)$$

This analysis assumes the electrode to be a complete sphere. As described in section 3.9, the electrodes used clinically had a considerable amount of their surface covered with epoxy resin adhesive. Making the assumptions of section 3.9 and following the above scheme of calculation the time response of such an electrode is found to be given by

$$I(t) = I_f + \frac{2I_f}{(Q_{s1} + Q_{s2})} \int_{n=1}^{\infty} \frac{\sin n\theta}{n} \left[ \int_0^{\theta_c} \sin\theta F(\theta) \exp\left[-Cn^2 F(\theta)^2\right] d\theta \right.$$

$$\left. + \int_{\theta_c}^{\theta_s} \frac{1}{\pi} (\pi - \psi) \sin\theta F(\theta) \exp\left[-Cn^2 F(\theta)^2\right] d\theta \right] \quad (5.6.10)$$

where

$$C = Dt \left[ \frac{I_f}{Dm\epsilon c_s} 2R^2 (Q_{s1} + Q_{s2}) \right]^2 \quad (5.6.11)$$

The derivation of equations 5.6.10 and 5.6.11 is given in full in appendix B.2. If there is no epoxy, then  $\theta_c \rightarrow \theta_s$  and the second integral  $\rightarrow 0$ . Also,  $Q_{s2}$  becomes zero and  $Q_{s1}$  becomes  $Q_s$  and equations 5.6.10 and 5.6.11 become identically equal to equations 5.6.9 and 5.6.7 respectively.

#### 5.7. The evaluation of the expressions obtained for the time response

As a result of the complexity of the time response expressions the use of a computer is required for their evaluation. The expressions have been cast in such a form that only the initial current  $I_i$ , the final current  $I_f$ , (or  $I_i/I_f$ ) and the variable  $\chi$  (for a disc) or  $\theta_c$  (for a sphere) need be entered as data into the evaluation programs.

The flow chart of the programs used for the enamelled discs and the sphere is given in appendix B.3. It is not proposed to describe the mechanical aspects of the computing in any great detail. However, some specific points do require comment.

The programs produce the variation of  $I$  with  $C$ , which is proportional to the real time  $t$ . It is then possible to plot values of  $C$ , corresponding to given currents, against the real time at which those values of current occurred. This process allows the diffusion coefficient  $D$  to be extracted, as for the steady state theory, as the independent variable for comparison with accepted values.

The summations in the time response expressions converge relatively rapidly. Usually only about fifteen terms were necessary for the accuracy of one in a thousand demanded by the programs. The integrals within the

the summations of equations 5.4.16, 5.5.8 and 5.6.9 are of the form of a decaying exponential term minus a complementary error function like term. The integrals are multiplied by the term  $\frac{\sin(an)}{an}$  where  $a = \pi \frac{I_f}{I_i}$ . Termination of a summation on a computer is usually achieved by checking if the last term is less than a given part of the sum so far. This method is not sufficient here since if  $I_i/I_f$  is close to an integer then  $\sin(an)$  regularly becomes zero or very small causing premature termination. This is overcome by the method shown in appendix B 3.

Figures 5.7.1., 5.7.2., 5.7.3., and 5.9.4. show the variation of  $I/I_f$  against  $C$  for the parallel disc, the perpendicular disc, the complete sphere and the epoxied sphere respectively. The curves were obtained by computation of the respective time response expressions as described above. The dependence of the time responses upon the ratio  $I_i/I_f$  is shown clearly.

The value of  $\chi$  chosen for the parallel and perpendicular discs (0.9) is typical of the values used for the experimental work. The separation point for the sphere  $\theta_g$ , is taken to be the theoretical value  $109.6^\circ$  for both the complete and the epoxied spheres. A typical value of the extent of epoxy,  $\theta_c$ , is used for the epoxied sphere.

As would be expected the shapes of the current decays for the complete sphere and the epoxied sphere are very similar. They are also similar to the shape of the current decay for the perpendicular disc. This is reasonable since a stagnation point exists for both types of electrode and around its stagnation point the sphere can be considered similar to a perpendicular disc.

Tables 5.7.1 and 5.7.2 show the effect upon the variation of  $I/I_f$  with  $C$  of varying  $\chi$ , for the parallel and perpendicular discs respectively. The effect is small. However,  $Q_{||}$  and  $Q_{\perp}$  in equations 5.4.7 and 5.5.6 are functions of  $\chi$  and so any error in the measured

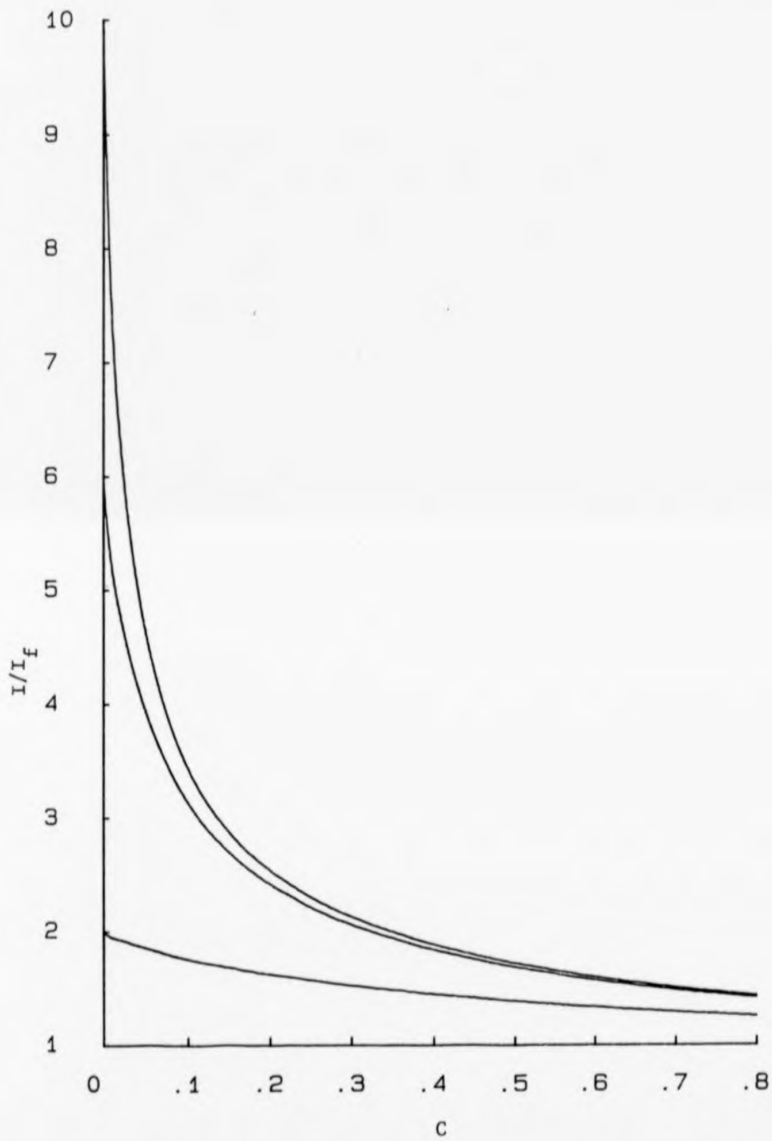


Figure 5.7.1 The variation of  $I$  with  $C$  for the enamelled parallel disc ( $\chi = 0.9$ ), at  $I_i/I_f = 2, 6$  and  $10$ .

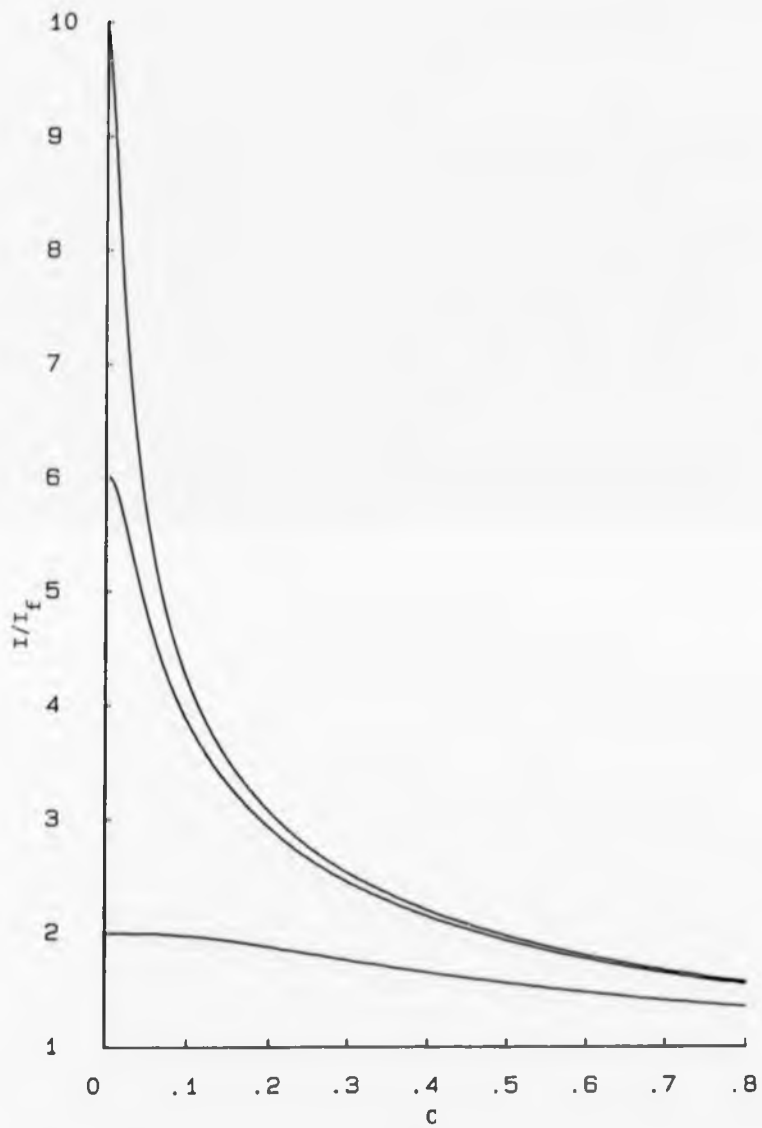


Figure 5.7.2 The variation of  $I$  with  $C$  for the enamelled perpendicular disc ( $\chi = 0.9$ ), at  $I_1/I_f = 2, 6$  and  $10$

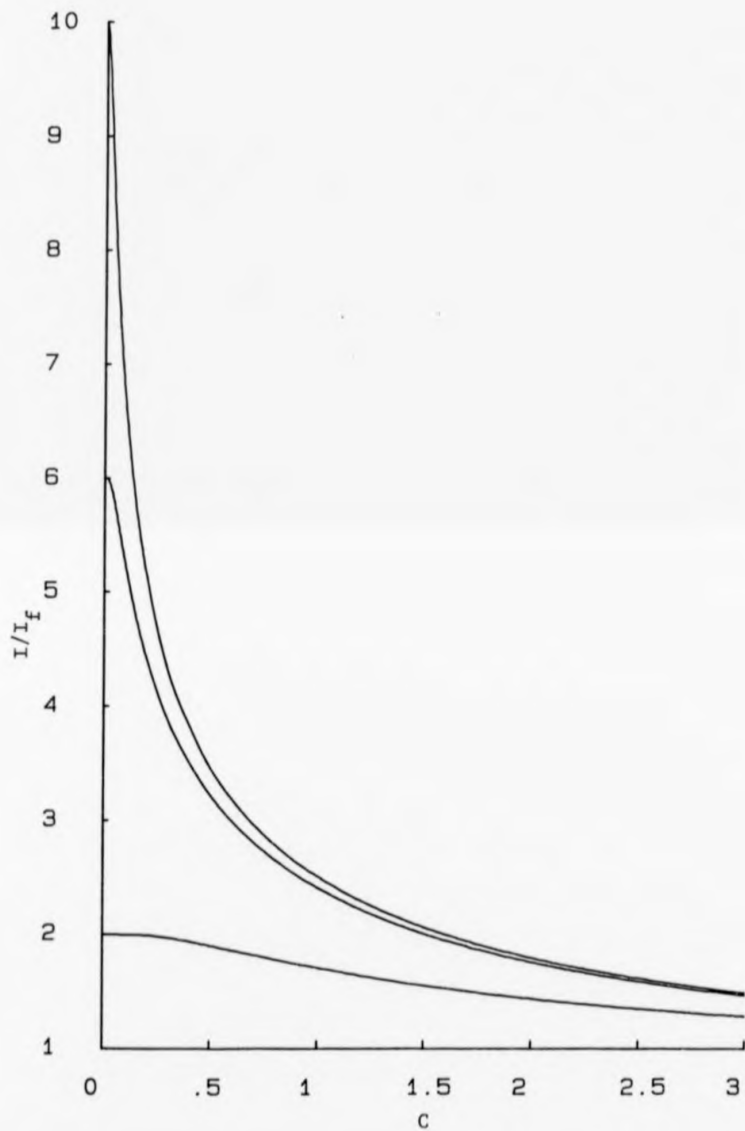


Figure 5.7.3 The variation of  $I$  with  $C$  for the complete sphere  
 ( $\theta_s = 109.6^\circ$ ), at  $I_1/I_f = 2, 6$  and  $10$

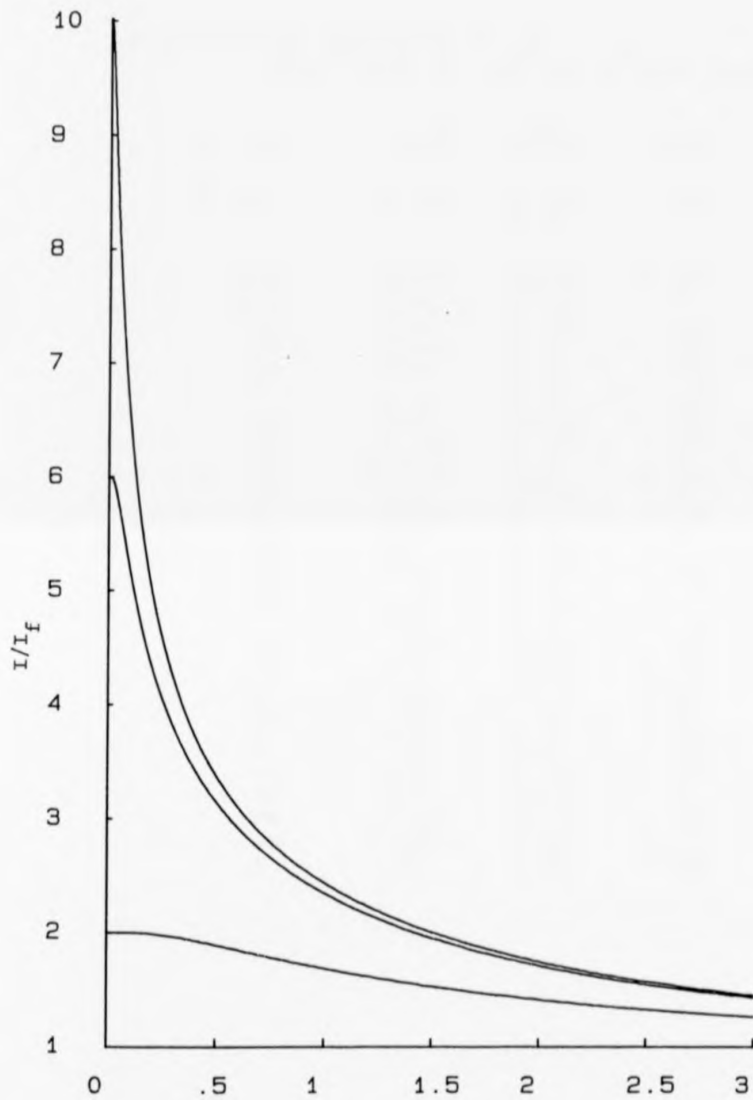


Figure 5.7.4 The variation of  $I$  with  $C$  for the epoxied sphere  
 $(\theta_c = 40^\circ)$ , at  $I_1/I_f = 2, 6$  and  $10$

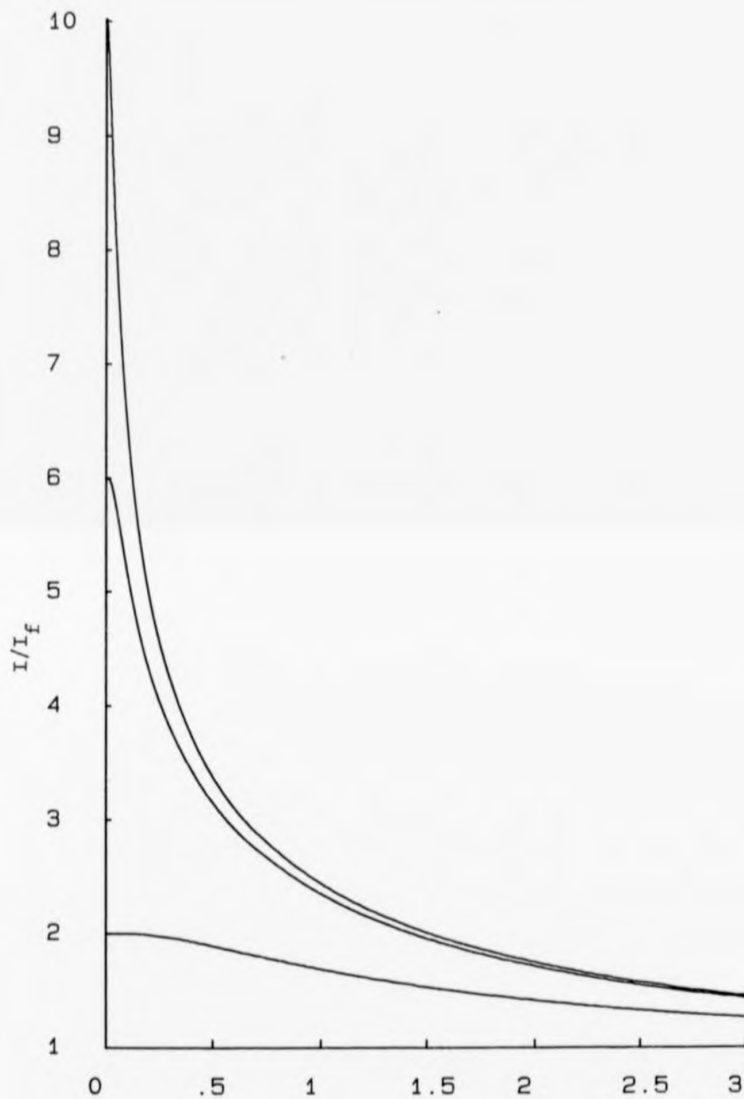


Figure 5.7.4 The variation of  $I$  with  $C$  for the epoxied sphere  
 ( $\theta_c = 40^\circ$ ), at  $I_1/I_f = 2, 6$  and  $10$

Table 5.7.1 The dependence of the variation of  $I/I_f$  with  $C$  upon  $\chi$ , for the parallel disc

$\chi$	-0.8	-0.85	-0.9	-0.95
$C$	$I / I_f$	$I / I_f$	$I / I_f$	$I / I_f$
0.00	6.000	6.000	6.000	6.000
.02	4.81	4.798	4.77	4.715
.04	4.152	4.155	4.142	4.105
.06	3.699	3.71	3.707	3.682
.08	3.366	3.381	3.384	3.369
.1	3.11	3.127	3.134	3.126
.12	2.906	2.925	2.935	2.932
.14	2.739	2.759	2.771	2.772
.16	2.599	2.62	2.634	2.637
.18	2.48	2.502	2.517	2.522
.2	2.378	2.4	2.416	2.423
.22	2.289	2.311	2.327	2.335
.24	2.21	2.232	2.248	2.257
.26	2.139	2.161	2.178	2.188
.28	2.076	2.098	2.115	2.125
.3	2.019	2.041	2.058	2.069
.32	1.967	1.989	2.006	2.017
.34	1.92	1.941	1.958	1.97
.36	1.876	1.897	1.914	1.926
.38	1.836	1.857	1.874	1.886
.4	1.799	1.82	1.837	1.849
.42	1.764	1.785	1.802	1.815
.44	1.732	1.753	1.77	1.782
.46	1.703	1.723	1.739	1.752
.48	1.675	1.694	1.711	1.724
.5	1.65	1.668	1.685	1.698

Table 5.7.2 The dependence of the variation of  $I/I_f$  with  $C$  upon  $\chi$ , for the perpendicular disc

$\chi$	-0.8	-0.85	-0.9	-0.95
$C$	$I / I_f$	$I / I_f$	$I / I_f$	$I / I_f$
0.00	6.000	6.000	6.000	6.000
.02	5.828	5.784	5.714	5.584
.04	5.287	5.214	5.096	4.91
.06	4.807	4.711	4.581	4.387
.08	4.411	4.312	4.182	3.991
.1	4.092	3.994	3.866	3.681
.12	3.831	3.735	3.61	3.433
.14	3.612	3.519	3.398	3.228
.16	3.426	3.336	3.219	3.055
.18	3.266	3.178	3.065	2.907
.2	3.126	3.041	2.932	2.779
.22	3.002	2.919	2.814	2.666
.24	2.892	2.812	2.709	2.566
.26	2.793	2.715	2.615	2.476
.28	2.704	2.627	2.53	2.395
.3	2.622	2.548	2.453	2.322
.32	2.548	2.475	2.382	2.255
.34	2.478	2.408	2.318	2.193
.36	2.416	2.346	2.258	2.137
.38	2.357	2.289	2.202	2.084
.4	2.303	2.236	2.151	2.035
.42	2.252	2.186	2.103	1.99
.44	2.204	2.138	2.058	1.948
.46	2.159	2.086	2.016	1.908
.48	2.117	2.054	1.976	1.871
.5	2.077	2.016	1.839	1.836

Table 5.7.3 The dependence of the variation of I/I<sub>f</sub> against C upon the separation point  $\theta_s$ , for the complete sphere

$\theta_s$	-100°	-109.6°	-120°
C	I /I <sub>f</sub>	I /I <sub>f</sub>	I /I <sub>f</sub>
0.00	6.000	6.000	6.000
.1	5.191	5.241	5.27
.2	4.335	4.43	4.49
.3	3.779	3.895	3.974
.4	3.39	3.514	3.606
.5	3.099	3.226	3.326
.6	2.872	2.999	3.104
.7	2.688	2.814	2.922
.8	2.535	2.659	2.77
.9	2.406	2.528	2.639
1	2.295	2.414	2.526
1.1	2.197	2.314	2.426
1.2	2.112	2.226	2.337
1.3	2.035	2.147	2.258
1.4	1.967	2.076	2.186
1.5	1.905	2.012	2.121
1.6	1.848	1.954	2.062
1.7	1.797	1.9	2.008
1.8	1.75	1.851	1.958
1.9	1.707	1.806	1.911
2	1.667	1.764	1.868
2.1	1.63	1.726	1.828
2.2	1.596	1.69	1.792
2.3	1.564	1.656	1.758
2.4	1.534	1.625	1.725
2.5	1.507	1.596	1.695

Table 5.7.4 The dependence of the variation of I/I<sub>f</sub> with C upon  $\theta_c$ , for the epoxied sphere

$\theta_c$	-20°	-30°	-40°	-50°
C	I /I <sub>f</sub>	I /I <sub>f</sub>	I /I <sub>f</sub>	I/I <sub>f</sub>
0.00	6.000	6.000	6.000	6.000
.1	5.192	5.185	5.186	5.194
.2	4.366	4.355	4.355	4.365
.3	3.829	3.817	3.817	3.827
.4	3.449	3.438	3.437	3.447
.5	3.164	3.152	3.152	3.161
.6	2.939	2.928	2.928	2.936
.7	2.756	2.746	2.745	2.753
.8	2.604	2.593	2.593	2.6
.9	2.474	2.464	2.464	2.471
1	2.362	2.352	2.352	2.359
1.1	2.264	2.255	2.254	2.261
1.2	2.177	2.168	2.168	2.174
1.3	2.1	2.091	2.09	2.097
1.4	2.03	2.022	2.021	2.027
1.5	1.967	1.959	1.958	1.964
1.6	1.91	1.902	1.901	1.907
1.7	1.858	1.85	1.849	1.855
1.8	1.81	1.802	1.802	1.807
1.9	1.766	1.758	1.758	1.763
2	1.725	1.718	1.717	1.722
2.1	1.688	1.68	1.68	1.685
2.2	1.653	1.646	1.645	1.65
2.3	1.62	1.613	1.613	1.617
2.4	1.59	1.583	1.582	1.587
2.5	1.562	1.555	1.554	1.559

values of  $\chi$  will manifest itself as an error in the value of  $D$  derived using these equations.

Table 5.7.3 for the complete sphere shows the effect upon the current decay of allowing  $\theta_s$  to vary around its accepted value of  $109.6^\circ$ . The effect is small, but again  $Q_s$  is a function of  $\theta_s$  so any difference in the actual value of  $\theta_s$  will manifest itself in  $D$  via equation 5.6.7.

Similarly table 5.7.4 for the epoxied sphere shows the value of  $\theta_c$  to have a small effect on the variation of  $I/I_f$  with  $C$ . Again any error in  $\theta_c$  will have effect through equation 5.6.11.  $\theta_s$  is assumed to be  $109.6^\circ$ .

#### 5.8. Discussion

The theory developed in this chapter states the time response to a decrease in flow is essentially decided by diffusion, convective effects only setting the initial and final conditions. The accuracy of this approach is strongly supported by the results presented in the following chapter.

The time response expressions arrived at only apply when the flow in the hydrodynamic boundary layer is laminar, as did the steady-state theory results of chapter 3, which are invoked to derive the results given here. Any further limits concerning the accuracy and applicability of the steady-state results must also apply to the final time response results, whatever the accuracy of the general theory of section 5.3.

The results of this chapter are given in terms of  $I$  not  $\bar{J}$ , partially for convenience (the average current density can easily be obtained), but mainly because it did not prove possible to find a general form of the time response expression directly involving the shape factor. Also, it is the value of current  $I$ , at a particular time that is actually

measured.

Given the theory is correct, this means that convection only sets the initial and final conditions and that diffusion controls the time response because it is so much slower than the convective changes. Supporting evidence comes from the time response to an increase in flow. Convective changes would be equally fast, and also the diffusion effects would be faster (though still the rate determining process) because the excess diffusion layer is essentially swept away by the increased flow.

The final time response expressions obtained, equations 5.4.16 , 5.5.8, 5.6.9 and 5.6.10 are dependent on the results of chapter 3. Unlike the steady state theory, however, the basic result, equation 5.3.39 is equally applicable to all the electrode shapes considered because of the generalised geometry used. It is because convective effects were assumed to only set the initial and final diffusion layer thicknesses that such a generalised geometry could be used. In chapter 3, the convection imposed its own symmetry and geometry upon each of the electrode shapes considered.

The success or failure, then of this theory depends upon two factors, the success of the general time response theory of section 5.3 and the success of the steady state results of chapter 3. Failure could be due to failure of either of these, irrespective of the accuracy of the other. Success however, must be very strong evidence for the accuracy of both.

As shown by the results of chapter 6 the theory presented in this chapter (section 5.3 onwards) is successful when applied to the parallel disc and the sphere, but some reservations remain about the accuracy of the shape factor of the perpendicular disc.

CHAPTER 6

## CHAPTER 6

### EXPERIMENTAL INVESTIGATIONS OF THE TIME RESPONSE

#### 6.1 Introduction

This chapter describes the experimental investigations of the time response of the parallel disc, the perpendicular disc and the sphere. Only the time response to a decrease in flow is considered as this is the limiting response. The time response of a given electrode is a function of many variables, and it was not practicable to investigate all dependencies for all electrodes. Also the theoretical descriptions of the time response did not exist in such an advanced form when these investigations were performed. A consequence of this is that only a limited range of  $\chi$  was used. Also, the effect of varying  $c_g$  was not investigated.

As with the steady state results (Chapter 4) the only experimentally independent variable in the equations for the time response is the diffusion coefficient of oxygen,  $D$ . The accuracy of the time response equations was therefore investigated by deriving a value of  $D$  for comparison with Figure 4.1.1. To obtain  $D$  knowledge of the oxygen concentration  $c_g$  (Figure 4.1.2) and the water vapour pressure  $P_w$  (Figure 4.1.3) was necessary. The value of the kinematic viscosity  $\nu$  was not necessary since the theory assumes that convective effects are not directly involved in the time response.

The value of  $D$  was obtained from the experimental results as follows : the values of  $I_i$ ,  $I_f$ , and  $\chi$  (if a disc) or  $\theta_c$  (if a sphere) were entered into the respective program (Chapter 5) to produce values of

I versus C. Then spot values of  $t$  against C were plotted for given values of I. The value of D was calculated from the applicable C versus  $t$  relationship (equation 5.4.7, 5.5.6, 5.6.7 or 5.6.11).

Whilst the results of Chapter 5 (equations 5.4.16, 5.5.8, 5.6.9 and 5.6.10) could have been cast in terms of velocities of flow, not currents, it is values of current that are actually measured. Further, during the response to a decrease in flow (that is during the decay of the current to its new level) the steady state current-flow velocity relationship (equation 3.1.2) does not hold. Therefore, this chapter is not concerned with the actual flow velocities, except in so far as they set the initial and final values of the current.

## 6.2 The Experimental Arrangement and Method

Two experimental arrangements were used. When  $U_f$  was the free convection velocity  $U_c$ , the arrangement used was exactly the same as that used to investigate the steady state response and is shown in Figure 4.4.1. The current was always displayed on the Tektronix model 7633 storage oscilloscope. The current was then either read off the screen or a polaroid photograph was taken.

The second arrangement was used when  $U_f > U_c$  and is shown schematically in Figure 6.2.1. Again, the current was recorded on the Tektronix oscilloscope. The velocity of flow down the tube ( $\equiv U_f$ ) was varied by altering taps  $T_1$  and  $T_2$ . Values of  $U_f$  up to about  $7 \text{ cm.s}^{-1}$  were used (measured using the electrode under investigation). Values above this could easily be obtained but were not usable because of fast variations in the flow velocity which proved impossible to remove. These variations were sufficiently fast to alter  $U_f$  (and therefore  $I_f$ ) during the time response so altering the time response curve obtained.

In the arrangement shown in Figure 6.2.1 the electrode transport and support of Figure 4.4.1 was placed behind the slot in the tube. Thus the cathode could be placed in the flowing NaCl solution in the tube and moved with respect to it. The minimum temperature of the 0.15M NaCl was controlled by the water bath, but during the experiment the temperature increased because of the heat dissipated by the pump. A record was therefore kept of the temperature of the solution as well as the atmospheric pressure.

With both arrangements the measurements were performed as follows. It was found most convenient to move the cathode along its transport by hand, suddenly stopping it. A sufficiently fast step decrease in velocity could easily be obtained by this method. It was necessary to assume  $U_f$  was constant during the decay of the current to its final value  $I_f$  (the reason  $U_f$  was limited to about  $7\text{cm}\cdot\text{s}^{-1}$  in Figure 6.2.1). If  $U_f$  varied significantly during the decay of the current it was in fact obvious because of the resulting discontinuity in the current decay. All decays showing a discontinuity were rejected.

Using these two arrangements the parallel and perpendicular enamelled disc electrodes and the spherical electrodes were investigated. The discs used were copper, the spheres gold. Ag/AgCl anodes were always used. The electrodes were aligned with the flow as described in Chapter 4.

Figures 3.9.7 and 3.9.8 show the geometry of the spherical electrodes used clinically. The analysis of the decays of this type of sphere was performed using equations 5.6.10 and 5.6.11. A special sphere was also constructed, as shown in Figure 6.2.2, to attempt to eliminate the effect of the epoxy resin. When used the epoxy resin was always downstream of the flow and in the analysis of the decays, using equations 5.6.7 and 5.6.9, it was assumed that the sphere was perfect.

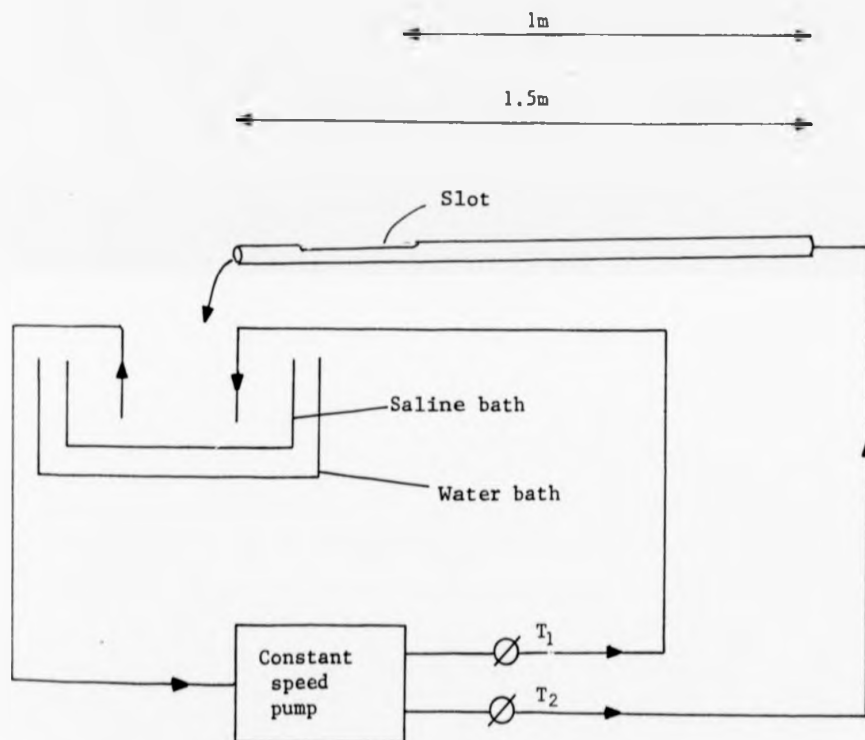


Figure 6.2.1 Diagram of the apparatus used to obtain values of  $U_f > U_c$ .

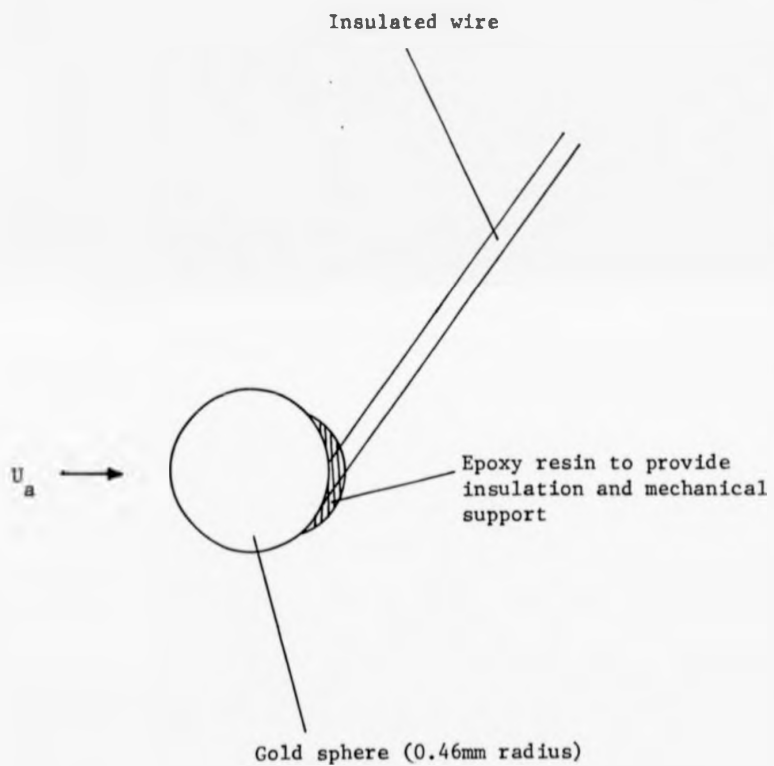


Figure 6.2.2 Schematic diagram of the special gold sphere constructed to eliminate the effects of epoxy resin.

### 6.3 Results

Typical current decays for the parallel disc, the perpendicular disc and the special sphere are shown in Figures 6.3.1, 6.3.2 and 6.3.3 with the corresponding theoretical curves. The theoretical variations of  $I$  with  $t$  were obtained using the relevant program as described below, to give the variation of  $I$  with  $C$  from which the value of  $M$  (equation 6.3.3) could be obtained, and thus the variation of  $I$  with  $t$ . The good agreement of the theoretical curves with the experimental points is not a trivial result since the shape of the current decays is complex and difficult to model.

The inadequacy of the initial theory (section 5.2) is shown clearly in Figure 6.3.4. Line (a) is obtained by applying equation 5.2.9 in the following form, to the current decay of Figure 6.3.1.

$$t = \frac{\pi (\text{mec}_g)^2 D \chi^2 R^4}{(I - I_f)^2} - \tau \quad (6.3.1)$$

That is, equation 5.2.9 has been cast in terms of  $I$ , not  $\bar{J}$ , and has been applied to the enamelled parallel disc. Line (a) is obtained with  $I_f = 3.5 \mu\text{A}$ , the experimentally observed value, and line (b) is obtained by setting  $I_f$  to zero. The linear relationship predicted by equation 6.3.1 can only be obtained by setting  $I_f$  to zero in an arbitrary manner. This result, with the theoretical reservations expressed in Chapter 5, clearly shows the inadequacy of this initial model.

For the moment, accepting this approach and applying equation 6.3.1, line (b) gives a value of  $D$  of  $1.94 \pm 0.06 \times 10^{-9} \text{ m}^2 \cdot \text{s}^{-1}$  at  $18^\circ\text{C}$ .

The remainder of the results presented are concerned only with the more advanced theory of Chapter 5. Figure 6.3.5 is obtained by applying this more advanced theory to the current decay for the parallel disc shown in Figure 6.3.1. That is,  $I_i$ ,  $I_f$  and  $\chi$  were entered into the

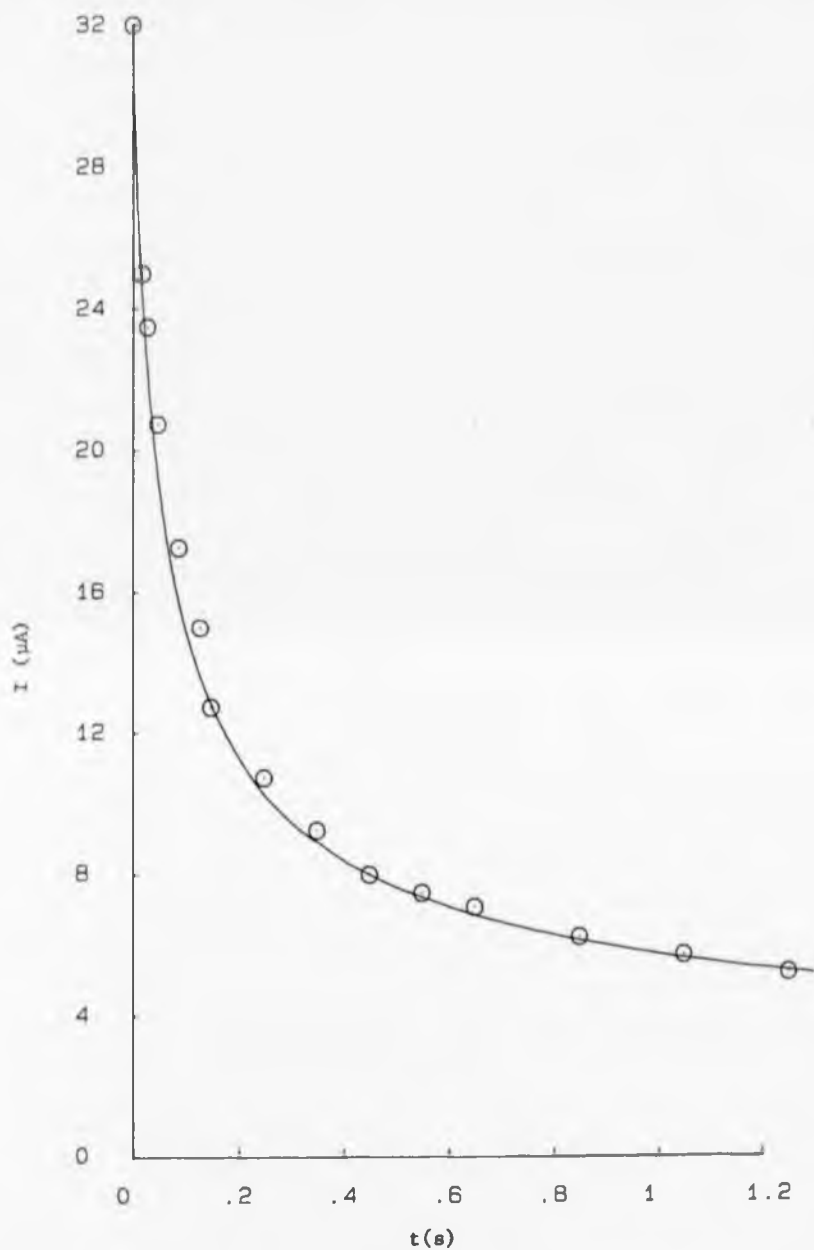


Figure 6.3.1 A typical time response of an enamelled parallel disc  
 ( $R = 8.5 \times 10^{-4}\text{m}$ ,  $\chi = 0.93$ ) at  $18^\circ\text{C}$ .  $c_g = 1.78 \times 10^{23}$   
 molecules. $\text{m}^{-3}$ .  $I_i = 31.0\mu\text{A}$ ;  $I_f = 3.5\mu\text{A}$   
 $M = 0.56 \pm 0.01\text{s}^{-1}$ .

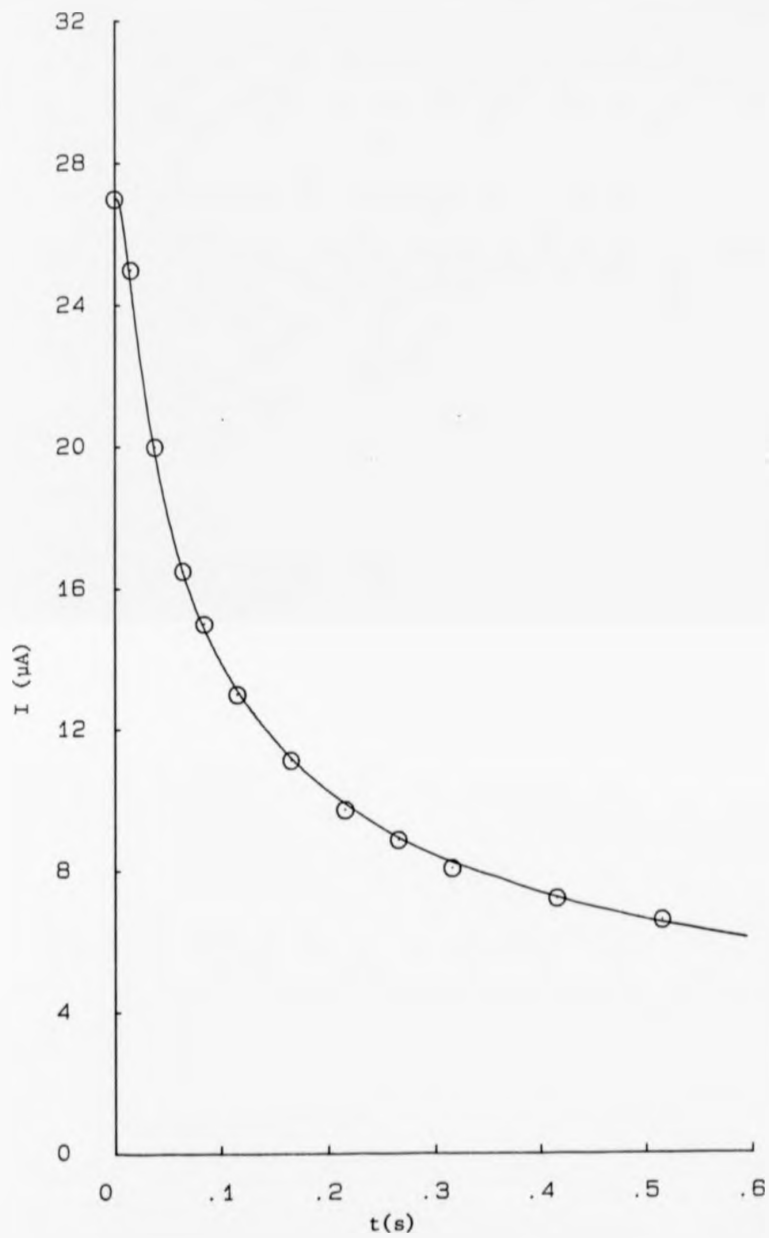
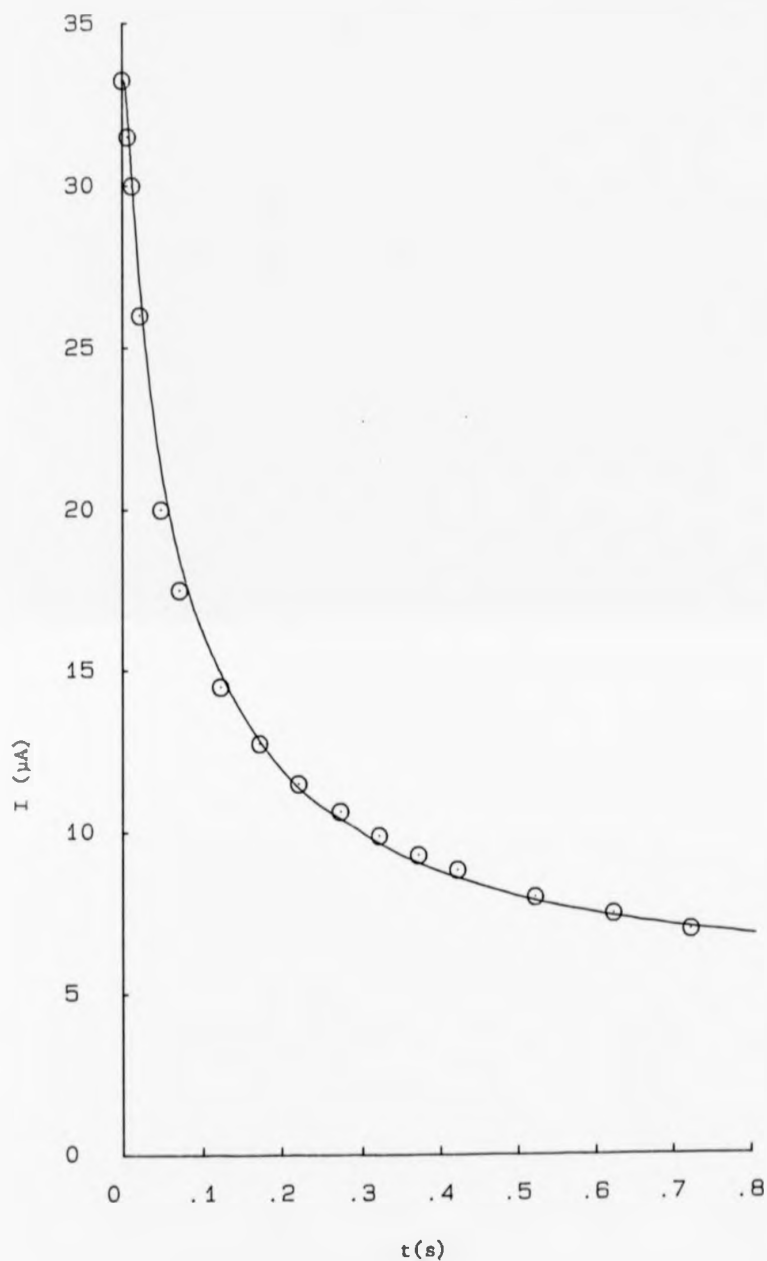


Figure 6.3.2 A typical time response of an enamelled perpendicular disc

( $R = 8.4 \times 10^{-4} \text{m}$ ,  $\chi = 0.95$ ) at  $20^\circ\text{C}$ .  $c_g = 1.69 \times 10^{23}$

molecules. $\text{m}^{-3}$ .  $I_i = 27.0 \mu\text{A}$ ;  $I_f = 2.7 \mu\text{A}$

$M = 0.56 \pm 0.01 \text{s}^{-1}$



**Figure 6.3.3** A typical time response of the special gold sphere  
 ( $R = 4.6 \times 10^{-4}\text{m}$ ) at  $37^{\circ}\text{C}$ .  $c_g = 1.23 \times 10^{23}$  molecules.  
 $\text{m}^{-3}$ .  $I_1 = 33.25\mu\text{A}$ ;  $I_f = 5.75\mu\text{A}$   
 $M = 6.8 \pm 0.2\text{s}^{-1}$ .

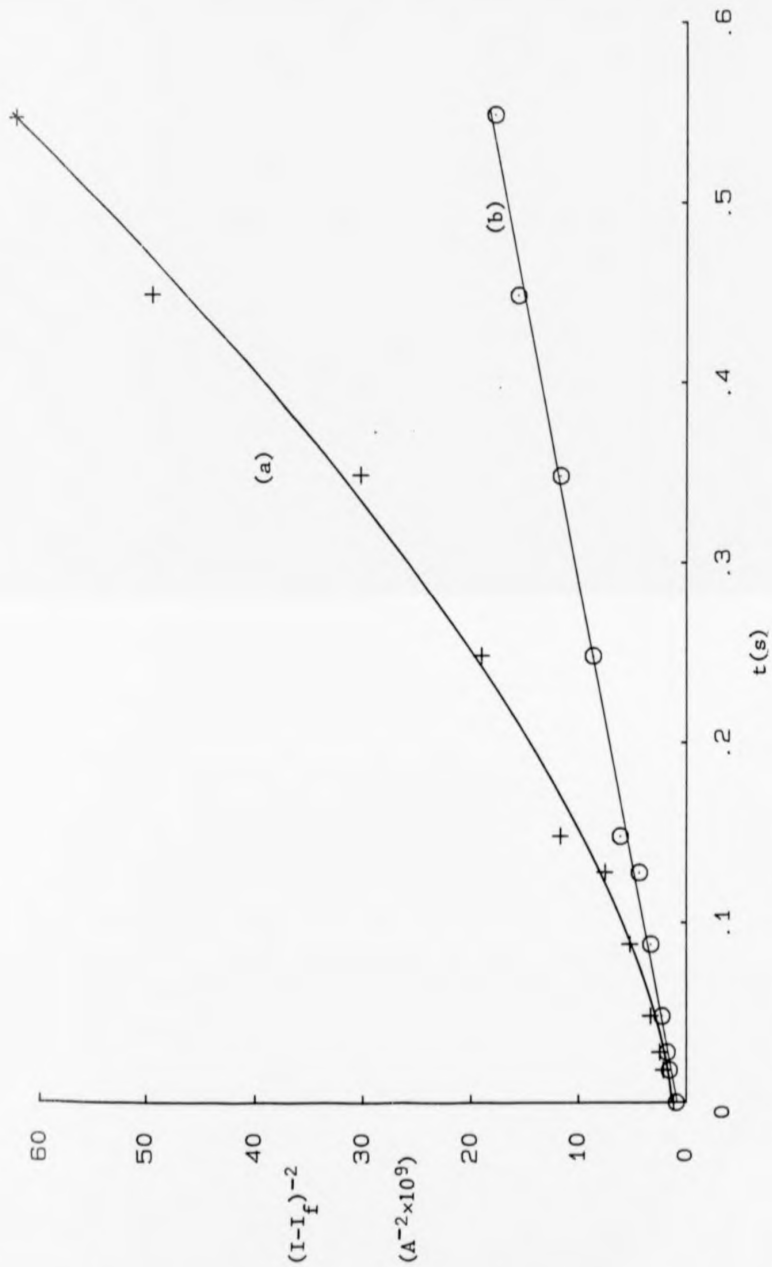


Figure 6.3.4 The time response of figure 6.3.1 analysed using the initial theory of section 5.2, with  $I_f = 3.5\mu A$ (a) and  $I_f = 0$ (b). The gradient of b is  $31.6 \pm 0.9 \times 10^9 A^{-2} \cdot s^{-1}$ .

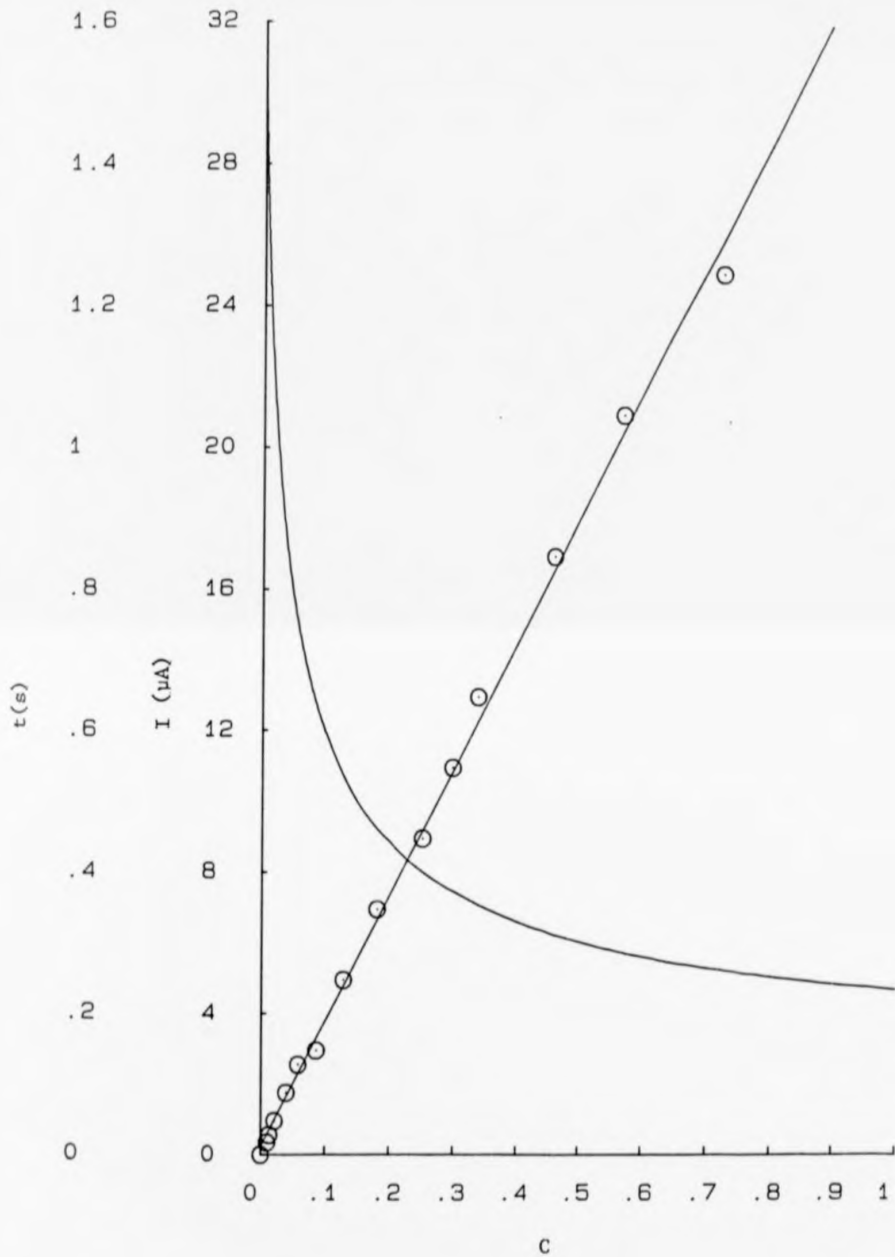


Figure 6.3.5 The computed variation of I with C, and the variation of t with C for the time response shown in figure 6.3.1.

Gradient =  $1/M = 1.78 \pm 0.03s$

Intercept =  $0.01 \pm 0.01s$

program for the parallel disc producing the variation of  $I$  with  $C$  shown. The values of  $t$  (from the experimental decay) were plotted against corresponding values of  $C$  as shown. Applying equation 5.4.7 to the  $t$ - $C$  graph gives a value of  $D$ , at  $18^\circ\text{C}$ , of  $1.76 \pm 0.03 \times 10^{-9} \text{ m}^2 \cdot \text{s}^{-1}$ .

Exactly the same process is used to analyse the current decays of the perpendicular disc and the sphere, using the corresponding programs and equations. Figure 6.3.2 for the perpendicular disc gives a value of  $D$  of  $1.53 \pm 0.03 \times 10^{-9} \text{ m}^2 \cdot \text{s}^{-1}$  at  $20^\circ\text{C}$ , and Figure 6.3.3 for the special sphere gives  $5.1 \pm 0.1 \times 10^{-9} \text{ m}^2 \cdot \text{s}^{-1}$  at  $37^\circ\text{C}$ .

Equations 5.4.7, 5.5.6, 5.6.7 and 5.6.11 relating  $C$  to  $t$  for the various disc and sphere electrodes can all be written in the form

$$C = I_f^2 \cdot K^2 \frac{t}{D} \quad (6.3.2)$$

where for a given electrode, oxygen concentration and temperature,  $K$  is a constant given by comparison with the respective equation. If  $M$  is the gradient of  $C$  versus  $t$ , then

$$M = I_f^2 K^2 \cdot \frac{1}{D} \quad (6.3.3)$$

Figures 6.3.6 and 6.3.7 show the variation of  $M$  with  $I_f^2$  for parallel and perpendicular discs respectively. These results were obtained using both experimental arrangements, that is,  $U_f$  varied between  $U_c$  and  $\sim 7 \text{ cm} \cdot \text{s}^{-1}$ . Values of the ratio  $I_i/I_f$  ranged between approximately 10 and 2 except when  $U_f$  approached  $7 \text{ cm} \cdot \text{s}^{-1}$  where maximum values of 2.5 are typical. These results were obtained using highly polished (with a 1 micron diamond wheel) electrodes. The experimental arrangement shown in Figure 6.2.1 was in a dusty environment and the electrode surfaces quickly acquired a greyish deposit which was easily removed. The electrodes were cleaned and repolished before each measurement. If this was not done then the value of  $D$  obtained from the

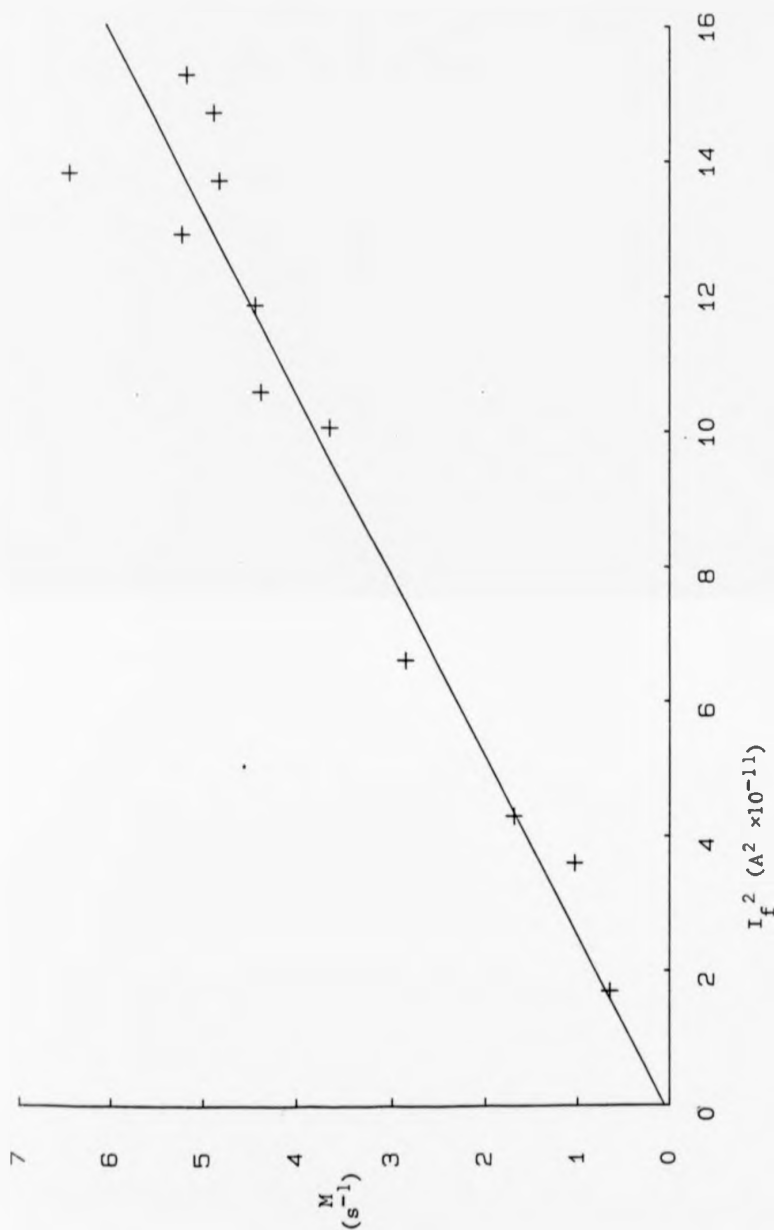


Figure 6.3.6 The variation of  $M$  with  $I_f^2$  for the parallel enamelled disc ( $R = 8.5 \times 10^{-4}\text{m}$ ,  $\chi = 0.93$ ) at  $18^\circ\text{C}$ .  
 $c_B = 1.78 \times 10^{23}$  molecules. $\text{m}^{-3}$ .  
 Gradient =  $3.7 \pm 0.5 \times 10^{10} \text{ A}^{-2}.\text{s}^{-1}$   
 Intercept =  $0.1 \pm 0.5\text{s}^{-1}$

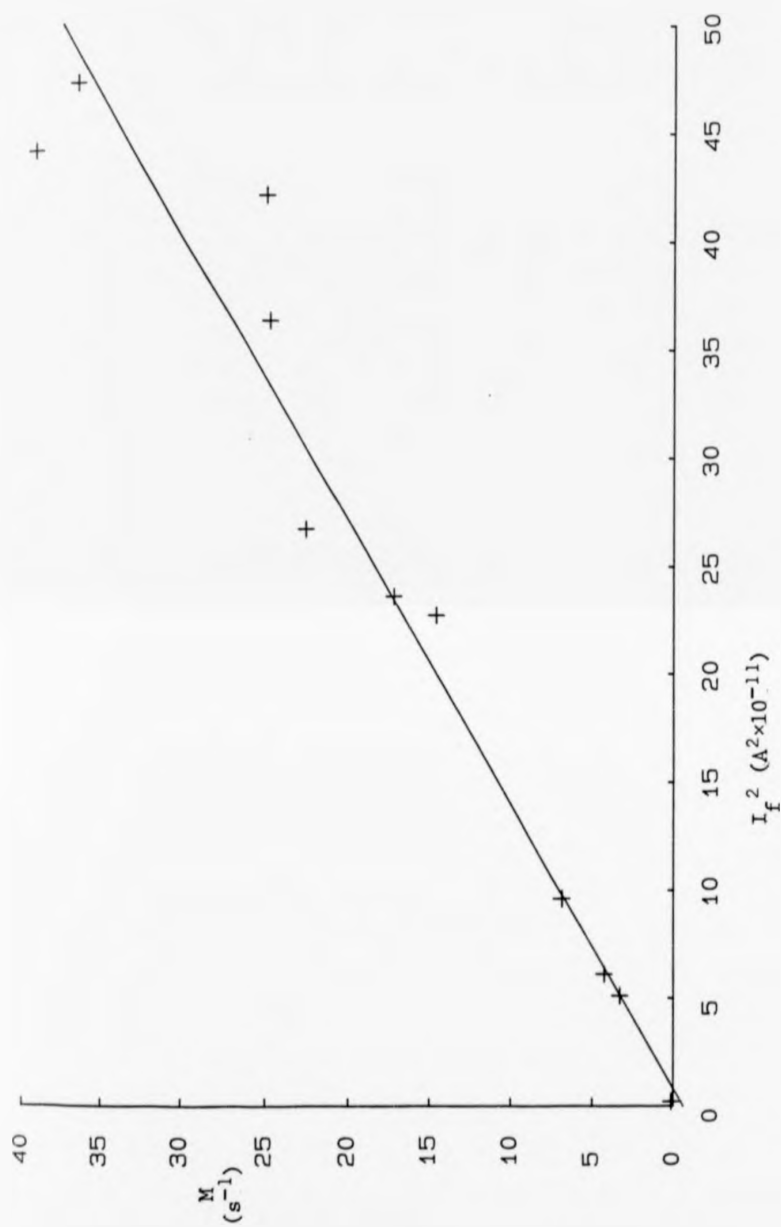


Figure 6.3.7 The variation of  $M$  with  $I_f^2$  for the perpendicular enamelled disc ( $R = 8.5 \times 10^{-4} \text{m}$ ,  $\chi = 0.93$ ) at  $18.5^\circ\text{C}$ .  
 $c_B = 1.76 \times 10^{23} \text{ molecules.m}^{-3}$ .  
 Gradient =  $7.6 \pm 0.6 \times 10^{10} \text{ A}^{-2}.\text{s}^{-1}$   
 Intercept =  $-1 \pm 3 \text{ s}^{-1}$ .

time response was unchanged (within the scatter), but the steady state current response was greatly reduced.

The value of  $D$  given by Figure 6.3.6 for the parallel disc at  $18^{\circ}\text{C}$  is  $2.2 \pm 0.3 \times 10^{-9} \text{ m}^2 \cdot \text{s}^{-1}$ . Figure 6.3.7 for the perpendicular disc gives a value of  $D$ , at  $18.5^{\circ}\text{C}$ , of  $1.4 \pm 0.2 \times 10^{-9} \text{ m}^2 \cdot \text{s}^{-1}$ . In both figures the scatter of the points increases as  $I_f$  increases, probably because of the increased variations in  $U_f$  described above. Fewer results were obtained with spherical electrodes, but they are similar to those of the parallel disc. In figures 6.3.6 and 6.3.7 the origin is not plotted as a point since a zero value of  $I_f$  is impossible to obtain. The intercept of Figure 6.3.6 is  $0.1 \pm 0.5 \text{ s}^{-1}$ , and that of Figure 6.3.7 is  $-0.6 \pm 3 \text{ s}^{-1}$ .

In Figures 6.3.8, 6.3.9 and 6.3.10 points are plotted for several current time responses at each electrode size or temperature. This contrasts with the corresponding graphs in Chapter 4 where single points were plotted, but each point was obtained from a steady state velocity response where many points were plotted.

The effect of varying the radius of the cathode was investigated only for the parallel disc. Re-arrangement of equation 5.4.7 shows that the radius dependence of the time response is probably best illustrated by plotting  $I_f^{1/2}/M^{1/2}$  against  $Q_{\infty}^{1/2}R$  as in Figure 6.3.8, where the gradient gives a value of  $D$ , at  $37^{\circ}\text{C}$ , of  $4.8 \pm 0.4 \times 10^{-9} \text{ m}^2 \cdot \text{s}^{-1}$ . As in Figure 4.4.6 (the steady state radius dependence) the origin has been plotted as a point, the intercept of Figure 6.3.8 being  $0.02 \pm 0.01 \times 10^{-3} \text{ A}^{1/2} \cdot \text{s}^{1/2}$ .

The variation of derived  $D$  with temperature is shown in Figures 6.3.9a and 6.3.9b. Current time responses were performed for the exposed sphere only at  $37^{\circ}\text{C}$ ; the results do, however, agree with those obtained with the special sphere, which is to be expected since the integration

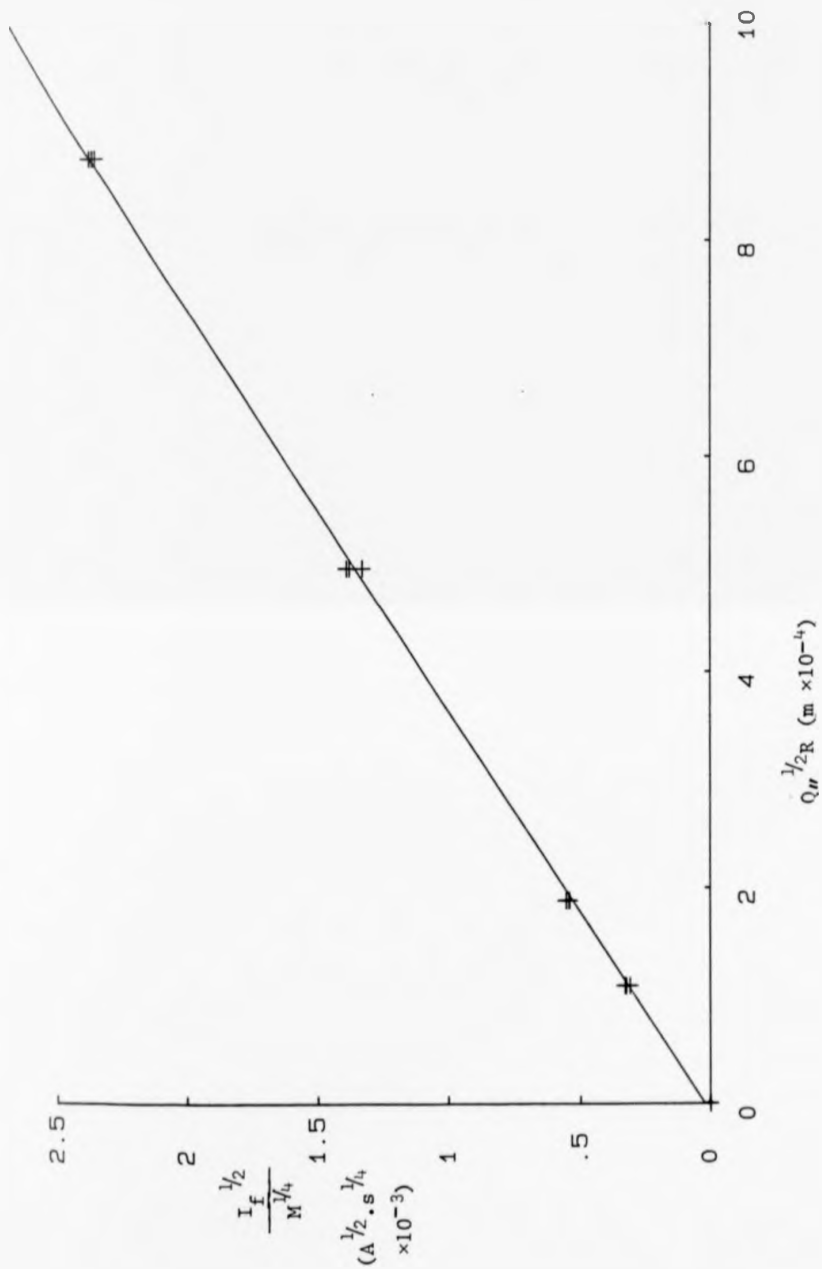


**Figure 6.3.8** The radius dependence of the speed of the time response for the parallel enamelled disc, at 37°C.  $c_B$  within 1% of  $1.28 \times 10^{23} \text{ molecules} \cdot \text{m}^{-3}$ .

$$\text{Gradient} = 2.69 \pm 0.02 \text{ A}^{1/2} \cdot \text{m}^{-1} \cdot \text{s}^{1/4}$$

$$\text{Intercept} = 2 \pm 1 \times 10^{-5} \text{ A}^{1/2} \cdot \text{s}^{1/4}$$

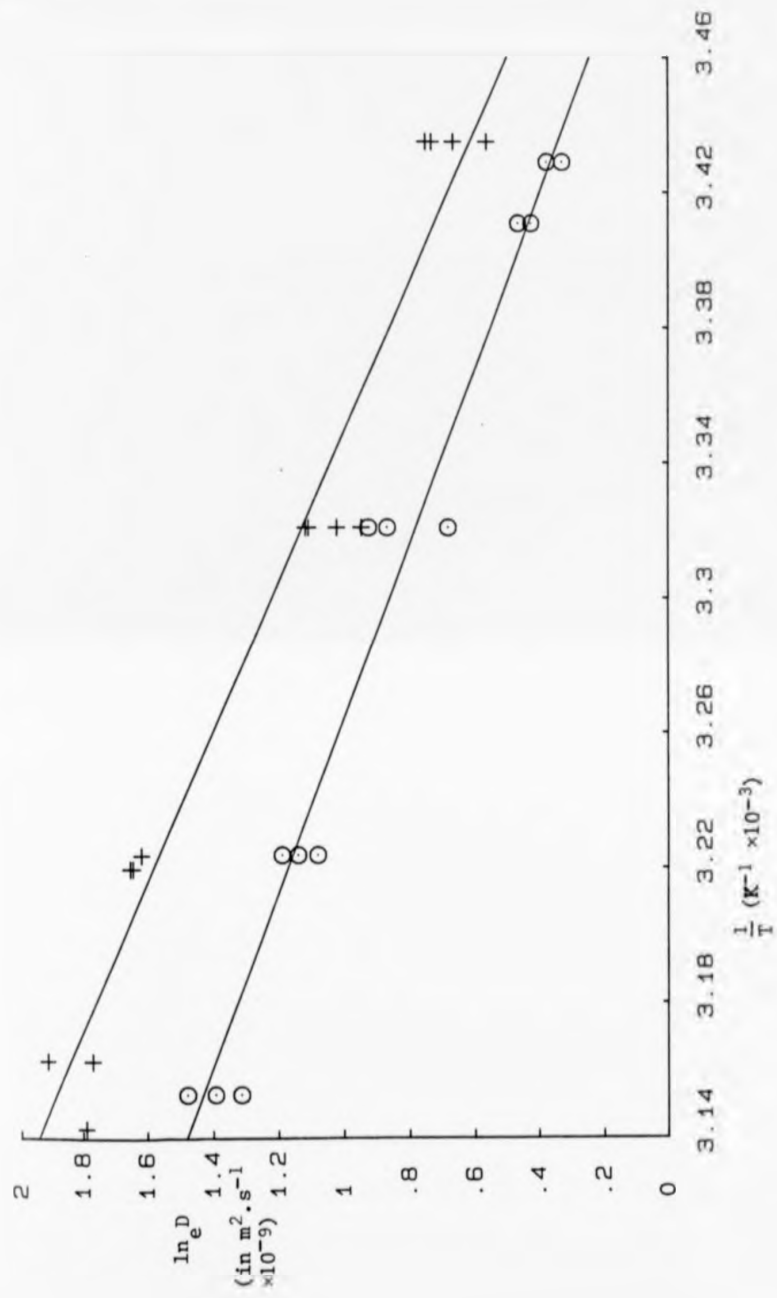


Figure 6.3.9a The variations of the values of D derived, with temperature for the enamelled parallel and perpendicular discs  
 Parallel disc ( + ) gradient =  $-4.5 \pm 0.4 \times 10^3 \text{K}$   
 Perpendicular disc ( o ) gradient =  $-3.9 \pm 0.3 \times 10^3 \text{K}$



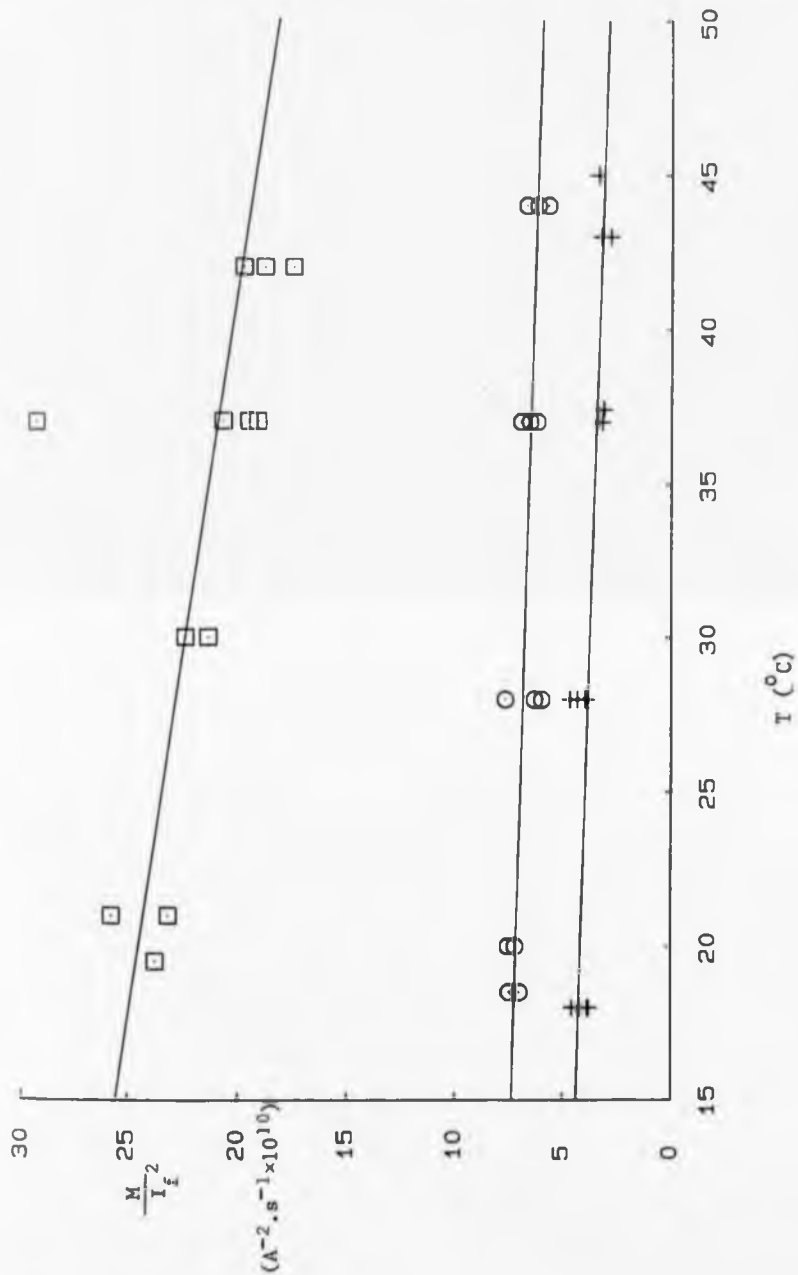


Figure 6.3.10 The effect of temperature on the speed of the time response.

- + Parallel disc  $R = 8.5 \times 10^{-4} \text{m}$ ,  $\chi = 0.93$  Gradient =  $-4 \pm 2 \times 10^8 \text{A}^{-2} \cdot \text{s}^{-1} / ^\circ\text{C}$
- Perpendicular disc  $R = 8.5 \times 10^{-4} \text{m}$ ,  $\chi = 0.95$  Gradient =  $-4 \pm 3 \times 10^8 \text{A}^{-2} \cdot \text{s}^{-1} / ^\circ\text{C}$
- Special sphere  $R = 4.6 \times 10^{-4} \text{m}$  Gradient =  $-20 \pm 10 \times 10^8 \text{A}^{-2} \cdot \text{s}^{-1} / ^\circ\text{C}$

of current density to obtain the current for the epoxied sphere is only a limited version of that for a complete sphere. The points plotted were obtained with single electrodes of each type. As in Figure 4.4.8 for the steady state the results do seem to confirm that  $\ln_e D$  varies as  $1/T$ , but the temperature range (from  $18^\circ\text{C}$  to  $44^\circ\text{C}$ ) is possibly too small.

The results of Figures 6.3.9a and 6.3.9b are re-plotted in Figure 6.3.10 to illustrate the variation of current time response with temperature. The results were obtained at atmospheric values of  $p\text{O}_2$  and show the combined effects of the decrease of  $c_s$  and the increase in  $D$  with temperature, upon the "speed" of the time response. It follows from equation 6.3.3 the faster a given time response is, the larger is the value of  $M$ , and also that the larger the value of  $I_f$  the faster the time response. The speed of the time response is, therefore, defined as  $M/I_f^2$  and in Figure 6.3.10  $M/I_f^2$  is plotted against temperature. The percentage change in the speed of the time response, per  $^\circ\text{C}$  is obtained by normalising the gradient against the best-fit value of  $M/I_f^2$ , at say  $37^\circ\text{C}$ . For the parallel disc the change in speed is  $-1.2 \pm 0.5\%/^\circ\text{C}$ , for the perpendicular disc  $-0.6 \pm 0.4\%/^\circ\text{C}$  and for the special sphere it is  $-1.0 \pm 0.5\%/^\circ\text{C}$ . So, the increase in  $D$  with temperature is more than offset by the decrease in  $c_s^2$  and the time response becomes slightly slower as temperature increases.

The effect upon the time response of varying  $c_s$  was not investigated, except in so far as  $c_s$  varied with temperature.

To this point, all errors quoted in this chapter refer only to the precision of the points plotted. As there was usually uncertainty in both the ordinate and the abscissa, the line drawn was evaluated from a least squares fit assuming independent uncertainties

in both co-ordinates, as in Chapter 4. A further discussion of possible errors is given below.

#### 6.4 Discussion

##### 6.4.1 General

Since the time response to a decrease in flow is the limiting response, effort has been concentrated upon it. No attempt has been made to describe the response to an increase in flow, which is regarded as being effectively instantaneous. The theory of section 5.3 onwards has been shown to fit the experiments well. The theoretical model applies to a step decrease in flow. This is likely to be close to that met in the C.S.F. and also had the advantage of being easy to achieve experimentally.

The inadequacy of the initial theory of section 5.2 is clearly shown in Figure 6.3.4. The failure of this theory to cope with values of  $I_f \gg 0$  made the development of the more advanced theory necessary. The more advanced theory has two distinct parts: that of section 5.3 which derives the time response of the current density at a point on a generalised electrode surface; and that of the following sections which uses the steady state results to obtain the time response of the current. To successfully describe the time response of the various electrodes, both parts must be accurate.

The values of  $D$  obtained from the parallel disc and sphere electrodes are in good agreement and also agree well with the values presented in Figure 4.1.1. Values of  $D$  from the perpendicular disc also fall within the range of those given in Figure 4.1.1, but are consistently smaller than those for the sphere and parallel disc (as was the case for the steady state results). Also, the values of  $D$  from the time response experiments are consistently greater than those from the steady state results. This is discussed in detail below.

#### 6.4.2 Comparison of the Derived Values of D with Accepted Values

Since there is a considerable scatter in the values of D in Figure 4.1.1 it is not possible to state whether the derived values of D are absolutely correct or not, but consideration of all potential sources of error is necessary. The errors previously quoted refer only to the scatter of the points plotted. Possible sources of error are as follows :

- (a) The values of D have been calculated assuming  $m = 4$ . Any over-estimate of m would cause a decrease in the value of D derived.
- (b) If the general theory of section 5.3 was inaccurate then errors would exist for all three electrode types. If an inaccuracy exists in any of the results of Chapter 3 only the electrode types concerned would be affected.
- (c) As detailed in point (c) of section 4.5, the experimental arrangements used may not reflect closely enough the idealised theoretical models.
- (d) Inaccuracies in the measurements of R,  $\chi$  and b. All dimensions quoted are average values, that is measurements in several different positions were averaged. The measurements therefore include any deviation from the ideal shape assumed theoretically. Also, inaccuracies in the dimensions will necessarily be greater, in percentage terms, for the smaller electrodes. Further, for the results given in Figure 6.3.8 for the parallel disc, it was not possible to polish the surface of the two smallest electrodes because of their small size, and here errors of type c (above) are likely to be large.

The experimental variable measured is current. Errors in the dimensions will not directly affect the values of  $I_i$  and  $I_f$  entered into the programs to give the variation of I with C. As shown by Tables 5.7.1, 5.7.2 and 5.7.4 an error in the value of  $\chi$  or  $\theta_c$  (related to b through equation 3.9.6) entered has a comparatively small effect

on the variation of  $I$  with  $C$ . Rather, an error in  $\chi$  (or  $\theta_c$ ) will have the greatest effect through equation 6.3.2 relating  $C$  to  $t$ , where the error manifests itself as an error in  $Q$ . Errors in  $R$  occur directly. Typically, an error of  $\pm 5\%$  in the dimensions could lead to an error in  $D$  of the order of  $\pm 30\%$ .

(e) An error in the value of  $I_f$ . During the time the current takes to decay to  $I_f$ ,  $U_f$  might have changed slightly altering the value of  $I_f$  read (large changes would cause obvious discontinuities and therefore be rejected). This could cause a typical error in the value of  $I_f$  used of  $\sim \pm 5\%$ , which through equation 6.3.2 would lead to an error in  $D$  of  $\sim \pm 10\%$ . An error of  $\pm 5\%$  in the ratio  $I_i/I_f$  would alter the variation of  $I$  with  $C$  slightly (Figures 5.7.1, 5.7.2, 5.7.3 and 5.7.4). A reasonable estimate of the error in  $D$  so caused would be  $\pm 10\%$ . That is, the total error in  $D$  caused by an error in  $I_f$  of say  $5\%$  might be  $\pm 20\%$ .

The cumulative error in  $D$  (if the errors are additive) caused by points (d) and (e) could total  $\pm 50\%$ . It must be emphasised, however, that this necessarily naive errors analysis has deliberately taken the worst possible errors.

(f) A further possible source of error exists. That is, the attitude of the final velocity to the cathode might not be that assumed.

The most likely plane for convection in the saline bath to be in is the vertical. This implies that, for the perpendicular disc,  $U_f$  might actually be parallel, and vice versa for the parallel disc. This potential problem could be of importance only when  $U_f \cong U_c$ . When the arrangement shown in Figure 6.2.1, to produce  $U_f > U_c$ , was used no such ambiguity could exist.

Such a change in  $U_f$  implies that the symmetry of the flow distribution

around the electrode would change during the current decay. This would be an extremely complex process, very difficult to describe theoretically. However, no evidence of such a process is seen in the results where the values of  $D$  obtained for  $U_f \equiv U_c$  are very similar to those for  $U_f > U_c$ .

A change in the attitude of  $U_f$  would be of less importance for spherical electrodes. The only effects would be to move the stagnation point and to alter the relative position of any epoxy resin.

#### 6.4.3 The Perpendicular Disc

As was the case for the steady state results the values of  $D$  obtained from the perpendicular disc are consistently smaller than those for the parallel disc and the sphere. Again then, consideration must be given to the perpendicular disc for sources of error peculiar to itself. Essentially, the points given in section 4.5 still apply here.

Given that the misalignment mechanism proposed in section 4.5 is valid then the perpendicular disc would in fact have a flow distribution symmetry similar to that for the parallel disc and perhaps its time response should be analysed using a method similar to that for the parallel disc. The effect of such a process can be roughly estimated as follows.

For a given electrode with  $\chi = 0.9$ ,  $C_1/C_{\parallel} \approx 1.6$  where  $C_1$  and  $C_{\parallel}$  are the values of  $C$  for the perpendicular and parallel discs respectively. Since  $D \propto 1/C$  (equation 6.3.2), the value of  $D$  obtained would be  $\sim 1.6$  times greater. Further, Figures 5.7.1 and 5.7.2 show that for the parallel disc a given value of  $I$  is achieved for a smaller value of  $C$  than for the perpendicular disc. Using the parallel disc program to analyse perpendicular disc decays would therefore further increase the value of  $D$  obtained. This is an extreme view since a misaligned per-

pendicular disc would not have exactly the same flow distribution as a parallel disc, but the argument does illustrate the possible results of even a slight misalignment.

#### 6.4.4 Comparison of the Time Response Results with the Steady State Results

Comparison of the values of  $D$  derived in Chapter 4 with those of Chapter 6 shows that the time response values are typically 1.5 to 2 times greater than the steady state values. Since the time response theory uses the steady state theory this implies that one or both theories are incorrect, or that some unaccounted mechanism is at work. [The rather poor agreement between corresponding gradients of Figure 4.4.8 and those of Figures 6.3.9a and 6.3.9b -  $\ln_e D$  vs  $1/T$  - can easily be explained by factors  $c$ ,  $d$  and  $e$  in section 6.4.2 above.]

If, in the analysis of the results too high a value of  $m$  was used (that is  $m$  should have been less than 4) the value of  $D$  obtained would have been decreased. However, the steady state value of  $D$  is proportional to  $m^{-3/2}$  whereas the time response value is proportional to  $m^{-2}$ . Therefore, decreasing  $m$  will increase the time response  $D$  to a greater extent than the steady state value. This is strong, though circumstantial, evidence for  $m$  being 4.

An explanation of the discrepancy in the results is now given. Point (c) of section 4.5 emphasises that the steady state theories of Chapter 3 are idealised models, very possibly not achieved in practice. Any deviation from this ideal is likely to decrease the current  $I$  from an electrode either by altering the flow pattern so that the hydrodynamic boundary layer and therefore the diffusion layer are thicker, or by possibly deactivating some points on the electrode surface (point b below) so that the diffusion layer is on average thicker.

To illustrate the effects of such a mechanism only the parallel

enamelled disc will be considered, but the same arguments apply to the other electrode geometries.

Given that the current density at a point  $J$  is decreased, then equation 3.6.1 becomes

$$J = k \times 0.34 \text{ m e c}_s D^{2/3} v^{-1/6} U_o^{1/2} x^{-1/2} \left[ 1 - \left( \frac{h}{x} \right)^{3/4} \right]^{-1/3} \quad (6.4.1)$$

where  $k \leq 1$  and is a constant for the particular electrode reflecting its deviation from the ideal. On integrating to obtain the total output current, equation 3.6.4 should now be written

$$I = k Q_{II} \times 4 \times 0.34 \text{ m e c}_s D^{2/3} v^{-1/6} U_o^{1/2} R^{3/2} \quad (6.4.2)$$

If  $k$  is not included in equation 6.4.2 then any value of  $D$  derived from it will be too low. Possible deviations from the ideal electrode causing a value of  $k < 1$  include :

- (a) If the electrode surface were rough, even microscopically so, the thickness of the hydrodynamic boundary layer, and the diffusion layer, would be increased and the current output for a given flow decreased.
- (b) Any random surface oxidation (or other poisoning) would effectively deactivate some elements of the electrode surface, decreasing the output current. If this were the only mechanism operating then  $k$  would represent the probability of a surface element being active.

This is distinct from the existence of enamelling, where the deactivated region is well defined and has predictable, quantifiable effects.

- (c) Geometrical deviations, such as the existence of the epoxy resin on the spheres, are likely to alter the flow pattern so as to increase the thickness of the diffusion layer and thus decrease the current.

The net effect of the above factors is to decrease the steady state current response and decrease the values of  $D$  derived using the results of Chapter 3.

Applying the same arguments and mechanisms to the time response theory gives a different result. The general time response theory of section 5.3 assumes some initial and final diffusion layer, set by some flow velocities, and equation 5.3.39 is obtained, giving the time response of the current density at a point on the generalised electrode surface. The actual flow velocities involved only appear indirectly in so far as they cause the initial and final current densities. Again considering the enamelled parallel disc, its current time response is obtained in section 5.4. If equations 6.4.1 and 6.4.2 are used in the analysis of section 5.4 instead of the unmodified equations 5.4.1 and 5.4.4 then the result obtained is unchanged, that is the extra factor  $k$  introduced cancels. So, when values of  $D$  are derived using equation 5.4.7 it is the actual measured value of  $I_f$  which is used, and the values of  $D$  derived from the time response equations are not reduced by any of the factors listed above, whereas those from the steady state theories are. This occurs because the value of  $D$  obtained from the time response depends only upon the functional dependence of current density  $J$  with position and the area over which  $J$  is integrated to give  $I$ .

A misaligned parallel disc electrode should be similar to the situation proposed here, except that  $k$  will be less than 1 in one flow direction and greater than 1 in the reciprocal direction as illustrated by the bifurcation of Figure 4.4.2. If a misaligned parallel disc is analogous, that is the misalignment does not alter the functional dependence of  $J$  with position, then the values of  $D$  derived from time responses in the reciprocal directions should be the same. This would

be a good test of the mechanism proposed above, but it was not performed explicitly (as care was usually taken to correctly align parallel discs when time responses were performed). However, none of the results obtained contradict the proposed mechanism.

#### 6.4.5 Scaling of Electrodes

From equations 5.4.7, 5.5.6, 5.6.7 and 5.6.11 it follows that the time taken for a given electrode to reach a given point in its time response, when responding to a particular change in flow velocity varies as

$$t \propto \left( \frac{R^2}{I_f} \right)^2 \quad (6.4.3)$$

For all electrode types considered  $I \propto R^{3/2}$  and therefore

$$t \propto R \quad (6.4.4)$$

So, reducing the size of an electrode will improve its time response, but will also decrease its steady state current output faster ( $I \propto R^{3/2}$ ). In practice the decrease in steady state current should be no problem because whilst the output of the electrodes used is typically  $\mu\text{As}$ , the noise current of the driving electronics was found to be only picoamps. The theoretical limit to reducing the electrode size is how far the theory applies. The time response theory is based on the steady state theory of Chapter 3. For there to be a diffusion layer there has first to be a hydrodynamic boundary layer which can exist when  $U_0 L / \nu \gg 1$  (Chapter 3). As  $\nu \sim 10^{-6}$  the requirement is  $U_0 L \gg 10^{-6}$ . So, to measure a minimum velocity of say  $1 \text{ cm.s}^{-1}$  the characteristic dimension  $L$  must be  $\gg 10^{-4}$ , say  $1 \text{ mm}$  which is typical of the spherical electrodes used.

This is the theoretical limit. The practical limit is likely to

be considerably less, since it is unlikely that the theory suddenly breaks down, and in fact it is likely that a perfectly functioning flow transducer could be considerably smaller than the above limit even if it could not be described theoretically. For example, the theoretical minimum velocity that could be measured by the electrode which produced the results shown in Figure 4.4.2 is  $\sim 5 \text{cm.s}^{-1}$ .

In this work no attempt was made to find the smallest functioning electrode size. The size of the sphere electrodes used was not dictated solely on theoretical grounds, but rather they were the smallest size it was reasonably convenient to construct using the methods described in Chapter 7.

#### 6.4.6 Conclusions

The theory developed in Chapter 5 to describe the time response has been shown to be successful, and its success must be taken as strong corroborative evidence for the accuracy of the steady state theory of Chapter 3. Some reservations still remain concerning the perpendicular disc but these are probably due to inadequacies of the experimental arrangement.

The experimental arrangement used for all electrodes is adequate for the purposes it was designed for, that is to test the functional dependence of current upon the main variables. However, the theories were not in such an advanced state when the experimental work was performed and the experimental arrangement is probably not adequate to test all the points of the theories.

For the flow variations met in the C.S.F. pathways it would be difficult to deconvolve the current time response to obtain the actual velocity variation and therefore information is lost during a decrease in flow velocity. However, if during a decrease in current the

velocity should increase again to a level corresponding to a current greater than the existing current, the decrease in current will immediately stop and the output current will again be an accurate reflection of the flow velocity.

In conclusion, the oxygen reducing cathode has been shown to be easily capable of functioning as a velocity transducer. A complete theoretical description has been developed and this description has been verified experimentally. The preferred form of transducer is a gold sphere and the remainder of this thesis is concerned with the development of a practical form of the transducer and its clinical

use.

CHAPTER 7

## CHAPTER 7

### THE DEVELOPMENT AND CONSTRUCTION OF THE FLOW TRANSDUCER; AND THE EXTENSION OF ITS CALIBRATION TO C.S.F.

#### 7.1 Introduction

Chapters 3 and 5 describe the theoretical aspects of the response of the cathode current to a steady flow velocity and its time response to a step decrease in flow. Chapters 4 and 6 describe the experiments performed to confirm these theoretical considerations.

The remainder of this thesis is concerned with the use of the flow transducer to measure the flow of cerebrospinal fluid. This chapter describes the development of the design of the transducer through to the form used in the clinical trials (Chapter 8) and the animal experiments performed to confirm its in-vivo operation.

Also described here are the in-vitro experiments performed to extend the calibration of the flow transducer from 0.15 M NaCl to C.S.F.

#### 7.2 Development of the cathode

##### 7.2.1. The copper enamelled parallel disc

The over-riding criterion in the design of the transducer was the need to measure flow and pressure simultaneously through the same point of access. As access to the C.S.F. pathways in humans was obtained via a spinal needle, through which the pressure was measured, it seemed sensible to produce a device which would enter the C.S.F. through this needle whilst still

permitting the measurement of pressure.

The first design that was tried is shown schematically in Figure 7.2.1. The P.T.F.E. bush to act as seal was first inserted into the luer -lock connector (the cut off bottom of a 5cm<sup>3</sup> disposable plastic syringe) into which the gold plated female connector had already been glued. The stainless steel tube\* (supplied by Goodfellows Metals of Cambridge) was then pushed through the P.T.F.E. bush. The P.T.F.E. bush, whilst acting as a fluid seal, allowed the stainless steel tube to move, so that the cathode face could be positioned with respect to the end of the spinal needle when in use.

The 36 swg enamelled copper wire was then carefully worked down the length of the steel tube until about one inch protruded at the bottom. The wire was then fixed in place top and bottom, with small blobs of insulating epoxy resin glue\* which also sealed the tube. Finally, the copper wire was soldered to the female connector. Continually, during construction, the integrity of the electrical insulation between the copper wire and the stainless steel tube was confirmed using an Avo meter. It was also found to be important to use a waterproof epoxy resin glue, so that the glue did not soften and detach after prolonged immersion.

In use, this design was inserted via a modified 3-way tap (as were all the other designs) into the spinal needle. This is illustrated in Figure 7.3.1. The tap was modified so that when turned to the correct position, it allowed fluid to flow between all its three ports simultaneously. Thus a fluid connection would exist from the C.S.F., along the annular space between the stainless steel tube and the spinal needle, and out through the 3-way tap allowing the simultaneous measurement of C.S.F. pressure.

\*  
See Table D.1.1

This design was intended to overcome the problem of the copper face of the cathode oxidising, since just before use a fresh face of copper could easily be cut. This design was used successfully in dogs but has obvious disadvantages. The working surface is, in principle, a parallel disc. In practice there is ambiguity since the attitude of the flow to the electrode is unknown. Also, after possibly only one use the transducer will have to be re-built if not enough copper remains. The cathode is also relatively sharp, increasing the possibility of damaging delicate tissues should contact occur.

#### 7.2.2. Copper sphere cathodes

To overcome the problem of ambiguous flow information copper sphere cathodes were used. These were made using 40 swg copper wire, rather than 36 swg, because it gave spheres of a more convenient diameter. Before inserting the copper wire into the stainless steel tube, its end was first placed in a Bunsen flame. A short length of the enamelling rapidly burnt off, and with practice it was relatively easy to form spheres, symmetrically placed on the end of the copper wires. Diameters up to 1mm were possible, but severe oxidation occurred which was removed by dipping in concentrated nitric acid until the sphere was bright, and washing in water.

This design of flow transducer is shown schematically in Figure 7.2.2. The enamel burnt off was replaced with lacquer thinned with amyl acetate and the sphere pulled back towards the stainless steel tube. After electrical isolation of the sphere from the stainless steel tube was confirmed, waterproof, insulating epoxy resin glue was applied as shown to seal the tube and give extra mechanical strength.

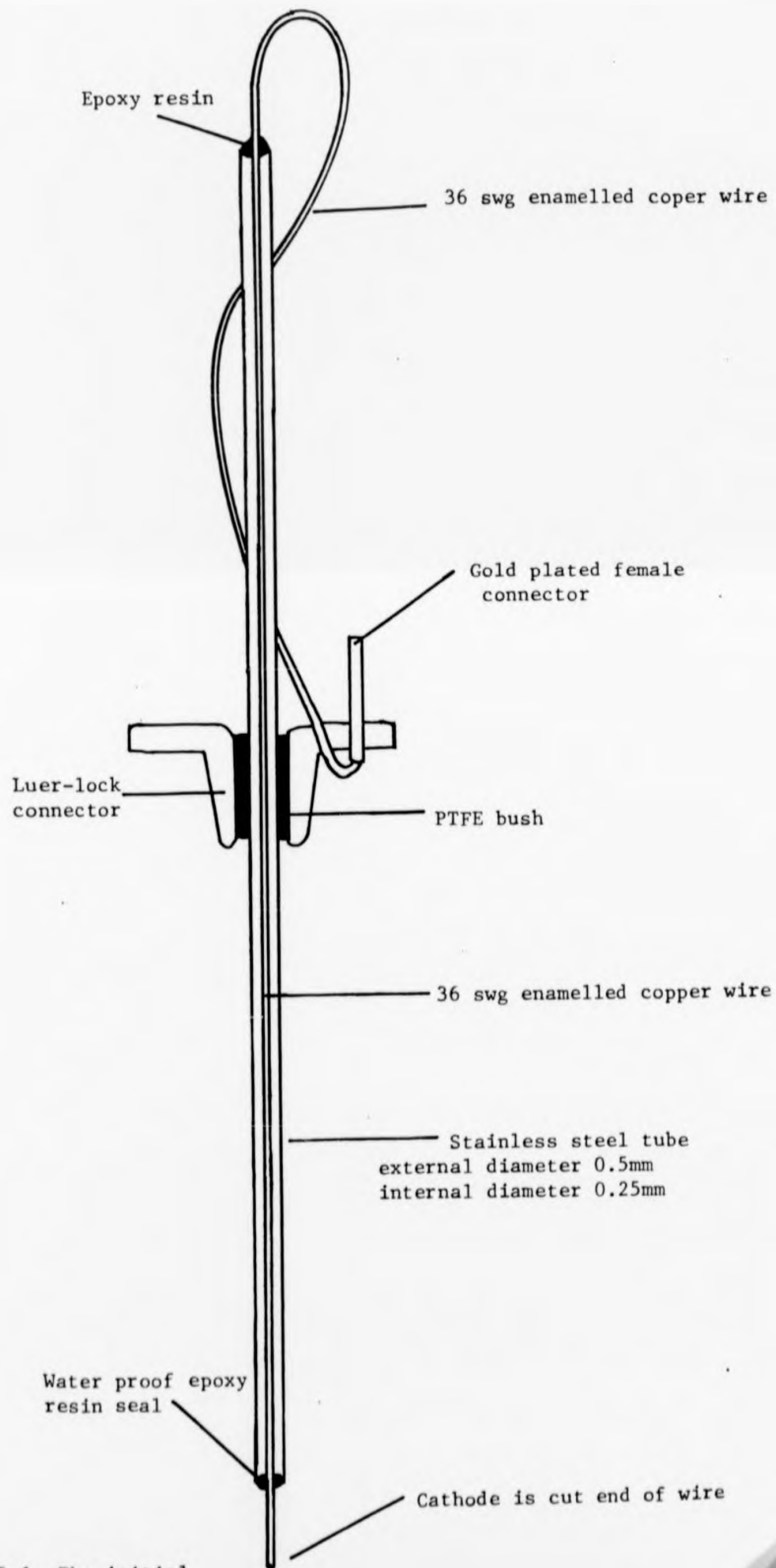


Figure 7.2.1 The initial design of flow transducer.

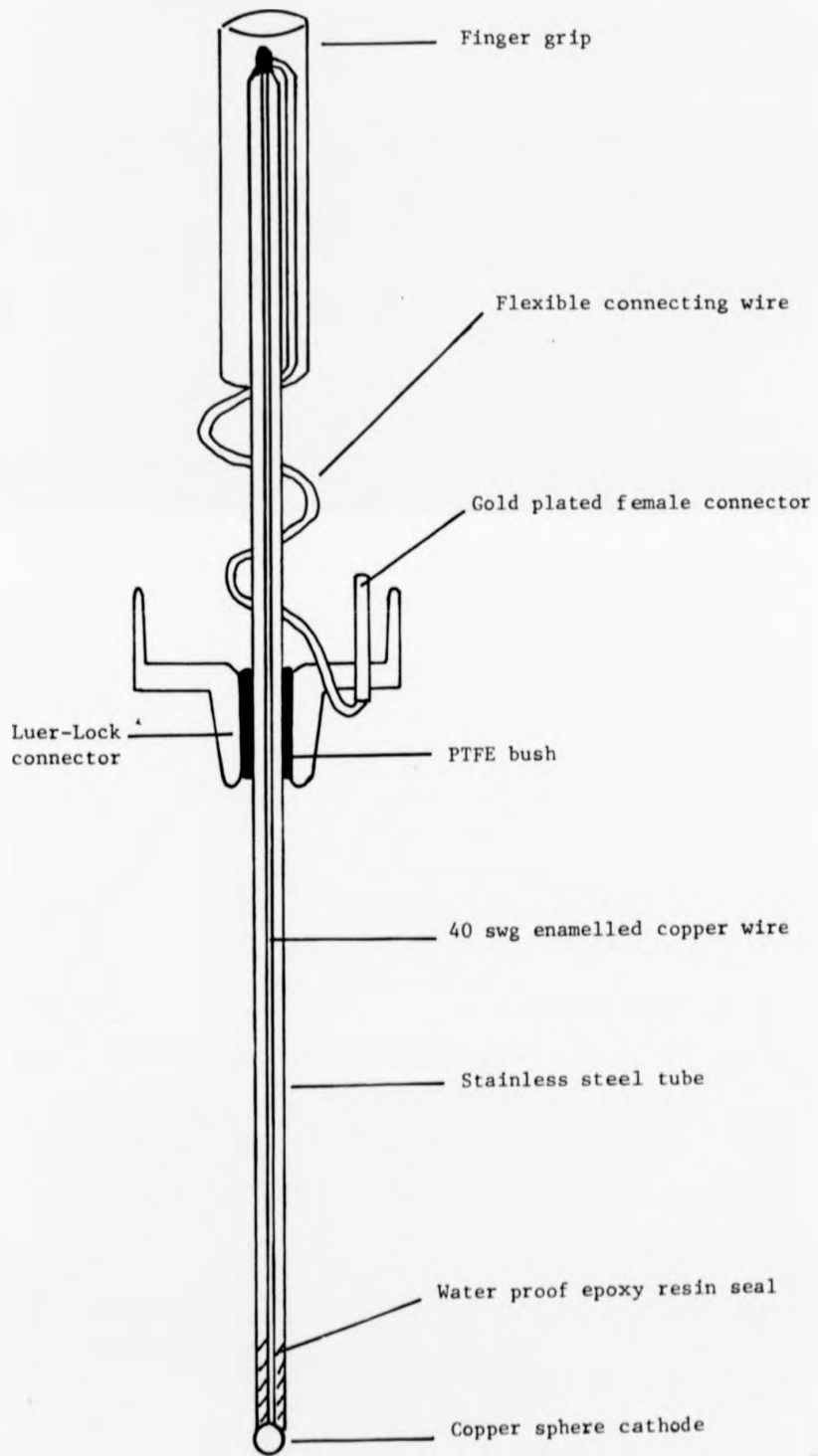


Figure 7.2.2 The flow transducer with the copper sphere cathode.

At the other end of the stainless steel tube the 40 swg copper wire was connected to the female connector using a thin, flexible, plastic insulated copper wire, the soldered connection being insulated and protected by epoxy resin glue. A convenient finger grip was then formed by placing a length of plastic sleeving (about 5cm long and  $\frac{1}{2}$ cm in diameter) over the end of the stainless steel tube. This was filled with epoxy resin glue and its ends capped with medical grade silicone rubber.

Whilst quite satisfactory in laboratory use, in spite of the often severe pitting caused by the flame and the nitric acid, this design of flow transducer would have been unsuitable for clinical use. Oxidation of the surface of the sphere would occur between sterilisation and use, the most convenient method of removal of the oxide, dipping the sphere in acid immediately before use, being obviously unsatisfactory.

To try to satisfy the need for a spherical cathode which did not suffer the problem of oxidation, copper sphere electrodes were electroplated with gold. The electroplating was performed using the method described by Wise (1964). This method was successful to the extent that the gold surface appeared shiny and complete under the microscope (40X), but often after use in saline verdigris was formed, indicating the gold layer was porous or incomplete. It was not considered worthwhile to attempt to perfect the electroplating especially since the copper sphere (the substrate) was often not perfect.

### 7.2.3 Gold sphere cathodes

All the problems detailed above were overcome by using a pure

gold sphere as the cathode, but at the cost of considerably increased difficulty of manufacture of the transducer.

Hard gold wire 0.125mm diameter\* (approximately 40 swg; supplied by Goodfellows Metals Ltd., Cambridge) was used. Gold spheres up to 1mm diameter could again be conveniently made by introducing the gold wire into a Bunsen flame. Best results were obtained with the flame horizontal and the wire introduced vertically from below, when a sphere symmetrically placed on the wire could be achieved with care. The major problem in manufacture was insulation of the sphere and its connecting wire from the stainless steel tube. It was not found possible to obtain sufficiently thin insulated gold wire and experiments at insulating long lengths of gold wire were not successful.

The approach adopted was to leave a stem of gold wire approximately 1cm long attached to the gold sphere. This wire was then butt-soldered to a 40 swg enamelled copper wire. Using a low temperature solder and soldering iron, it was possible to produce a good electrical joint though its mechanical strength often left much to be desired. The solder joint and the uninsulated stem of gold wire were then insulated with a thin coat of epoxy resin glue (this also increased the strength of the joint) and when this had set the wire was pulled up the tube until the sphere was in position. Epoxy resin glue was then gradually built up around the bottom of the tube and the base of the sphere to provide a seal and mechanical strength (the bottom of the tube had been scored to provide a key) to minimise the risk of the sphere falling off into the C.S.F. pathways. This process is illustrated in the series of photographs comprising Figure 7.2.3.

Construction was then completed as for the copper sphere cathodes.

\*  
See Table D.1.1

Figure 7.2.4. is a schematic diagram of the gold sphere transducer. The silicone rubber seal shown was added after the first clinical trials, when it was found that the P.T.F.E. bush alone was not sufficient to prevent leakage of the C.S.F.

This design of flow transducer was found to meet all the design criteria in that it allowed the simultaneous measurement of flow and pressure through the same orifice; reduced as far as possible the ambiguity of the flow information; and suffered no oxidation problem so that long term storage was not a problem. Importantly, no difference in calibration was found after ethylene oxide sterilisation.

### 7.3 The Anode

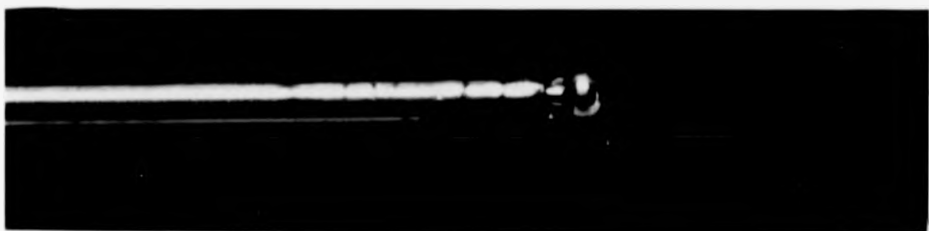
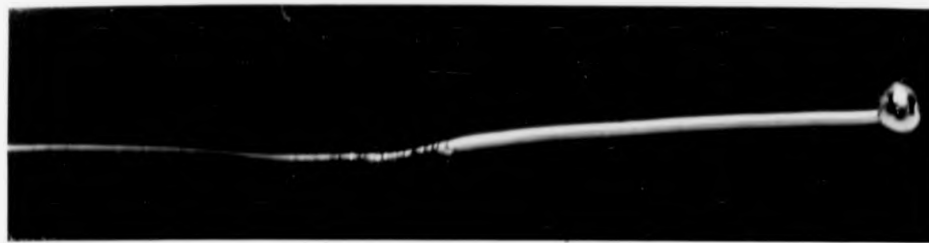
#### 7.3.1 General considerations

In principle the choice of anode is simple, the anode only being needed to complete the circuit. The criteria relating to the choice of anode material are discussed in section 4.3.3.

Two main types of anode present themselves : an anode in a reservoir with a direct fluid connection to the cathode in the C.S.F. pathways; or an anode on a suitably prepared region of skin. Both methods were tried in dogs, and clinically, and found acceptable. The choice was essentially one of convenience.

#### 7.3.2 The reservoir

Figure 7.3.1. shows schematically the type of reservoir used. It was constructed from two cut down  $5\text{cm}^3$  disposable plastic syringes, stuck together to give a volume of about  $2\text{cm}^3$ . The anode was a button type Ag/AgCl electrode. Figure 7.3.1. also shows diagrammatically the arrangement of reservoir and cathode assembly as used in practice. The advantage of this arrangement is that there



0 10 mm

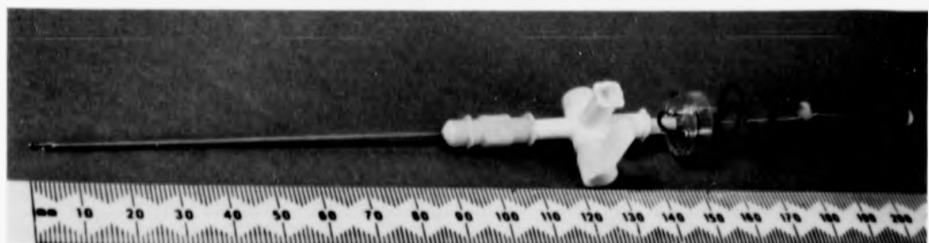


Figure 7.2.3 Series of photographs of the construction of the gold sphere transducer showing (from top to bottom): the butt-soldered joint; the epoxy resin insulation; the epoxy resin seal; and the completed transducer mounted in a spinal needle.

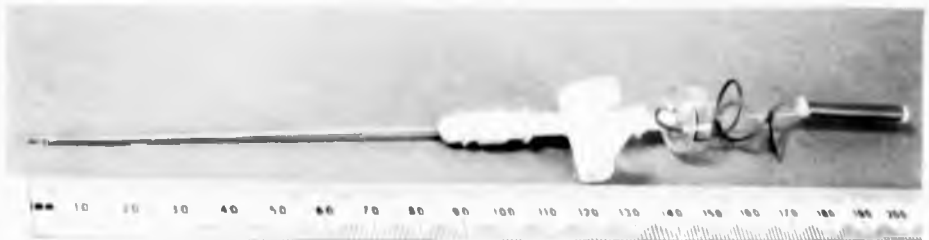
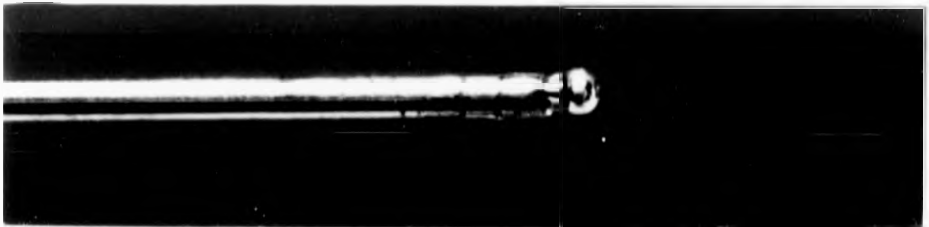
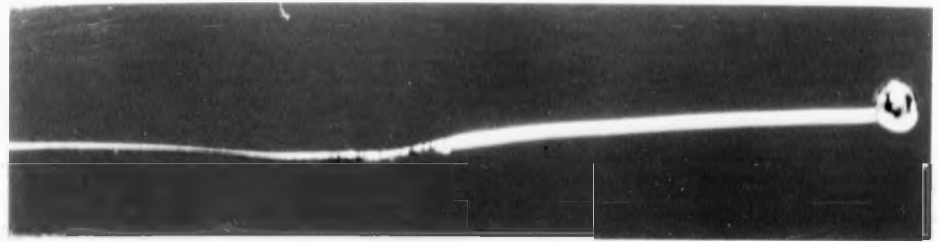
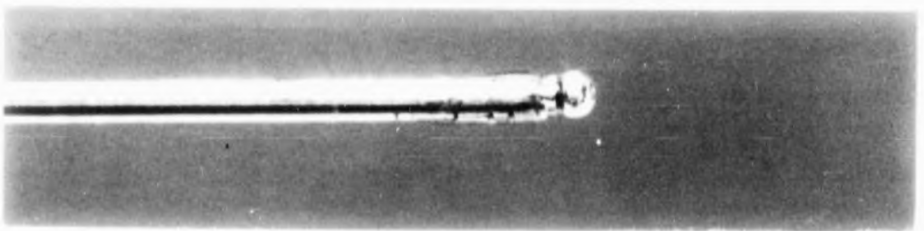
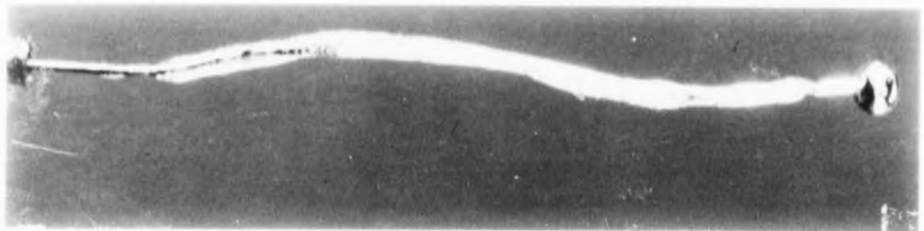


Figure 7.2.3 Series of photographs of the construction of the gold sphere transducer showing (from top to bottom): the butt-soldered joint; the epoxy resin insulation; the epoxy resin seal; and the completed transducer mounted in a spinal needle.



Micrograph showing a long, thin, straight biological specimen, possibly a nematode, with a small circular feature at the right end.

Micrograph showing a long, thin, straight biological specimen, possibly a nematode, with a small circular feature at the right end.

Micrograph showing a long, thin, straight biological specimen, possibly a nematode, with a small circular feature at the right end.

Micrograph showing a long, thin, straight biological specimen, possibly a nematode, with a small circular feature at the right end.

Micrograph showing a long, thin, straight biological specimen, possibly a nematode, with a small circular feature at the right end.

Micrograph showing a long, thin, straight biological specimen, possibly a nematode, with a small circular feature at the right end.

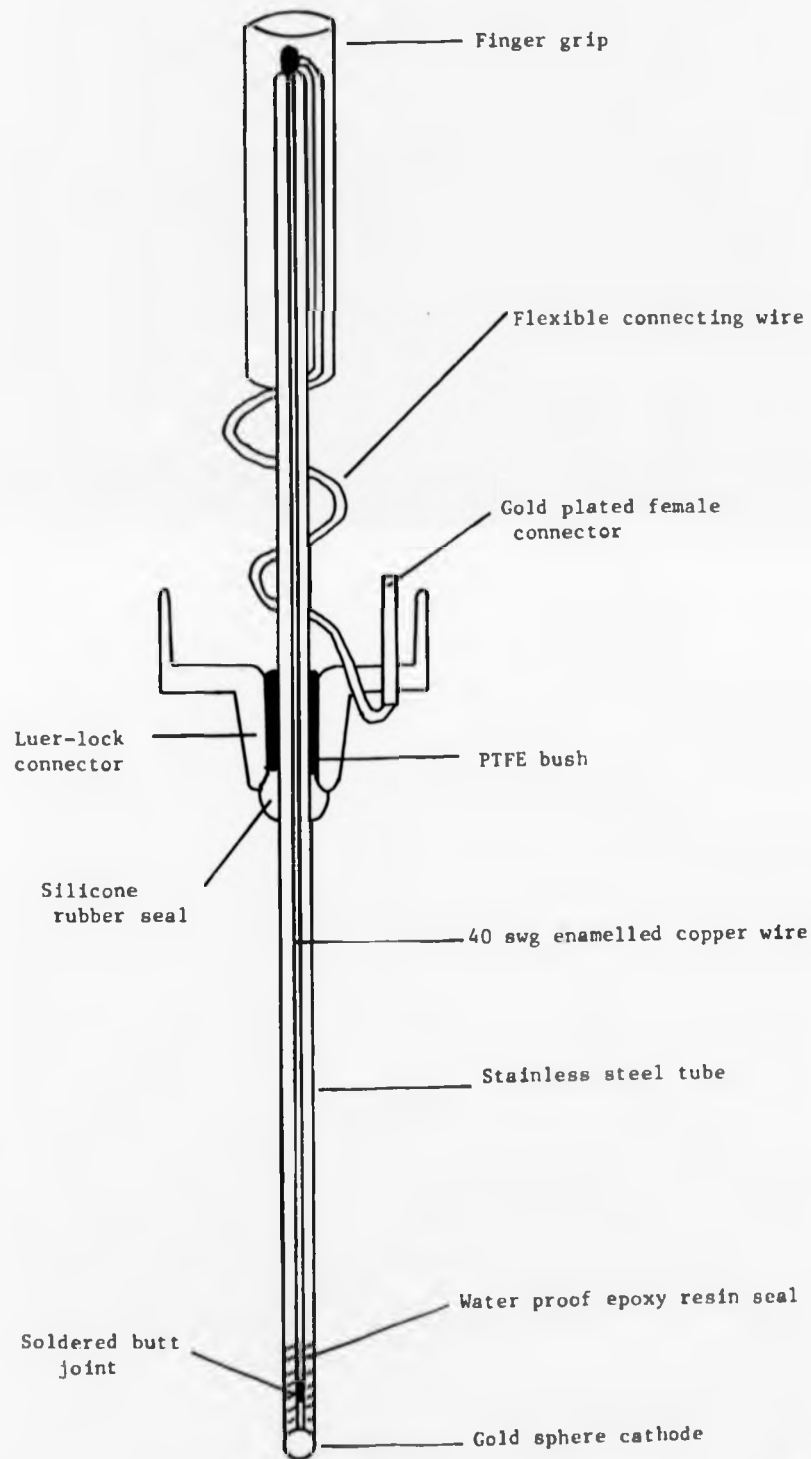


Figure 7.2.4 The flow transducer with the gold sphere cathode.

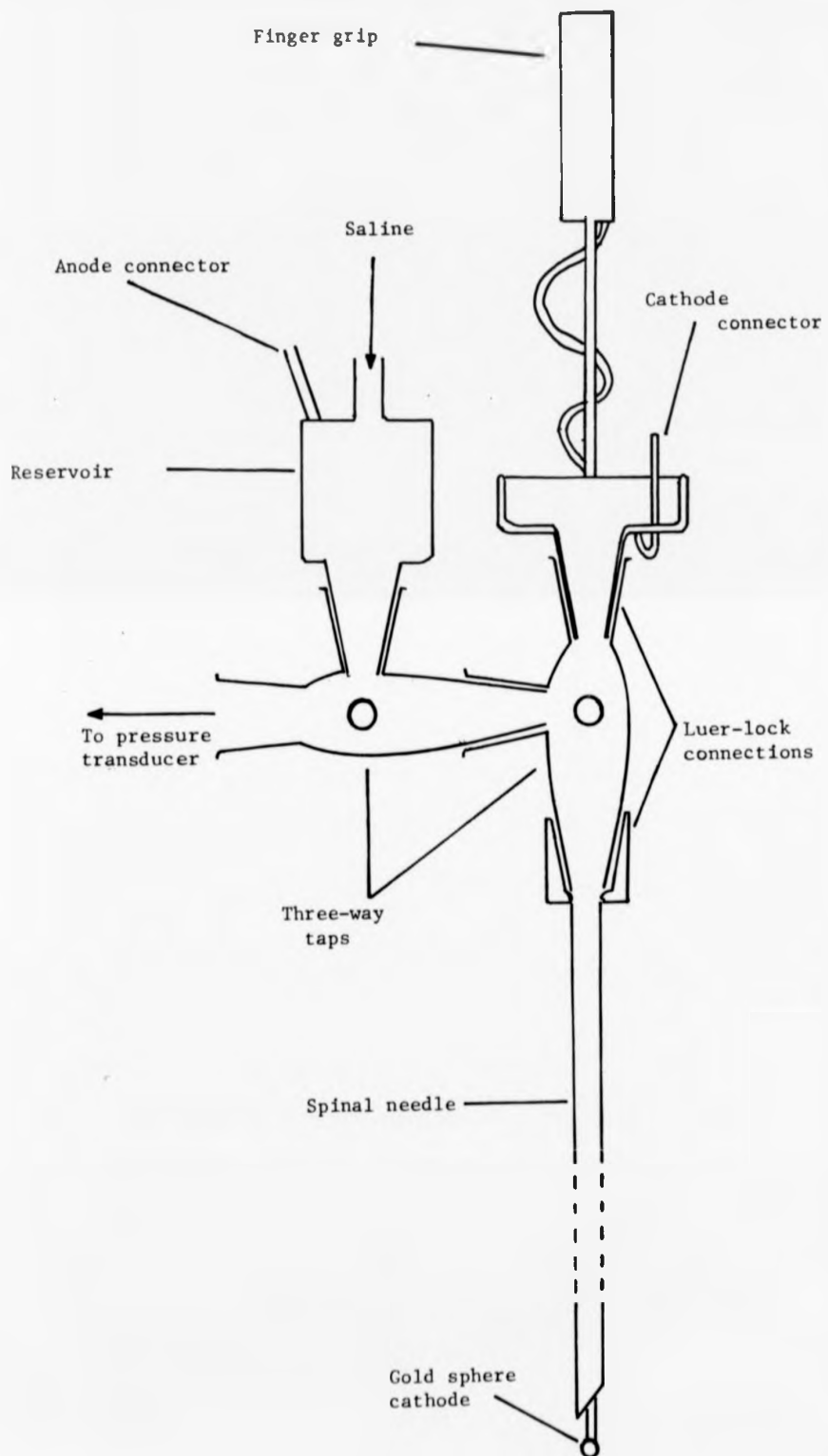


Figure 7.3.1 Schematic diagram of the arrangement of reservoir and cathode assembly used in practice.

is a direct fluid connection between anode and cathode ensuring that the resistance between the two is always low.

The disadvantages are the extra weight at the end of the spinal needle when inserted and that the reservoir is an extra volume from which air must be removed by flushing to ensure good quality pressure measurements. The use of a reservoir tended to complicate the procedure and so skin electrodes were favoured during the clinical trials.

In the initial dog experiments a copper anode in a reservoir was used. This was not suitable for clinical use because of the oxidation problem and because copper ions enter solution during use. Another problem was that after a period of use the concentration of copper ions in the reservoir increased sufficiently to cause a significant increase in  $V_a$  with a corresponding decrease in  $V_c$ , affecting the response of the flow transducer. This was, however, easily reversed by flushing the reservoir with fresh saline.

### 7.3.3. Skin electrodes

When the anode was a skin electrode the transducer assembly was as shown in Figure 7.3.1., with the omission of the reservoir assembly. Whilst the use of skin electrodes offers simplicity and convenience it also introduces problems. The resistance between anode and cathode must be sufficiently small so that when an increased current passes the cathode potential  $V_c$  stays on the plateau of the  $I-V_c$  characteristic (Figure 3.2.2.). The plateau is typically .3V wide and the maximum current expected is approximately  $10\mu A$ , so a resistance between anode and cathode of  $30k\Omega$  should be tolerable,

though a value of  $\leq 10k\Omega$  would be preferable. With correct skin preparation, that is scraping to remove the stratum corneum, and the application of electrode gel (Webster, 1978; Strong, 1970) skin resistance values of  $\leq 10k\Omega$  should easily be obtainable in the majority of cases. This problem and also that of motion artefact are discussed in Chapter 8.

The skin electrodes used were : Ag/AgCl button type electrodes, usually used as an array of 2 or 4 in parallel; and a German Silver plate electrode approximately 55mm x 45mm and slightly curved (section 8.3).

Two other types of electrode were tried. They were the shaft of the spinal needle (stainless steel) and the stainless steel tube supporting the cathode. Stainless steel does not make as stable an electrode as Ag/AgCl (Webster, 1978; Strong, 1970) but if its use had been successful there would have been obvious advantages. However, as expected, both were found to be unsuitable in that velocity calibrations performed using them as anodes were both unstable and non-repeatable.

#### 7.4 The Animal Experiments

##### 7.4.1 Introduction

The animal experiments were performed in parallel with and in conjunction with the development of the flow transducer design as described in sections 7.2 and 7.3. The experiments highlighted problems in the design of the transducer which were corrected and tested in further experiments.

The experiments were performed to confirm the ability of the transducer to measure the flow of C.S.F. in-vivo, and to gain experience of its in-vivo use. No attempt was made in any of the experiments to model the flow of C.S.F. in the human situation.

In addition to the design problems of the flow transducer which were overcome, there were also surgical problems because the C.S.F. pathways in animals are much smaller than in humans. Thus the animal experiments were a series of experiments, each of which was designed to overcome problems, both technical and surgical, highlighted in previous experiments.

The dog experiment described below, and the results presented, are the culmination of the animal work. The final form of cathode (a gold epoxied sphere) and a Ag/AgCl skin electrode were used. The results confirmed the in-vivo functioning of the transducer and no further animal experiments were performed since there was no sufficiently good reason to do so.

In total six animal experiments were performed, including one rhesus monkey and five dogs. The animals were always anaesthetised.

#### 7.4.2 Experimental arrangement and methods

Measurement of C.S.F. pressure (or flow) is more difficult in animals than in humans because of the smaller size of animal C.S.F. pathways. This caused considerable problems in the placement of the spinal needle/flow transducer assembly. No imaging was used in any of the animal work.

In the initial experiments the transducer was placed in the spinal C.S.F. pathways (either lumbar or cisternal), with the animal lying on its abdomen. A flow of C.S.F. could then be imposed by

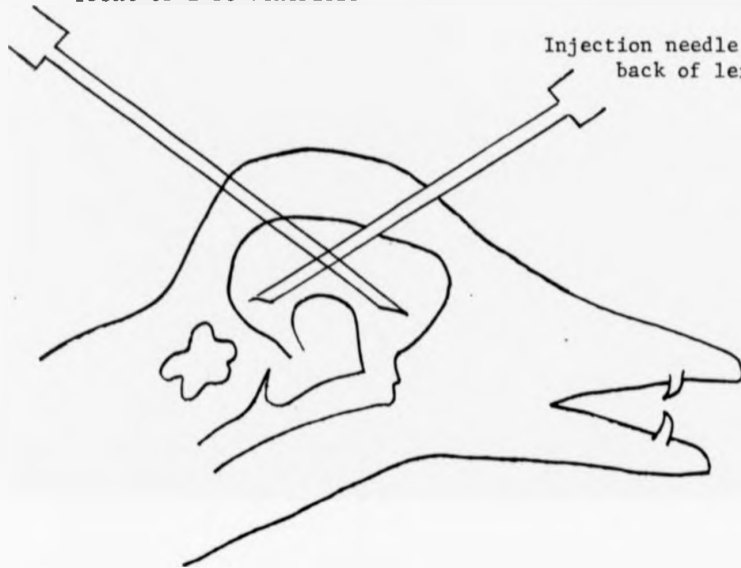
squeezing the animal's abdomen. This arrangement was unsatisfactory because of difficulty in positioning the transducer and difficulty in producing a controllable flow of C.S.F. of reasonable magnitude.

The arrangement now described was designed to overcome these problems. The dogs used had previously been given injections of kaolin cisternally to cause hydrocephalus, so increasing the size of the ventricles and permitting easy access. The experimental arrangement is shown schematically in Figure 7.4.1. Injection needles were placed in the left and right lateral ventricles as shown and a spinal needle was placed in the left ventricle into which the flow transducer was inserted and through which pressure was measured. Figure 7.4.2. is a photograph showing this particular experimental arrangement. The anode was a Ag/AgCl button type electrode taped to a shaven patch of skin on the dog's skull. Electrode gel was used. The cathode assembly had previously been positioned with respect to the spinal needle used (the spinal needles had been found to differ slightly in length) so that the cathode was 2 to 3mm beyond the point of the needle when inserted; its position could then be adjusted if required.

No imaging was used so it was not possible to know exactly the position of the cathode in the ventricle, nor was it possible to know exactly the position of the cathode relative to any flow pattern caused by manually pumping, using syringes, from one injection needle to the other. The cathode was known to be in a confined space (the left ventricle) in which a flow of C.S.F. could be imposed.

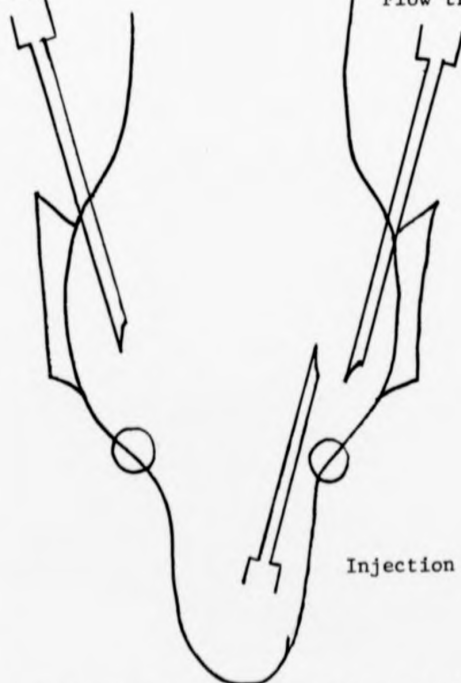
The pressure was recorded so as to show when a flow of C.S.F. was imposed and to allow the pressure within the ventricles to be

Flow transducer and pressure needle:  
front of left ventricle



Injection needle:  
back of left ventricle

Injection needle:  
right ventricle



Flow transducer and pressure  
needle

Injection needle: left ventricle

Figure 7.4.1 Diagrams showing the positions of the flow transducer and injection needles in the dog experiment.

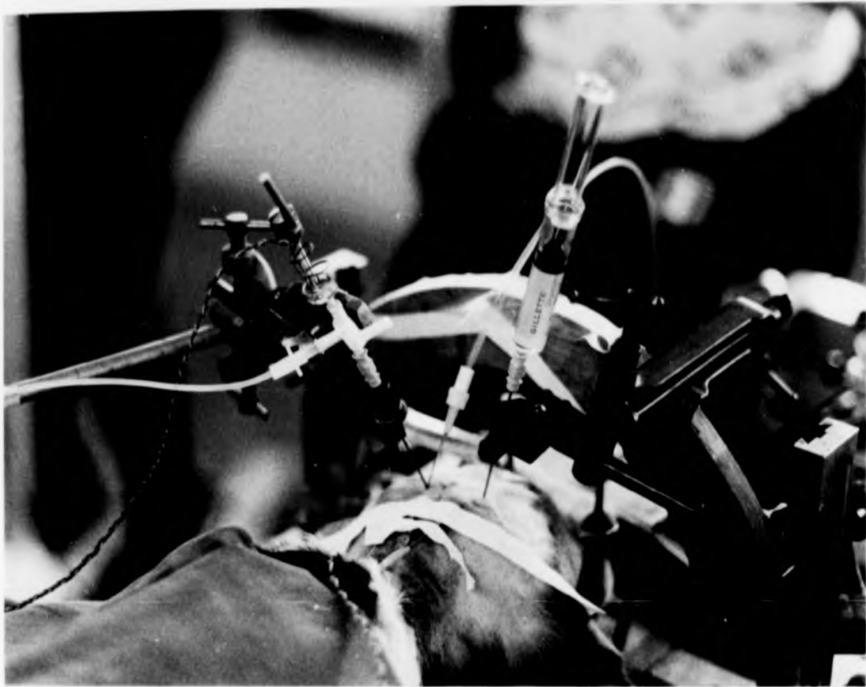


Figure 7.4.2 Photograph of the dog experiment described in the text.

The electrochemical flow transducer and the injection needles are clearly shown. The Ag/AgCl anodes are taped to the skull immediately below the flow transducer.



Figure 7.4.2 Photograph of the dog experiment described in the text.

The electrochemical flow transducer and the injection needles are clearly shown. The Ag/AgCl anodes are taped to the skull immediately below the flow transducer.

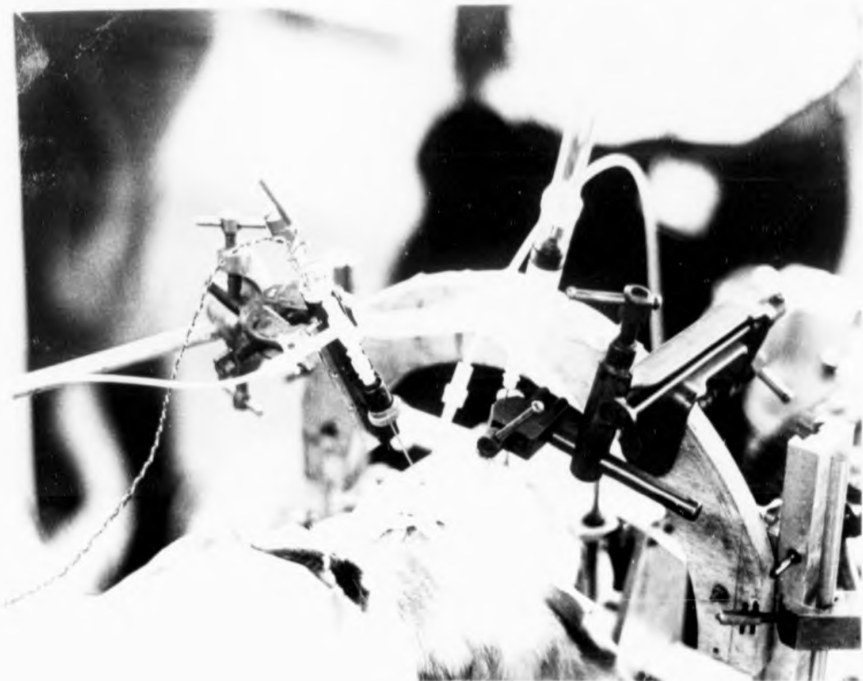


Fig. 2 Photograph of the dog experiment described in the text.

The electrochemical flow transducer and the injection needles are clearly shown. The Ag/AgCl anodes are taped to the skull immediately below the flow transducer.

kept within reasonable limits. The voltage clamp circuit used was the same as that shown in Figure 4.4.1. The pressure and flow waveforms were recorded on a Devices M19 chart recording system. The flow signal was fed to a Devices 3461 d.c. amplifier with variable low pass filtering. The filter setting was adjusted to sufficiently reduce any 50Hz noise on the trace; for the results shown the filter had a 3dB point of 30Hz. The pressure transducer was a Statham P23 and was driven by a Devices 3552 pressure pre-amplifier.

The cable to the anode and cathode was 3m long, screened for the first 2m. The last metre was thus flexible unscreened cable. In this application cable capacitance is of no consequence as the input to the voltage clamp (Figure 4.4.1.) is a virtual earth.

#### 7.4.3. Results

Figure 7.4.3. shows the output current  $I$  of the flow transducer and the pressure in the same ventricle as recorded through the same spinal needle. The cathode was an epoxied gold sphere 0.56mm in diameter, and the anode was a Ag/AgCl button type electrode taped to the dog's head (the skin had been shaved and scraped and electrode gel was used). The potential  $V_{ac}$  set between cathode and anode was 1 volt.

The large swings in pressure occurred when a flow was imposed by manually pumping. Originally  $I^2$  was not recorded. Figure 7.4.3. was obtained by digitising the original recordings (using a Hewlett Packard model 7220 digital plotter, accurate to .025mm) and storing the data. Replay from a computer onto the digital plotter allowed the variation of  $I^2$  with time to be shown accurately. The relative

magnitudes of the free convection and the imposed flows are more easily seen on the  $I^2$  trace. On the right hand side of the figure is shown the velocity calibration for the flow transducer assuming a temperature of  $37^{\circ}\text{C}$  and corrected for the measured  $p\text{O}_2$ .

Initially one of the pumping syringes was filled with physiological concentration saline. The measured  $p\text{O}_2$  (of a sample of C.S.F. removed for analysis) at the time the results shown on Figure 7.4.3. were recorded was 100mm of Hg. This value is higher than would normally be expected because the saline used had an atmospheric concentration of oxygen. It is also possible that oxygen was diffusing directly into the C.S.F. because of the experimental arrangement; this is supported by an earlier experiment when the measured  $p\text{O}_2$  was seen to increase from approximately 50mm of Hg to approximately 110mm of Hg during the course of the experiment. Another explanation of the high value of  $p\text{O}_2$  is that oxygen was allowed to enter the sample taken for analysis. If this is so then the magnitude of the flow past the cathode was greater than that implied by the calibration shown.

The external pumping arrangement also introduces an uncertainty into the temperature (the temperature of the C.S.F. was not measured) because of possible cooling of C.S.F. in the syringes and because the saline used was originally at room temperature.

Since no independent accurate measure of the flow was possible, neither of the above mentioned uncertainties is of importance. The experiment was designed to allow the imposition of a flow at a known time and to monitor the response of the flow transducer. In this respect the experiment was completely successful.

Each imposed flow shown in Figure 7.4.3. is marked with an arrow

denoting pumping from the left ventricle to the right, or vice versa. The response was consistently greater when pumping from the left ventricle into the right, as it was for similar flow events not shown. As no imaging was used the attitude of the cathode with respect to the imposed flow was unknown, and also the dimensions of the ventricles were unknown. However, typically  $4\text{cm}^3$  were pumped during each imposed flow and the magnitude of the transducer output current is consistent with such a volume flow.

The results of Figure 7.4.3. show that the transducer is capable of responding consistently and reasonably to the in-vivo flow of C.S.F.

Figure 7.4.4. illustrates the sensitivity of the transducer. The gain has been increased by a factor of 1000 and the dc component backed off. The rhythmical variations in current are attributed to flow of C.S.F. caused by movements of arteries and artery walls during the cardiac cycle. The dog was shivering periodically during its respiratory cycle in this part of the experiment and when this occurred the current trace (at such high gain) exceeded the range of the chart recorder. Figure 7.4.5. shows similar information except that the gain of the pressure recording has been increased by a factor of 10 and the chart speed increased to show more detail.

As shown in Chapters 5 and 6 the response of the output current to a decrease in flow is complex. The flow information content of the decreasing portions of the  $I$  and  $I^2$  traces of Figure 7.4.3. is degraded by the time response characteristics of the flow transducer. The time response is fastest when the velocities are highest and at the initial parts of the current decays. Therefore, at the higher flow magnitudes of Figure 7.4.3. the initial current decays are possibly reasonable representations of the actual flow occurring. During a

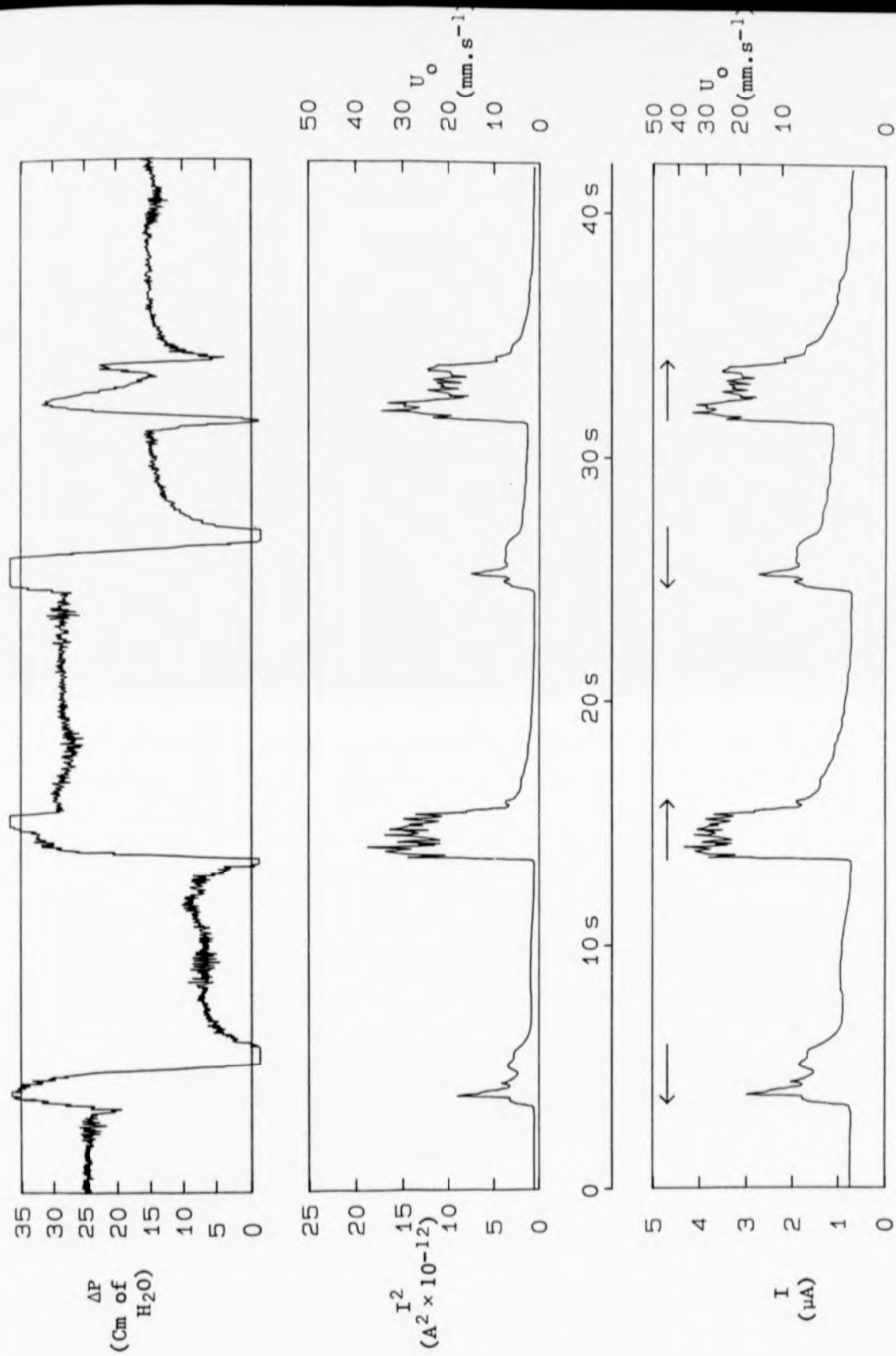


Figure 7.4.3  $I$  and  $I^2$  during pumping. The velocity calibration has been corrected for the measured  $pO_2$  of 100mm of Hg. The arrows indicate the direction of pumping.

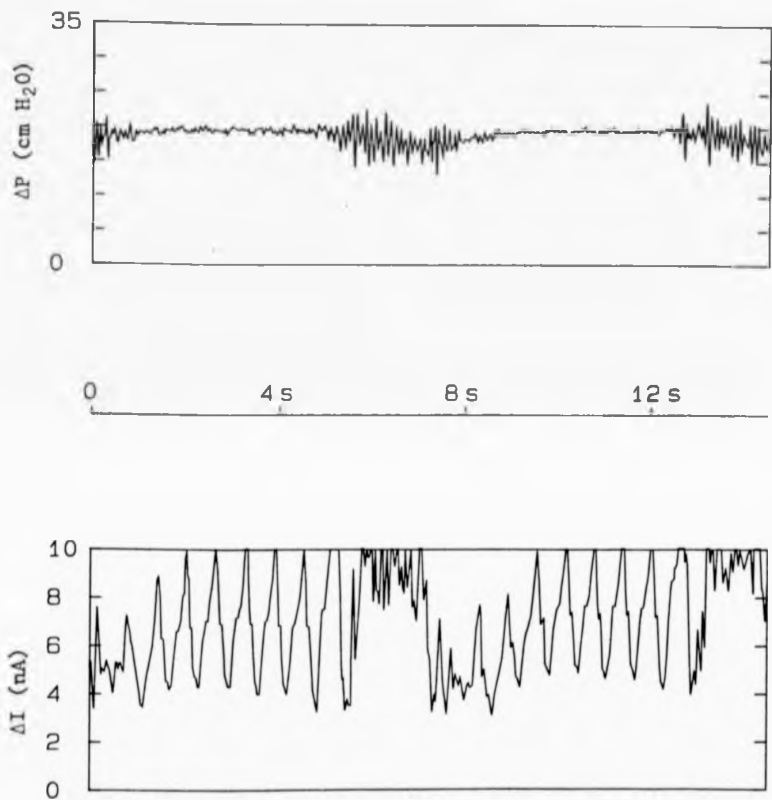


Figure 7.4.4 Rhythmical variations in  $I$ , attributed to movement of CSF caused by cardiac activity. The dog was shivering periodically.

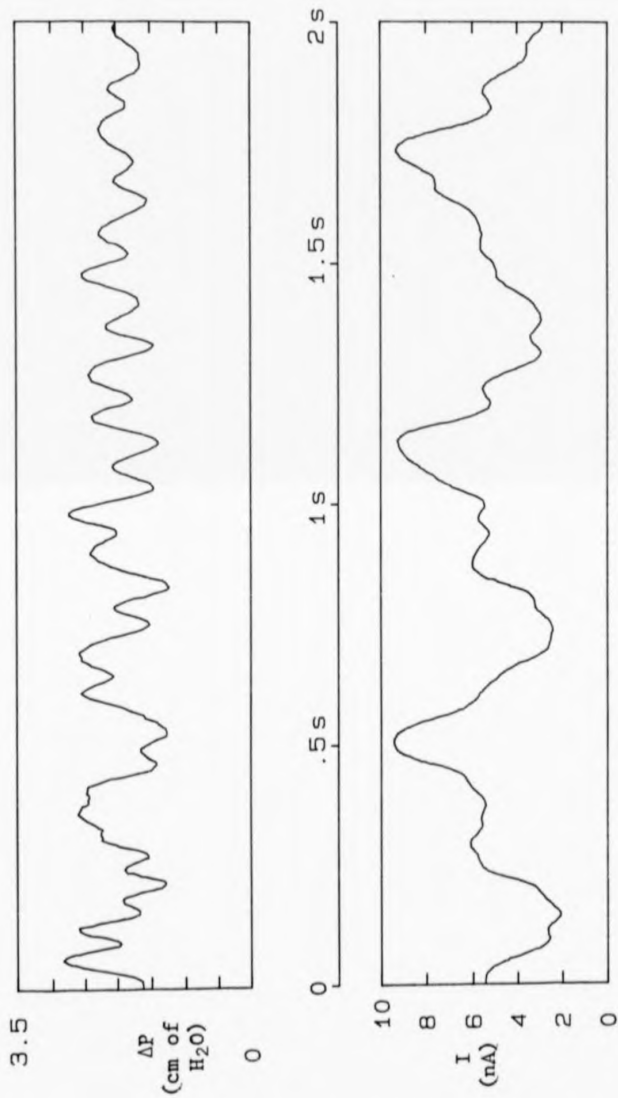


Figure 7.4.5 Rhythmical variations in  $I$  recorded with a faster time base to show more detail. The pressure scale is 10 times more sensitive than in figure 7.4.4.

current decay, if the flow increases to a value corresponding to a greater value of I than that reached in the current decay then the output current will again accurately follow the magnitude of the flow. As would be expected in a small container with good temperature control the free convection occurring is smaller than in a saline bath heated to 37°C. This is shown by the small value of I when no flow is imposed.

The cathode and anode used were calibrated in air equilibrated saline at 37°C before and after the experiment and no difference in calibration was seen. The cathode was in place in the ventricle for approximately 30 minutes and so there is no evidence of protein poisoning of the cathode over this time span. In this experiment no traces of blood were visible in the C.S.F. In earlier experiments traces of blood were seen in the C.S.F., but again no evidence of poisoning was observed even after several hours. In the initial experiments, where enamelled copper disc cathodes were inserted into the lumbar or cisternal C.S.F. pathways, the response of the cathode was sometimes greatly decreased. After visual inspection of the cathode this decrease in flow sensitivity was attributed to the cathode having come into intimate forcible contact with tissue. This is the only evidence of poisoning of the cathode, of any sort, noted in the animal experiments.

## 7.5 Extension of the Calibration to C.S.F.

### 7.5.1 The constituents of the C.S.F.

All the laboratory work described to this point was carried out in 0.15M NaCl (approximately physiological concentration saline). The functioning of the flow transducer was shown in Chapter 3 to be insensitive to changes in NaCl concentration. C.S.F., whilst basically physiological saline, also contains other constituents as shown in

Table 7.5.1.

The inorganic constituents of the C.S.F. would not be expected to interfere with the electrochemical reduction of oxygen (Charlot, 1962). Also, the viscosity and density of C.S.F. is very similar to that for the saline used to this point; as the kinematic viscosity  $\nu$  appears in equation 3.1.2 as  $\nu^{-1/6}$  any slight differences in the kinematic viscosity would have a negligible effect on the velocity response.

Also, the oxygen concentration of C.S.F. is considerably less than that of air equilibrated 0.15M NaCl (Campkin et al, 1974; Chapter 8). When in-vivo measurements are performed the  $pO_2$  of the C.S.F. must be measured.

The major constituents of the C.S.F., besides the inorganic ions, are glucose, urea and protein. The effects of the addition of these three constituents to 0.15M NaCl are described in section 7.5.2. Further, the pH of C.S.F. differs from that of air-equilibrated saline. The effect of altering the pH is described in section 7.5.3.

#### 7.5.2. The effect of protein upon the velocity response

Many workers with invasive  $pO_2$  electrodes have commented upon the adverse effects of protein on the oxygen reducing cathode. Meldrum et al (1973) state that "Protein molecules and other substances in solution are also attracted to the cathode surface, altering its reactivity with oxygen.", and Silver (1972) refers to "...the unfortunate effects of protein deposition and the formation of-SH complexes upon the catalytic surface ....". Cater et al (1959) whilst commenting upon the poisoning of bare oxygen cathodes attribute poisoning by glutathione to formation of Pt or Au -

Table 7.5.1 PROPERTIES AND MAJOR CONSTITUENTS OF C.S.F.

Specific gravity		1.007
Relative viscosity (38 C)		1.020-1.027
pH		7.327-7.371
Major inorganic constituents:		Typical Ratio of C.S.F./Plasma
sodium	128-157 mEq/l	0.98
potassium	2.06-3.86 mEq/l	0.62
chloride	110-129 mEq/l	1.14
bicarbonate	21.3-25.9 mEq/l	1.01
magnesium	.45-4.01 mEq/l	1.39
calcium	1.96-2.60 mEq/l	0.49
carbon dioxide	39.5-50.9 mm of Hg	1.28
other elements in trace amounts e.g., copper, iron and manganese		
Glucose	480-860 mg/l	0.64
Nitrogenous substances:		
Total nitrogen	157-220 mg/l	---
Non-protein	110-200 mg/l	---
Urea	138-364 mg/l	0.80
Amino-acids	9.6-15.2 mg/l	---
Protein	171-313 mg/l (approx 50% as albumin)	0.003

Abtacted from Gangong W F, Review of Medical Physiology, 1981  
and Diem K and Lentner C, Scientific Tables, 1970.

sulphydryl complexes on the surface of the platinum or gold cathode. Zick (1976) when using gold cathodes states "Polarized electrodes attract proteins making them more susceptible to poisoning".

The above references indicate that poisoning of the cathode, and the resulting decrease in the velocity response, caused by organic compounds such as protein could be a problem. An advantage here though, is that C.S.F. contains far less protein than blood or tissue (Table 7.5.1.).

Using the experimental method of section 4.4 the effects upon the velocity response of adding glucose, urea and protein to the 0.15M NaCl (to make a mock C.S.F.) were investigated. The protein used, which was in limited supply, was bovine albumin. The cathode was an epoxied gold sphere (as used clinically) and the anode was a Ag/AgCl electrode.

A velocity calibration was first carried out in 0.15M NaCl at 37°C, and then repeated immediately after the successive addition of each of the following: 0.8g/1000cm<sup>3</sup> glucose; 0.4g/1000cm<sup>3</sup> urea; 0.1g/1000cm<sup>3</sup> albumin; a further 0.1g/1000cm<sup>3</sup> albumin; and finally 0.2g/1000cm<sup>3</sup> albumin giving a total of 0.4g/1000cm<sup>3</sup> albumin.

Each velocity calibration was found to be identical within the normal scatter. This result indicates that the addition of albumin, and glucose and urea, in concentrations typical of C.S.F. does not, at least in the short term, alter the velocity calibration.

If left immersed in the mock C.S.F. for some time, the velocity response of the flow transducer, whilst still exhibiting the same functional relationship with applied velocity, was found to decrease in magnitude. Replacing the anode did not reverse the decrease, but dipping the cathode in concentrated nitric or hydrochloric acid

restored the velocity response to its original magnitude. This is indicative of some poisoning process at the cathode.

The long-term effects of exposure to the main constituents of C.S.F. (urea, glucose and protein) were investigated by leaving the electrodes (operational, but stationary) in the mock C.S.F. and repeating the velocity calibration at intervals. This was done at albumin concentrations of  $0.4\text{g}/1000\text{cm}^3$  and  $0.8\text{g}/1000\text{cm}^3$ . The concentration of glucose was  $0.8\text{g}/1000\text{cm}^3$  and that of urea was  $0.4\text{g}/1000\text{cm}^3$  in both cases. The results are shown in Figure 7.5.1.

In Chapter 4 the gradient of the  $I^2 - U_a$  graph was defined as  $g$ , the expression for an epoxied sphere being equation 4.4.3.  $g'$  is the normalised gradient of the  $I^2 - U_a$  graph, that is the value of  $g$  at some time  $t$  after immersion, divided by the value of  $g$  at  $t = 0$ .

The results of Figure 7.5.1 show the poisoning process to cause an **exponential** decay of the current, probably proportional to the albumin concentration (more results are needed to be certain). The rate of decrease of  $I$  at  $0.4\text{g albumin}/1000\text{cm}^3$  is  $3.5 \pm 0.7\%$  per hour and that at  $0.8\text{g}/1000\text{cm}^3$  is  $6 \pm 1\%$  per hour.

To conclude, the results suggest that the presence of glucose and urea (at concentrations typical of the C.S.F.) has no effect upon the velocity response. Albumin, in the short term has no effect, but on prolonged immersion an **exponential** decay of the output current occurs which is probably proportional to the albumin concentration. The poisoning process occurs at the cathode and is probably randomly scattered over the whole surface.

This work was performed after the dog experiments had been completed. No protein poisoning problem was identified during the dog experiments though this is not evidence for its absence. The dog experiments were solely concerned with establishing that the

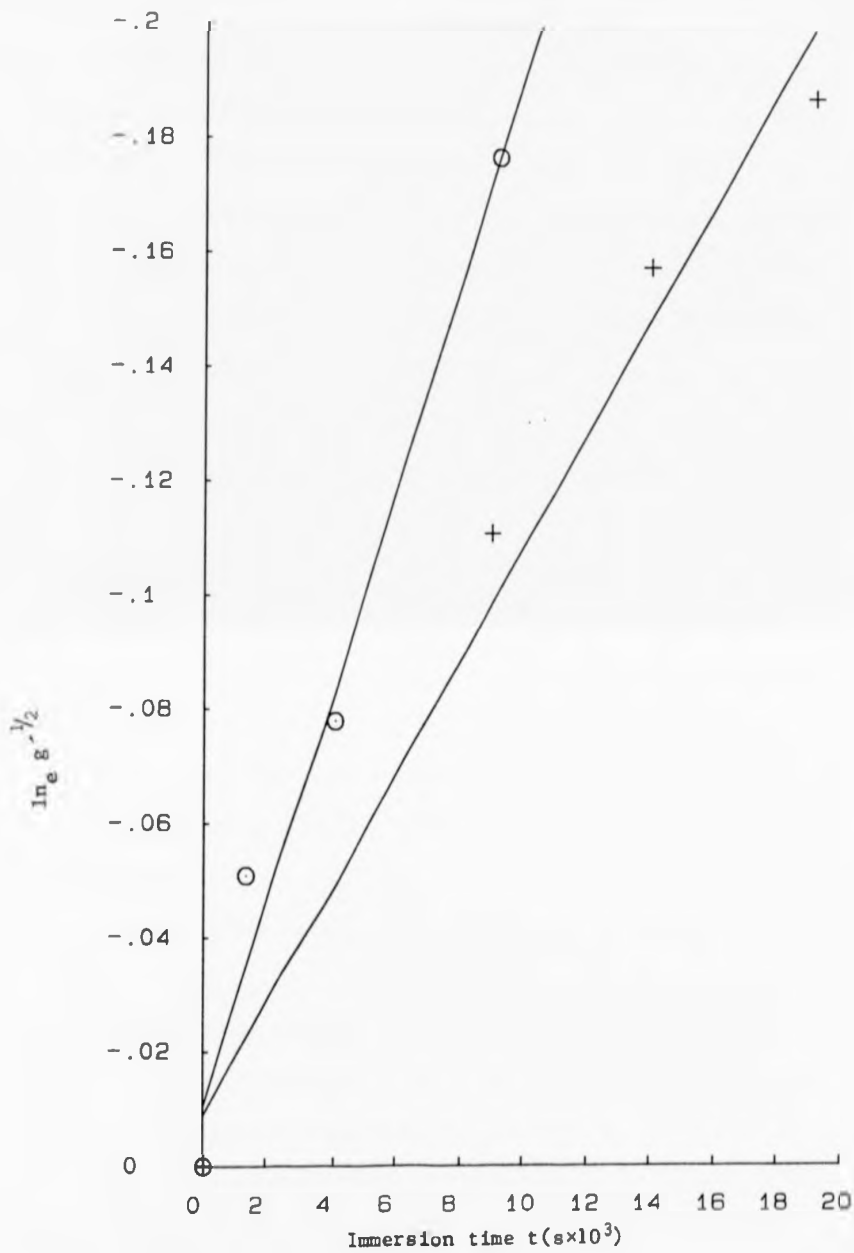


Figure 7.5.1 The effect upon the velocity response of a gold sphere cathode (at  $37^{\circ}\text{C}$ ) of immersion in mock CSF containing bovine albumin.

$g'$  is the gradient of the  $I^2-U_a$  graph, normalised against the value at  $t=0$ .

+  $0.4\text{g}/1000\text{cm}^3$ ; o  $0.8\text{g}/1000\text{cm}^3$  bovine albumin.

flow transducer would function in-vivo.

In Figure 7.5.1, at  $0.4\text{g}/1000\text{cm}^3$  albumin, a 7% decrease in  $I^2$  occurs in one hour. In clinical use such a poisoning rate would be acceptable, but in the clinical trials (Chapter 8) no evidence of poisoning was identified. Consequently, no further investigation of this process was performed.

### 7.5.3 The effect of pH upon the velocity response

0.15M NaCl as used in the laboratory work is slightly acidic because of dissolved carbon dioxide, whereas C.S.F. is slightly alkaline (Table 7.5.1). To investigate the effect of pH, the pH of 0.15M NaCl was varied by the addition of hydrochloric acid or by sodium hydroxide. The pH was measured using an "Orion research" analogue pH meter (Model 301). Velocity calibrations were performed at  $37^\circ\text{C}$  using a gold epoxied sphere cathode and a Ag/AgCl anode.

At pH 11.25 the velocity calibration was unchanged from that in unadulterated saline. However, when a velocity calibration was attempted at pH 2.7 not only was  $I_p$  an order of magnitude greater than usual, but the velocity response was also very large with an extremely large scatter. This is evidence of a different, or extra, reaction occurring at the cathode at low pH (the cathode being the current limiting electrode).

To investigate this a series of  $I-V_{ac}$  curves were carried out at various values of pH, at  $37^\circ\text{C}$  using the same electrodes. The device described in section 4.3.1 to limit the free convection was used.

Figure 7.5.2 shows some of the  $I-V_{ac}$  curves obtained at the lower values of pH (for clarity not all the curves are shown). Figure 7.5.3 shows the variation of  $I_p$  with pH. Figure 7.5.2 illustrates how, as the pH is decreased, the second reaction increases in magnitude and masks the oxygen reaction. From Figure 7.5.3 it seems likely that the rate of the second reaction (probably the evolution of hydrogen gas at the cathode) is proportional to the hydrogen ion concentration. Above pH 4.5 the effect of the second reaction is negligible and the flow transducer functions normally.

As shown in Figure 7.5.2 the second reaction also possesses a plateau and is therefore transport limited, though in this case as the hydrogen ion is charged there would also be transport by drift. The results of Figure 7.5.3 show that even at high values of pH when the hydroxide ion concentration could have been sufficiently high to interfere with the transport of hydroxide ions from the cathode (to the extent that this became the rate determining step - section 3.1), the flow transducer still functioned normally.

#### 7.6 Discussion

The development of the preferred form of flow transducer (the gold sphere cathode) has been described, together with results from an animal experiment which confirm that the transducer can measure the in-vivo flow of C.S.F. Having obtained these results it was not considered necessary to perform any further animal experiments.

Whilst the effect of the presence of the cathode assembly upon

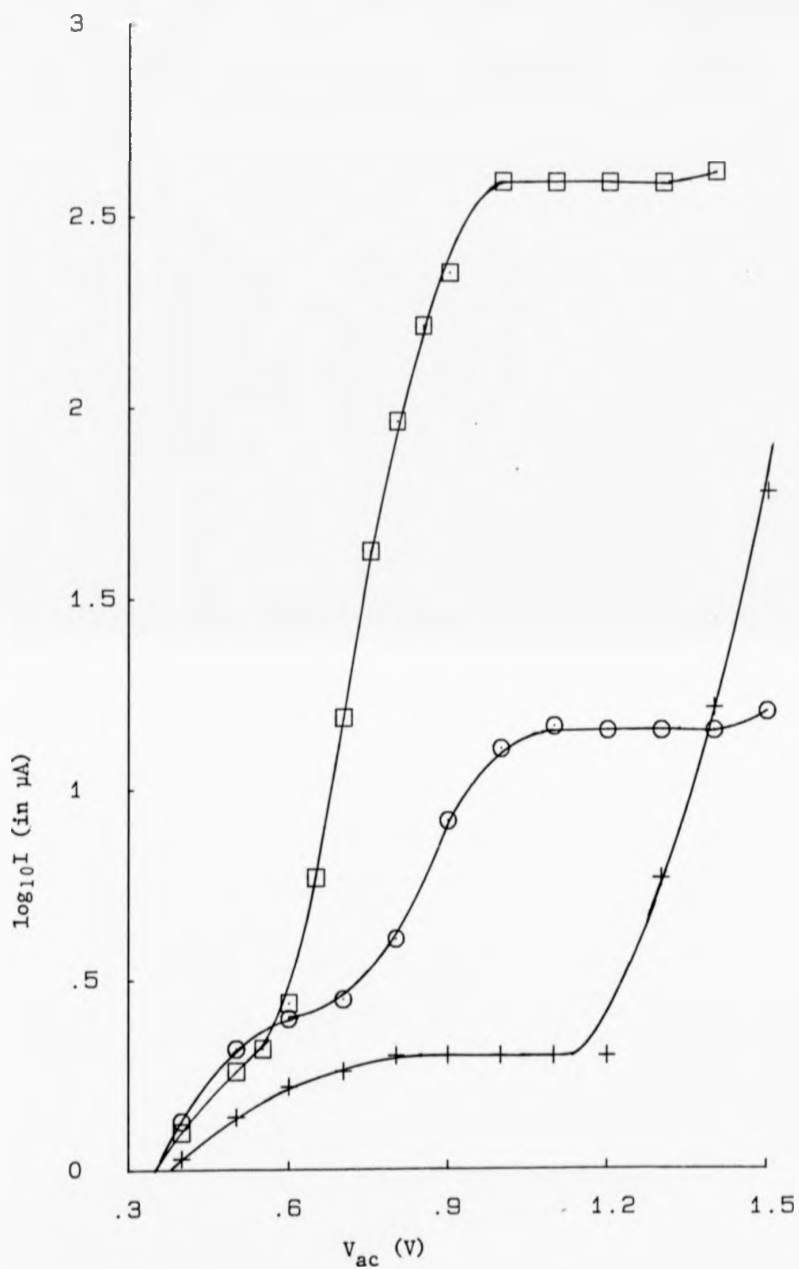


Figure 7.5.2  $I-V_{ac}$  curves at low values of pH for a gold cathode and Ag/AgCl anode at  $37^{\circ}C$ .

+ pH 6.2; O pH 3.5;  $\square$  pH 2.2

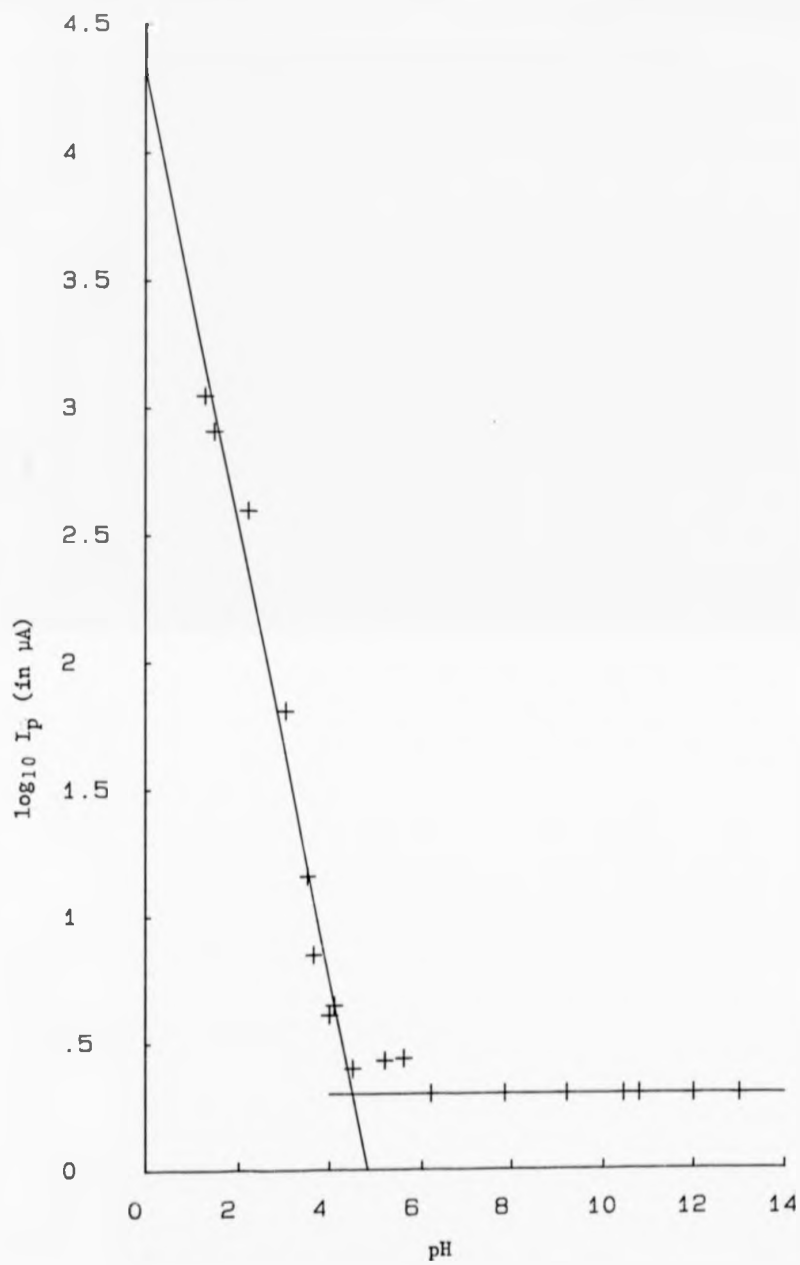


Figure 7.5.3 The variation of plateau current  $I_p$  with pH for a gold cathode and Ag/AgCl anode at  $37^\circ\text{C}$ .

the pressure measurements was not explicitly investigated, no degradation of the pressure recordings was noticed. If a simple lumped parameter model of the pressure recording system is assumed (Webster, 1978), the most likely effect of the presence of the cathode assembly would be to increase the damping by effectively decreasing the radius of the spinal needle. To first order there would be no effect upon the resonant frequency.

The work described in section 7.5 shows that the calibration of the transducer in 0.15M NaCl can be directly applied to C.S.F., assuming the mock C.S.F. used was a good enough model. The results from mock C.S.F. show that protein poisoning can occur, though at a tolerably slow rate. However, in the animal work performed, and in the clinical trials (Chapter 8) no evidence of protein poisoning of the cathode was observed. The absence of any observed protein poisoning does not mean that it cannot, or indeed did not, occur. Protein poisoning should be considered a potential problem.

The complete investigation of the poisoning problem would require considerable work, which was not considered worthwhile at this stage. However, if the flow transducer is to be used to measure blood flow, then since blood contains typically 200 times as much protein as C.S.F. (Table 7.5.1) more work must be done to overcome the problem.

In conclusion, the gold sphere cathode has been shown to successfully measure the flow of C.S.F. in-vivo. It should be emphasised that the device measures the magnitude of the flow velocity in its immediate vicinity, effectively at a point. The following chapter describes the clinical trials conducted using the flow transducer.

CHAPTER 8

CHAPTER 8THE CLINICAL TRIALS8.1 Introduction

The clinical trials reported here were performed at the Midland Centre for Neurosurgery and Neurology (MCNN), Smethwick, West Midlands, under the direction of Mr. B.N. Williams, Consultant Neurosurgeon. Ethical Committee approval for the trials had been obtained. In all cases the patients were to be subjected to the CSF pressure measurements routinely performed by Mr. Williams. The flow measurements, using the electrochemical flow transducer, were a minimal extension of the procedure. The flow measurements, in this diagnostically unproven state, took second place to the pressure measurements.

The gold sphere cathode (Chapter 7) was used in all cases. A variety of anodes was used. The flow transducer met the criteria set, that is that it should be capable of measuring CSF flow when inserted through a spinal needle, whilst allowing the simultaneous measurement of pressure through the same needle.

The results presented in this chapter are by their very nature initial results. At this stage it is not possible to say (and is beyond the scope of this work) if the flow information obtained using the electrochemical flow transducer is diagnostically useful. The results presented are typical of those obtained in various patients in response to the stimuli used (section 8.3). Simultaneous flow and pressure measurements were performed in 11 patients.

## 8.2 Electronics

The voltage-clamp circuit used in the clinical trials is shown in figure 8.2.1. The voltage-clamp stage (OA1) is based on an LH0042CD junction field-effect operational amplifier. The operational amplifier OA2 allowing a variable back-off  $V_{bo}$  was a 741. The potential  $V_{ac}$  was set using the potentiometer P1 and appeared between the points IH and IL which were connected to the cathode and anode respectively via the interface unit shown in figure 8.2.2.  $V_{ac}$  was monitored using a Keithley model 602 electrometer through the port on the interface unit.

The switches S1 were ganged together so that the feedback resistors of both stages switched together. The output voltage of the voltage-clamp stage  $V_{vc}$  is

$$V_{vc} = -IR_f + V_{ac} \quad (8.2.1)$$

The feedback resistors of the second stage were pre-set to give accurate range calibration (the values of  $R_f$  being nominal). The gain of the second stage, which introduces a second inversion, is then effectively unity and the output voltage  $V_o$  is

$$V_o = IR_f - V_{ac} + V_{bo} \quad (8.2.2)$$

The back-off  $V_{bo}$  was set using S2, P2 and P3.  $V_{ac}$  was backed-off exactly by setting S4 (figure 8.2.2) to o/c, S5 to one of the meter positions and setting S2, P2 and P3 so that the meter read zero, when  $V_{bo}$  exactly cancelled  $V_{ac}$ . When the flow transducer was being used S5 was set to o/c. Automatic back-off of  $V_{ac}$  could have been achieved by



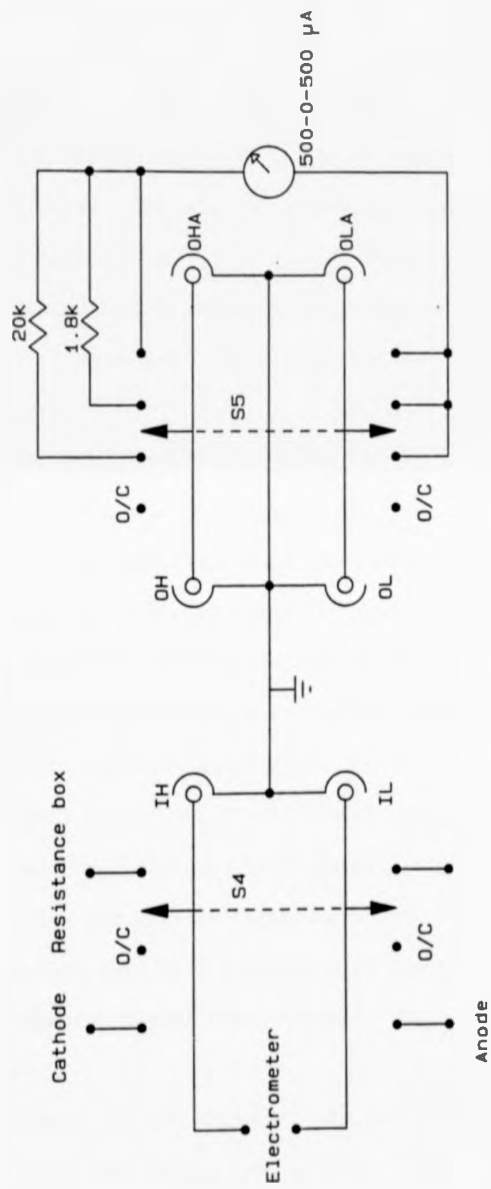


Figure 8.2.2 The interface unit.

connecting P1 to the non-inverting input of OA2, but the greater flexibility allowed by this circuit was preferred.

The switches S3 were ganged together and allowed the optional 50Hz notch filter to be switched in. The interface unit (figure 8.2.2) was used to facilitate connection to the Devices M19 multi-channel chart recorder used clinically to record the data. It also allowed accurate back-off of  $V_{ac}$  as described above, and calibration of the flow measuring system by switching S4 to the decade resistance box. The outputs OHA and OHB fed the signal to the chart recorder.

The earth shown in figures 8.2.1 and 8.2.2 is the metal of the containing boxes. The 0 volt line (the anode) is not connected to the earth, except at the connection into the chart recorder. All electrical interconnections were made using BNC plugs and co-axial cable, the screen of which was connected to the metal boxes. For the clinical work the  $\pm 15$  volt supply was obtained from four PP9 batteries via a  $\pm 15$  volt voltage regulator.

Connections to the flow transducer electrodes were made via 2.5 metres of 6-way, screened cable, 3 wires being used for each electrode. The screening and plastic sheathing of the last metre had been removed, and each pair of 3 wires plaited together. This gave light, flexible and convenient connections to the flow transducer electrodes.

The frequency response of the voltage-clamp circuit (figure 8.2.1), including the flexible electrode cables, was, with  $R_f = 1M\Omega$ , perfectly flat to 1kHz with no phase shift. Even though the flow transducer electrodes are of quite high impedance, cable capacitance is of no importance because the input to the voltage-clamp is a virtual earth.

The noise current of the voltage-clamp was of the order of tens of pico-amps, orders of magnitude less than the micro-amps measured clinically.

Patient safety was the responsibility of the Medical Physics Department staff at MCNN and the equipment used was cleared by them. As the equipment was battery powered the electrical safety problems were reduced but the following precautions were taken to limit the current that could flow through the patient in the event of a fault.

The voltage-clamp was powered by a total of 36 volts of batteries. The inclusion of the  $2.2\text{M}\Omega$  resistor (figure 8.2.1) at the inverting input to OA1 and the smallest value of  $R_f$  being  $1\text{M}\Omega$  ensured that the maximum current that could flow through the patient, in the event of a fault in OA1 and the voltage regulator, was 36 micro-amps. The Keighley electrometer was powered by batteries with a total of 55 volts. A  $10\text{M}\Omega$  resistor was placed in series with its connection to the cathode line so that no more than 5.5 micro-amps could flow in the event of a fault. This  $10\text{M}\Omega$  resistor and the  $2.2\text{M}\Omega$  resistor and the resistors  $R_f$  in figure 8.2.1, and their connections to the cathode lead, were encased in epoxy resin potting compound.

### 8.3 Methods and Procedures

The flow measurements were always performed as an adjunct to the pressure measurements. The pressure measurement techniques used have been well described by Williams (for example, Williams, 1981a) and will be only briefly described here. During the procedure the

patients were conscious and sitting upright.

Access to the CSF pathways was gained at two of three possible sites; lumbar, cisternal and ventricular. Access to the first two was by 18 gauge spinal needles typically 9cm long, and to the ventricles by a catheter inserted through a hole drilled in the forehead. Entry to the lumbar and cisternal pathways is illustrated in figures 2.2.1 and 2.2.2 respectively.

Figure 8.3.1 illustrates the pressure measurements, showing all three points of entry and the level against which the pressures were referred. When investigating the response to the stimuli he uses such as coughs, Williams is not particularly concerned with absolute pressures, rather he is concerned with the magnitudes of changes in CSF pressure which occur in response to the stimuli, and their time variations. Therefore, the pressure transducers are zeroed such that the vertical height differences between the points of entry and the reference level are removed from the pressures measured. Using this method, for example, the recorded baseline pressures in the normal case, at different points of entry to the CSF pathways, are equal apart from temporary differences in pressure caused by pulsation.

In these measurements the points of entry to the CSF pathways used were usually lumbar and cisternal, and sometimes lumbar and ventricular. The pressure measurements were made with Ailtech model MSD10-E miniature pressure transducer coupled directly to the spinal needle or to the flow transducer assembly (figure 7.3.1). CSF pressure (and flow) measurements were recorded in response to the following stimuli : a cough or a series of coughs; cardiac pulsation; blowing against a resistance (equivalent to a Valsalva manoeuvre); and Queckenstedt's test (bilateral jugular compression). In addition an

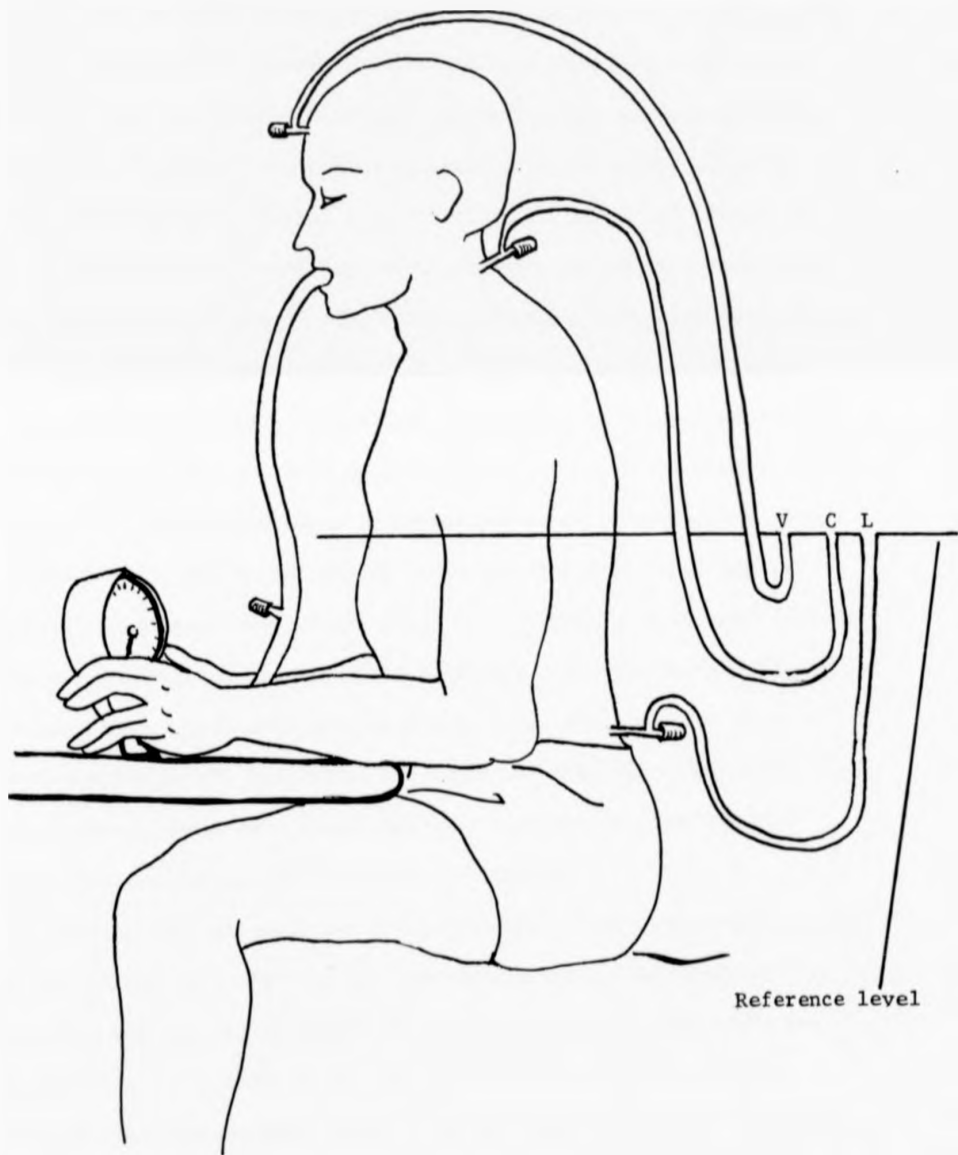


Figure 8.3.1 Schematic illustration of the pressure measurements.

V - ventricular pressure; C - cisternal pressure;  
L - lumbar pressure

ECG was usually recorded but no arterial or venous pressures were measured.

The flow transducers were always gold sphere cathodes (section 7.2.3) and the flow transducer assembly was as shown in figure 7.3.1, with or without the reservoir depending upon what type of anode was used. The gold cathodes used had diameters in the range 0.50 to 0.71 mm and  $\theta_c$  (the angle from the stagnation point at which the epoxy resin glue began - equation 3.9.6) varied between 11 and 44 degrees.

Three types of anode were used : Ag/AgCl button type electrodes in the reservoir shown in figure 7.3.1; Ag/AgCl skin electrodes taped to a suitably prepared region of skin; and a slightly curved plate electrode approximately 45mm x 55mm of the type commonly used to record ECGs. This was held onto the upper arm using a rubber strap. The plate electrode was made of German Silver (a nickel-silver alloy, Webster, 1978) and in laboratory tests was very similar to Ag/AgCl anodes except that the optimum value of  $V_{ac}$  (when using a gold cathode) was 0.1 volts lower for the plate electrode. The use of skin electrodes as the anode, especially the plate electrode, was found far more convenient than the reservoir, and therefore skin electrodes were mainly used. When skin electrodes were used the skin was scraped with a wooden spatula and electrode gel applied.

The cathode assembly was always pre-positioned with respect to the spinal needle such that the gold sphere protruded approximately 2 to 3mm from the tip of the needle when inserted. This positioning was done before the spinal needle was inserted into the CSF pathways. When the flow measurements were to be performed the cathode assembly was inserted into the CSF pathways through the spinal needle.

Before the cathode and anode were switched in circuit the value of  $V_{ac}$  for the electrode pair being used was set (1.0 volt for the Ag/AgCl anode and 0.9 volt for the German Silver anode) and exactly backed off as described in section 8.2.  $V_{ac}$  was then set to zero and the electrodes switched in circuit, and  $V_{ac}$  gradually increased to the pre-set value. This procedure avoided any current spike caused by suddenly switching on in an oxygen rich environment.

During the measurements procedure at least one sample of CSF was taken for analysis in a glass syringe which was capped as quickly as possible to prevent any influx of oxygen.

All the measurements made were recorded continuously on the Devices M19 6 channel chart recorder, the signal from the flow transducer voltage-clamp being fed to a Devices 3461 DC amplifier with variable low pass filtering. This was almost always set to have a 3dB point of 30Hz and was the only filtering of the flow signal that was used.

#### 8.4 Results

##### 8.4.1 General considerations

As measurements have only been performed in a limited number of patients the results obtained can only be considered as initial. It is therefore not sensible to, as yet, attempt to correlate the flow results with disease process or anatomical abnormalities, even though all the patients investigated had some abnormality of the CSF pathways. Rather, the results shown are intended to show that the measurement of the flow of CSF is feasible, whilst still allowing the simultaneous measurement of pressure through the same needle. Therefore,

results typical of the range of measurements made are presented.

It is dangerous to generalise from such early results, especially in such a complex hydrodynamic system. However, the following general comments are, tentatively, made.

Either end of the CSF pathways, that is the lumbar sac and the ventricles, can be thought of as dead ends. Therefore little flow would be expected in response to the pressure stimuli. It is also likely that at these sites, especially the lumbar sac, that there would be as much radial as axial flow, as the changes in the local volume of CSF occurring are accommodated by the elasticity of the pathways. In the first 3 trials the flow transducer was only placed in the lumbar pathways. The flows recorded were both small and featureless compared to those obtained cisternally. On one occasion the flow transducer was placed in the ventricles and again the measured flow in response to the various stimuli used was very small, although this could have been caused by a large (suspected) blockage of the CSF pathways.

The cisternal pathways are most likely to give rise to the largest flows (of the sites available for measurement) and this flow would be expected to be primarily up/down as CSF moves between the spinal and intracranial CSF spaces. Most of the flow measurements made, and all those presented here, were made cisternally, and as expected were usually of larger magnitude than those made in the lumbar CSF pathways.

In general a flow of CSF would be expected when the lumbar pressure minus the cisternal pressure (L-C) is greater than, or less than, zero; or, if there is a standing pressure difference, when it changes.

This is probably so for the large pressure stimuli such as coughs. However, local flow will depend on local pressure differences, but the lumbar and cisternal sites of pressure measurement are some distance apart. That is, a flow could still be expected when there is no change, or only a small change, in the L-C trace. Also, because of the distance between the pressure measurement sites, events on the flow and the L-C traces would not necessarily be synchronous.

In the initial trials the probe was calibrated in physiological saline at 37°C immediately after removal from the CSF pathways. No difference was found between this calibration and that before sterilisation in ethylene oxide. As this immediate calibration was extremely inconvenient in the limited space and time available, and as no change was found in the first three trials, this practice was stopped. Instead, a laboratory calibration was performed the next day, when again no difference in calibration was found.

These results show that ethylene oxide, and subsequent storage of the sterilised flow transducer, have no effect on the velocity response. Also, they show that no poisoning of the cathode by protein occurred, or rather was detected. The cathodes were typically in the CSF pathways for approximately 30 minutes, and so no significant protein poisoning occurred on this time scale, even though the CSF was sometimes noticeably bloody. After each use, and subsequent re-calibration the gold cathodes were cleaned in acid and so no cumulative poisoning effect could have been observed.

#### 8.4.2 Typical responses to the stimuli

Typical flow responses to the pressure pulsations used are presented here. Figures 8.4.1 to 8.4.5 show the flow signal in response

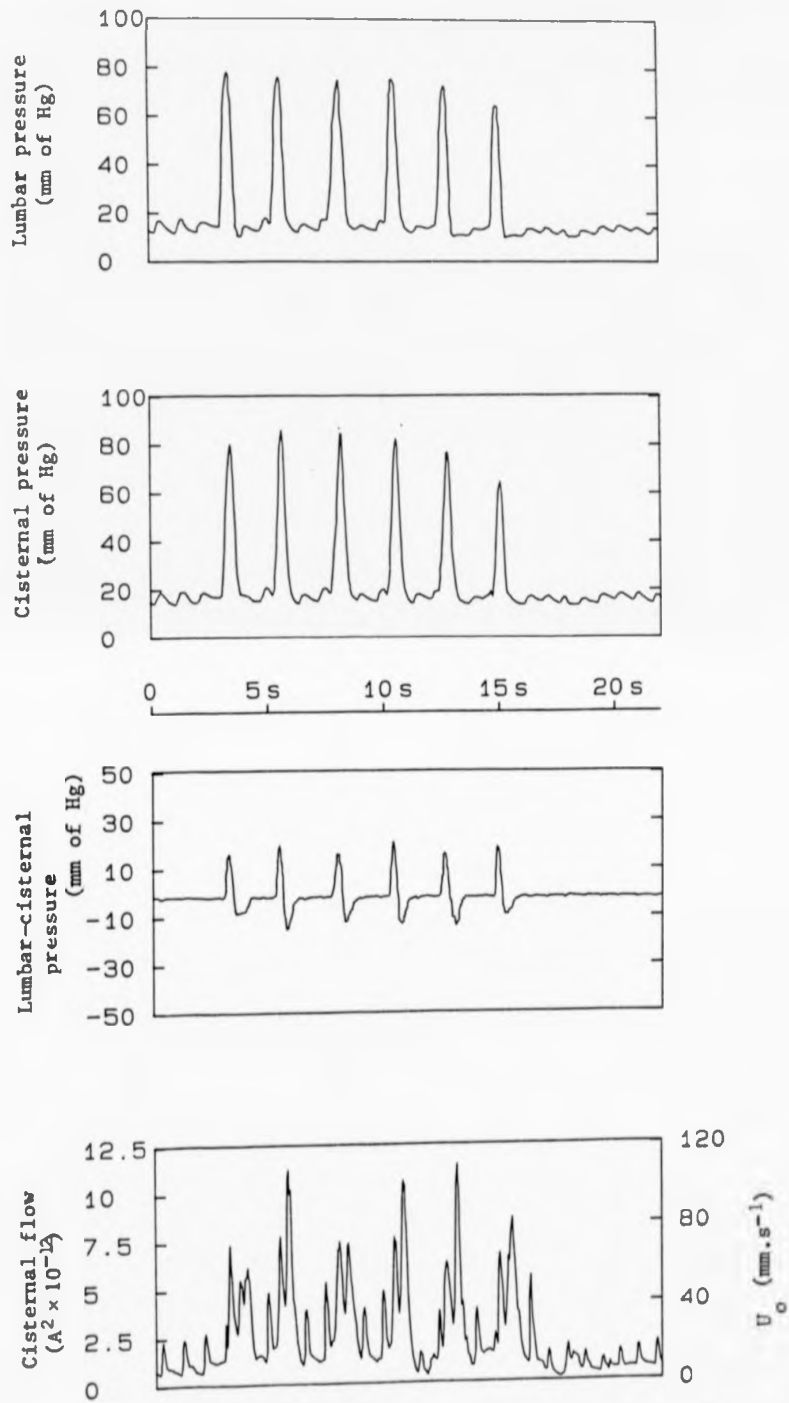
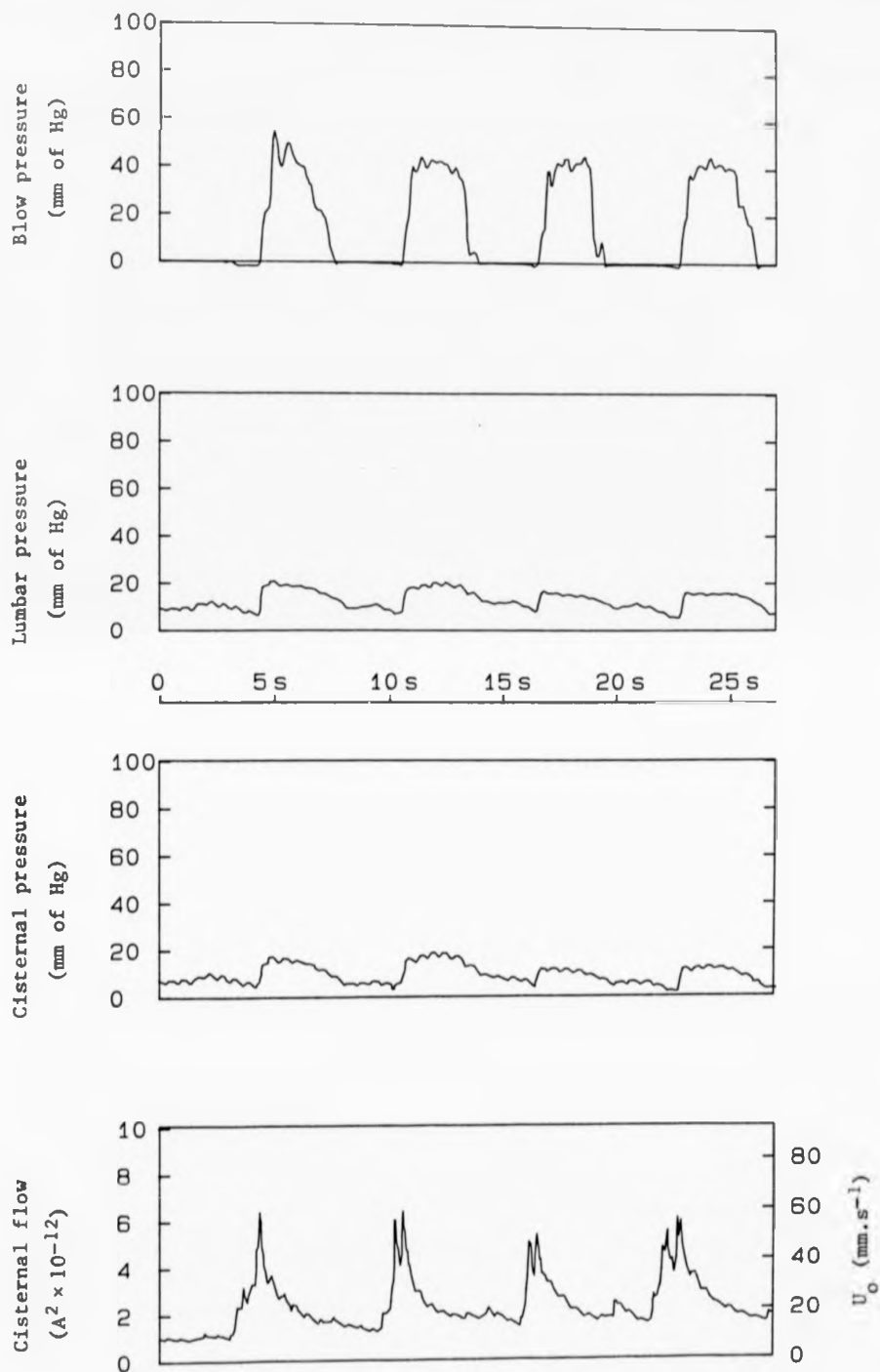
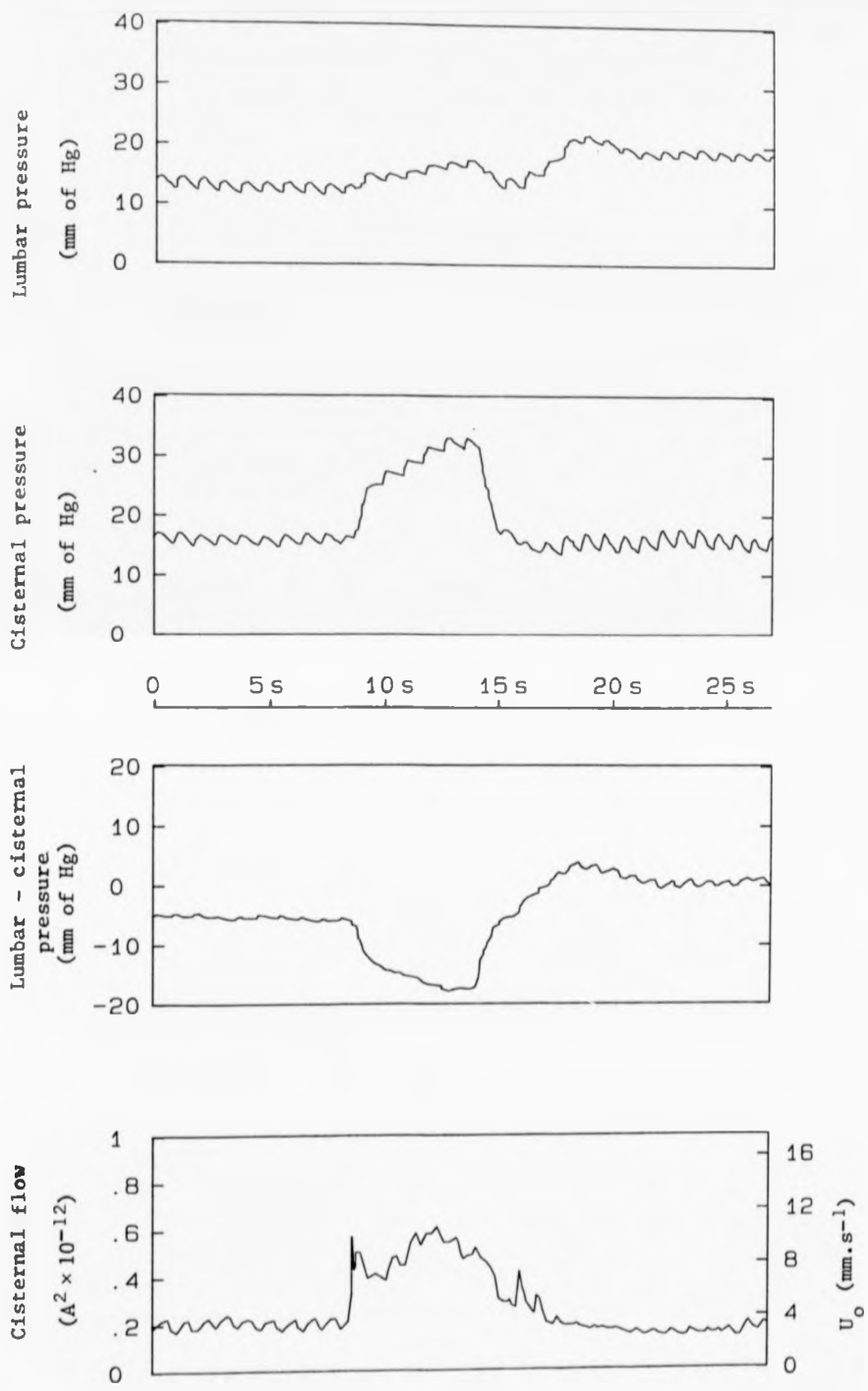


Figure 8.4.1 The response to a series of coughs.  $pO_2 = 40\text{mm of Hg}$ .  
Cathode dimensions:  $R = 3.1 \times 10^{-4}\text{m}$ ;  $b = 1.4 \times 10^{-4}\text{m}$ .



**Figure 8.4.2** The response to a series of blows.  $pO_2 = 49$  mm of Hg.  
 Cathode dimensions:  $R = 3.1 \times 10^{-4}$  m;  $b = 1.4 \times 10^{-4}$  m.



**Figure 8.4.3** The response to Queckenstedt's test.  $pO_2 = 52$  mm of Hg.  
 Cathode dimensions:  $R = 2.5 \times 10^{-4}$  m;  $b = 0.5 \times 10^{-4}$  m.

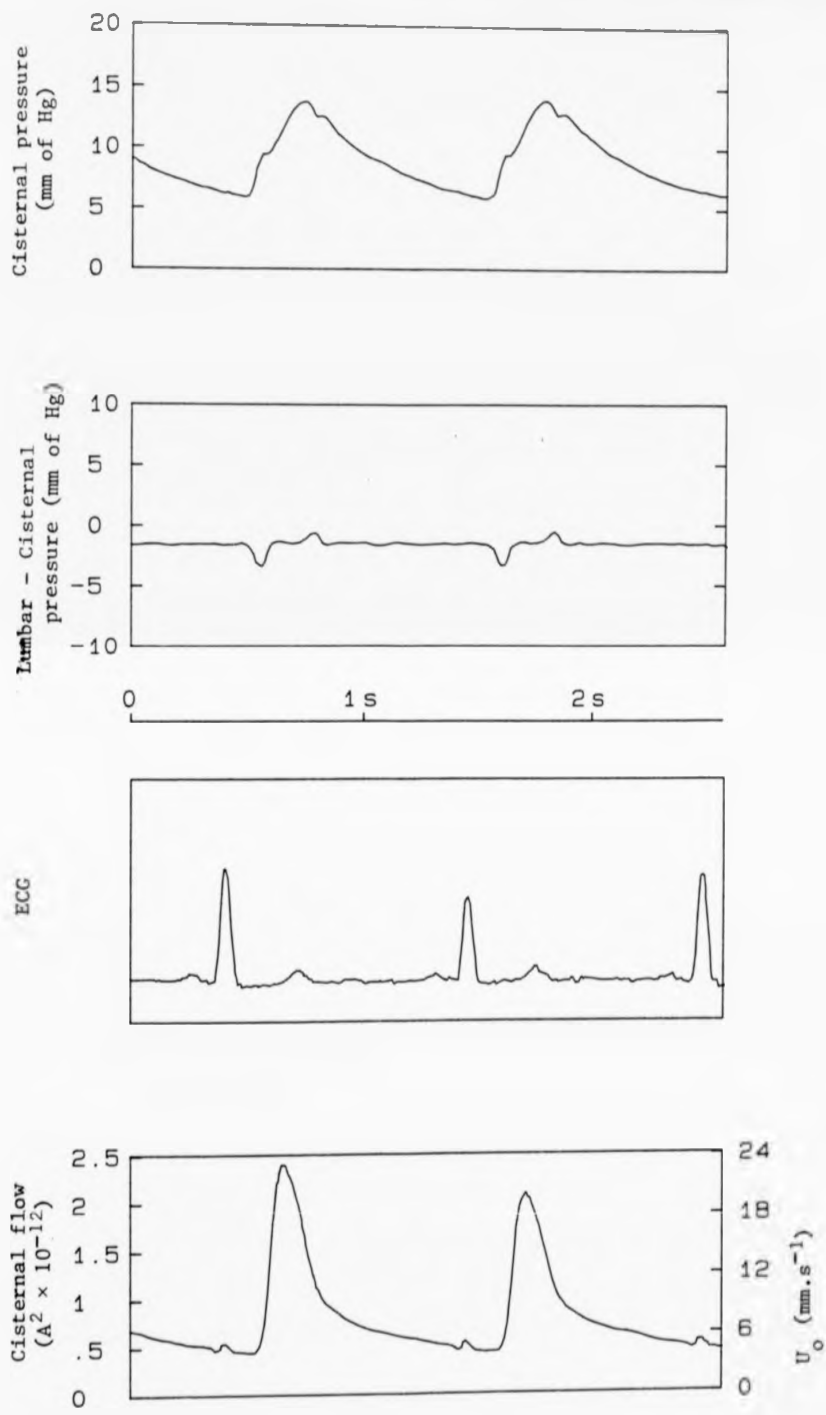
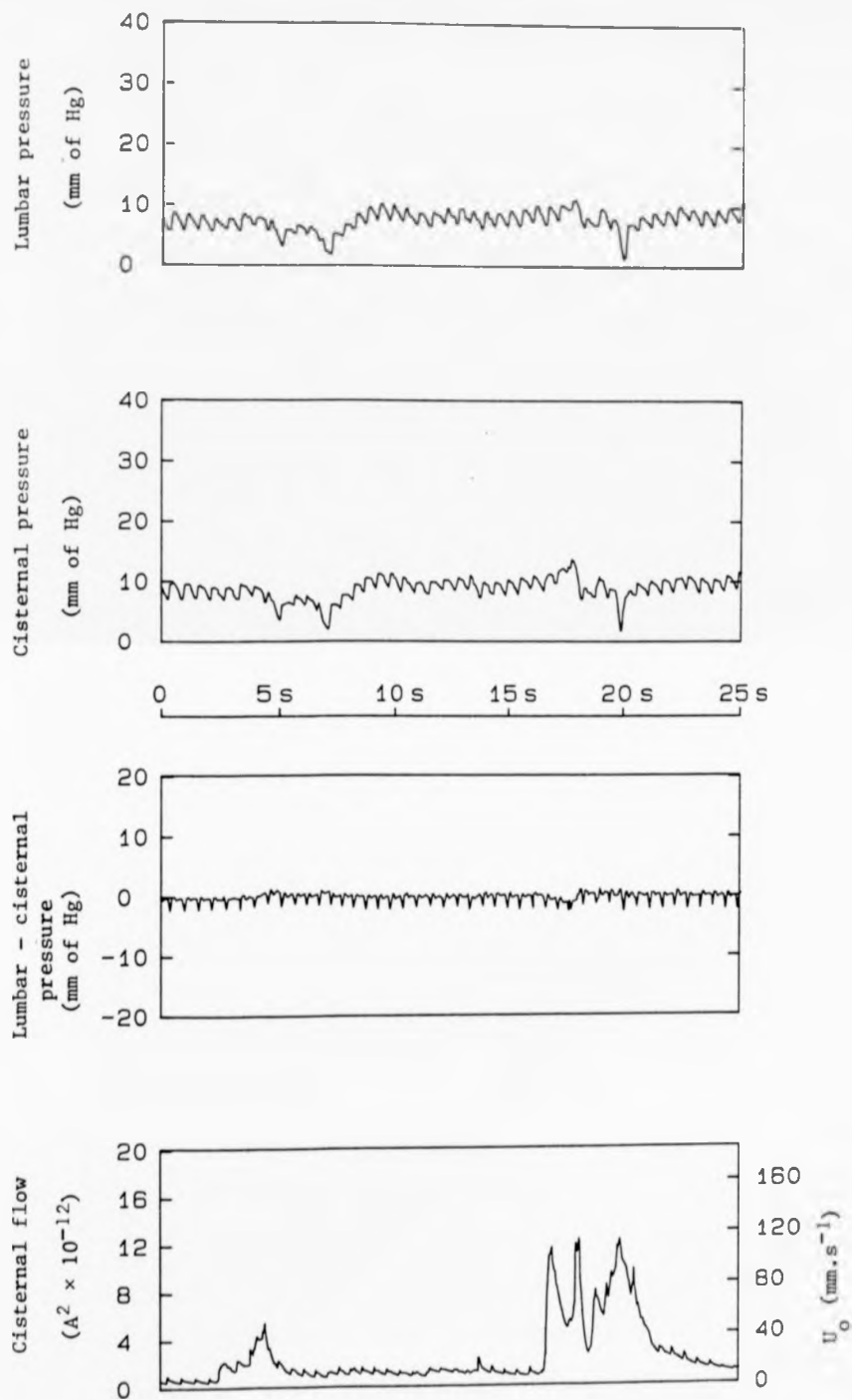


Figure 8.4.4 The response to cardiac pulsation.  $pO_2 = 40\text{mm}$  of Hg.  
 Cathode dimensions:  $R = 3.1 \times 10^{-4}\text{m}$ ;  $b = 1.4 \times 10^{-4}\text{m}$ .



**Figure 8.4.5** The response to movements of the patient's right arm, to which the anode was strapped.  $pO_2 = 49$  mm of Hg. Cathode dimensions:  $R = 3.1 \times 10^{-4}$  m;  $b = 1.4 \times 10^{-4}$  m.

to : a series of coughs; a series of blows; Queckenstedt's test; cardiac pulsation; and movement of the patient. For all the results presented the flow transducer was in the cisternal pathways, the cisternal pressure being measured through the same needle.

All the figures show  $I^2$ , and various pressure traces, and in the case of figure 8.4.4 the ECG. The original results were digitised (as for the animal experiments - Chapter 7) and the output of the voltage-clamp squared using a computer. The results were then replotted with the  $I^2$  trace which is proportional to flow velocity, thus allowing easier interpretation of the results. The velocity scale shown was obtained by adjusting the velocity calibration of the particular flow transducer to the measured  $pO_2$ .

All the results shown were obtained with a German Silver plate strapped to the upper right arm as anode, except for figure 8.4.4 where the plate was strapped to the lower right leg.

The response to a series of coughs is shown in figure 8.4.1. As in this patient, coughs generally produce the largest pressures and flows. The flow trace is double peaked, as would be expected with flow first into, and then out of, the head and so the flow trace correlates with the L-C trace. During the cough the cardiac flow is augmented and interspersed with the flow peaks due to the cough. These results are from the same patient as those shown in figure 8.4.4 (cardiac pulsation). This patient had a higher than average cardiac flow, as can be seen by comparison of figures 8.4.1 and 8.4.4 with figures 8.4.2 and 8.4.3.

A typical response to a series of blows is shown in figure 8.4.2. The flow trace shows flow before the blow, which was caused by the patient breathing in before blowing. A double peak exists

at the beginning of the blow. This can be explained by the flows caused by breathing in and by blowing being in opposite directions; that due to breathing in (when the pressure in the abdominal and thoracic cavities falls) being away from the head, and vice versa. When the pressure traces are constant the flow decreases but no large flow signal exists when the blow ceases. The L-C trace was essentially constant during this series of blows. In general blows caused the second largest flows.

Figure 8.4.3 shows a typical response to a Queckenstedt's test. As here, the flow caused by a Queckenstedt's test was usually small. The flow correlates well with the L-C trace, which is offset at the end suggesting not all the CSF displaced from the head was able to return. Interestingly the magnitude of the cardiac flow is diminished after the Queckenstedt's test.

Figure 8.4.4 shows the cardiac pulsation flow trace in the same patient as the series of coughs. Here, however, the plate anode was on the right leg rather than the right arm. The main flow signal, whilst synchronous with the cisternal pressure peak is not synchronous with the events in the L-C trace. Just before each flow peak there is a small disturbance of the otherwise smooth time response of the flow transducer current. This is synchronous with the R-wave of the ECG and is believed to be caused by ECG pick up. This point is discussed in detail in section 8.5.1. The cardiac pulsation flow seen was not usually so large. In this patient the magnitude of the pulsation varied with head position.

Figure 8.4.5 shows traces obtained, in the same patient as figure 8.4.2, when movements of the patient's right arm (to which the plate anode was strapped) occurred. Whilst the movements do cause

pressure changes the flow signal obtained, especially for the second event, is unreasonably large. A naive comparison with figure 8.4.2 shows that there the pressure changes caused by the blows are approximately twice as great, whilst the flow caused is approximately half the magnitude. The flow signal during the movements could conceivably represent a true flow, but it is most likely that the signal obtained is a mixture of flow and motion artefact at the anode. This is discussed in greater detail in section 8.5.3.

All the results shown were obtained with the plate skin anode. An Ag/AgCl anode in a reservoir was used in the early trials and no difference between it and skin anodes was seen except that no motion artefact was observed. Skin electrodes, especially the plate, were preferred during the trials because they were found far more convenient to use.

## 8.5 Sources of Artefact

### 8.5.1 ECG pick up

The artefact in figure 8.4.4 synchronous with the ECG R-wave is believed to be caused by the time varying electrical potentials in the body caused by the electrical activity of the heart. In the same way that the potential difference between two points on the surface of the body (for example the right arm and the left arm) changes during the cardiac cycle, the potential difference between the two points at which the anode and cathode are, will change by some amount  $v_e$ . Since the voltage-clamp maintains the potential between the anode and cathode at  $V_{ac}$ , this means that the potential of either the anode or cathode (or both) will change with respect to the electrolyte

surrounding it. That is, the overpotential  $V_a$  at the anode (section 3.2.1) or  $V_c$  at the cathode (or both) will change by a total of  $v_e$ .

The anode is on the steeply rising part of the  $I-V_a$  curve (section 4.3.3) and so any change in  $V_a$  must be accompanied by a large change in  $I$ . However, the current is limited by the rate of transport of oxygen to the cathode, and so no change in  $I$  can occur unless there is another, extra, source of current. The cathode is on the plateau of the  $I-V_c$  curve and a large change in  $V_c$  can be accommodated with no change in current. It is therefore proposed that the external potential  $v_e$  only perturbs the overpotential at the cathode  $V_c$ , and that the artefact seen is caused by this perturbation of  $V_c$ . That is

$$V_{ac} = V_a + V_c' + v_e \quad (8.5.1)$$

where

$$V_c' = V_c - v_e \quad (8.5.2)$$

This was investigated using the arrangement shown in figure 8.5.1. In principle it should have been arranged that  $v_e$  was somehow actually generated in the saline bath, but this was considered unnecessary since the anode can be neglected compared to the cathode. This is so, both because of the arguments above, and because experimentally and in the equivalent circuit the anode was found to behave as a small resistance.

The cathode was a gold sphere 0.63mm in diameter and the anode a pair of Ag/AgCl electrodes in parallel. The temperature of the saline bath was 17°C and the method described in section 4.3.1 was

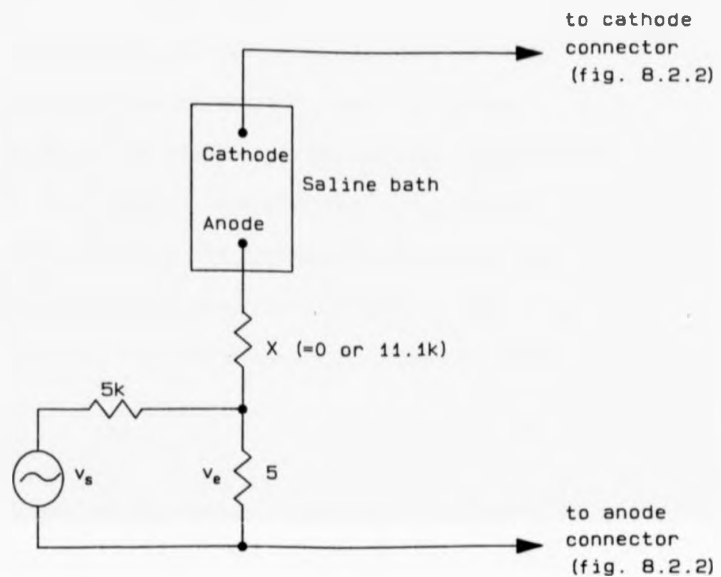
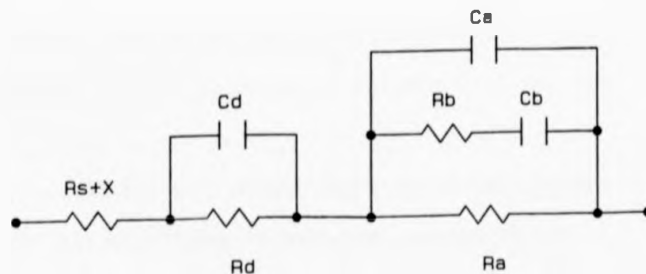


Figure 8.5.1 The simulation of ECG pick-up.



Values used for the theoretical curves of figs 8.5.3 and 8.5.4  
 $R_d=800k$     $C_d=0.43\mu$   
 $R_a=25k$     $C_a=0.22\mu$   
 $R_b=1k$     $C_b=0.36\mu$   
 $R_s=500$

Figure 8.5.2 The proposed equivalent circuit of the cathode to perturbations of  $V_c$ .

employed to reduce the free convection past the cathode.  $V_{ac}$  was 0.9V and  $v_e$  30mV peak to peak, so ensuring that the electrodes always remained on the plateau of the  $I-V_{ac}$  and  $I-V_c$  curves.

Appendix C1 analyses the response of the voltage-clamp circuit to this situation. The response of the voltage-clamp to the perturbation  $v_e$  is  $v_o$ , and  $Z$  is the impedance of the anode and cathode (primarily the cathode) when on the plateau of the  $I-V_{ac}$  curve. The result of the analysis is given in terms of  $H$  where

$$H = v_o / (v_e R_f) = 1/Z \quad (8.5.3)$$

If  $Z$  is a complex impedance then  $H$  will be a function of frequency. The artefact of figure 8.4.4 strongly suggests that the ECG pick up is frequency dependent since only the higher frequency components of the ECG (the QRS complex) produce a noticeable effect.

An attempt was made to model the equivalent circuit of the flow transducer electrodes and the circuit is shown in figure 8.5.2. The model was obtained as follows : a dc path must exist since a direct current flows. The resistance of the dc path can to some extent be identified with  $I/V_{ac}$ , though on the plateau  $I$  is independent of  $V_{ac}$ .

Oxygen can be said to carry pseudo-charge since the passage of oxygen across the diffusion layer is necessary for the charge exchange process at the cathode to occur.  $R_d$  is identified with the resistance the diffusion layer presents to the passage of oxygen, and  $C_d$  with the separation of pseudo-charge across the diffusion layer.

The reduction of oxygen at the cathode (section 3.2) is a multistep process and occurs very close to the surface.  $R_a$ ,  $R_b$  and

$C_b$  are identified with the electrochemical processes involved at the electrode/electrolyte interface (Bockris and Reddy, 1970; Eyring, Henderson and Jost, 1970) and  $C_a$  with the effective capacitance of the intermediaries in the reaction.

In general, there should also be a parallel resistor and capacitor to represent the saline between the anode and cathode, and a parallel resistor and capacitor to represent the anode. However, when a similar experiment was performed with the gold cathode replaced by a Ag/AgCl electrode the impedance was found to be purely resistive and, compared to when the gold cathode was used, of negligible magnitude. Therefore,  $R_s$  represents the resistance of the anode, the saline, and any other unidentified series resistance in the equivalent circuit. The equivalent circuit for the flow transducer electrodes is thus primarily that for the cathode. Also, all components of the equivalent circuit, especially  $R_d$  and  $C_d$ , are likely to be functions of the flow past the cathode, though this was not investigated. The full equation of the equivalent circuit is given in appendix C2.

Figure 8.5.3 compares the measured and computed variations of  $|H|$  and the phase lead of  $v_o$  over  $v_e$  for  $X=0$  (the series resistor shown in figure 8.5.1). Figure 8.5.4 shows the same variations for  $X=11.11k\Omega$ , which was intended to simulate a large skin resistance. In the region of interest for physiological measurement the two figures are very similar. The computed variations were obtained with the equations of appendix C2 and the component values shown in figure 8.5.2. At frequencies below 1Hz the frequency and magnitude of  $v_o$  was such that it was extremely difficult to separate from the changes in the output of the voltage-clamp caused by the random

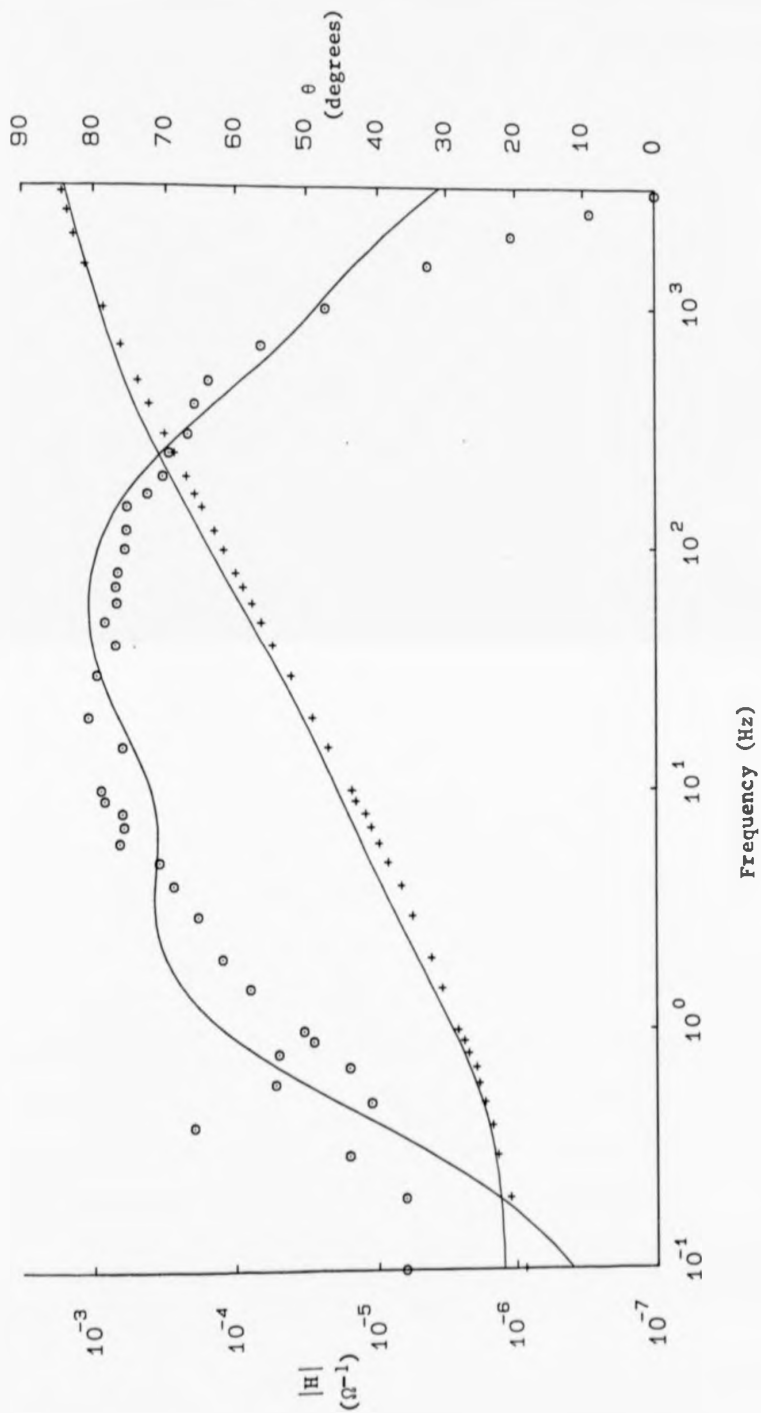
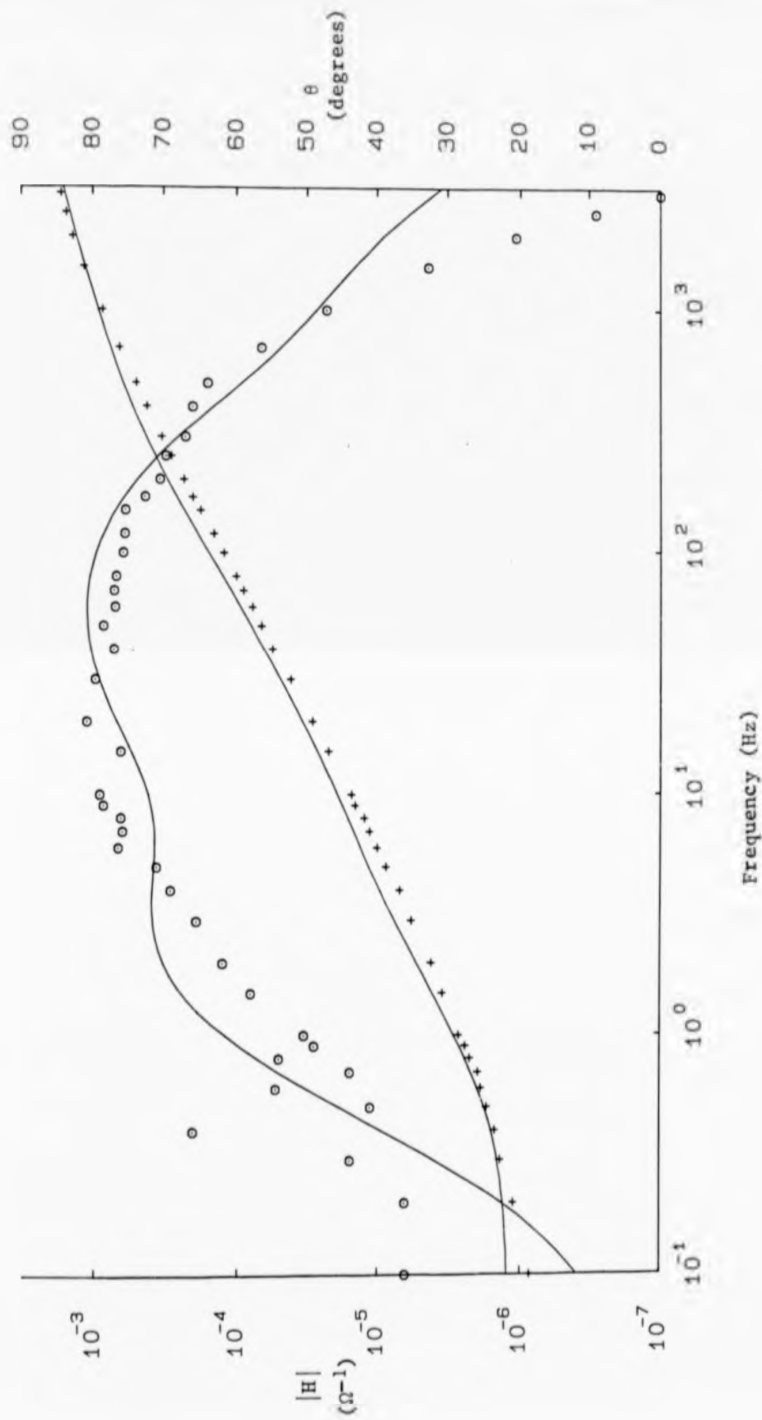
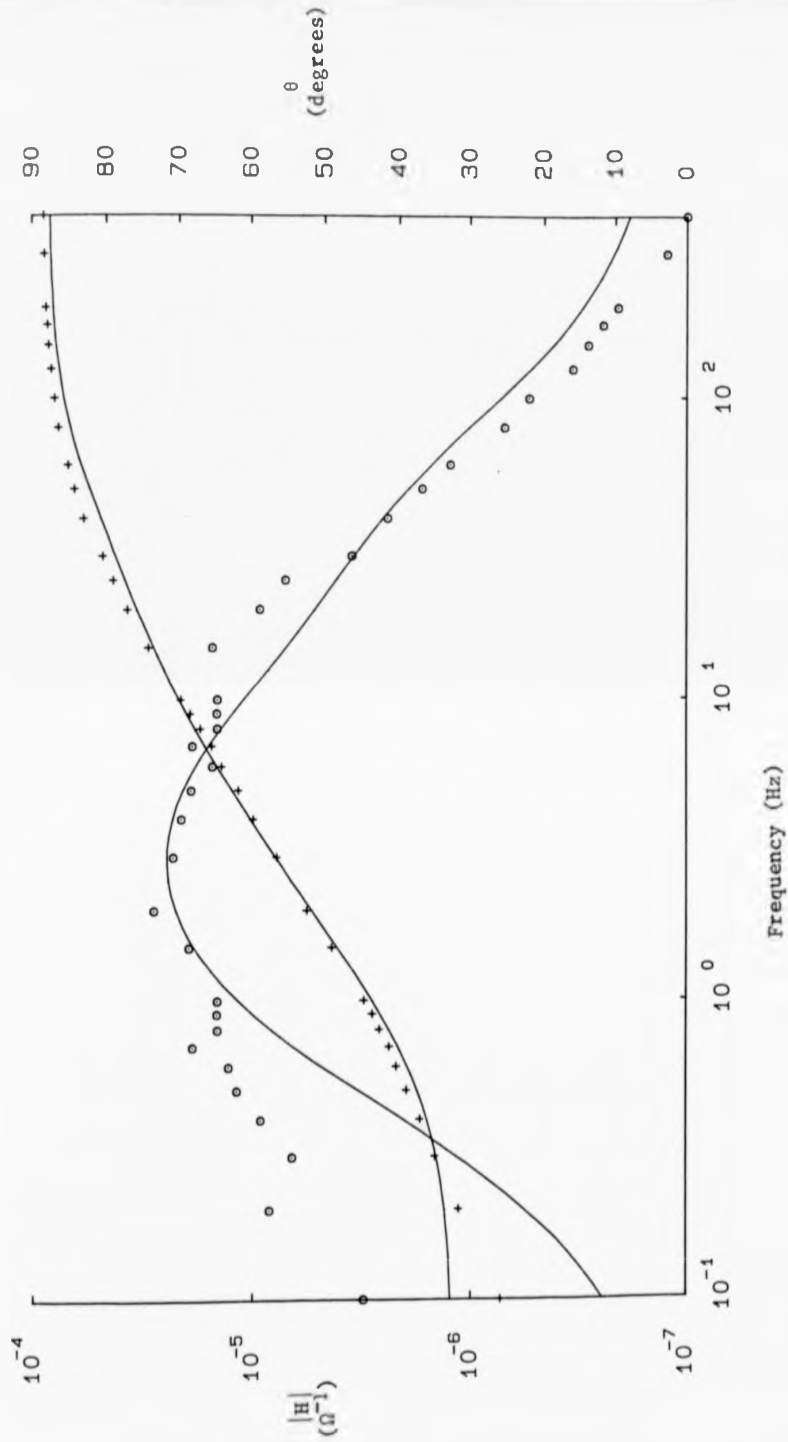


Figure 8.5.3 The results of the simulation of ECG pick-up with  $X=0\Omega$  (figure 8.5.1). The solid lines were computed using the circuit and values of figure 8.5.2.  $\times |H|$ ;  $\circ \theta$ , the phase lead of  $v_o$  over  $v_e$ .



**Figure 8.5.3** The results of the simulation of ECG pick-up with  $X=0\Omega$  (figure 8.5.1). The solid lines were computed using the circuit and values of figure 8.5.2.  $\times |H|$ ;  $\circ \theta$ , the phase lead of  $v_o$  over  $v_e$ .



**Figure 8.5.4** The results of the simulation of ECG pick-up with  $X = 11.1k\Omega$  (figure 8.5.1). The solid lines were computed using the circuit and values of figure 8.5.2.  $+ |H|$ ;  $o \theta$ , the phase lead of  $v_o$  over  $v_e$ .

changes in the free convection past the cathode. Given the complexity of the system being modelled, and the simplicity of the model the computed curves are a good fit to the experimental points.

The results of figures 8.5.3 and 8.5.4 show the response of  $v_o$  to  $v_e$  to be a function of frequency,  $v_o$  increasing in magnitude rapidly with frequency. This explains the observations made in the clinical trials, where only the fastest components of the ECG produced observable artefact.

Figure 8.4.4 was recorded with the anode strapped to the right leg so as to maximise the distance between anode and cathode and therefore, hopefully,  $v_e$ .  $R_f$  was  $1M\Omega$  and the peak to peak value of  $v_o$  equivalent to the artefact of figure 8.4.4 is approximately 75mV. At, say 20Hz,  $|H|$  is approximately  $2.5 \times 10^{-5}$  mhos, giving a value of  $v_e$  of approximately 3mV. This is typical of the peak to peak height of the QRS complex.

In conclusion, the explanation of the ECG pick up presented here can be summarised as follows : the electrical activity of the heart causes a time varying potential difference in the electrolyte between the flow transducer electrodes  $v_e$ ; this causes a change in the overpotential  $V_c$  at the cathode of  $v_e$ ; it is this change in  $V_c$  which causes the frequency dependent artefact  $v_o$  in the output of the voltage-clamp.

It should be possible to remove, or at least minimise, the ECG pick up by placing the anode as close to the cathode as possible, preferably in the CSF. This would have other advantages which are discussed below.

### 8.5.2 The effects of skin impedance

Two basic types of anode were considered (Chapter 7); an anode in a reservoir with a direct fluid connection to the cathode, and an anode on the skin. In the clinical trials the anode on the skin was preferred for its greater convenience.

The importance of the magnitude of skin impedance was realised. If the impedance was too great then the volts lost across the skin impedance, when an increased current caused by CSF flow passed, would cause the electrodes to fall off the plateau of the  $I-V_{ac}$  curve. The plateau of the  $I-V_{ac}$  curve is typically 0.3V wide, and the maximum current that could reasonably be expected is  $10\mu A$ . A value for the skin impedance of less than  $30k\Omega$  was therefore necessary, and preferably less than  $10k\Omega$ .

The wrist to wrist impedance was measured in 5 patients using 1.5V dc. The electrodes used were German Silver plates (usually used as anode) and the skin was prepared as normal. The resistances were found to be stable after approximately ten minutes. The resistances were measured with both polarities, and averaged. The mean resistance in the 5 patients was  $5.0 \pm 2.4 k\Omega$ . The resistance of the skin could therefore be expected to be of the order of  $2.5k\Omega$  (neglecting the internal resistance of the body) in most patients. An anode on the skin was therefore thought perfectly satisfactory.

However, the model for the ECG pick up (section 8.5.1) can be applied to this situation.

If the impedance of the skin (and, in principle, the impedance of the body tissue between the anode and cathode) is represented by  $Z$ , then

$$V_{ac} = V_a + V_c + IZ \quad (8.5.4)$$

If the flow of CSF changes, then  $I$  will change by  $\Delta I$  and

$$V_{ac} = V_a + V_c' + (I+\Delta I).Z \quad (8.5.5)$$

that is

$$V_c' = V_c - \Delta I.Z \quad (8.5.6)$$

If  $\Delta I.Z$  is identified with the perturbation potential  $v_e$ , then the situation here is exactly analogous to that in section 8.5.1. That is, the change in the current passing through the impedance between the electrodes causes a perturbation  $v_e$  in the overpotential  $V_c$  at the cathode and an artefactual signal  $v_o$  is present in the output of the voltage-clamp. The case in figure 8.5.1, when  $X = 11k\Omega$ , was an attempt to model a high series skin impedance and the results are presented in figure 8.5.4.

The above argument states, that for anodes on the skin, part of the signal recorded will be the artefact  $v_o$ . The amount of artefact will be a function of the frequency of the changes in flow and of the magnitude of the skin impedance.

In figure 8.4.2 the current changes from  $\sim 1\mu A$  to  $\sim 2.5\mu A$  at each blow, so  $\Delta I$  is  $1.5\mu A$ . If the skin impedance is assumed to be  $2.5k\Omega$ , and the dominant frequency of change  $10\text{Hz}$ , then  $v_o$  can be estimated. From figure 8.5.3, at  $10\text{Hz}$   $|H| \sim 1.5 \times 10^{-5} \Omega^{-1}$  and with  $R_f = 1M\Omega$   $v_o \sim 50\text{mV}$ . At  $R_f = 1M\Omega$   $50\text{mV}$  is equivalent to  $.05\mu A$  and in this case represents approximately 2% of the peak current measured.

This is an acceptable level of error, but  $v_o$  is proportional to the magnitude of the skin impedance, and it is very possible that the error could be large without it being realised. It is far better to remove the source of error and this can easily be done by placing the anode in the CSF, as with the reservoir.

The extreme case of this argument is that the change in  $V_a$  when  $I$  changes will also produce a perturbation  $v_e$  in  $V_c$ . However, with a correctly functioning anode, that is it is on the steeply rising part of the  $I-V_a$  curve, this must be negligible.

### 8.5.3 Motion artefact

The response of the flow trace in figure 8.4.5 must, at least in part, be due to artefacts at the anode/skin interface caused by motion of the arm. The model developed in section 8.5.1 can, again, be applied here to explain the motion artefact. Since the impedance of the skin is not negligible  $V_{ac}$  is given by equation 8.5.4. If the movement of the arm causes a change  $\Delta Z$  in this impedance, then

$$V_{ac} = V_a + V_c' + (Z + \Delta Z) \cdot I \quad (8.5.7)$$

where

$$V_c' = V_c - I \cdot \Delta Z \quad (8.5.8)$$

If  $I \Delta Z$  is identified with  $v_e$  then the situation is analogous to that in section 8.5.1. An upper limit for the change in impedance  $\Delta Z$ , which occurred in figure 8.4.5 can be established as follows. All of the second event is assumed to be artefact and since  $R_f = 1M\Omega$   $v_o \sim 2.5V$ , with the principal frequency approximately 10Hz, when from figure 8.5.3  $|H| \sim 1.5 \times 10^{-5}\Omega^{-1}$ . Therefore, from equation 8.5.3  $v_e \sim 0.16V$ . The current immediately before the event is approximately  $1\mu A$  and if  $v_e$  is identified with  $I \Delta Z$ ,  $\Delta Z \sim 160k\Omega$ .

Assuming all of the second event to be artefactual is the worst case, and produces a surprisingly high value of  $\Delta Z$ . However, this example does emphasise the importance of motion artefact. Whilst it is

thought unlikely that there is a significant motion artefact present in the other flow traces presented, it is impossible to be sure since, for example, a cough could quite easily involve movement of the right arm.

Fortunately, this source of artefact can again be easily removed by using an anode in the CSF.

#### 8.6 Discussion

The results presented in section 8.4 show that the electrochemical flow transducer is capable of measuring the magnitude of CSF flow velocity in humans, whilst still allowing the measurement of pressure through the same needle. Also, the flow measurement procedure was simple enough to be a minimal extension of the pressure measurements. The results obtained are only initial results and it would be premature to say whether or not the flow information has any diagnostic value. However, these results do justify further trials to investigate the usefulness of the flow information.

The electrochemical flow transducer is very sensitive to low flow velocities, and therefore suited to this application. However, at low velocities its time response to a decrease in flow velocity is very long. Since the flow transducer is also insensitive to the direction of flow, its output at low flow velocities is effectively a time averaged representation of the flow, weighted towards the peak flows; for example, the peak cardiac flow is accurately represented but smaller flow velocities are masked within the time response of the output.

It is difficult to compare the direct flow velocity measurements given in section 8.2 with the volume flow results summarised in table 2.3.1, which were obtained using indirect radiographic and pressure measurement procedures. Only a naive comparison is possible and for this it is necessary to make some gross assumptions, as follows : it is assumed that the CSF pathways around the flow transducer are essentially circular and of approximately 10mm radius; that the pathways are empty of any structure which might shield the cathode; and that the flow velocity profile is flat. Then by estimating, for the various pressure stimuli, the average flow velocity and the duration of this flow velocity, it is possible to obtain an estimate of the volume flow occurring for comparison with table 2.3.1.

In figure 8.4.1 the maximum velocity is  $\sim 100\text{mm}\cdot\text{s}^{-1}$  and the average velocity of flow into the head is  $\sim 50\text{mm}\cdot\text{s}^{-1}$  for approximately 0.5s. This suggests a volume flow into the head, during a cough, of  $\sim 8\text{cm}^3$ .

For figure 8.4.2 (blows being equivalent to a Valsalva manoeuvre) the maximum velocity is  $\sim 60\text{mm}\cdot\text{s}^{-1}$ , and the average velocity of flow in either direction is, say,  $\sim 30\text{mm}\cdot\text{s}^{-1}$  for approximately 0.5s. During the blows, therefore, the volume flow out of and into the head is approximately  $5\text{cm}^3$ .

In the Queckenstedt's test of figure 8.4.3 the average velocity is  $\sim 6\text{mm}\cdot\text{s}^{-1}$  and lasts  $\sim 5\text{s}$  suggesting a volume flow out of the head of  $\sim 9\text{cm}^3$ .

The structure of the cardiac flow trace (figure 8.4.4) can only be explained by assuming that the CSF is rapidly ejected from the head, and then slowly returns. Assuming an average velocity of  $15\text{mm}\cdot\text{s}^{-1}$  for  $1/8\text{s}$  gives a volume flow out of the head during each heart beat of

$\sim 0.6\text{cm}^3$ .

Such a crude analysis is prone to large errors, and also the results were obtained in patients with abnormalities of the CSF pathways, but given these reservations the volume flow figures estimated above compare favourably with those of table 2.3.1.

The velocity calibration of the flow traces is critically dependent upon the measured  $pO_2$  since  $U_o \propto 1/c_s^2$ . The  $pO_2$  was measured by extracting a sample of CSF with a glass syringe which was capped as quickly as possible. If in error, the  $pO_2$  measured is most likely to be an overestimate since oxygen could enter the sample, causing the velocity calibration used to be an underestimate. The  $pO_2$ s measured were in the range 40 to 69mm of Hg, with a mean value of  $57 \pm 9$ mm of Hg. Campkin et al (1974) found the  $pO_2$  to be  $46.2 \pm 20.1$ mm of Hg in three conscious patients during ventriculography, and Fishman (1980) gives the average value of the CSF  $pO_2$  as 43.0mm of Hg.

Three possible sources of artefact have been identified (section 8.5), deriving primarily from the use of a skin electrode as anode. The problems of skin impedance and motion artefact can be eliminated by the use of an anode in the CSF (for example, the reservoir) and the problem of ECG pick up can be minimized by placing the anode as close to the cathode as possible. An obvious course of action is to construct an electrochemical flow transducer with the anode on the same assembly as the cathode. This would solve the artefact problems whilst being more convenient to use than the reservoir.

CHAPTER 9

CHAPTER 9CONCLUDING REMARKS

The work presented can be divided into three parts :-

- (i) the development of theoretical descriptions of the steady state response of various electrode geometries, and the development of a theory of the time response which can be applied to all the electrode geometries considered.
- (ii) the experimental investigation of the factors affecting the output current.
- (iii) the development of a practical electrochemical flow transducer and its use in the measurement of CSF flow in-vivo.

Chapter 3 describes the theory of the steady state response of disc electrodes, parallel and perpendicular to the flow, and of spherical electrodes. The description of the parallel disc is an extension of the theory of Levich (1962) for the semi-infinite parallel plate. The descriptions of the finite perpendicular disc and of the sphere are believed original; the model of the sphere is particularly successful since it extends to the separation point.

No satisfactory description of the time response (to decreases in flow) of the electrodes could be found, and so it was necessary to develop the time response theory presented in Chapter 5. The time response theory uses a generalised geometry and its application to particular electrodes involves the use of the steady state flow response results for those electrodes; its success therefore depends upon the accuracy of the steady state theories for the individual electrodes.

The experimental investigations of the various electrode geometries were performed before the theoretical descriptions were complete. They were designed to investigate the factors affecting the output current, not to explicitly test the more detailed facets of the theoretical models. Whilst, then, the experimental testing of the theories is in some ways incomplete, the degree of agreement obtained between theory and experiment is encouraging. The ability of the somewhat complex expressions obtained in Chapter 5 to describe the response of the various electrodes to a step decrease in flow is believed a considerable success.

Agreement between theory and experiment is worst for the disc perpendicular to the flow. This may be because of deficiencies in the theoretical model (for example, the way in which the potential flow components are obtained for this electrode - section 3.7), or because of deficiencies in the experimental investigation of this electrode. The latter could be the case because, for the perpendicular disc unlike the parallel disc and the sphere, any slight misalignment of the electrode is likely to drastically alter the geometry of the flow over the electrode (this is discussed in section 4.5).

The third aspect of this work, the development and use of a CSF flow transducer, was independent of the theoretical descriptions of the electrodes; the experimental work done was sufficient to allow the construction of such a transducer.

The initial clinical trials described could only be of use in showing whether or not the transducer worked in-vivo, and in exposing problems. The trials were successful on both counts. The results obtained showed that the flow of CSF could be measured in-vivo (though

no simultaneous independent measure of CSF flow is possible) whilst allowing the simultaneous measurement of pressure along the same spinal needle. The results also exposed three sources of artefact (section 8.5) which, fortunately, should be easily removable by placing the anode in the CSF, close to the cathode.

At this stage it is not possible to say what medical value the flow information has; only further trials can decide this issue. Volume flow information might well be of more use, but at the moment this is available only from radiographic procedures, which are time consuming and difficult to interpret; or from pressure studies as described in section 2.3.1 which give flow information of dubious value because of the gross perturbation of the CSF pathways they occasion. Certainly, development of the electrochemical flow transducer to provide directional flow information would increase its value in the measurement of CSF (and other) flows. One possible method of providing directional information is discussed below.

The electrochemical flow transducer is small, and neither it, nor the associated electronics, is costly. It might therefore be of use in other applications, for example the measurement of blood flow. As a research tool the flow transducer, or a simple linear array of transducers, might be of use in measuring velocity profiles across blood vessels in animal models. A possible clinical application could be as a catheter-tip flow transducer.

Protein poisoning of the cathode was not found to be a problem in the clinical trials, but blood contains approximately 200 times more protein. Therefore, for the electrochemical flow transducer to be of use in blood further work to find methods of removing or accommodating the protein poisoning is required.

Protein poisoning of the cathode could possibly be prevented by coating the cathode with a layer of an oxygen permeable substance so thin that the diffusion layer extends beyond it. This method would, however, decrease the output current, and increase the response time, since the diffusion coefficient of oxygen in the coating substance would be smaller than in water; and there would also be an upper limit to the flow velocity measurable, which would occur when the flow limited the diffusion layer to the coating.

The usefulness of the flow transducer would be greatly increased by the development of a directionally sensitive version. For example, if all that is required is "up or down", as for flow in a tube, this could be achieved by mounting two independent cathodes on opposite sides of a suitable support. The upstream cathode would give a greater output (when differences in flow sensitivity had been allowed for) than the downstream cathode. Subtraction of the two signals would give a signal whose polarity depended on the direction of flow, flow magnitude information being obtained from the cathode currently facing into the flow, or from an independent spherical cathode. Since the time response to an increase in flow is fast, and the initial response to a decrease in flow is also relatively fast, the direction signal would respond quickly to reversals of flow.

Another way of improving the electrochemical flow transducer would be to improve its time response to a decrease in flow. An obvious way is to decrease the size of the cathode (this is discussed in section 6.4.5). Zick (1976) describes the operation of  $pO_2$  electrodes in which the potential applied between anode and cathode was pulsed on and off. The currents flowing during the formation and destruction of the

diffusion layer, when processed, were found to produce a signal which varied with oxygen concentration. This type of stimulation of the cathode might be of value in improving the time response of the electrochemical flow transducer.

It is conceivable that the current, or its rate of change, early in the formation of the diffusion layer, is a function of flow velocity. If no significant perturbation of the oxygen concentration occurs (for this to be so a small cathode and a short on-pulse time would be necessary) then it is possible that the time response to a decrease in flow would be limited, not by the diffusion rate of oxygen, but by the time response of the hydrodynamic boundary layer, or the pulse repetition frequency.

A P P E N D I C E S

APPENDIX A.1 Calculation of the current response of an enamelled plate parallel to flow

The geometry is illustrated in figure 3.6.2. The plate is considered to be infinite in the z-direction, so that edge effects can be ignored. The potential flow  $U_0$  is parallel and constant and therefore  $\partial p / \partial x = 0$ . Therefore, the boundary layer equations (3.4.7 and 3.4.8) become

$$u \frac{\partial u}{\partial x} + v \frac{\partial u}{\partial y} = \nu \frac{\partial^2 u}{\partial y^2} \quad (\text{A.1.1})$$

$$\frac{\partial u}{\partial x} + \frac{\partial v}{\partial y} = 0 \quad (\text{A.1.2})$$

with boundary conditions

$$y = 0 : u = v = 0 \quad ; \quad y \rightarrow \infty : u \rightarrow U \quad (\equiv U_0 \text{ here}) \quad (\text{A.1.3})$$

Schlichting (1960) introduced the dimensionless co-ordinate  $\mu$ , and the stream function  $\psi(x,y)$

$$\mu = y \left( \frac{U_0}{\nu x} \right)^{1/2} \quad (\text{A.1.4})$$

$$\psi = \left( \nu x U_0 \right)^{1/2} f(\mu) \quad (\text{A.1.5})$$

where  $f(\mu)$  is the dimensionless stream function.

Transforming the boundary layer equations (A.1.1 and A.1.2) into terms of  $\mu$  gives

$$f f'' + 2f''' = 0 \quad (\text{A.1.6})$$

with boundary conditions

$$\mu = 0 : f(\mu) = f'(\mu) = 0 \quad ; \quad \mu \rightarrow \infty : f' \rightarrow 1 \quad (\text{A.1.7})$$

The primes denote differentiation with respect to  $\mu$ .

Equation A.1.6 can only be solved numerically, using the Blasius expansion (Schlichting 1960). Expanding around  $\mu = 0$  gives

$$f(\mu) = \sum_{n=0}^{\infty} \left(-\frac{1}{2}\right)^n \frac{\alpha^{n+1} C_n \mu^{3n+2}}{(3n+2)!} \quad (\text{A.1.8})$$

Here the viscous flow components are required at  $y \rightarrow 0$  and it is sufficient to take only the first term in A.1.8. Thus

$$f(\mu) \approx \frac{\alpha \mu^2}{2} \quad (\text{A.1.9})$$

From figure A.1.1 it will be seen that  $\alpha = 0.332$ .

The convective-diffusion equation (3.3.1) becomes here

$$u \frac{\partial c}{\partial x} + v \frac{\partial c}{\partial y} = D \left( \frac{\partial^2 c}{\partial x^2} + \frac{\partial^2 c}{\partial y^2} \right) \quad (\text{A.1.10})$$

with boundary conditions

$$\begin{aligned} \frac{\partial c}{\partial y} &= 0 \text{ at } y = 0, x < h \\ c &= 0 \text{ at } y = 0, x > h \end{aligned} \quad (\text{A.1.11})$$

$$c \rightarrow c_s \text{ as } y \rightarrow \infty$$

$$\text{At } x = y = 0 \quad c = c_s$$

However,  $\frac{\partial c}{\partial y} > \frac{\partial c}{\partial x}$  and  $u > v$  (Levich 1962) and, therefore, equation A.1.10 becomes

$$u \frac{\partial c}{\partial x} + v \frac{\partial c}{\partial y} = D \frac{\partial^2 c}{\partial y^2} \quad (\text{A.1.12})$$

with

$$u = \frac{\partial \psi}{\partial y} = U_0 f'(\mu) = U_0 \alpha \mu \quad (\text{for } \mu \sim 0) \quad (\text{A.1.13})$$

and

$$v = - \frac{\partial \psi}{\partial x} = \frac{1}{2} \left( \frac{v U_0}{x} \right)^{1/2} \cdot \frac{\alpha \mu^2}{2} \quad (\text{A.1.14})$$

Transforming  $y \rightarrow \psi$ , equation (A.1.12) becomes

$$x^{1/2} \frac{\partial c}{\partial x} = \beta \frac{\partial}{\partial \psi} \left( \sqrt{\psi} \frac{\partial c}{\partial \psi} \right) \quad (\text{A.1.15})$$

where

$$\beta = \frac{U_0^{3/4} \alpha^{1/2} 2^{1/2} D}{v^{1/4}} \quad (\text{A.1.16})$$

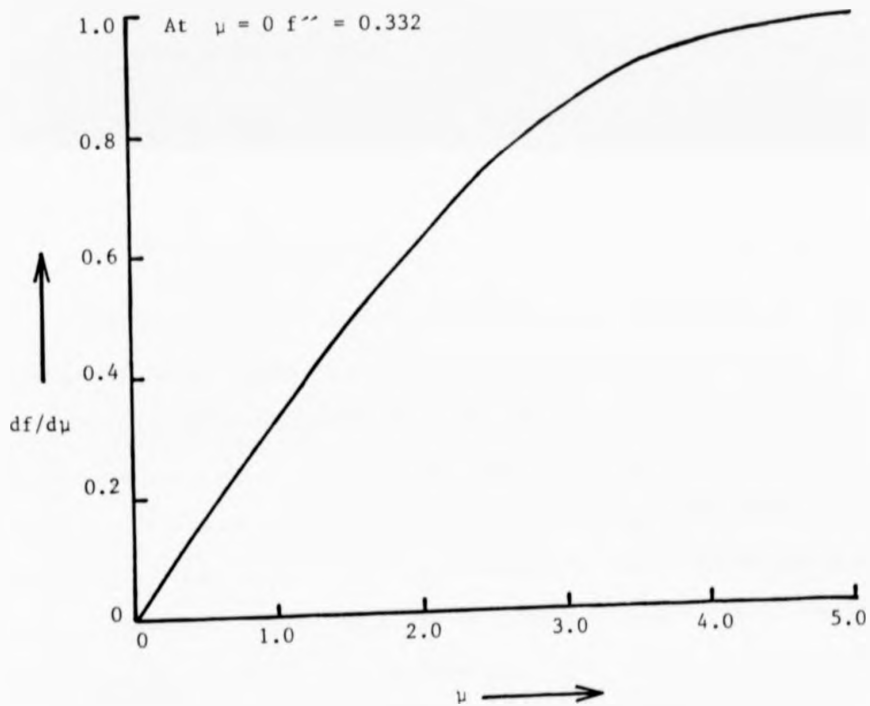


Figure A.1.1 The variation of  $df/d\eta$  with  $\eta$  for the parallel plate adapted from Schlichting (1960)

Equation A.1.15 then becomes, by introducing the variables

$$\zeta = x^{3/4} \quad \text{and} \quad \phi = \sqrt{\psi}$$

$$\frac{\partial c}{\partial \zeta} = \frac{\beta}{3\phi} \quad \frac{\partial^2 c}{\partial \phi^2} \quad (\text{A.1.17})$$

with boundary conditions

$$c \rightarrow c_s \quad \text{as} \quad \phi \rightarrow \infty$$

$$\frac{\partial c}{\partial \phi} = 0 \quad \text{for} \quad \zeta < h^{3/4}, \quad \phi = 0 \quad (\text{A.1.18})$$

$$c = 0 \quad \text{for} \quad \zeta \geq h^{3/4}, \quad \phi = 0$$

Re-introduction of the variable  $\mu$ , transforms equation A.1.17 into

$$\frac{\partial^2 c}{\partial \mu^2} = -\frac{\nu}{D} \frac{\alpha}{4} \mu^2 \frac{dc}{d\mu} \quad (\text{A.1.19})$$

since

$$\mu = \frac{\phi}{(\nu U_0)^{1/4} (\alpha/2)^{1/2} (\zeta)^{1/3}} \quad (\text{A.1.20})$$

Equation A.1.19 can be derived directly from equation A.1.12. The reason for the intermediate steps therefore requires explanation.

Levich (1962) has demonstrated that equation A.1.17 with its boundary conditions has a unique solution and states that this solution can be found from the solution to the analogous problem where the entire surface is reactive, that is for  $h = 0$ . Equation A.1.17 can be solved for  $h = 0$  by transformation into A.1.19. The importance of equation A.1.17 is that it is invariant in  $\zeta$  if  $\zeta \rightarrow \zeta + \text{constant}$ . Equation A.1.17 has effectively separated the concentration and velocity profiles, so that the above transformation, whilst representing a changed concentration profile, leaves the velocity dependence upon  $x$  unaltered.

If, having found a solution of equation A.1.17 for  $h = 0$ , the transformation

$$\zeta \rightarrow \zeta - h^{3/4} \quad (\text{A.1.21})$$

in the solution is made, the solution will still be a solution of equation A.1.17, but that corresponding to the required boundary conditions.

The solution to equation A.1.19 for  $h = 0$ , found by integration

is,

$$c(\mu) = \frac{c_s}{\int_0^\infty \exp\left(\frac{-\nu\alpha}{4D} \frac{\mu^3}{3}\right) d\mu} \cdot \int_0^\mu \exp\left(\frac{-\nu\alpha}{4D} \frac{\mu^3}{3}\right) d\mu \quad (\text{A.1.22})$$

Now,

$$\int_0^\infty \exp\left(\frac{-\nu\alpha}{4D} \frac{\mu^3}{3}\right) d\mu = \left(\frac{12D}{\nu\alpha}\right)^{1/3} \Gamma\left(\frac{4}{3}\right) \quad (\text{Dwight 1961})$$

(A.1.23)

Using a result from the Survey of Applicable Mathematics (Rektorys 1969) (p554, Theorem 12)

$$\left. \frac{dc}{d\mu} \right|_{\mu=0} = c_s \left(\frac{\nu\alpha}{12D}\right)^{1/3} \frac{1}{\Gamma(4/3)}$$

The solution for  $h \neq 0$  is obtained by inserting A.1.21 into A.1.20. Thus now,

$$\mu = \frac{\phi}{(\nu U_0)^{1/4}} \frac{1}{(\alpha/2)^{1/2}} \cdot \frac{1}{(x^{3/4} - h^{3/4})^{1/3}} \quad (\text{A.1.24})$$

and therefore

$$\left. \frac{\partial c}{\partial y} \right|_{y=0} = c_s \left(\frac{\nu\alpha}{12D}\right)^{1/3} \cdot \frac{1}{\Gamma(4/3)} \sqrt{\frac{U_0}{\nu}} \cdot \frac{1}{x^{1/2} \left(1 - \left(\frac{h}{x}\right)^{3/4}\right)^{1/3}} \quad (\text{A.1.25})$$

Finally, with  $\alpha = 0.332$  and  $\Gamma(4/3) = 0.893$  the current density at a point  $J$  for the enamelled plate is obtained

$$J = 0.34 \text{ mec}_s D^{2/3} \nu^{-1/6} U_0^{1/2} x^{-1/2} \left[1 - \left(\frac{h}{x}\right)^{3/4}\right]^{-1/3} \quad (\text{A.1.26})$$

APPENDIX A.2 A series expansion solution of the convective-diffusion equation

The form of the equation to be solved is

$$u \frac{\partial c}{\partial x} + v \frac{\partial c}{\partial y} = D \frac{\partial^2 c}{\partial y^2} \quad (\text{A.2.1})$$

with boundary conditions

$$y = 0 : c = 0 ; \quad y \rightarrow \infty : c \rightarrow c_s \quad (\text{A.2.2})$$

The velocity components  $u$  and  $v$  are expanded as

$$u = u_0 y x \left[ 1 + m_2 \frac{x^2}{R^2} + m_4 \frac{x^4}{R^4} + \dots \right] \quad (\text{A.2.3})$$

$$v = -u_0 y^2 \left[ 1 + n_2 \frac{x^2}{R^2} + n_4 \frac{x^4}{R^4} + \dots \right] \quad (\text{A.2.4})$$

The assumption is made that the concentration  $c$  is of the form

$$c = c_0 + \frac{c_2}{R^2} + \frac{c_4}{R^4} + \dots \quad (\text{A.2.5})$$

and that

$$\frac{\partial c_0}{\partial x} \equiv 0 \quad (\text{A.2.6})$$

The assumption  $\partial c_0 / \partial x \equiv 0$  is justified since it is known  $\partial c / \partial y > \partial c / \partial x$ .

Substitution into equation A.2.1 gives, to this order,

$$\begin{aligned} & u_0 y x \left[ 1 + m_2 \frac{x^2}{R^2} + m_4 \frac{x^4}{R^4} \right] \left[ \frac{1}{R^2} \frac{\partial c_2}{\partial x} + \frac{1}{R^4} \frac{\partial c_4}{\partial x} \right] \\ & - u_0 y^2 \left[ 1 + n_2 \frac{x^2}{R^2} + n_4 \frac{x^4}{R^4} \right] \left[ \frac{\partial c_0}{\partial y} + \frac{1}{R^2} \frac{\partial c_2}{\partial y} + \frac{1}{R^4} \frac{\partial c_4}{\partial y} \right] \\ & = D \left[ \frac{\partial^2 c_0}{\partial y^2} + \frac{1}{R^2} \frac{\partial^2 c_2}{\partial y^2} + \frac{1}{R^4} \frac{\partial^2 c_4}{\partial y^2} \right] \quad (\text{A.2.7}) \end{aligned}$$

Equating terms in powers of  $1/R$  gives

$$-u_0 y^2 \frac{dc_0}{dy} = D \frac{d^2 c_0}{dy^2} \quad (\text{A.2.8})$$

$$u_0 y x \frac{\partial c_2}{\partial x} - u_0 y^2 \left[ n_2 x^2 \frac{dc_0}{dy} + \frac{\partial c_2}{\partial y} \right] = D \frac{\partial^2 c_2}{\partial y^2} \quad (\text{A.2.9})$$

$$\begin{aligned} & u_0 y x \left( \frac{\partial c_4}{\partial x} + n_2 x^2 \frac{\partial c_2}{\partial x} \right) - u_0 y \left( \frac{\partial c_4}{\partial y} + n_2 x^2 \frac{\partial c_2}{\partial y} + n_4 x^4 \frac{dc_0}{dy} \right) \\ &= D \frac{\partial^2 c_4}{\partial y^2} \end{aligned} \quad (\text{A.2.10})$$

Equation A.2.8 is solved by integration to give

$$\frac{dc_0}{dy} = A e^{-u_0 y^3/3D} \quad (\text{A.2.11})$$

$$c_0 = B + A \int_0^y e^{-u_0 y^3/3D} dy \quad (\text{A.2.12})$$

A and B are constants.

A solution of the form

$$c_2 = \phi_2(y) x^2 \quad (\text{A.2.13})$$

is assumed to equation A.2.9 giving, on substitution

$$D \frac{d^2 \phi_2}{dy^2} + u_0 y^2 \frac{d\phi_2}{dy} - 2u_0 y \phi_2 = -u_0 y^2 n_2 A e^{-u_0 y^3/3D} \quad (\text{A.2.14})$$

This is consistent in that equation A.2.14 does not involve  $x$ .

A trial solution of the form  $\phi_2 = \gamma y e^{-u_0 y^3/3D}$ , where  $\gamma$  is some constant, requires  $\gamma = \frac{n_2}{5} A$  for consistency, that is

$$c_2 = \frac{n_2}{5} A x^2 y e^{-u_0 y^3/3D} \quad (\text{A.2.15})$$

A solution of the form

$$c_4 = \phi_4(y) x^4 \quad (\text{A.2.16})$$

is assumed to equation A.2.10 giving, on substitution

$$\begin{aligned} D \frac{d^2 \phi_4}{dy^2} + u_0 \frac{y^2 d\phi_4}{dy} - 4 u_0 y \phi_4 \\ = u_0 y^2 A e^{-u_0 y^3/3D} \left[ \frac{2n_2 m}{5} - \frac{n_2^2}{5} \left( 1 - \frac{u_0 y^3}{D} \right) - n_4 \right] \end{aligned} \quad (\text{A.2.17})$$

Equation A.2.17 is consistent in that it does not involve  $x$ .

A trial solution of the form

$$\phi_4 = \alpha A y e^{-u_0 y^3/3D} + \beta A y^4 e^{-u_0 y^3/3D}$$

requires for consistency that

$$\alpha = -\frac{1}{7} \left[ \frac{2m_2}{5} n_2 - \frac{n_2^2}{5} - n_4 + \frac{6}{5} \cdot \frac{n_2^2}{5} \right] \quad (\text{A.2.18})$$

$$\beta = -\frac{1}{10} \frac{u_0}{D} \frac{n_2^2}{5} \quad (\text{A.2.19})$$

that is

$$c_4 = A y x^4 e^{-u_0 y^3/3D} (\alpha + \beta y^3) \quad (\text{A.2.20})$$

$$\begin{aligned} \therefore c = B + A \int_0^y e^{-u_0 y^3/3D} dy + \frac{n A}{5R^2} x^2 y e^{-u_0 y^3/3D} \\ + \frac{A}{R^4} y x^4 e^{-u_0 y^3/3D} (\alpha + \beta y^3) \end{aligned} \quad (\text{A.2.21})$$

Now, when  $y = 0$ ,  $c = 0$  (equation A.2.2) and, therefore,

$$B = 0 \quad (\text{A.2.22})$$

and when  $y \rightarrow \infty$ ,  $c \rightarrow c_s$ , and therefore,

$$A = \frac{c_s}{\int_0^{\infty} e^{-u_0 y^3/3D} dy} \quad (\text{A.2.23})$$

Or from Dwight (1961)

$$A = \frac{c_s}{\Gamma(4/3)} \left( \frac{u_0}{3D} \right)^{1/3}$$

Now since,

$$J = D e m \left. \frac{\partial c}{\partial y} \right|_{y=0} \quad (\text{A.2.24})$$

$$J = \frac{c_s}{\Gamma(4/3)} \left( \frac{u_0}{3D} \right)^{1/3} m e D \left[ 1 + \frac{n_2}{5} \frac{x^2}{R^2} + a \frac{x^4}{R^4} \right] \quad (\text{A.2.25})$$

This equation for the current density is used for the perpendicular disc (section 3.7) and for the sphere (section 3.8).

### APPENDIX A.3 General solution of the hydrodynamic boundary layer equation for a body of revolution

The co-ordinate system used is shown in figure 3.4.1. The flow is assumed to be parallel to the axis of revolution. The boundary layer equations (3.4.11 and 3.4.12) and the boundary conditions (3.4.13) are

$$u \frac{\partial u}{\partial x} + v \frac{\partial u}{\partial y} = -\frac{1}{\rho} \frac{\partial p}{\partial x} + \nu \frac{\partial^2 u}{\partial y^2} \quad (\text{A.3.1})$$

$$\frac{\partial(ur)}{\partial x} + \frac{\partial(vr)}{\partial y} = 0 \quad (\text{A.3.2})$$

$$y = 0 : u = v = 0 \quad ; \quad y \rightarrow \infty : u \rightarrow \bar{U} \quad (\text{A.3.3})$$

Solution is facilitated by the introduction of the stream function  $\psi(x,y)$ . Equation A.3.2 is satisfied identically if

$$u = \frac{1}{r} \frac{\partial(\psi r)}{\partial y} = \frac{\partial \psi}{\partial y} \quad (\text{A.3.4})$$

$$v = -\frac{1}{r} \frac{\partial(\psi r)}{\partial x} = -\frac{\partial \psi}{\partial x} - \frac{1}{r} \frac{dr}{dx} \psi \quad (\text{A.3.5})$$

[This is an alternative form of the stream function to that used in section 3.7.]

If the body contour is given by

$$r(x) = r_1x + r_3x^3 + r_5x^5 + \dots \quad (\text{A.3.6})$$

the potential flow is given by

$$U\phi = u_1x + u_3x^3 + u_5x^5 + \dots \quad (\text{A.3.7})$$

and the distance from the surface by

$$\mu = y \left( \frac{2u_1}{v} \right)^{1/2} \quad (\text{A.3.8})$$

then, Schlichting found the stream function to be

$$\psi(x, y) = \left( \frac{v}{2u_1} \right)^{1/2} \left[ u_1x f_1(\mu) + 2u_3x^3 f_3(\mu) + 3u_5x^5 f_5(\mu) + \dots \right] \quad (\text{A.3.9})$$

where

$$f_3 = g_3 + \frac{r_3 u_1}{r_1 u_3} h_3 \quad (\text{A.3.10})$$

$$f_5 = g_5 + \frac{r_5 u_1}{r_1 u_5} h_5 + \frac{u_3^2}{u_1 u_5} k_5 + \frac{r_3 u_3}{r_1 u_5} j_5 + \frac{r_3^2 u_1}{r_1^2 u_5} q_5 \quad (\text{A.3.11})$$

The functions of  $\mu$ , that is  $g_3, h_3, g_5, h_5$  etc., were found numerically.

The important point here, where  $u$  and  $v$  are required at small  $y$ , is

that at small  $\mu$  these functions of  $\mu$  behave such that

$$f_3 \sim \alpha_3 \mu^2 \quad (\text{A.3.12})$$

$$f_5 \sim \alpha_5 \mu^2 \quad (\text{A.3.13})$$

The values of  $u$  and  $v$  are found from equation A.3.9, A.3.4 and A.3.5.

APPENDIX B.1. Calculation of the time response of a parallel disc with no enamel.

The relevant geometry is given in figure 3.6.3. If there is no enamel then  $h = 0$  and  $\chi = 1$ , and from equation 3.6.5  $Q_{II}$  becomes 1.23.

The variation of current with time then becomes, from equation 5.4.8

$$I(t) = \frac{I_f}{2R^{3/2} Q_{II}} \int_0^R db \int_0^{\ell} x^{-1/2} dx + \frac{I_f}{R^{3/2} Q_{II}} \int_{n=1}^{\infty} \frac{\sin an}{an} \int_0^R db \int_0^{\ell} x^{-1/2} \exp\left[-\frac{Cn^2 R}{x}\right] dx \quad (\text{B.1.1.})$$

The first double integral has been evaluated in section 3.6 and is equal to  $2R^{3/2} Q_{II}$ , if  $h = 0$  and  $\chi = 1$ .

The inner integral of the second double integral can be evaluated by setting

$$x^{-1/2} = \xi \quad (\text{B.1.2.})$$

when

$$\int_0^{\ell} \rightarrow 2 \int_{\ell^{-1/2}}^{\infty} \exp\left[-Cn^2 R \xi^2\right] d(-\xi^{-1}) \quad (\text{B.1.3.})$$

This is integrated by parts to give

$$2 \left[ \exp \left[ \frac{-\text{Cn}^2 \text{R}}{\ell} \right] \ell^{1/2} - 2\text{Cn}^2 \text{R} \int_{-\ell^{1/2}}^{\infty} \exp \left[ -\text{Cn}^2 \text{R} \xi^2 \right] d\xi \right] \quad (\text{B.1.4})$$

now,

$$(1 - \text{erf } z) = \frac{2}{\sqrt{\pi}} \int_z^{\infty} e^{-t^2} dt \quad (\text{Rektorys, 1969}) \quad (\text{B.1.5})$$

and it therefore follows that

$$\int_0^f x^{-1/2} \exp \left[ -\frac{\text{Cn}^2 \text{R}}{x} \right] dx = 2 \left[ \exp \left[ -\frac{\text{Cn}^2 \text{R}}{\ell} \right] \ell^{1/2} - \sqrt{\pi \text{Cn}^2 \text{R}} \left[ 1 - \text{erf} \left( \frac{\text{Cn}^2 \text{R}}{\ell} \right)^{1/2} \right] \right] \quad (\text{B.1.6})$$

From equation 5.4.13, with  $\chi = 1$

$$\ell = 2\text{R} \sqrt{1 - \epsilon^2} \quad (\text{B.1.7})$$

where, from equation 5.4.12

$$b = \epsilon \text{R} \quad (\text{B.1.8})$$

Substitution of equations B.1.6, B.1.7 and B.1.8 in equation

B.1.1 gives

$$I(t) = I_f + \frac{2I_f}{Q_H} \int_{n=1}^{\infty} \frac{\sin an}{an} \int_0^t \exp \left[ -\frac{\text{Cn}^2}{2\sqrt{1-\epsilon^2}} \right] \cdot \left[ 2(1-\epsilon^2)^{1/2} \right]^{1/2} \\ - \sqrt{\pi \text{Cn}^2} \left[ 1 - \text{erf} \left( \frac{\text{Cn}^2}{2\sqrt{1-\epsilon^2}} \right)^{1/2} \right] d\epsilon \quad (\text{B.1.9})$$

APPENDIX B.2. Calculation of the time response of a sphere partially covered with epoxy.

The geometry relevant to this calculation is given in figures 3.9.8a and b.

The total steady state current is given by equation 3.9.10, which becomes with  $r = R \sin \theta$

$$I = \int_0^{\theta_c} \int_0^{2\pi} d\phi R^2 \sin \theta J(\theta) d\theta + \int_{\theta_c}^{\theta_s} \int_0^{2(\pi-\psi)} d\phi R^2 \sin \theta J(\theta) d\theta \quad (\text{B.2.1.})$$

or in integrated form, from equation 3.9.12

$$I = 2\pi R^{3/2} 1.04 (Q_{s1} + Q_{s2}) \text{mec}_s D^{2/3} v^{-1/6} U_o^{1/2} \quad (\text{B.2.2.})$$

$J(\theta)$  is the current density at a point on the surface of the sphere and is given by equation 3.8.20

$$J(\theta) = 1.04 R^{-1/2} F(\theta) \text{mec}_s D^{2/3} v^{-1/6} U_o^{1/2} \quad (\text{B.2.3.})$$

where  $F(\theta)$  is given by equation 5.6.2.

As in section 5.6. the subscript  $f$  is introduced and equations B.2.2. and B.2.3. are combined to give

$$J_f = \frac{I_f F(\theta)}{2\pi R^2 (Q_{s1} + Q_{s2})} \quad (\text{B.2.4.})$$

Equation B.2.4. is substituted into equation 5.3.39 to give the time response of the current density at a point on the surface of the sphere.

$$J(\theta, t) = \frac{I_f F(\theta)}{2\pi R^2(Q_{s1} + Q_{s2})} + \frac{2I_f F(\theta)}{2\pi R^2(Q_{s1} + Q_{s2})} \cdot \sum_{n=1}^{\infty} \frac{\sin an}{an} \exp \left[ -Cn^2 F(\theta)^2 \right] \quad (\text{B.2.5})$$

where

$$C = \left[ \frac{I_f}{Dmecs} \frac{1}{2R^2(Q_{s1} + Q_{s2})} \right]^2 Dt \quad (\text{B.2.6})$$

The time variation of the total current is found by performing the integrations of equation B.2.1 upon the terms of equation B.2.5, to give (using equations 3.9.13 and 3.9.14)

$$I(t) = \frac{I_f}{2\pi(Q_{s1} + Q_{s2})} \cdot 2\pi(Q_{s1} + Q_{s2}) + \frac{I_f}{\pi(Q_{s1} + Q_{s2})} \cdot \sum_{n=1}^{\infty} \frac{\sin an}{an} \times$$

$$\left[ \int_0^{\theta_c} 2\pi \sin\theta F(\theta) \exp \left[ -Cn^2 F(\theta)^2 \right] d\theta + \right.$$

$$\left. \int_{\theta_c}^{\theta_s} 2(\pi - \psi) \sin\theta F(\theta) \exp \left[ -Cn^2 F(\theta)^2 \right] d\theta \right] \quad (\text{B.2.7})$$

Equation 5.6.10 is then obtained by rearrangement.

APPENDIX B.3. The flow chart of the programs used to evaluate the time response expressions.

Equations 5.4.16, 5.5.8 and 5.6.9 describing the time response of the enamelled parallel disc, the enamelled perpendicular disc and the sphere can all be cast in the following form:

$$I(C) = I_f + \frac{2I_f}{Q} \int_{n=1}^{\infty} \text{TERM}(C,n) \quad (\text{B.3.1.})$$

where

$$\text{TERM}(C,n) = \frac{\sin an}{an} \times \text{INTEGRAL}(C,n) \quad (\text{B.3.2.})$$

and

$$a = \pi \times \frac{I_f}{I_i} \quad (\text{B.3.3.})$$

Therefore, the flow charts for each program . are very similar and only one general flow chart, figure B.3.1. will be given. Specific differences are discussed below.

The method of termination of the summation, shown in figure B.3.1. requires that at least ten terms are calculated. Termination occurs if the present sum minus the sum five terms ago is less than one thousandth of the present sum. This method overcomes the problem described in section 5.7.

The actual integrals are calculated either using Simpson's method (the parallel disc) or by using a standard routine resident in the computer (the perpendicular disc and the sphere). Convenience was the only deciding factor.

The double integral in equation 5.4.16 for the parallel disc is evaluated as follows.  $h'$ ,  $l'$  and  $z$  are functions of  $\epsilon$ . Each value of  $\epsilon$  used in the Simpson's method evaluation of the outer integral is also used to

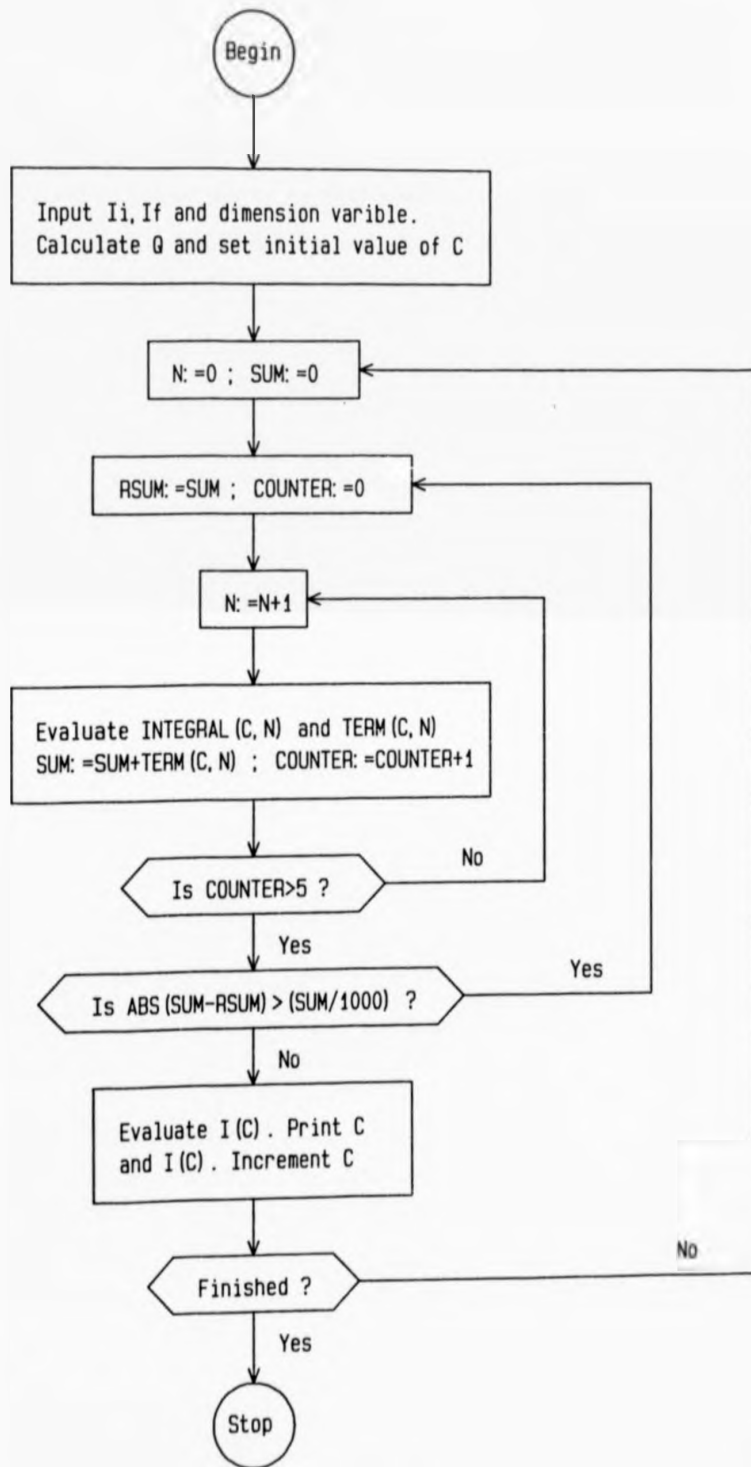


Figure B.3.1 Simplified flow chart of the programs used to evaluate the time response expressions.

evaluate the upper limit of the inner integral, which is itself calculated using Simpson's method. However, when  $\epsilon = 0$  the inner integral contains the term  $e^{-\frac{1}{\epsilon}}$ , which whilst equal to zero cannot be evaluated numerically by a computer. This term is set explicitly to zero.

APPENDIX C1 The response of the voltage-clamp to constant A.C. voltage perturbation

Since A.C. perturbations are being considered let  $v_{ac} = 0$ . The circuit describing the situation is shown in figure C.1.1.  $Z$  is the impedance of the flow transducer electrodes when the transducer is operating (i.e.  $v_{ac} \neq 0$ ). The equations of the circuit are

$$v_o - v_i = i_f R_f \quad (C.1.1)$$

$$v_e - v_i = iZ \quad (C.1.2)$$

$$v_o = -Av_i \quad \left[ \text{the open loop gain } A > 10^5 \text{ (Jones, 1977)} \right] \quad (C.1.3)$$

$$i + i_f = 0 \quad (C.1.4)$$

Substitution of equation C.1.3 into C.1.1 gives

$$i_f = v_o (1 + 1/A) / R_f \quad (C.1.5)$$

and substitution of equations C.1.3 and C.1.4 into C.1.2 gives

$$v_e + v_o/A = -i_f Z \quad (C.1.6)$$

Combining equations C.1.5 and C.1.6 gives

$$v_e = -v_o \left[ Z(1+A)/R_f + 1/A \right] \quad (C.1.7)$$

Since  $A \gg 1$  and if  $AZ \gg R_f$  equation C.1.7 becomes

$$v_o/v_e = -R_f/Z \quad (C.1.8)$$

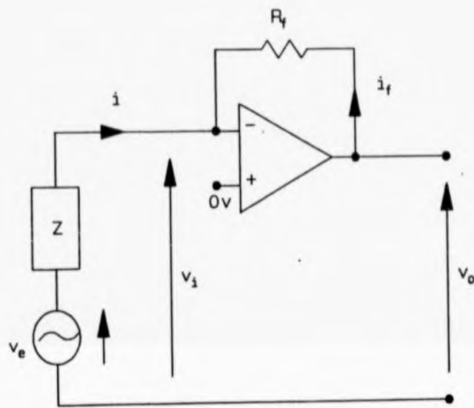


Figure C.1.1 Constant alternating voltage perturbation of the voltage-clamp.

The output of the second, inverting, unity gain stage of the voltage-clamp is then

$$v_o/v_e = R_f/Z \quad (\text{C.1.9})$$

or

$$H = 1/Z \quad (\text{C.1.10})$$

where

$$H = v_o/(v_e R_f) \quad (\text{C.1.11})$$

H is a function of the electrode impedance Z and if Z is a complex frequency then H will be a function of frequency.

APPENDIX C2 The equation of the equivalent circuit of figure 8.5.2

$$H = \frac{X1.X2 + Y1.Y2 + 1 (X1.Y2 - X2.Y1)}{X1^2 + Y1^2} \quad (\text{C.2.1})$$

where

$$X1 = R_d(1-\omega^2AB) + R_b(1-\omega^2AB - \omega^2T[A+B+E]) + R_a(1-\omega^2BT) \quad (\text{C.2.2})$$

$$Y1 = \omega \left[ R_d(A+B+E) + R_b(A+B+E+T-\omega^2TAB) + R_a(T+B) \right] \quad (\text{C.2.3})$$

$$X2 = 1 - \omega^2AB - \omega^2T(A+B+E) \quad (\text{C.2.4})$$

$$Y2 = \omega(A+B+E+T-\omega^2TAB) \quad (\text{C.2.5})$$

and  $A = C_a R_a$ ;  $B = C_b R_b$ ;  $E = C_b R_a$ ;  $T = C_d R_d$

Table D.1.1

## Materials and Items used.

Item	Comment	Supplier
Enamelled copper wire	Commercial grade	The Temple Electrical Co Ltd Temelec House 291 Lower High St Watford WD1 2HZ
Copper sheet	99.99% pure	Johnson Matthey Chemicals Ltd Orchard Rd Royston SG8 5HE
Gold wire 0.125 mm hard	99.99+% pure Impurities (ppm by weight): Ag 10; Ca 1; Cu 1; Fe 2; Mg 1; Pd <1; Si 5	Goodfellow Metals Ltd Cambridge Science Park Milton Rd Cambridge CB4 4DJ
Ag/AgCl electrodes	Button type (as used for EEGs)	Specialised Laboratory Equipment Ltd 15 Campbell Rd Croydon Surrey CR0 2SQ
Oxygen electrode	Model DOS-450-M Lead-Silver oxygen electrode with polythene membrane Output typically 5 microamps (into 1 kohm load) in air equilibrated saline at 20 C	A.Gallenkamp & Co Ltd PO Box 290 Technico House Christopher St London EC2P 2ER
Stainless steel tube	0.500 mm OD, 0.125mm wall thickness Cr18/Ni10/Fe	Goodfellow Metals Ltd Cambridge Science Park Milton Rd Cambridge CB4 4DJ
Epoxy resin glue	Quick set	RS Components Ltd PO Box 427 13-17 Epworth St London EC2P 2HA
Chemicals	e.g., NaCl Analytical Reagent Grade. All solutions made up in de-ionised water	Fisons Scientific Apparatus Ltd Bishop Meadow Rd Loughborough LE11 0RG

R E F E R E N C E S

REFERENCES

- Arvia A.J., and Marchiano S.L. (1971)  
In: Modern Aspects of Electrochemistry. No.6.  
Eds: Bockris J. O'M. and Conway B.E.  
London : Butterworths.
- Barnett H.J.M., Foster J.B. and Hudgson P. (1973)  
Syringomyelia.  
London : Saunders.
- Battocletti J.H., Sances A., Larson S.J., Evans S.M., Bowman R.L.,  
Kudravcev V. and Ackmann J.J. (1975)  
Clinical applications and theoretical analysis of NMR blood  
flowmeter.  
Biomed. Eng., 10; 12-15 & 20.
- Bell G.H., Emslie-Smith D. and Paterson C.R. (1980)  
Textbook of Physiology. 10th edition.  
Edinburgh : Livingstone.
- Bellhouse B.J. and Bellhouse F.H. (1968)  
Thin film gauges for the measurement of velocity or skin  
friction in air, water or blood.  
J. Phys. E., 1; 1211-1213.
- Bellhouse B.J., Bellhouse F.H. and Cunning A. (1969)  
A straight needle-probe for the measurement of blood velocity.  
J. Phys. E., 2; 936-938.
- Bellhouse B.J., Clark C. and Schultz D.L. (1972)  
Velocity Measurements with Thin Film Gauges.  
In: Blood Flow Measurement.  
Ed: Roberts V.C.  
London : Sector
- Bering E.A.Jr. (1955)  
Choroid plexus and arterial pulsation of CSF.  
Arch. Neurol. Psychiat. (Chicago), 73; 165-172.
- Bevir M.K. (1971)  
Sensitivity of electromagnetic velocity probes.  
Phys. Med. Biol., 16; 229-232.
- Bockris J.O'M. and Reddy A.K.N. (1970)  
Modern Electrochemistry. Vol.2.  
London : MacDonald.

- Campkin T.V., Barker R.G., Pabari M. and Grove L.H. (1974)  
Acid-base changes in arterial blood and cerebrospinal fluid during craniotomy and hyperventilation.  
Br. J. Anaesth., 46; 263-267.
- Cater D.B., Silver I.A. and Wilson G.M. (1959)  
Apparatus and technique for the quantitative measurement of oxygen tension in living tissues.  
Proc. R. Soc. B., 151; 256-276.
- Charlot G., Badoz-Lambling J. and Tremillon B. (1962)  
Electrochemical Reactions : The Electrochemical Methods of Analysis.  
Amsterdam : Elsevier.
- Chopp M. and Portnoy H.D. (1980)  
Systems analysis of intracranial pressure.  
J. Neurosurg., 53; 516-527.
- Clark C. (1974)  
Thin film gauges for fluctuating velocity measurements in blood.  
J. Phys. E., 7; 548-556.
- Clark L.C.Jr. (1956)  
Monitor and control of blood and tissue oxygen tensions.  
Trans. Am. Soc. Artif. Int. Organs, 2; 41-48.
- Crank J. (1975)  
The Mathematics of Diffusion. 2nd edition.  
Oxford : Clarendon.
- Damjanovic A. (1969)  
In: Modern Aspects of Electrochemistry. No.5.  
Eds: Bockris J. O'M. and Conway B.E.  
London : Butterworths.
- Davson H. (1967)  
Physiology of the Cerebrospinal Fluid.  
London : Churchill.
- Dereymaeker A., Stevens A., Rombouts J.J., Lacheron J.M. and Pierquin A. (1971)  
Study on the influence of the arteial pressure upon the morphology of cisternal CSF pulsations.  
Europ. Neurol., 5; 107-114.
- Diem K. and Lentner C. (1970)  
Documenta Geigy : Scientific Tables.  
Basle : Geigy J.R.

- Du Boulay G.H. (1966)  
Pulsatile movements in the CSF pathways.  
Br. J. Radiol., 39; 255-262.
- Du Boulay G.H., O'Connell J.E.A., Currie J., Bostick T. and Verity P. (1972)  
Further investigations of pulsatile movements in the cerebrospinal fluid pathways.  
Acta. Radiologica (Stockholm), 13; 496-523.
- Dwight H.B. (1961)  
Tables of Integrals and other Mathematical Data. 4th edition.  
New York : MacMillan.
- Ekstedt J. (1977)  
CSF hydrodynamic studies in man : 1. Method of constant pressure CSF infusion.  
J. Neurol. Neurosurg. Psychiat., 40; 105-119.
- Ekstedt J. (1978)  
CSF hydrodynamic studies in man : 2. Normal hydrodynamic variables related to CSF pressure and flow.  
J. Neurol. Neurosurg. Psychiat., 41; 345-353.
- Eversden I.D. (1973)  
Monitoring intracranial pressure.  
Biomed. Eng., 8; 192-197.
- Eyring H., Henderson D. and Jost. W. (1970)  
Physical Chemistry : An Advanced Treatise. Vol. 1XB.  
London : Academic.
- Fishman R.A. (1980)  
Cerebrospinal Fluid in Diseases of the Nervous System.  
Philadelphia : Saunders W.B.
- Ganong W.F. (1981)  
Review of Medical Physiology. 10th edition.  
Los Altos (Calif) : Lange Medical Publications.
- Gardner W.J. (1945)  
Cerebrospinal Fluid : Dynamics.  
In: Medical Physics.  
Ed: Glaser O.  
Chicago : Year Book Co.
- Gilland O. (1966)  
CSF Dynamic Diagnosis of Spinal Block.  
Stockholm : Almqvist and Wiksell.

- Gilland O., Chin F., Anderson W.B. and Nelson J.R. (1969)  
A cinemyelographic study of cerebrospinal fluid dynamics.  
Am. J. Roentgenography, 106; 369-375.
- Guinane J.E. (1972)  
An equivalent circuit analysis of cerebrospinal fluid hydrodynamics.  
Am. J. Physiol., 223; 425-430.
- Jackson J.R. and Williams B.N. (1979)  
Errors in velocity measurement by the Pitot principle in fluids with slowly propagated pressure waves.  
J. Biomed. Eng., 1; 50-54.
- Jenkins C.O. and White D.N. (1972)  
The rise time of intracranial echo pulsations and intracranial pressure.  
Acta. Neurol. Scand., 48; 115-123.
- Jones M.H. (1977)  
A Practical Introduction to Electronic Circuits.  
Cambridge : Cambridge University Press.
- Laitinen L. (1968)  
Origin of the arterial pulsation of cerebrospinal fluid.  
Acta. Neurol. Scand., 44; 168-176.
- Lakke J.P.W.F. (1969)  
Queckenstedt's Test.  
Amsterdam : Excerpta Medica.
- Landolt-Börnstein. (1969)  
Numerical Values and Functions from Physics, Chemistry, Astronomy, Geophysics and Technology.  
Berlin : Springer.
- Levich V.G. (1962)  
Physicochemical Hydrodynamics.  
London : Prentice-Hall.
- Ling S.C., Atabek H.B., Fry D.L., Patel D.J. and Janick J.S. (1968)  
Application of heated-film velocity and shear probes to haemodynamic studies.  
Circ. Res., 23; 789-801.
- Lockey P., Poots G. and Williams B.N. (1975)  
Theoretical aspects of the attenuation of pressure pulses within cerebrospinal fluid pathways.  
Med. Biol. Eng., 14; 861-869.

- Mackay R.S. (1970)  
Biomedical Telemetry.  
New York : Willey.
- Marchiano S.L. and Arvia A.J. (1968)  
Diffusional flow under non-isothermal laminar free convection  
at a thermal convective electrode.  
Electrochim. Acta., 13; 1657-69.
- Matsuda H. (1967)  
Zur theorie der Stationärenstrom-Spannungs-Kurven von Redox-  
Elektrodenreaktionen in Hydrodynamischer Voltammetrie.  
J. Electroanal. Chem., 15; 109-127.
- Meldrum S.J., Watson B.W. and Becker G.A. (1973)  
A catheter tip transducer for continuous measurement of  
blood oxygen tension in neonates.  
Biomed. Eng., 8; 470-471 and 479.
- Mochizuki M., Koyama T. and Yokota K. (1962)  
Monograph Series of the Research Institute of Applied  
Electricity. 10.  
Ed: Higasi K.  
Sapporo : Hokkaido University.
- O'Connell J.E.A. (1953)  
The cerebrospinal fluid as an aetiological factor in the  
development of lesions affecting the central nervous system.  
Brain, 76; 279-298.
- O'Connell J.E.A. (1970)  
Cerebrospinal fluid mechanics.  
Proc. R. Soc. Med., 63; 507-518.
- Oeseburg B., Zijlstra W.G. and Ing T.G. (1968)  
Uncovered platinum electrodes for the measurement of  $\Delta P_{O_2}$   
as an aid in diagnostic cardiac catheterisation.  
Cardiovasc. Res., 4; 394-403.
- Parker D., Scopes J.W., Key A., Davies R. and Marcovitch H. (1971)  
A disposable catheter-tip transducer for continuous measurement  
of blood oxygen tension in vivo.  
Biomed. Eng., 6; 313-317.
- Perry R.H., Chilton C.H. and Kirkpatrick S.D. (1963)  
Chemical Engineers' Handbook. 4th edition.  
New York : McGraw Hill.

Prandtl L. (1963)

Fluid Dynamics.  
London : Blackie.

Prytherch D.R. and Smith M.J.A. (1979)

A velocity magnitude transducer for use with saline  
containing dissolved oxygen.  
J. Phys. E., 12; 195-200.

Prytherch D.R., Smith M.J.A. and Williams B. (1979)

The measurement of cerebrospinal fluid flow.  
Phys. Med. Biol., 24; 1196-1208.

Reitan H. (1941)

On movements of fluid inside the cerebrospinal space.  
Acta. Radiologica (Stockholm), 22; 762-779.

Rektorys K. (1969)

Survey of Applicable Mathematics.  
London : Iliffe.

Roberts V.C. (1972)

Blood Flow Measurement.  
London : Sector.

Rosenhead L. (1963)

Fluid Motion Memoirs : Laminar Boundary Layers.  
Oxford : Clarendon.

Schlichting H. (1960)

Boundary Layer Theory.  
New York : McGraw Hill

Seed W.A. (1972)

Hot Film Anemometry in the Human Aorta.  
In: Blood Flow Measurement.  
Ed: Roberts V.C.  
London : Sector.

Seed W.A. and Wood N.B. (1970a)

Use of a hot-film velocity probe for cardiovascular studies.  
J. Phys. E., 3; 377-384.

Seed W.A. and Wood N.B. (1970b)

Development and evaluation of a hot-film velocity probe for  
cardiovascular studies.  
Cardiovasc. Res., 4; 253-263.

- Shapiro K., Marmarou A. and Shulman K. (1980)  
Characterization of clinical CSF dynamics and neural axis compliance. 1. The normal pressure-volume index.  
Annal. Neurol., 7; 508-514.
- Silver I.A. (1972)  
Problems in the investigation of tissue oxygen microenvironment.  
Chem. Eng. Med., 17; 343-351.
- Spertell R.B. (1981)  
On the transmission of external pressure fluctuations to the cerebrospinal fluid.  
J. Theor. Biol., 88; 309-321.
- Spiegel M.R. (1964)  
Theory and Problems of Complex Variable : Schaum's Outline Series.  
New York : McGraw Hill.
- Strong P. (1970)  
Biophysical Measurements.  
Beaverton, Oregon : Tektronix Inc.
- Tunturi A.R. (1977)  
Elasticity of the spinal cord dura in the dog.  
J. Neurosurg., 47; 391-396.
- Washburn E.W. (1929)  
International Critical Tables of Numerical Data : Physics,  
Chemistry and Technology. Volume V.  
New York : McGraw Hill.
- Weast R.C. (1978)  
Handbook of Chemistry and Physics. 59th edition.  
West Palm Beach, Florida : Chemical Rubber Co. Press.
- Webster J.G. (1978)  
Medical Instrumentation : Application and Design.  
Boston : Houghton Mifflin.
- Williams B.N. (1973)  
Syringomyelion and its surgical treatment.  
Nursing Times; 24th May 1973.
- Williams B.N. (1974)  
A demonstration analogue for ventricular and intraspinal dynamics (DAVID).  
J. Neurol. Sci., 23; 445-461.

- Williams B.N. (1976)  
Cerebrospinal fluid pressure changes in response to coughing.  
*Brain*, 99; 331-346.
- Williams B.N. (1977)  
On the pathogenesis of the Chiari malformation.  
*Zeitschrift fur Kinderchirurgie*, 22; 533-554.
- Williams B.N. (1981a)  
Simultaneous cerebral and spinal fluid pressure recordings : 1.  
Technique, physiology and normal results.  
*Acta. Neurochirurgica*, 58; 167-185.
- Williams B.N. (1981b)  
Simultaneous cerebral and spinal fluid pressure recordings : 2.  
Cerebrospinal dissociation with lesions at the Foramen Magnum.  
*Acta. Neurochirurgica.*, 59; 123-142.
- Williams B.N. (1981c)  
Chronic herniation of the hindbrain.  
*Annals R. College Surgeons of England*, 63; 9-17.
- Williams B.N. (1981d)  
Syringomyelia as a sequel to traumatic paraplegia.  
*Paraplegia*, 19; 67-80.
- Williams B.N. and Guthkelch A.N. (1974)  
Why do central arachnoid pouches expand?  
*J. Neurol. Neurosurg. Psychiat.*, 37; 1085-1092.
- Wise E.M. (1964)  
*Gold: Recovery, Properties and Applications.*  
Princeton, N.J : Van Nostrand.
- Woodcock J.P. (1976)  
Physical properties of blood and their influence on blood flow measurement.  
*Reports Prog. Phys.*, 39; 65-127.
- Yuan S.W. (1970)  
*Foundations of Fluid Mechanics.*  
London : Prentice Hall.
- Zick G.L. (1976)  
Determination of oxygen tension by measurement of net charge transport.  
*IEEE Trans. Biomed. Eng.*, BME 23; 472-477.